UNIVERSITY OF GENOVA

POLYTECHNIC SCHOOL

Department of Mechanical, Energy, Management and Transportation Engineering

DOCTORAL THESIS

Design Methods and Optimization Tools for the Development of Upper Limbs Exoskeletons

Supervisor:
Prof. Giovanni Berselli
Prof. Antonio Frisoli

Candidate:
Greta Vazzoler

December 2024

Design Methods and Optimization Tools for the Development of Upper Limbs Exoskeletons

Greta Vazzoler

A dissertation submitted to the faculty of
University of Genova
in partial fulfillment of the requirements for the degree of

Doctor of Philosophy

Department of Mechanical, Energy, Management
and Transportation Engineering

University of Genova

December 2024

Abstract

This thesis aims to provide an in-depth analysis of innovative design strategies and advanced modelling techniques in the field of upper limbs exoskeletons. It focuses on two key areas: first, the development of optimization tools for designing passive balancing systems that enable the creation of cost-effective and lightweight exoskeletons to prevent injuries among industrial workers while performing repetitive overhead tasks; and second, the application of conventional robotic systems techniques to produce a complete device for robot-assisted therapy, specifically targeting rehabilitation for post-stroke and orthopaedic patients. The research not only addresses the complexities of replicating human limb anatomy, but also offers practical insights for developing user-friendly exoskeletons, either for injury prevention or to foster recovery of arm function after impairment. The proposed strategy strengthens the theoretical foundations of exoskeleton design and offers significant potential for real-world advancements, aiming to greatly improve the quality of life for both workers and injured patients thanks to the usage of innovative upper limbs exoskeleton solutions.

The essence of this thesis is embodied in Chapter 3 and Chapter 4, where the proposed systems are presented. Before developing novel devices, the research started by tackling a detailed examination of upper limbs exoskeletons available in the scientific literature including the analysis of the human upper limb anatomy to understand the natural movement of the human art. After identifying key design principles for the development of exoskeleton systems, the current technologies in the field have been reviewed and a classification of upper limbs exoskeletons has been provided by leveraging the state of the art. In detail, this study explores devices that find application in both industrial and healthcare fields, with a focus on shoulder-elbow exoskeletons for helping industrial workers in executing overhead tasks and medical devices for the rehabilitation of the wrist.

Chapter 3 deploys the Shoulder-Elbow Exoskeleton (SEES), focusing on its analysis and preliminary design. The SEES is a passive upper limb exoskeleton intended to support workers in industrial environments by assisting in repetitive tasks and reducing the risk of injuries. Its main purpose is to compensate for gravity loads on the human arm. The system is implemented via a 6-Degrees Of Freedom (DOFs) kinematic model (5-DOFs for the shoulder and 1-DOF for the elbow) and employs passive elastic elements to achieve gravity compensation, minimizing both weight and costs of the overall structure. This chapter introduces a detailed analytical tool to aid in the exoskeleton design, examining its kinetic-static behaviour and optimizing the design of the elastic springs to balance gravity across several arm movements. Different kind of balancer models, i.e., with 1-DOF or 3-DOFs, and various arrangements of the springs, either linear or torsional springs, have been evaluated. One optimal configuration is proposed as a case study, and results are validated using a multi-body simulation tool for specific tasks.

Chapter 4 focuses on the Wrist EXOSkeleton (W-EXOS), detailing its mechanical design and performance evaluation as a 3-DOFs device for rehabilitating orthopaedic and post-stroke patients. The W-EXOS covers the 93.3% of the human Range Of Motion (ROM) and can simulate specific wrist movements (i.e., pronation-supination, radial-ulnar deviation, and flexion-extension). The device has been designed with a handle as end-effector and is powered by electric motors via an efficient cable transmission system performing high torque-to-weight and torque-to-volume ratios. Its kinematic structure includes three rotational joints with non-perpendicular axes, allowing for a compact design and effective mass

distribution. Theoretical modelling facilitated the evaluation of the exoskeleton and the human joints matching, assessing the device ROM and torque for each joint. The performance assessment of the system included a position control test and a Virtual Reality (VR) serious game trial involving voluntary healthy subjects. The VR test has been performed in two conditions, namely enabling and disabling the exoskeleton assistance while the subject was asked to complete specific orientation tasks of the wrist while wearing the device. Obtained results showed that the system significantly improved performance and reduced muscle stress by approximately the 30% when the exoskeleton assistance was provided. Additionally, the W-EXOS was proved to be adaptable in the integration with different exoskeleton systems. Indeed, the handle can be replaced with a hand exoskeleton, allowing the combined motion of the human wrist and hand; then, the overall system can be attached to a rehabilitation station or a shoulder-elbow exoskeleton, enabling the motion of the upper limb within its natural workspace and the simulation of bimanual tasks in both configurations.

Alongside its theoretical and practical insights, this thesis promotes accessibility and encourages broader adoption of the proposed innovative techniques within the scientific community by sharing the codes in the Appendix. The code for the parametric design tool of the SEES is attached to be run in the software *Matlab* and customize the system as needed. Since the model is fully parametric, features of the user (e.g., the arm weight and length), of the exoskeleton (e.g., the dimension and material of links, the type of balancer and its configuration), and the simulated movement can be customized. The *Matlab* code for the kinematic model of the W-EXOS, of particular interest due to the non-perpendicular axes scheme, is provided to evaluate the matching with the axes of the human wrist joint (perpendicular) while performing a specific movement.

Further works include the active prototyping and experimental testing of the SEES, along with the clinical trials of the W-EXOS, the latter being already tested in the laboratory to prove the system functionalities.

List of Publications

Journal Papers

1. **Vazzoler, G.,** Shimohara, S., Berselli, G., Hopkins, J.B., 2024. "Designing Multi-axis Compliant Mechanisms with Lockable Decoupled Inputs: A Tip-tilt Case Study". *IDETC24 Special Issue, Journal of Mechanical Design, Transactions of the ASME* (Q1 Journal) - DOI.

2. **Vazzoler, G.,** Camardella, C., Gabardi, M., Marcheschi, S., Solazzi, M., Berselli, G., Frisoli, A., 2024. "Design and Performance Assessment of a Modular, Cable-Driven, 3-DoFs Exoskeleton for Orthopedic and Post-Stroke Rehabilitation of the Wrist". *IEEE/ASME Transactions on Mechatronics* (Q1 Journal) - UNDER REVISION.

3. Gallerani, M., **Vazzoler, G.,** De Novi, G., Ottensmeyer, M.P., Razzoli, R., Berselli, G., 2023. "Integrated Design and Prototyping of a Robotic Eye System for Ocular and Craniofacial Trauma Simulators". *International Journal on Interactive Design and Manufacturing* (Q2 Article) - DOI.

4. Merlo, F., **Vazzoler, G.,** Berselli, G., 2023. "Eco-Programming of Industrial Robots for Sustainable Manufacturing via Dynamic Time Scaling of Trajectories". *Robotics and Computer-Integrated Manufacturing* (Q1 Article) - DOI.

5. **Vazzoler, G.,** Bilancia, P., Fontana, M., Frisoli, A., Berselli, G., 2022. "Analysis and Preliminary Design of a Passive Upper Limb Exoskeleton". *IEEE Transactions on Medical Robotics and Bionics* (Q1 Article). Special Section entitled on *20th International Conference on Advanced Robotics (ICAR2021)* - DOI.

Conference Papers

1. **Vazzoler, G.,** Camardella, C., Gabardi, M., Marcheschi, S., Solazzi, M., Berselli, G., Frisoli, A., 2023. "Evaluating Efficacy of Continuous Assistance Control during Orientation Tasks with an Active Wrist Exoskeleton". *21st International Conference on Advanced Robotics (ICAR 2023)* - DOI.

2. **Vazzoler, G.,** Berselli, G., Frisoli, A., 2022. "A Concept for a Gravity-Balanced Upper-Limb Exoskeleton". *4th Italian Conference for Robotics and Intelligent Machines (I-RIM 2022)* - **BEST PAPER AWARD, finalist** - DOI.

3. Merlo, F., **Vazzoler, G.,** Berselli, G., 2022. "A Computer-Aided Tool for the Energy Optimization of Industrial Robots in Manufacturing Applications". *International Joint Conference on Mechanics, Design Engineering and Advanced Manufacturing (JCM 2022) - In book: Advances on Mechanics, Design Engineering and Manufacturing IV* - DOI.

4. **Vazzoler, G.,** Bilancia, P., Fontana, M., Frisoli, A., Berselli, G., 2021. "Preliminary Design and Virtual Prototyping of an Upper Limb Exoskeleton". *20th International Conference on Advanced Robotics (ICAR 2021)* - DOI.

Patents

1. *Esoscheletro robotico di polso*; number: 102023000021408; deposit: 13/10/2023; inventors: Berselli, G., Frisoli, A., Gabardi, M., Solazzi, M., **Vazzoler, G.** (ITALIAN PATENT GRANTED - EUROPEAN EXTENSION UNDER EVALUATION).

2. *Arto Protesico Superiore Motorizzato Avente una Configurazione Costruttiva Ottimizzata*; number: 102023000019935; deposit: 27/09/2023; inventors: Berselli, G., Baggetta, M., **Vazzoler, G.,** Palli, G., Melchiorri, C. (ITALIAN PATENT GRANTED - EUROPEAN EXTENSION UNDER EVALUATION).

Acknowledgements

To Professor Giovanni Berselli,
My heartfelt gratitude for guiding me from my very first steps in scientific research. Thank you for your unwavering support, availability, and collaboration. Your passion and dedication to our work have been a constant source of inspiration, setting an example that I will carry throughout my career. I am also grateful for your leadership in establishing the Mechanical Computer Aided Engineering Laboratory (MCAE-Lab) at the Department of Mechanical, Energy, Management, and Transportation Engineering, University of Genova. The MCAE-Lab has been a truly enjoyable and dynamic environment, and I am fortunate to have witnessed its growth, alongside colleagues with whom I will always be eager to collaborate.

To Professor Antonio Frisoli,
My sincere thanks for welcoming me to the Institute of Mechanical Intelligence at the Scuola Superiore Sant'Anna of Pisa, an exceptional laboratory rich in knowledge, experience, and future-forward technological solutions. Thank you for introducing me to the field of robotic rehabilitation and offering me the opportunity to work on exciting and rewarding projects. These experiences have not only expanded my skills and knowledge but have also allowed me to collaborate with diverse professionals, contributing to improving people's lives through technological advancements.

To Professor Jonathan Hopkins,
I am truly grateful for the opportunity to visit your laboratory, the Flexible Research Group, in the Mechanical and Aerospace Engineering Department at the University of California, Los Angeles (UCLA). Collaborating with you and your team, and sharing your research approach and ideas, has been an inspiring experience, enriching both my personal and professional growth.

To my colleague and friend Mario Baggetta,
Thank you for contributing your ideas, insights, concerns, and solutions throughout our research journey. Your collaboration and support have been invaluable along this path.

To my family,
For being my secure, constant source of support and strength.

Greta Vazzoler

Genova,
December 2024

Contents

List of Figures

List of Tables

List of Abbreviations

D	Dimensional
ADL	Activities of Daily Living
AI	Artificial Intelligence
CAD	Computer Aided Design
CAE	Computer Aided Engineering
COM	Centre Of Mass
DH	Denavit Hartenberg
DOF	Degree Of Freedom
FE	Flexion Extension
HP	HyPothesis
LS	Linear Spring
NZFL	Non-Zero Free Length
PC	Personal Computer
PS	Pronation Supination
R	Revolute
ROM	Range Of Motion
RUD	Radial Ulnar Deviation
SEES	Shoulder-Elbow ExoSkeleton
TS	Torsional Spring
VR	Virtual Reality
W-EXOS	Wrist EXOSkeleton
ZFL	Zero Free Length

Chapter 1

Introduction

The field of upper limbs exoskeletons made substantial progress in recent years, driven by the better understanding of human requirements and the incorporation of cutting-edge technologies. These advancements led to the development of systems designed to assist individuals while also aiding in the prevention and rehabilitation of injuries.

The present thesis seeks to investigate the complex relationship between the needs of users, whether industrial workers or rehabilitation patients, the natural dexterity of the human upper limb, and the creation of innovative design methods. These methods involve optimization routines and the integration of both rigid and compliant elements in the development of upper limbs exoskeletons, specifically the SEES (Shoulder-Elbow ExoSkeleton) and the W-EXOS (Wrist EXOSkeleton). Since recognizing the diverse and changing needs of users is fundamental to the progression of exoskeleton technologies, this research examines multiple dimensions of user experiences, focusing on the development of robotic solutions that meet functional requirements and also enhance the quality of life for individuals dealing with upper limb muscular strain or impairments.

The human upper limb, celebrated for its exceptional dexterity and adaptability, serves as an ideal benchmark for advancements in exoskeleton design. This thesis aims to bridge the gap between conventional exoskeleton technologies and the intricate capabilities of the natural limb by closely examining the complexities of human movement and the seamless interaction between biological and mechanical systems. Central to this shift is the incorporation of passive elements, which represents a significant departure from traditional exoskeleton design. These passive elements mimic the natural compliance and adaptability of biological systems, bringing exoskeletons closer to replicating the fine-tuned movements of the human upper limb. A key focus of this research is on the SEES, where passive elements are dimensioned through a theoretical optimization tool, enabling the exoskeleton to be quickly customized for specific applications. Since passive elements vary depending on the case

study, this tool allows for an efficient and tailored design process. In contrast, the W-EXOS has been developed using a more conventional approach, employing rigid components powered by motors and a cable-system transmission. The focus here has been on creating a complete system, embedding motors, electronics, serious games and Virtual Reality (VR) advanced software, ready for clinical use in robot-assisted rehabilitation.

A crucial aspect of this research lies in understanding the current advancements in upper limbs exoskeletons, focusing on both passive and active devices for industrial and medical applications. These diverse fields present unique requirements and needs, which in turn lead to distinct design decisions. By employing advanced methodologies including optimization routines and analytical techniques for robotic system design (e.g., the Denavit Hartenberg (DH) method), this thesis aims to present two different approaches for developing upper limbs exoskeletons tailored to various demands. Optimization techniques play a central role in this process, ensuring the solutions to be compact enough to minimize costs while addressing the needs of users. The goal is to create systems that are not only effective but also comfortable and user-friendly, making them more likely to be adopted and worn for extended periods.

This study encompasses a wide range of disciplines, including the human anatomy, the needs of industrial workers and of post-stroke and orthopaedic patients, the design of passive balancer and cable-driven systems, and the development of advanced optimization techniques. By integrating these elements, the research not only aims to enhance functional outcomes in both industrial exoskeletons and robot-assisted therapy, but also points out the importance of a more empathetic and user-centred approach to exoskeleton design. This holistic perspective seeks to create solutions that address both the physical and emotional needs of users, ultimately improving their quality of life.

1.1. Thesis Contribution

This thesis outlines the design of upper limbs exoskeleton systems including a passive exoskeleton for the shoulder-elbow joint (i.e., the SEES) and an active exoskeleton for the wrist joint (i.e., the W-EXOS).

The main contributions of the thesis are summarized in the next points.

- *State of the art on upper limbs exoskeletons*: A study on the state of the art with an eye towards advantages and disadvantages between passive and active upper limbs exoskeletons has been carried out. By focusing on the user needs, solutions able to achieve good performances while being flexible in the setup configuration and in the field of application has been tackled, depending on the case study of interest.

- *Theoretical optimization tool*: A new methodology for designing the SEES, i.e., a 6-Degrees of Freedom (DOFs), passive, shoulder-elbow exoskeleton suitable for industrial applications, has been developed. A case study is presented to show the potentiality of the proposed optimization process; however, since the model is parametric, it can be customized to design specific devices depending on the needs. Theoretical results have been validated via the virtual prototyping of the device, and a detailed mechanical engineering process has been carried out to prepare the system to be physically produced as the next step.

- *Physical production and testing*: The mechanical design and physical prototyping of the W-EXOS, i.e., a 3-DOFs, cable-driven, wrist exoskeleton actuated through an efficient cable transmission, has been presented. Optimization techniques have been used to meet the specific requirements of each component, and validation of results have been carried out thanks both virtual and physical prototypes. Experiments have been made with voluntary healthy subjects, and certifications have been obtained, thus, confirming the system to be ready for clinical trials.

1.2. Research Methods

The research has been carried out proceeding with a precise methodology, as explained in the following steps.

- *Human body analysis*: The human body anatomy has been studied in detail, including the skeletal and articular systems.

- *Users' needs analysis*: The users' necessities when wearing a robotic system have been considered, focusing on designing a comfortable device able to simulate the natural motion of the human body.

- *State of the art analysis*: The current scientific literature on upper limbs exoskeletons has been analysed and reviewed. Given the broad context where upper limbs exoskeletons find application, this thesis takes into consideration both passive and active devices for either industrial or medical applications. Specifically, passive shoulder-elbow exoskeletons for workers and active wrist exoskeletons with 3-DOFs for post-stroke and orthopaedic patients have been considered.

- *Conceptual design development*: Several conceptual designs for upper limbs exoskeletons have been elaborated aiming at overcoming limitations of the current devices through analytical optimization techniques and methods based on Computer Aided Design/Computer Aided Engineering (CAD/CAE) investigated in the proposed case studies.

- *Virtual prototyping and theoretical validation*: The proposed devices have been designed in commercial multi-body software to better visualize the system and validate the theoretical models thanks to virtual prototypes.

- *Physical prototyping and experimental validation*: The device (in this case, the W-EXOS) has been physical produced and tested in the laboratory via an experimental assessment including a position control test, without the human in the loop, and a VR test with voluntary subjects wearing the exoskeleton.

1.3. Thesis Outline

By leveraging the conceptual diagram of Figure 1.1, this thesis aims to provide a general overview of the current advancements in the design of upper limbs exoskeletons and introduces two novel robotic systems by leveraging classic design methods of traditional robotics integrated with novel optimization techniques. The first proposed device is the SEES, a shoulder-elbow exoskeleton mostly useful in industrial contexts: it has 6-DOFs and is equipped with passive balancing elements to simulate specific overhead tasks. The second system is the W-EXOS, a wrist exoskeleton mainly developed for robot-assisted therapy: it is actuated by electric motors via a cable transmission system to reproduce several orientation tasks of the human wrist in a VR serious game scenario. Thanks to its flexibility

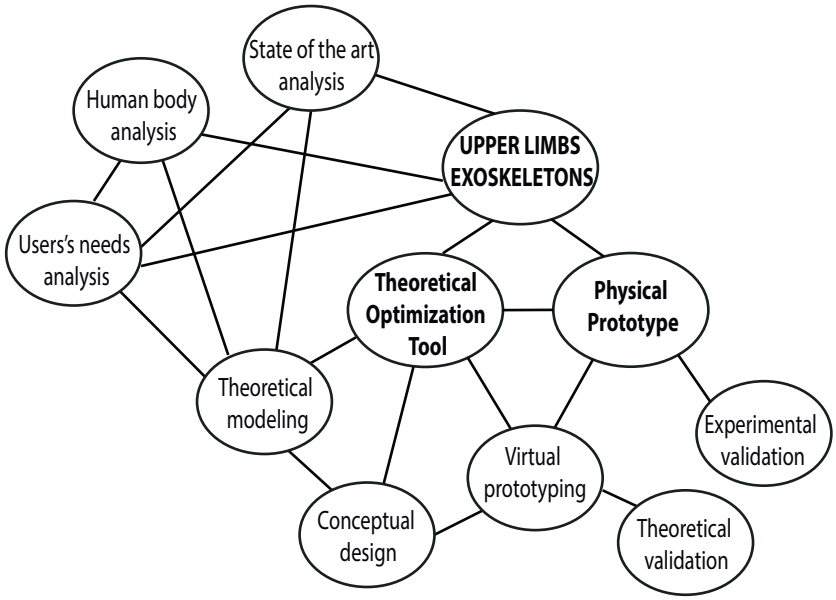

Figure 1.1: Thesis conceptual diagram.

in the flanges of attachment, W-EXOS can be mounted on a rehabilitation station or in a shoulder-elbow exoskeleton, and its end-effector, i.e., an handle, can be replaced with a hand exoskeleton. Thus, it allows to achieve a complete system able to perform natural motion of the human upper limb, including the simulation of bimanual tasks. Even if born by common needs from the state of the art, the SEES and the W-EXOS have been studied as independent devices; indeed, Chapter 3 and Chapter 4 include initial and final considerations for each exoskeleton.

The rest of the manuscript is organized as in the bullet point list below.

- Chapter 2 is about upper limbs exoskeletons. Starting from the anatomy of the human upper limb, the skeletal and articular systems are investigated to understand the natural functioning of the human body. Then, design considerations are made to identify the most relevant aspects to be considered for designing an upper limbs exoskeleton. Also, the state of the art is studied focusing on the devices of interest for the present thesis. After providing guidelines for classifying upper limbs exoskeletons and pointing out design principles to direct the engineering of the proposed devices, exoskeletons for industrial and healthcare applications are listed and described in their main features. In particular, two main categories are considered: industrial exoskeletons for the shoulder-elbow joint, and medical devices for the upper limb, with focus on ex-

oskeletons with three rotational DOFs for the rehabilitation of the wrist joint. The first concern is due to the needs of workers, mainly straining the shoulder joint while reproducing repetitive overhead tasks. The second choice is due to project requirements where the device is born: the wrist exoskeleton has to allow the simulation of all the three DOFs of the human wrist; moreover, it has to be integrated with a shoulder-elbow exoskeleton and a hand exoskeleton, so to reach a complete system for the upper limb.

- Chapter 3 is about the SEES. It reports the analysis and preliminary design of a passive, wearable, upper limb exoskeleton to support workers in industrial environments in a vast range of repetitive tasks, offering an effective strategy to reduce the risk of injuries in production lines. The system primary purpose is to compensate for gravity loads acting on the human upper limb. The proposed exoskeleton is based on a 6-DOFs kinematics with 5-DOFs for the shoulder joint (two displacements plus three rotations) and 1-DOF for the elbow. Gravity compensation is implemented with passive elastic elements to minimize the weight and reduce the cost of the overall system. A detailed analytical tool is developed to support the designer in the preliminary design stage, investigating the exoskeleton kinetic-static behaviour and deriving optimal design parameters for the springs over the human arm workspace. By defining specific functional requirements (i.e., the user's features and simulated movements), computationally efficient optimization studies are carried out to determine the optimal coefficients and positions of the springs, thus, maximizing the accuracy of the gravity balancing. Both linear and torsional springs are investigated, and obtained results are validated with a commercial multi-body tool for some relevant movements of the user's arm. To sum up, after presenting the proposed exoskeleton design concept, the background theory on balancers is studied. Then, the proposed methodology involving the exoskeleton analytical model and the design optimization process is presented, and final remarks are drawn. A list of notations is provided to simplify the reading of the overall Chapter, and the developed design tool is shared in the Appendix A.

- Chapter 4 is about the W-EXOS. It presents the mechanical design and performance evaluation of a novel 3-DOFs wrist exoskeleton to fulfil the rigid requirements for orthopaedic and post-stroke patients' upper limbs rehabilitation. The device covers the

93.3% of the human Range Of Motion (ROM), simulating the Pronation Supination (PS), Radial Ulnar Deviation (RUD), and Flexion Extension (FE) movements. It can be integrated with a rehabilitation station or a 4-DOFs shoulder-elbow exoskeleton, its end-effector being a sensorised handle or a hand exoskeleton, and it allows bimanual tasks performance thanks to the lateral arrangement of all components. W-EXOS is actuated through electric motors via an efficient cable transmission, having high torque-to-weight and torque-to-volume ratios. Its kinematics is a serial chain of three rotational joints with non-perpendicular axes competing at the wrist rotation centre. So, the device joints are coupled but the structure is compact and with good mass distribution. Theoretical modelling allowed the study of the human wrist and the device axes matching, evaluating the ROM and torques at each joint. The device performance assessment is done using a position control test, and a VR serious game with assistive control. With the W-EXOS in the basic configuration embedding the handle and integrated into the rehabilitation platform, a position control test is carried out for the device ROM validation, whereas, a VR serious game experience is made to test thirteen healthy subjects and prove the device assistance strategy during wrist motion tasks in a typical rehabilitation session. Subjects experienced the system under two different conditions, i.e., considering the device assistance on/off. Results showed a significantly higher performance under assistance, rather than without it, on the exploitation of the wrist ROM and on the intuitiveness of movements during the orientation task. A reduction of around the 30% of the overall muscle stress is measured, highlighting the assistance efficacy of the system. Further, the W-EXOS handle is replaced by the hand exoskeleton and the system is mounted on the shoulder-elbow exoskeleton, proving the W-EXOS configuration in multiple, highly wearable, compact, and usable, bimanual, upper limbs robotic setups.

- Chapter 5 contains final remarks on the achieved results and further works.
- The Appendix contains the parametric design optimization tool of the SEES to be run in the software *Matlab* (Appendix A), and the *Matlab* code to solve the kinematic model of the W-EXOS compared to the one of the human wrist (Appendix B). A list of related activities is reported in Appendix C.

Chapter 2

Upper Limbs Exoskeletons

Exoskeletons are wearable devices whose primary aim is balancing gravitational loads on the user while simulating a movement, thus, enhancing the user's physical capabilities. They can aid specific human joints, such as those of the upper and lower limb, neck, ankle and back, reducing efforts on the human exoskeletal system while preventing and/or treating injuries [33]. When designing exoskeletons, aspects in line with the principle of human-centred design [34] need to be considered: indeed, wearable robots ought to be ergonomic, mediating between the needs of users and those of the system itself. These devices must provide a force proportional to motion, avoiding abrupt movements that could lead to unwanted displacements and/or forces, thus, causing discomfort to the user. From a kinematic point of view, an exoskeleton have to be almost equivalent to the human limb: the alignment of the mechanical system with the human art during all motion time is of primary concern to follow the movements of each joint within their workspace. To this end, the knowledge of the human body parts and joints is essential. The human body flexibility and its musculoskeletal apparatus is, in fact, of fundamental interest to the present study, constituting the starting point for the design of upper limbs exoskeletons. The human body characteristics change according to the person's age, sex and state of health; for this reason, the design of an exoskeleton is inevitably linked to the subject who will wear the device. These aspects are highlighted more in the design of support devices for upper limbs, as the latter are smaller and more delicate than the lower limbs and present a wide range of possible movements [35].

2.1. General Requirements

General requirements for upper limbs exoskeletons in healthcare applications can be summarised as in the next points, focusing on assistive (from point 1 to 7) and rehabilitation (from point 8 to 14) applications.

1. *Ergonomics and comfort*: The device should fit a wide range of users comfortably and allow for long-term use without causing discomfort or fatigue. Lightweight designs with optimized load distribution are critical.

2. *Ease of use*: The system should be intuitive to operate, with minimal training required for users or caregivers. Quick donning and doffing mechanisms are essential for usability.

3. *Adaptability*: The exoskeleton should support users with different levels of physical abilities, including impaired individuals, and adjust to their specific needs and body dimensions.

4. *Power and autonomy*: Assistive exoskeletons in industrial settings or for daily living tasks require efficient power systems to ensure extended operation. Hybrid solutions combining active and passive elements may reduce energy consumption.

5. *Functionality*: The device must enhance the user's strength and mobility while maintaining precise and naturalistic motion patterns to avoid discomfort or injury.

6. *Safety*: Integrated safety mechanisms, such as collision avoidance, overload protection, and emergency stop functions, are vital to prevent accidents during use.

7. *Durability and maintenance*: In industrial or personal settings, the exoskeleton must withstand repetitive use and exposure to varying environmental conditions with minimal maintenance requirements.

8. *Therapeutic effectiveness*: The exoskeleton should provide measurable benefits in promoting motor recovery, such as guiding correct movement patterns and providing feedback to encourage neuroplasticity.

9. *Flexibility in modes*: A rehabilitation exoskeleton should support both active and passive training modes, allowing users to progress from assisted movements to more independent control as they recover.

10. *Customizability*: The device must be capable of tailoring resistance, ROM, and other parameters to suit the patient's specific therapeutic needs and goals.

11. *Data collection and monitoring*: Sensors should record detailed performance metrics, such as movement quality, ROM, and force exertion, to track progress and adapt therapy plans accordingly.

12. *Interoperability*: Integration with other rehabilitation tools and systems, such as VR environments or biofeedback devices, can enhance the overall therapy experience.

13. *Safety and compliance*: Exoskeletons must adhere to strict safety standards for medical devices, ensuring reliable operation during therapeutic use and compliance with regulatory requirements.

14. *Psychological considerations*: The device design should consider patients' engagement and motivation, incorporating elements such as gamification or real-time feedback to make rehabilitation sessions more engaging.

When addressing the requirements of upper limbs exoskeletons, it is essential to consider the actions of muscles and tendons, as these biological components play a crucial role in natural movement and force generation. Indeed, the next features need to be evaluated.

- *Biomechanical compatibility*: Exoskeletons should align closely with the anatomy and biomechanics of the human upper limb. The actions of muscles and tendons must be mirrored in the device movement patterns to ensure naturalistic and comfortable operation. Misalignment can lead to unnatural joint loading, discomfort, or even injury over time.

- *Force transmission*: Muscles and tendons work together to transmit forces efficiently, allowing precise control of movement. Exoskeletons should either augment or replicate this force transmission, especially in rehabilitation or assistive scenarios. For example, actuators or elastic elements could simulate tendon-like behaviour to provide smooth and responsive force delivery.

- *Joint dynamics*: Muscle actions determine the torque and ROM at joints. Exoskeletons must accommodate the dynamic forces generated by these muscles and provide appropriate resistance or assistance. Passive or active elements may need to adjust dynamically to match the natural muscle-tendon behaviour.

- *Muscle engagement in rehabilitation*: For rehabilitation purposes, exoskeletons should encourage active muscle engagement rather than fully replacing it. Devices that allow for muscle activation, guided by the exoskeleton, can promote neuroplasticity and functional recovery. This can be achieved through adjustable levels of assistance or resistance.

- *Tendon elasticity and energy storage*: Tendons act as biological springs, storing and releasing energy during movement. Exoskeleton designs could integrate elastic components that mimic this behaviour, improving efficiency and reducing energy consumption in both active and passive devices.

- *Minimizing interference*: Exoskeletons should minimize interference with natural muscle and tendon actions. Overly rigid or restrictive designs may limit the user's ability to engage muscles effectively, reducing the therapeutic or functional benefits of the device.

By considering the actions of muscles and tendons in exoskeleton design, it is possible to create devices that not only assist or rehabilitate but also enhance the user's ability to perform natural movements while respecting the body's biomechanics. Thanks to the considerations of all these requirements, upper limbs exoskeletons can better meet the specific needs of users in both assistive and rehabilitation contexts, promoting wider adoption and improved outcomes in healthcare applications.

2.2. Human Upper Limb

This section will primarily draw upon three books as key references: *Netter's Atlas of Human Anatomy* [36], *Principles of Anatomy and Physiology*, [37] and *The Physiology of the Joints* [38]. These outstanding resources are essential for exploring the anatomy, kinesiology, and functional aspects of the human body. While the first two books [36, 37] are updated sources (published in the 2022 and 2018 respectively), the third one [38] is somewhat older (originally published in 1982); however, it remains a thorough guide, providing extensive information on the biomechanics of the human body and rehabilitative methods within the field.

2.2.1. Anatomy

The upper limb is an extraordinarily complex mechanical system, consisting of over thirty muscles, thirty major bones (with twenty-seven in the hand alone), eighteen joint articulations, and thirty-four DOFs, twenty-seven of which are unique to the hand. Within this system, the arm primary role is to position the hand in space, while the hand is responsible for grasping and manipulating tasks. In this context, the term *manipulation* refers to the ability to move and adjust the orientation of objects in space using one or both hands.

2.2.2. Skeletal System

As shown in Figure 2.1, the major upper limb bones are distributed across four main areas:

1. The scapula and clavicle, in the shoulder.
2. The humerus, in the arm.
3. The radius and ulna, in the forearm.
4. The carpal, in the wrist (eight bones), the metacarpal, in the palm (five bones), and the phalanges, in the fingers (fourteen bones).

The humerus, or arm bone, is the longest and largest bone in the upper limb, connecting proximally with the scapula and distally with the ulna and radius at the elbow. The ulna, located on the medial side of the forearm (toward the little finger), is longer than the radius. In contrast, the radius, which is found on the lateral side of the forearm (toward the thumb), is smaller and has a narrow proximal end that broadens distally. Both bones articulate with the humerus at the elbow joint.

2.2.3. Articular System

Joints, or articulations, are classified both structurally (Section 2.2.3.1), based on their anatomical features, and functionally (Section 2.2.3.2), according to the enabled movements.

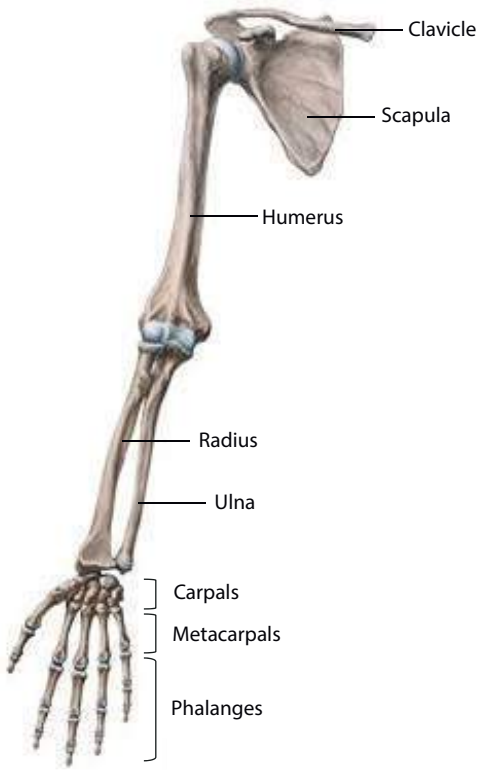

Figure 2.1: Skeletal system of the human upper limb: main bones and areas.

2.2.3.1. Structural Classification

The structural classification depends on the presence or absence of a synovial cavity (i.e., a space between the articulated bones) and on the type of connective tissue joining the bones. Three main joint types can be identified:

1. Fibrous joints.
2. Cartilaginous joints.
3. Synovial joints.

Fibrous and cartilaginous joints do not have a synovial cavity: the firsts consist in bones held together by dense, irregular, connective tissue that is rich in collagen fibres; the seconds have cartilage serving to connect the bones. Synovial joints include a synovial cavity, and the bones are linked by dense, irregular, connective tissue within an articular capsule, often supported by additional ligaments.

2.2.3.2. Functional Classification

The functional classification of joints refers to the ROM they permit and involves the next points:

1. Synarthroses joints.
2. Amphiarthroses joints.
3. Diarthroses joints.

The motion kind of these joints can be defined as fixed, slightly free, and free. It is worth noting that all diarthroses joints are structurally classified as synovial joints (Section 2.2.3.1), which come in different shapes and allow several types of movements. These joints are the most relevant for the present thesis, and will be further investigated in Section 2.2.3.3.

2.2.3.3. Synovial Joints

2.2.3.3.1. Structure

Referring to the joints structural classification (Section 2.2.3.1), the upper limb mainly consists of synovial joints, with one notable exception: the interosseous membrane, which is a type of fibrous joint. This membrane is a thick, dense sheet of irregular connective tissue that links adjacent long bones and allows for limited movement, known as amphiarthrosis. It is found between the radius and ulna in the forearm (Figure 2.1).

Synovial joints are unique and have specific features that distinguish them from other types of joints; their main structure is shown in Figure 2.2, taking as example the shoulder articulation. A defining feature is the synovial cavity **(1)**, a space between the articulating bones **(2)** (in this case, the scapula and the humerus). The presence of the synovial cavity enables free movement, which classifies all synovial joints functionally as diarthroses (Section 2.2.3.2). The bones within the joint are also covered with a layer of hyaline cartilage, known as articular cartilage **(3)**. This cartilage creates a smooth, slippery surface on the bones, minimizing friction during movement and helping to absorb shock. Moreover, the joint is enclosed by a sleeve-like articular capsule **(4)**, which surrounds the synovial cavity and connects the articulating bones. This capsule is made up of two layers:

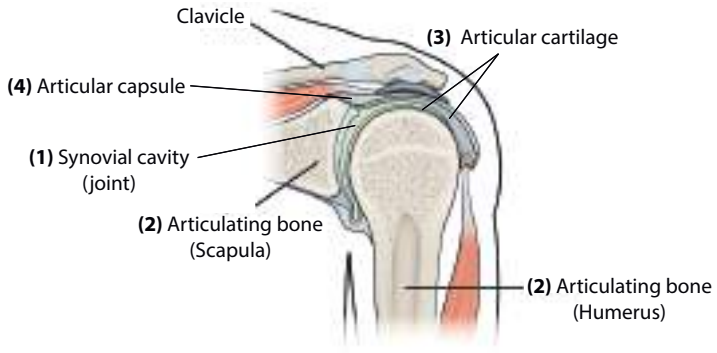

Figure 2.2: Synovial joint structure (e.g., shoulder joint).

- *Outer fibrous membrane*: It typically consists of dense, irregular connective tissue primarily made up of collagen fibres, which connect to the periosteum of the bones involved in the joint. The fibrous membrane acts as a thickened extension of the periosteum between the bones; its flexibility allows for significant joint movement, while its strong tensile properties help prevent bone dislocation. In some cases, the fibrous membrane contains parallel bundles of dense regular connective tissue, known as ligaments, which provide crucial mechanical support to keep the bones securely together in a synovial joint.

- *Inner synovial membrane*: It consists of areolar connective tissue with elastic fibres. This membrane produces the synovial fluid, i.e., a viscous and clear, or pale yellow, liquid that plays several important roles, such as lubricating the joint cavity between the synovial membrane and the articular cartilage, forming a thin layer over the surfaces within the capsule. Moreover, it helps reducing friction and absorbing shocks, and it delivers oxygen and nutrients to the chondrocytes within the articular cartilage, while removing carbon dioxide and metabolic waste from these cells.

2.2.3.3.2. Classification

Although all synovial joints have a similar structure, the shapes of their articulating surfaces differ, enabling a wide ROM. These joints are classified into six types based on their mechanical motion: ball-and-socket (or spherical), hinge, pivot (or pin), condyloid (or ellipsoidal), planar, and saddle. The ones of interest for the present research are illustrated in Figure 2.3 and will be described in the next list, matched with the upper limb joint of interest

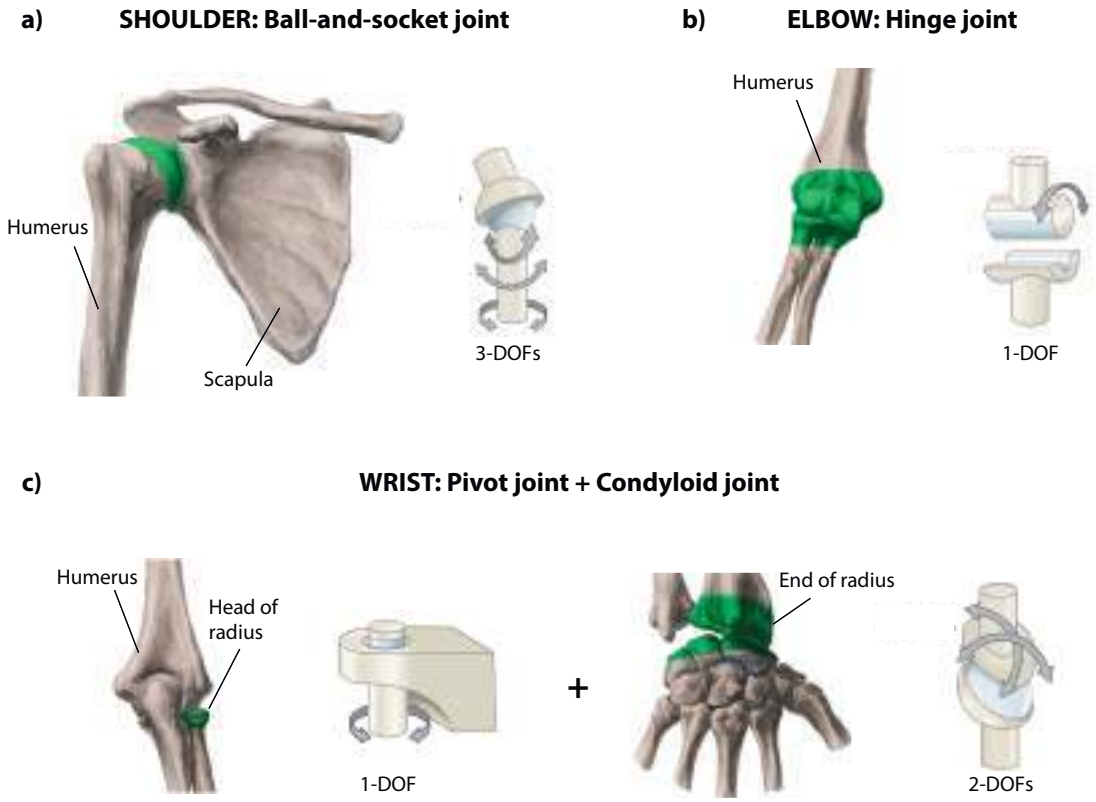

Figure 2.3: Articulations of the human upper limb: ***a)*** *Shoulder: 3-Degrees Of Freedom (DOFs) ball-and-socket joint;* ***b)*** *Elbow: 1-DOF hinge joint;* ***c)*** *Wrist: 3-DOFs joint (1-DOF pivot plus 2-DOFs condyloid).*

(**a)** shoulder, **b)** elbow, and **c)** wrist):

a) *Ball-and-socket joint*: A ball-and-socket joint (also known as spherical joint) is characterized by the spherical surface of one bone fitting into a cup-shaped cavity of another bone, and enables rotational movements around three axes, thus, having 3-DOFs. The upper limb joint that can be schematized with this kind of synovial articulation is the shoulder, where the head of the humerus fits into the glenoid cavity of the scapula.

b) *Hinge joint*: A hinge is a 1-DOF joint where the convex surface of one bone fits into the concave surface of another producing an angular motion similar to that of a hinged door. Typically, one bone remains stationary while the other rotates around an single axis, simulating an opening/closing movement. The flexion-extension of the elbow joint of the human upper limb is an examples of hinge joint.

c) *Pivot joint and Condyloid joint*: In a pivot joint (also known as pin), the rounded or pointed surface of one bone fits into a ring formed partially by another bone and

partially by a ligament, thus, allowing 1-DOF (i.e., a rotation around one axis). This joint respects the behaviour of the radio-ulnar joint, which allows the hand to rotate anteriorly and posteriorly, reproducing the PS motion; it is usually classified as one of the three DOFs of the human wrist. The other two DOFs, i.e., the wrist RUD and FE, can be schematized with a condyloid joint. In this joint, also known as ellipsoidal joint, the convex, oval-shaped end of one bone fits into the oval-shaped cavity of another bone letting rotational movements around two axes.

The shoulder joint deserves particular attention due to its complexity. It is worth noting that the human shoulder is not one single joint but a combination of five joints; this aspect will be further investigated in Section 2.2.3.4. Moreover, the choice of classifying the shoulder like a ball-and-socket joint is an approximation, since, in the human body, the shoulder centre of rotation is not fixed during the motion; this theme will be studied in deep in Section 2.2.4.1.

2.2.3.4. Shoulder Joint

As shown in Figure 2.4, the shoulder is a multi-articular complex composed of five distinct joints, which can be divided into two groups:

- *GROUP 1* contains two joints: the shoulder and the subdeltoid. The shoulder joint (or scapulo-humeral joint) **(1)** is a true anatomical joint where two articular surfaces, lined with hyaline cartilage, come together. The subdeltoid joint (or second shoulder joint) is not an anatomical joint, but it functions as a physiological joint, consisting of two surfaces that slide against each other. The subdeltoid joint is mechanically linked to the shoulder joint; this means that any movement in the shoulder joint triggers a movement in the subdeltoid joint.

- *GROUP 2* involves three joints: the scapulo-thoracic **(2)**, the acromio-clavicular **(3)**, and the sterno-clavicular **(4)**. The first is the most significant joint (physiological) in this group but depends on the other two joints (anatomical), with which it is mechanically connected. The acromio-clavicular joint is located at the clavicle acromial end, whereas the sterno-clavicular joint is situated at the sternal end of the clavicle.

To sum up, *GROUP 1* includes an anatomical joint (the shoulder joint) mechanically linked to a physiological joint (the subdeltoid joint), whereas *GROUP 2* includes a physiological

joint (the scapulo-thoracic joint) mechanically linked to two anatomical joints (the acromio-clavicular and the sterno-clavicular joints). Within each group, the joints are mechanically interconnected, meaning they must work together. In practice, both groups function simultaneously, with each set contributing differently depending on the specific movement.

2.2.3.5. Elbow Joint

The distal end of the humerus features two primary articular surfaces (i.e., the trochlea and the capitulum) that form a complex resembling a ball and spool threaded onto the same axis. This axis roughly corresponds to the axis of flexion-extension for the elbow joint. However, the joint capsule encloses a single anatomical joint cavity with two functional joints:

- *Elbow joint*: It allows the elbow flexion-extension.
- *Superior radio-ulnar joint*: It is essential for the human forearm pronation-supination.

It is worth noting that most of the works in the literature consider the superior radio-ulnar joint as one of the three DOFs of the wrist (i.e., the PS).

2.2.3.6. Wrist Joint

This articular complex of the wrist is composed of two joints that allows the wrist RUD and FE movements:

- *Radio-carpal joint*: Being an ellipsoidal joint, it is commonly referred to as the wrist joint, and is located between the radial head and the proximal row of carpal bones (Figure 2.1).

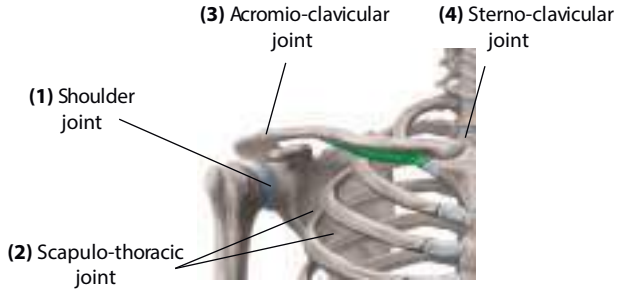

Figure 2.4: The complex of the shoulder.

- *Mid-carpal joint*: it is situated between the proximal and distal rows of carpal bones (Figure 2.1).

A third DOF of the wrist (i.e., the PS) is usually considered to be the one enabled by the superior radio-ulnar joint of the elbow, as explained in Section 2.2.3.5.

2.2.4. Range of Motion

The functional ability of the upper limb depends on the coordinated movements of the shoulder, elbow, wrist, and hand, which together create multiple integrated spheres of action. This capability is naturally constrained by the proportional relationships of the limb segments within the available space. When standing, the upper limb ROM typically reaches down to the midthigh, like shown in Figure 2.5. To extend beyond this point and reach farther down the lower extremity or to the ground, additional mobility from the hip, knee, ankle, and trunk is required. Furthermore, integrating upper limb actions with gait increases the reach of the upper extremity to more distant locations. To visualize the maximum achievable field of the upper limb (i.e., the envelope of action denoted as E_n, $n = 1,\ 2,\ 3,\ 4$), one can trace the path of the farthest point of the upper extremity as the shoulder moves, while keeping all other joints in extension. Within this envelope, the elbow, wrist, and hand each have their own specific ROM, represented by E_2, E_3, and E_4 respectively. These distinct movements collectively enhance the overall functional performance of the upper extremity, broadening its range of actions.

2.2.4.1. Shoulder Joint

The shoulder, as the proximal joint of the upper limb, is the most mobile joint in the human body. It has three DOFs, allowing the upper limb to move across three spatial planes and around three primary axes (Figure 2.6a):

1. *Transverse axis*: Positioned in the frontal plane, this axis controls flexion and extension movements, which occur in the sagittal plane (Figure 2.6b, plane A, Figure 2.7a).

2. *Antero-posterior axis*: Located in the sagittal plane, this axis governs abduction (moving the upper limb away from the body) and adduction (moving the upper limb toward

the body), both of which take place in the frontal plane (Figure 2.6b, plane B, Figure 2.7b,c).

3. *Vertical axis*: This axis runs through the intersection of the sagittal and frontal planes, corresponding to the third axis in space. It controls rotational movements of flexion and extension in the horizontal plane when the arm is abducted to $90\ deg$ (Figure 2.6b, plane C, Figure 2.7d,e,f).

Referring to Figure 2.6a, there are two distinct types of lateral and medial rotation of the arm and the upper limb around the long axis of the humerus (4): voluntary and automatic rotations. The first occurs when the arm rotates freely, depending on the third DOF, which is possible only in triaxial ball-and-socket joints. This movement is generated by the contraction of the rotator muscles. The second happens without conscious effort, either in biaxial joints or in triaxial joints when only two of the available axes are engaged. The reference position is defined when the upper limb hangs vertically at the side of the trunk, aligning the long axis of the humerus with the vertical axis of the limb. The long axis of the humerus also aligns with the transverse axis when the arm is abducted to $90\ deg$, and with the anteroposterior axis when the arm is flexed to $90\ deg$. As a result, the shoulder joint possesses three primary axes and three DOFs. The long axis of the humerus can align with any of these axes

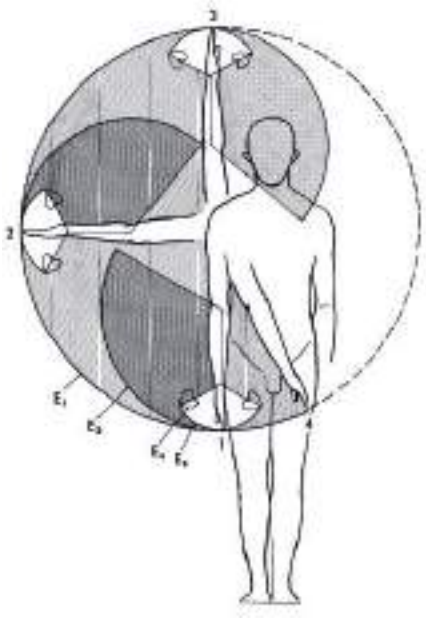

Figure 2.5: Upper limb elevation in the frontal plane: shoulder, elbow, wrist, and hand envelopes of action (E_n, $n = 1,\ 2,\ 3,\ 4$).

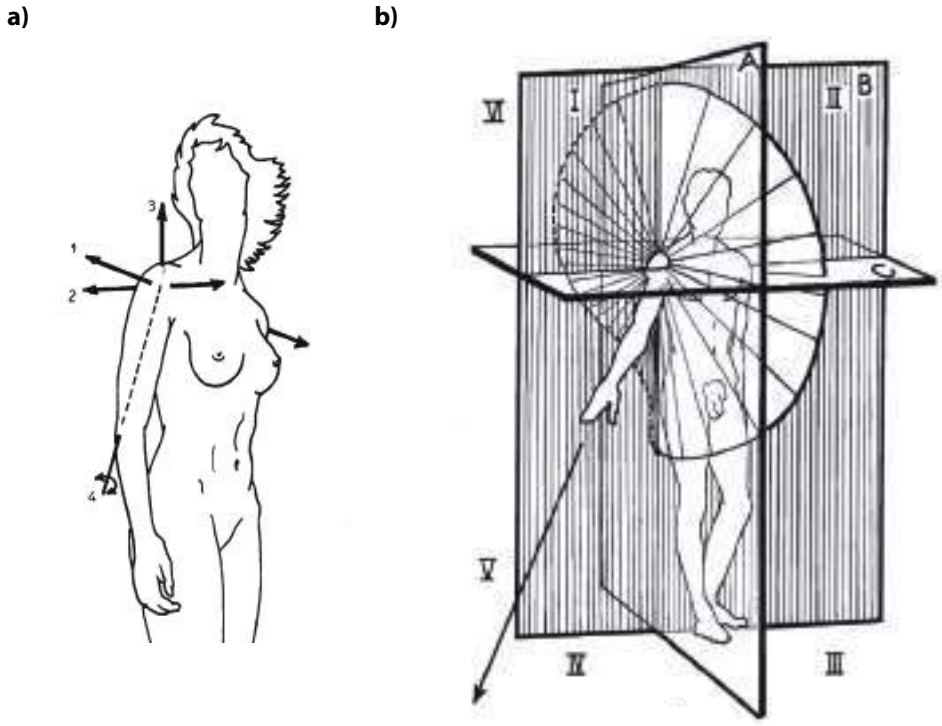

Figure 2.6: ***a)*** *Shoulder axis of rotation: (1) Transverse; (2) Antero-posterior; (3) Vertical; (4) Humerus.* ***b)*** *Shoulder circumduction and main planes: (A) Sagittal; (B) Frontal; (C) Transverse.*

or occupy an intermediate position, enabling both lateral and medial rotation movements.

The movements of the shoulder are explained in detail in the next points:

- *Flexion and extension*: These movements are shown in Figure 2.7a and performed in the sagittal plane (Figure 2.6b, plane A) around the transverse axis (Figure 2.6a, (1)). The flexion is up to $180\ deg$, whereas the extension is up to 45 or $50\ deg$.

- *Adduction*: As visible from Figure 2.7b, it happens in the frontal plane (Figure 2.6b, plane B) around axis (2) of Figure 2.6a and is possible only if combined to extension, thus allowing a trace of adduction, and flexion, reaching nearly 30 or $45\ deg$.

- *Abduction*: This movement is shown in Figure 2.7c and takes place in the frontal plane (Figure 2.6b, plane B) around axis (2) of Figure 2.6a, achieving a full ROM of $180\ deg$.

- *Axial rotation of the arm*: It happens around its long axis (Figure 2.6a, (3)) in the transverse plane (Figure 2.6b, plane C) and can occur in any position of the shoulder. This is a voluntary movement of joints with three axes and three DOFs. Typically,

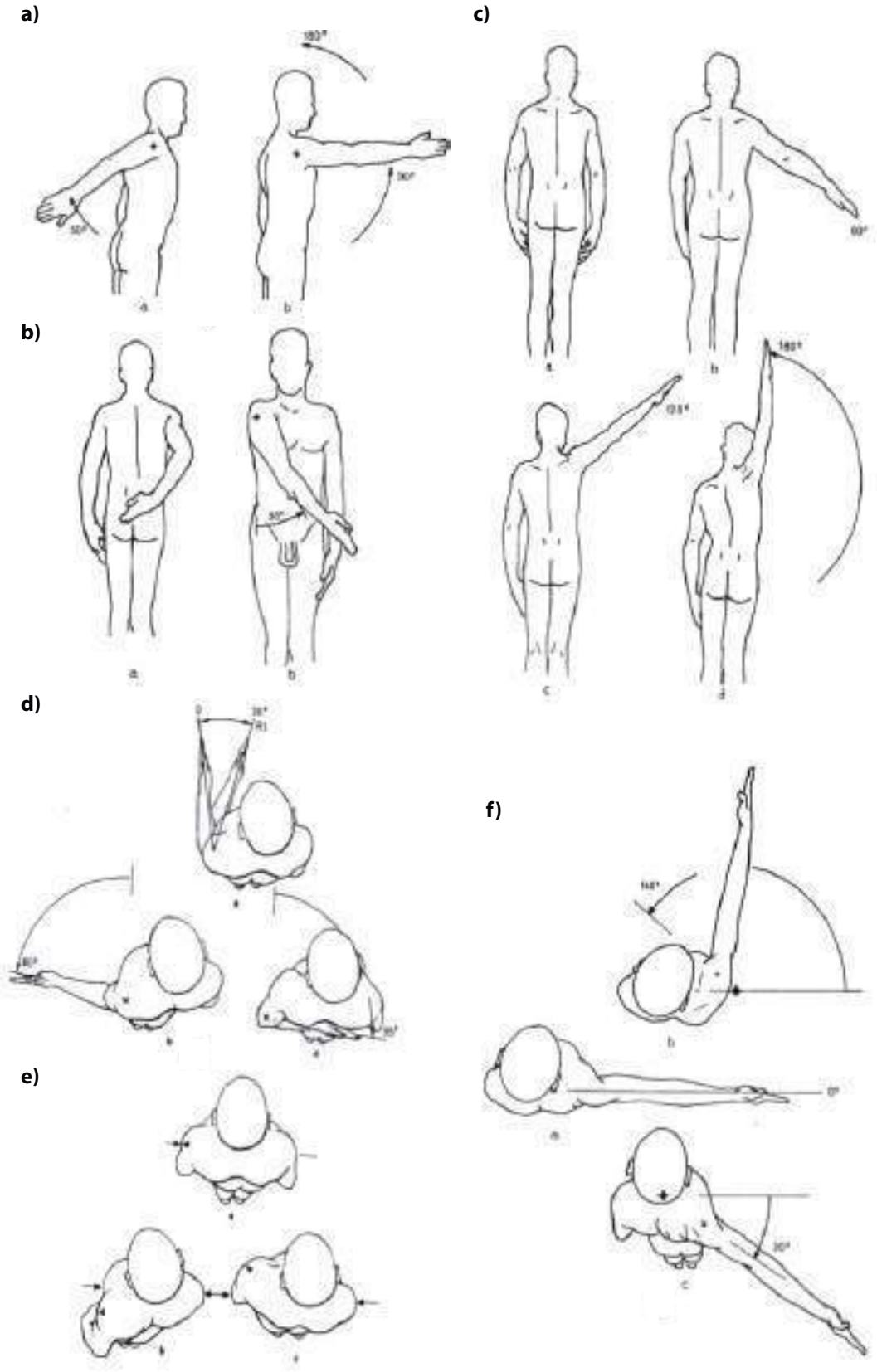

Figure 2.7: Upper limb movements. ***a)*** *Shoulder flexion-extension;* ***b)*** *Shoulder adduction;* ***c)*** *Shoulder abduction;* ***d)*** *Arm axial rotation;* ***e)*** *Shoulder girdle movement in the horizontal plane;* ***f)*** *Shoulder flexion-extension in the horizontal plane.*

this rotation is measured beginning from the reference position, where the arm hangs vertically alongside the body, as visible from Figure 2.7d. Being the reference position with the elbow at $90\ deg$, the lateral rotation is up to $80\ deg$ (maximum $90\ deg$), whereas the medial rotation is up to $100\ deg$ (maximum $110\ deg$).

- *Shoulder grindle*: From the reference position shown in Figure 2.7e, this movement involves a forward (around $20\ deg$) and backward (around $15\ deg$) rotation around the long axis in the transverse plane (Figure 2.6a, (3); Figure 2.6b, plane C).

- *Horizontal flexion and extension*: It occurs in the horizontal plane (Figure 2.6b, plane C) around the vertical axis of Figure 2.6a, (4). As illustrated in Figure 2.7f, starting from the reference position with the open arm aligned with the the upper limb abducted of $90\ deg$ in the frontal plane, it ranges from $140\ deg$ (flexion), to 30 or $40\ deg$ (extension).

- *Circumduction*: This motion, shown in Figure 2.6b, combines the elementary movements about the three cardinal axes. The curve represents the base of the circumduction cone (the path traced by the fingertips), intersecting various spatial sectors defined by the shoulder joint reference planes (A: sagittal plane (flexion-extension); B: frontal plane (adduction-abduction); C: horizontal plane (horizontal flexion-extension)).

Once defined the shoulder movements, it is worth studying the instantaneous centre of rotation of this joint during the motion. Historically, the head of the humerus was thought to resemble a portion of a sphere, leading to the assumption that it had a fixed, unchanging, instantaneous centre of rotation. However, recent researches revealed that there are actually multiple instantaneous centres of rotation, each corresponding to the centre of movement between two very close positions. These centres are calculated using a computer, based on a series of sequential radiographs. Figure 2.8 shows in detail the motion phases of the shoulder instantaneous centre of rotation:

a) b) *Abduction*: During abduction, when considering only the rotational component of the humerus in the frontal plane, two distinct sets of instantaneous centre of rotation, separated by a distinct gap, can be identified. The first set is located within a circular domain (C1), near the inferomedial aspect of the humeral head. The centre of grav-

ity of this domain serves as the reference point, with the radius determined by the average distance between the centre of gravity and each instantaneous centre of rotation. The second set is situated in another circular domain (C2), near the upper half of the humeral head. Notably, these two domains do not overlap. MOreover, during the shoulder abduction, the movement of the shoulder joint can be divided into two distinct phases, essentially acting as two separate joints:

  - *Abduction up to* $50\ deg$: In this phase, the humeral head rotates around a point located within the circular domain referred to as C1.
  - *Abduction from* $50\ deg$ *to* $90\ deg$: As abduction continues beyond $50\ deg$, the centre of rotation shifts to lie within the circular domain C2. There is a noticeable change in movement, causing the rotation centre to shift to a position that is superior and medial to the humeral head.

c) *Flexion*: During flexion, a similar analysis of the instantaneous rotation centres shows no such discontinuity; these latter all lie within a single circular domain located in the lower part of the humeral head, approximately midway between its two borders.

d) *Rotation*: During axial rotation, the circular domain of the instantaneous centre of rotation is positioned at the junction between the head and shaft of the humerus, midway between the lateral borders of the humeral head.

2.2.4.2. Elbow Joint

The human elbow consists in a single joint that permits two functions: the pronation-supination, which is an axial rotation involving the superior radio-ulnar joint, and the elbow flexion-extension. In the present thesis, like commonly done in the scientific literature, the first movement has been considered as one of the wrist DOFs (i.e., the PS) and will be discussed in Section 2.2.4.3; whereas, the second movement is illustrated in Figure 2.9: the elbow allows the hand to be moved towards or away from the body, rotating of around $145\ deg$ from the reference position, namely, when the arm is relaxed down along the body.

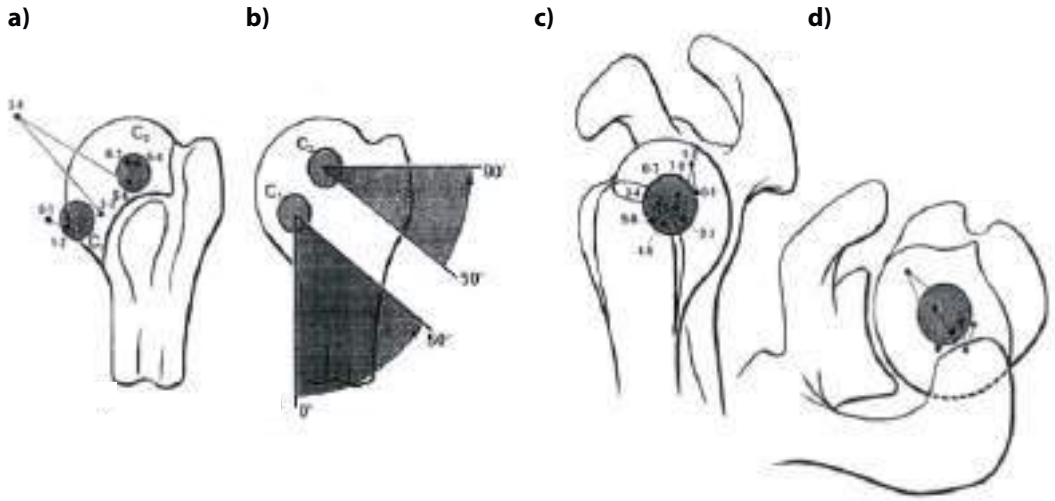

*Figure 2.8: Motion of the shoulder instantaneous centre of rotation. Phase of **a), b)** Abduction; **c)** Flexion; **d)** Rotation.*

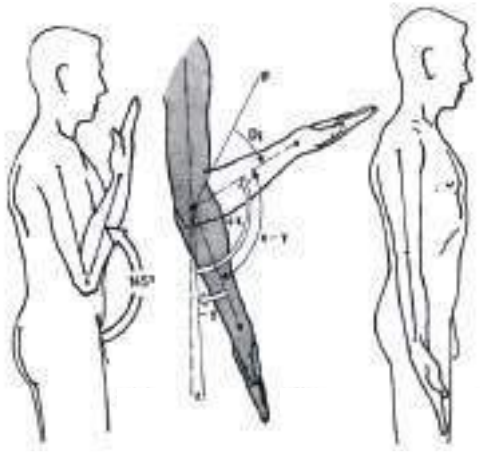

Figure 2.9: Upper limb movement: elbow flexion-extension.

2.2.4.3. Wrist Joint

The wrist is the distal joint of the upper limb and plays a crucial role in positioning the hand for optimal grasping. As explained in Section 2.2.3.6, the wrist articular complex primarily has two DOFs. However, when combined with pronation and supination (i.e., the rotation of the forearm around its long axis), the hand can be oriented at any angle necessary for grasping or holding objects. Given this consideration, the wrist movements are shown in Figure 2.10, including the **a)** PS, **b)** RUD, and **c)** FE motions.

Figure 2.10a shows the PS joint, that refers to the movement of the forearm around its longitudinal axis. This DOF involves two interconnected joints: 1) the superior radio-ulnar joint, which is anatomically part of the elbow; and 2) the inferior radio-ulnar joint, which is

anatomically separate from the wrist. The longitudinal rotation of the forearm adds a third DOF to the wrist articular complex. This allows the hand, as the functional end of the upper limb, to be positioned in any orientation necessary to grasp or support an object. Starting from the initial position of the forearm with the elbow flexed at $90\ deg$ and resting against the trunk, the supination consists in the palm facing up and the thumb pointing laterally (for a maximum of $90\ deg$), indeed the pronation is achieved when the palm faces down and the thumb is pointing medially (for a maximum of $85\ deg$).

The other two DOFs of the wrist (RUD, FE) are visible from Figure 2.10b,c and occur around two primary axes when the hand is positioned anatomically, namely, in full supination (Figure 2.11a):

- *Transverse axis*: The axis AA' lies in the frontal plane (vertically hatched) and governs the movements of flexion and extension, which occur in the sagittal plane (horizontally hatched): flexion (arrow 1) occurs when the palm (anterior surface) of the hand moves towards the anterior side of the forearm; extension (arrow 2) happens when the back (posterior surface) of the hand moves towards the posterior side of the forearm.

- *Anteroposterior axis*: The axis BB' lies in the sagittal plane (horizontally hatched) and controls the movements of adduction and abduction, which occur in the frontal plane (vertically hatched): adduction or ulnar deviation (arrow 3) consists in the hand moving towards the body midline, causing its medial (ulnar) edge to form an obtuse angle with the forearm medial border; abduction or radial deviation (arrow 4) involves the hand motion away from the body midline, creating an obtuse angle between its lateral (radial) edge and the forearm lateral border.

The range of wrist movements around the transverse axis is assessed from a reference position shown in Figure 2.10b, where the axis of the hand running through the middle finger and the third metacarpal aligns with the axis of the forearm. Abduction does not exceed $15\ deg$, whereas adduction is typically $45\ deg$ when measured as the angle between the reference line and a line connecting the middle of the wrist to the tip of the middle finger (represented by a broken line). It is worth noting that the range of adduction is two-to-three times greater than that of abduction. The range of wrist movements around the anteroposterior axis is assessed from a reference position shown in Figure 2.10c, which is achieved when the posterior aspect

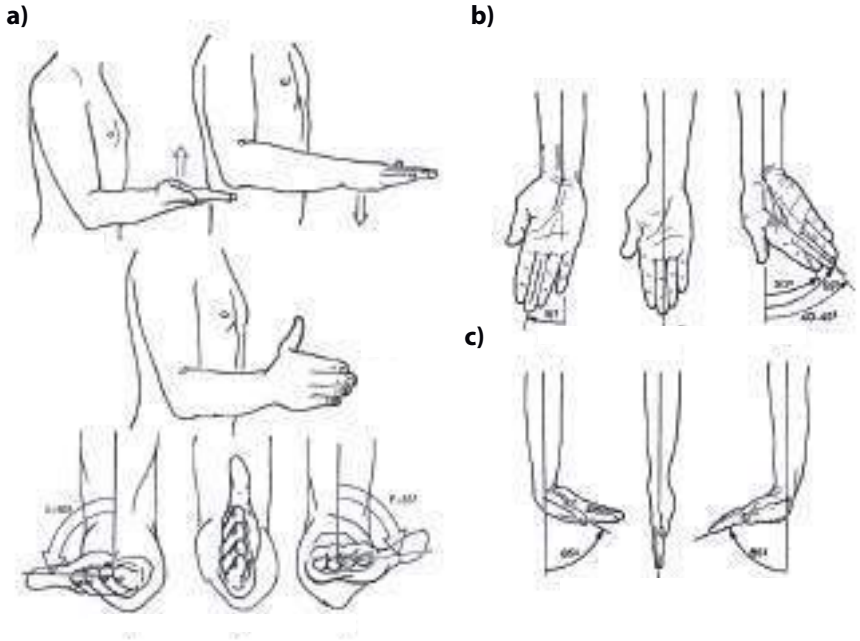

Figure 2.10: Wrist movements: ***a)*** *Pronation-supination;* ***b)*** *Radial-ulnar deviation;* ***c)*** *Flexion-extension.*

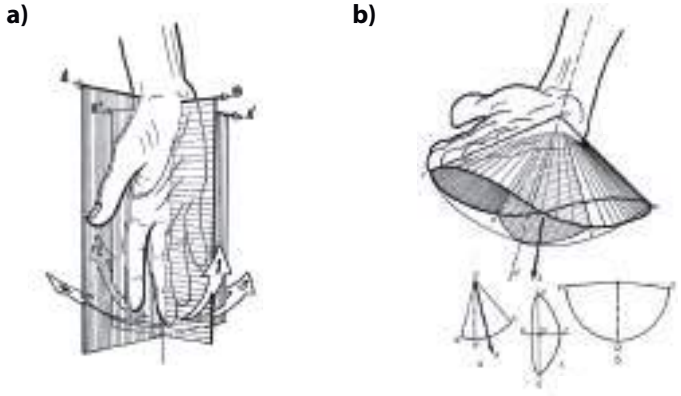

Figure 2.11: ***a)*** *Wrist axis of rotation: (AA') Transverse; (BB') Anteroposterior.* ***b)*** *Wrist circumduction.*

of the hand is in line with the posterior surface of the forearm. Both flexion and extension achieve a maximum of around $85\ deg$.

The combination of the flexion, extension, adduction and abduction movements defines the circumduction of the wrist, which takes place simultaneously about the two axes like shown in Figure 2.11b. When circumduction reaches its maximum extent, the axis of the hand traces a conical surface in space, known as the cone of circumduction. The apex of this cone is located at point O, which is considered the centre of the wrist, while the base of the cone is represented by the points F, R, E, and C. These points indicate the path that the

middle finger covers during maximal circumduction. Since the cone of circumduction is not a perfect geometric cone, its base is not circular. This irregularity arises because the range of the various simple movements that combine to form circumduction is not symmetrical around the axis of the forearm, labelled as 00'. The ROM is greater in the sagittal plane (FOE) and smaller in the frontal plane (ROC). As a result, the cone is flattened from side to side, and its base forms an ellipsoidal shape with the major axis (FE) running in a postero-anterior direction. This ellipse is further distorted medially (C) due to the greater range of ulnar deviation. Consequently, the axis of the cone of circumduction (OA) does not align with the axis of the forearm (00') but instead deviates towards the ulnar side at an angle of approximately $15\ deg$. This position, with the hand in $15\ deg$ of adduction, represents an equilibrium point for the muscles responsible for adduction and abduction, making it one of the elements of the hand functional position.

2.3. State of the Art on Upper Limbs Exoskeletons

Nowadays, exoskeletons are taking the field in hospitals and industries; according to [39], their market will reach $2500\ Mn$ of $US\$$ within the 2030, and in 2021, the 50% of the exoskeleton market took place in healthcare (vs. around the 15% in the industrial environment). Due to the high interest in robot-assisted rehabilitation integrated with VR for physical interaction, exoskeletons are assuming a critical role in developing innovative systems founding spread application in rehabilitation and teleoperation [40, 41]. Also, manufacturing companies are increasingly introducing automation technologies to comply with the high requests of modern markets [42, 43]. Nevertheless, industrial operators are still involved in many repetitive manual tasks [44]. So, the use of an exoskeleton can provide muscle fatigue relief and reduce the risk to undergo work-related musculoskeletal disorders [45].

2.3.1. Classification

Exoskeleton classification may depend on several aspects, such as the field of application, kinematics and number of DOFs, dynamics, rigidity (related to the softness of materials), type of actuation (i.e., active, passive, hybrid) and control system, ergonomics, safety, kind of experimental evaluation and presence of Artificial Intelligence (AI) associated with serious games or VR. Figure 2.12 reports a scheme of a possible classification of upper limbs

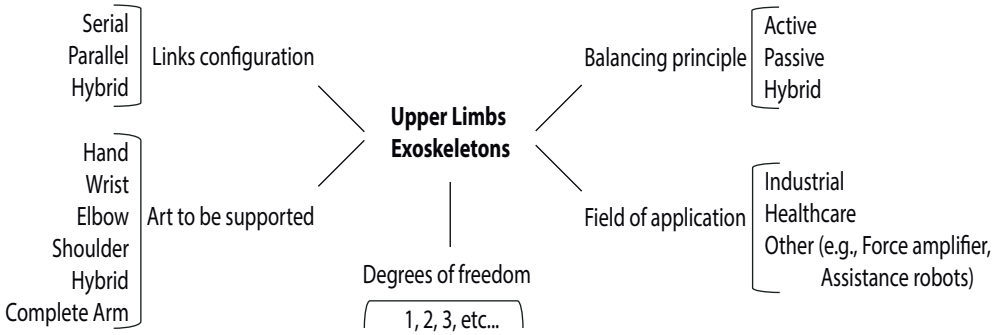

Figure 2.12: Classification of exoskeletons for the upper limb.

exoskeletons. The following categories can be identified:

- *Art to be supported*: Upper limbs exoskeletons can be identified for supporting a joint singularly (e.g., hand, wrist, elbow, shoulder), or for allowing a combined motion of more than one joint.

- *Degrees of freedom*: Mechanisms are classified according to the number of active joints, i.e., according to the number of DOFs (1-DOF, 2-DOFs, etc.).

- *Field of application*: Depending on the desired function, there are different types of robotic systems, such as rehabilitation robots, assistance robots and force amplifiers, that can find application in the industrial sector or in healthcare.

- *Links configuration*: An exoskeleton is composed of a structure of links connected by joints. Depending on the structure chosen to define the kinematic chain of the mechanism, exoskeletons can be classified as serial, parallel or hybrid.

- *Balancing principle*: Exoskeletons must be statically balanced to compensate for the gravitational load due to the limb and the weight of the device itself. There are two types of balancing (that, eventually, can be combined to achieve an hybrid solution):

    1. *Active*: The mechanism requires a continuous power supply and achieves balance via external actuators, with the aid of additional components such as sensors, cables and a control system. An additional classification can be made according to the method of actuation (e.g., electric, pneumatic, hydraulic, hybrid), the method of power transmission (e.g., gear-drive, cable-drive, belt-drive, mixed methods), and the type of control (e.g., impedance control, force control or other).

2. *Passive*: Passive elastic components acting as springs are used to balance the gravitational force.

An evaluation of these categories, involving pro and cons, is further provided in Section 2.3.2.

2.3.2. Design Principles

An important aspect to be considered when designing an exoskeleton is the reachable workspace. Studying the achievable ROM of a limb provides an understanding of the limb functioning itself. In robotics, the concept of *reachable workspace* of a mechanisms occurs when analysing a manipulator or a kinematic chain. It is defined as the region achievable by the end-effector reference system (i.e., the end part of the mechanism) with at least one movement, and its study is the basis for developing various mechanisms, from industrial ones, for specific working environments, to medical ones.

As a first step in the design of a robotic arm, the development of a kinematic model allows a better understanding of the attainable workspace. Of course, the knowledge of the human body anatomy, along with its skeletal and articular system, is of primary concern to design an exoskeleton with a kinematic chain that replicates as good as possible the one of the human limb. Basing upon the human upper limb functional aspects described in Section 2.2, the preliminary design phase of an upper limb exoskeleton consists in the next main points:

- *Biomechanics of the human limb*: The structure of the articulation to be supported can influence the choice of balancing type and constraint some design features of the overall system. Significant remarks can be made considering multi-DOFs or single-DOF kinematics:

  – For a muli-DOFs kinematics, such as the one of the shoulder joint, the choice of an active or passive balancing system has a valuable impact. The human shoulder joint is complex, so, it is usually balanced via active systems. Nowadays, designing a passive balancer for fully supporting the shoulder in its complete workspace is a challenge that leaves space to the research. In case of active balancing, there are problems with handling due to the installation of additional elements that contribute to a larger footprint and an increase in the overall weight of the structure,

but accurate motion is preferred. Instead, passive balancing allows the exoskeleton part to be simplified, but loses quality in terms of motion accuracy. Aiming at designing a lightweight but accurate system, a partial solution could be, for instance, to use an active system with a remote control realized via cable transmission: in this case, the motors do not have to be positioned directly on the joint to be actuated, but can be fixed on an external base.

  - For a simple 1-DOF kinematic chain, such as that one of the elbow, the choice of balancing principle is not binding: either active or passive balancing can be applied. When implementing a passive balancing, considerations on the material properties and the additive-manufacturing technique to be applied for manufacturing specific passive elements to support the art of interest need to be made. Optimization techniques can be implemented to size the passive elements, e.g., springs, to balance the system. In case of active balancing, several components come into play: it is therefore necessary to think about various aspects, including the correct positioning of the actuation system (i.e., motors, transmission system), so that it do not occupy space by restricting the human limb workspace and do not excessively increase the overall weight of the mechanism, affecting its compactness. Also, the system is common to be equipped with additional elements, such as a user interface to provide input data to the operator for actuating the exoskeleton.

- *Balancing action*: This aspect is linked to the application field. The functions of an exoskeleton may be manifold, and the device usage in industrial or medical environments entails different design requirements. To balance an exoskeleton, the main motion conditions, either static or dynamics, must be identified: if the mechanism reproduces slow movements (e.g., for rehabilitation purposes), the conditions can be defined as static; conversely, for fast movements (for instance, repetitive tasks to be performed by workers), the balancing should be done in the dynamic range. The last case prefers active balancing solutions, thus, using motors to counterbalance the gravity action.

- *Balancing precision*: This aspect is strongly influenced by the type of balancing. In the case of active balancing, the motors allow the exoskeleton to cover a wide ROM,

thanks to the feedback system realized by the sensors and the rapid control. Conversely, the use of passive exoskeletons limits the number of tasks that can be performed, the mechanism design being closely linked to the type of movement to be reproduced. In this case, the balancing can be optimized for a single movement by correctly positioning the passive components and assigning a specific elastic constant. The reproduction of a different movement leads to accept a greater balancing error than for the optimized case. In the medical field, where the patient must/can not move the limb by himself, a perfect balancing of the device is required. By contrast, in the industrial environment, a certain balancing error can be accepted because the worker owns sufficient strength to achieve the needed balance.

- *Weight*: This point, like the previous one, is directly related to balancing kind. A bulky and heavy exoskeleton requires motors to be moved (i.e., needs an active balancing); whereas, a passive balancing is only possible in the case of a light and compact device.

Combining all these aspects, an intermediate solution can be considered: hybrid exoskeletons comprise both motors and elastic elements. The partly-passive balance allows the use of smaller motors, reducing the risk of collision between the various components of the mechanism, and the performance of different tasks, minimizing the energy required to activate the system.

2.3.3. Industrial Applications

In the industrial sector, the production lines of manufacturing factories now require high dynamism as a result of an increasing development of automation according to the industry 4.0 trend [42]. Despite the strong increase in robotization within industries, workers are still forced to perform repetitive manual operations, such as assembling parts, handling tools, overhead tasks, loading and unloading machines, lifting and transporting heavy components [44, 46]. These operations make the human work strenuous and especially hazardous to health. In this context, the aid of a wearable robot can relieve human fatigue during movement and reduce the risk of developing work-related musculoskeletal disorders [45]. If workers were to suffer injuries, performing manual operations within an assembly line would be time-consuming, resulting in a loss of productivity in the industrial process. Therefore, the

adoption of wearable devices has a twofold advantage: on one hand, the workers' health is protected, on the other hand, industrial requirements, such as reduced costs and production time, are fulfilled while product quality is increased [43].

Referring to existent prototypes, important considerations can be made based on their field of application. Different exoskeleton types have been conceived and presented in past researches (see [47–49] for a review). These recent, commercially-available, industrial exoskeletons are designed to be light and manoeuvrable to not interfere with worker's movements, although they may be constrained in accuracy because of their limited motion capabilities. A simple structure with a reduced number of parts is preferred since additional components (e.g., motors, sensors and cables) may affect the overall weight reducing the exoskeleton comfort.

Figure 2.13 shows the most recent upper limbs exoskeletons available in the market and Table 2.1 summarise their main features. Given the industrial needs, as it can be noticed, most of them are passive, or at least hybrid, and focus on supporting the shoulder upper limb joint. Due to commercial interest, not all technical information are easy to be found. Below is reported the description of available devices (Figure 2.13) with their main features:

a) *MATE*: The COMAU exoskeletons (MATE-XT and MATE-XT 4.0) [1] are systems

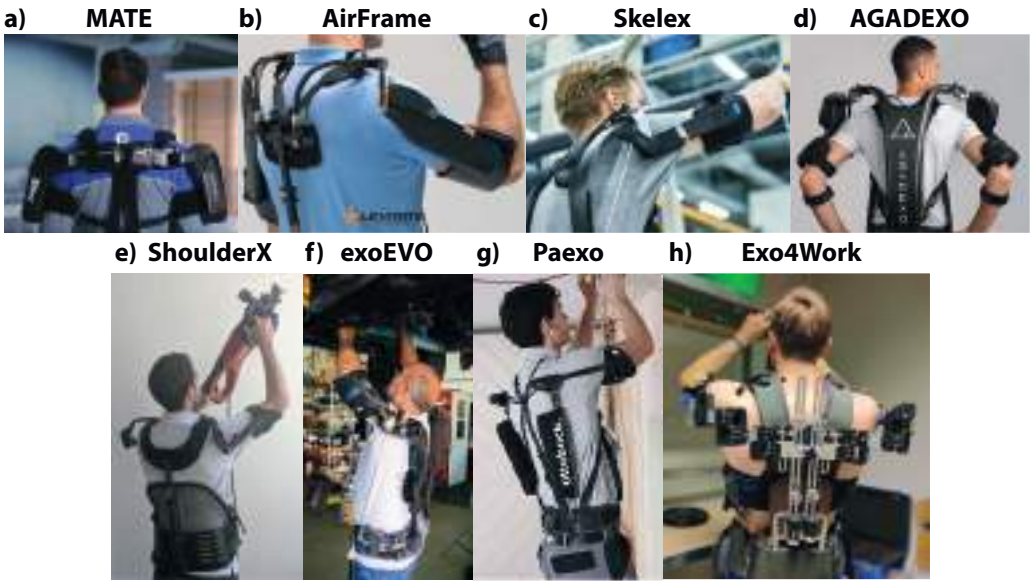

Figure 2.13: Upper limbs commercial industrial exoskeletons (examples on the current market – 2024): ***a)*** *MATE [1];* ***b)*** *AirFrame [2];* ***c)*** *Skelex [3];* ***d)*** *AGADEXO [4];* ***e)*** *ShoulderX [5];* ***f)*** *exoEVO [6];* ***g)*** *Paexo [7];* ***h)*** *Exo4Work [8].*

that enhance human potential by relieving the user from excessive strain in the shoulder joint. These exoskeletons provide strength, control and stability by allowing dynamic shoulder movements to be replicated. Their ergonomics lets the exoskeleton parts in direct contact with the wearer's skin to be adjusted into different sizes. MATE-XT and MATE-XT 4.0 offer a steady reduction in shoulder muscle activation (around the 30%), being particularly effective during overhead activities and manual handling of weights from the ground. They help improving posture and alleviate muscular strain, making tasks less physically taxing and promoting better overall ergonomics for the user; depending on the task to be performed and the user's physical capabilities, they let to select seven assistance levels, choosing the intensity of auxiliary force.

b) *AirFrame*: This upper limb support device [2], made by Levitate Technologies INC, reduces effort levels by up to 80%. The AirFrame distributes the weight of the user's arms between the shoulders, neck and back, shifting it towards the outside of the hips, to distribute energy and reduce physical stress. It is equipped with a mechanical support system that activates progressively with movement, adapting in real time. A new version of the exoskeleton (AirFrame FLEX) offers enhanced flexibility and comfort, supporting several working postures and functions.

c) *Skelex*: Skelex 360-XFR [3], designed to be suitable for 80% of the population, uses

*Table 2.1: Upper limbs commercial industrial exoskeletons main features (examples on the current market − 2024). From Figure 2.13: **a)** MATE [1]; **b)** AirFrame [2]; **c)** Skelex [3]; **d)** AGADEXO [4]; **e)** ShoulderX [5]; **f)** exoEVO [6]; **g)** Paexo [7]; **h)** Exo4Work [8]. The assistance level indicates the amount or intensity of support provided by the exoskeleton to the user's movements; the Degree Of Freedom (DOF) column indicates the joint supported by the device (Shoulder (S) and/or Elbow (E) joint), and, if available, the exact number of DOFs; the elbow column indicates whether the device kinematics includes the elbow joint; the adjustment refers to the exoskeleton's ability to adapt to the user's body shape, posture, or activity. Note that devices marked with N for the passive feature are semi-passive, such as the MATE, which uses a mechanical system based on springs and cables to provide biomechanical support without motors or batteries.*

Device	Passive	Assistance Level	DOF	Elbow	Multi-task	Weight [∼kg]	Adjustment	Cost
MATE	N	8	S-E (3)	N	Y	1.6	Customizable	Medium-high
Airframe	Y	Adjustable	S-E (3)	N	Y	5.4	Simple	Medium
Skelex	Y	Dynamic	S-E (2)	Y	Y	2.5	Advanced	High
AGADEXO	N	7	S-E (2)	N	Y	3.2	Customizable	Medium-high
ShoulderX	N	5	S-E (2)	Y	N	2.8	Simple	High
exoEVO	Y	Fixed	S (1)	Y	N	1.5	Simple	Medium
Paexo	Y	Customizable	S (1)	N	N	5.5	Customizable	Medium
Exo4Work	Y	Adjustable	S-E (2)	N	Y	7.8	Simple	Medium

the Skelex patent Flex Frame technology to provide upper body support focusing on the arms. It offers adjustable support ranging from $0.5\ kg$ to $4\ kg$ per arm, customized based on the user's needs. Despite its robust support, the 360-XFR is lightweight (it weights $2.3\ kg$), allowing for ease of use, comfort during extended periods of wear, and full $360\ deg$ ROM, ensuring flexibility and motion freedom.

d) *AGADEXO*: AGADEXO Shoulder [4] is a smart industrial exoskeleton suitable for different case studies designed to reduce the risk of shoulder muscular disorders during manual material handling tasks. It is fast to be installed and equipped with a sensorized bracelets with AI algorithms: this allows the system to activate automatically only when the user lifts/lowers a payload, providing assistance as needed. The mechanical structure is in carbon fibre, to guarantee maximum freedom of movement, lightness and resistance, whereas the actuation technology is hybrid, embedding semi-active actuators composed of an elastic mechanism paired with an electric motor. So, power consumption is minimized, weight of motors and batteries is reduced, and user's comfort is enhanced.

e) *ShoulderX*: The exoskeleton produced by SUITX [5] augments its wearer by reducing gravity-induced forces at the shoulder complex, enabling the user to perform chest-to-ceiling level tasks for longer durations and with less effort. It can be combined with the modulus for the back and the legs, so to achieve a complete exoskeleton to support the human body (i.e., the Modular Agile eXoskeleton (MAX) [50]). An improved device is the IX SHOULDER AIR [51]: it functions without a battery and uses only the body own energy allowing the 40% fatigue reduction for shoulder muscles and joints; it is lightweight (it weights around $2.2\ kg$), and allows a $360\ deg$ ROM.

f) *exoEVO*: The exoEVO by exoBIONICS [6] is designed with minimal touch points to provide power allowing the natural motion of the upper limb. The exoskeleton features a patented stacked-link structure designed to closely follow the user's arm and elbow throughout their full ROM. This innovative design ensures that the exoskeleton maintains proper joint alignment during repetitive movements, providing consistent support and reducing strain on the user's joints. exoEVO is equipped with adjustable, high-force actuators known for their durability, capable of withstanding over a million

cycles before needing replacement. The device allows for easy customization of the assistance level for each arm, making it adaptable to the specific needs of the user and the task at hand. This is achieved by simply swapping out the compact gas springs, which control the amount of support provided. The ability to independently adjust the support level for each arm ensures optimal performance and comfort, especially in tasks requiring varied assistance levels for different movements.

g) *Paexo*: The Paexo Shoulder by Ottobock [7] is a lightweight industrial exoskeleton designed to alleviate shoulder strain during overhead work. It weighs $1.9\ kg$ and supports users with a height range from $160\ cm$ to $190\ cm$. It allows users to lift up to $6\ kg$ per arm, enhancing productivity and reducing physical strain. A successor of the Paexo Shoulder is the Ottobock Shoulder [52], which embodies some improvements such as the faster donning/doffing, the reversible magnetic closure, the tool-free sizing and torque adjustment, and the improved arm cuffs.

h) *Exo4Work*: This device [8] is a 5-DOFs passive shoulder exoskeleton weighting $3.8\ kg$. It provides assistance to the shoulder thanks to a passive remote actuation mechanism that applies a force perpendicular to the humerus. By adjusting the spring pretension, the assistance level provided by the device can be regulated. The torque profile of the exoskeleton is strategically designed to offer higher assistance during the lifting phase of tasks, which helps in significantly reducing muscle activation and strain when elevating the arms. However, this torque profile leads to an increase in muscle activation during the lowering phase. This happens because the exoskeleton assistance decreases, requiring the user's muscles to engage more actively to control the descent. While this might seem counterproductive, it is often a trade-off in exoskeleton design to ensure that the lifting phase, which generally requires more force, is adequately supported. Additionally, the exoskeleton is designed to provide minimal assistance when the shoulder elevation angles are low, such as during walking or other non-overhead activities. This is important to avoid hindering natural movement and to ensure that the exoskeleton does not interfere with tasks that involve lower shoulder positions, thereby allowing for more flexibility and freedom of movement during these activities.

Although the just presented devices are not yet used on a large scale, several studies show

that their use in industry has positive effects on operators' health [43, 53, 54]. Thanks to the aid provided by these systems, there is a reduction in the risk of injury for workers, with a consequent reduction in healthcare costs, and an increase not only in company productivity, but also in quality and precision in production. Indeed, the interest in the use of these devices is wide, but some problems, such as the lack of specific safety regulations, hinder their diffusion in the industrial world. One technical aspect that must be evaluated is the discomfort in wearing the device, due to both the weight and the bulkiness of the device itself. In fact, the user, accustomed to moving normally with fluidity, is forced to follow the mechanism, limiting his movements in terms of working space and fluidity. Exoskeletons for industrial application privilege aspects such as lightness and manoeuvrability, a reduced footprint, and the possibility of performing multiple operations, at the expense of a lower accuracy of motion: using a limited number of DOFs, they do not follow the exact movement of the human limb, risking to cause discomfort to the user.

Given this background, the present thesis developed a shoulder-elbow exoskeleton, aiming at providing a solution to find a trade-off depending on the needs of both workers and industries. Details will be discussed in Chapter 3, providing an efficient methodology to design a passive exoskeleton to be customized as desired.

2.3.4. Healthcare Applications

Concerning the rehabilitation field, robotic devices are designed to provide several advantages beyond human capabilities and improve the efficacy of traditional therapy. Mainly, exoskeletons for medical applications are designed to reach high motion capabilities in the workspace with the drawback of being heavy, due to the use of lots of components. As studied for example in [26], the effectiveness of robot-aided rehabilitation can be compared to the conventional one, proving the decrease in therapists' effort and the increase of the assessment repeatability and accuracy thanks to its continuous usage. Rehabilitation systems can provide movement guidance to the user's upper limb in a 3-Dimensional (3D) space, offering aid to the patient and therapist. In this way, the physical exertion of therapists due to manual labour can be relived, without excluding their professional role, overcoming most of the standard treatment limits. Indeed, the practice can be prevented due to the severity of the injury and the patient may lose motivation because of the repetitiveness of exercises;

moreover, the therapist must be present during the rehabilitation process to check the user response under therapy, always incurring the risk to collect unclear results due to the rough feedback. In this regard, using a system equipped with sensors allows to take objective and large-scale measurements, thus, offering a custom control strategy that the therapist can set and adapt to the user's needs. Also, the doctor can treat more patients at the same time and elaborate recorded data remotely.

Among the major companies in the rehabilitation robots market, Hocoma, Bionik, and Fourier Intelligence can be mentioned [55–57]. Their primary aim is to develop systems able to provide human body weight support and movement guidance in a 3D workspace, ensuring the increase of the patient's ROM, and augmented strength and endurance.

Focusing on upper limb exoskeletons including the wrist modulus, the available devices are shown in Figure 2.14 and explained in detail in the next bullet list:

- *Hocoma products*: These devices have been designed for arm and hand therapy of patients with moderate impairments providing assist-as-needed support to the patient's individual abilities [55]. **a)** *Armeo Power* is useful for guiding the initial phases of arm and hand function recovery. **b)** *Armeo Spring* and **c)** *Armeo Spring Pro* include an ergonomic exoskeleton to guide self-initiated movement therapy and allow the simultaneous motion of arm and hand in 3D space. Also, motivating exercises can be performed, thanks to the adaptation of difficulty level to the patient's capabilities. **d)** *Armeo Senso* is for self-directed arm therapy; it is easy to use and configure, being portable and with an intuitive user interface.

- *Bionik products*: Bionik [56] offers different rehabilitation platforms for physical and occupational therapy, allowing the simultaneous/single usage of the arm/hand modulus and including a user interface helping therapists in task control. An interesting device is **e)** the *Bionik InMotion Arm*, distinguished among other therapy systems by the ability to assess patients and deliver real-time interactive responses. This robot is designed to sense patients' movements and adapt to their constantly changing abilities. Key features include adaptive assistance (if a patient struggles to move, the robot gently assists in initiating the movement towards the target), guided movements (for patients with coordination issues, the robot guides the movement, ensuring that the

patient practices correctly and moves towards the target efficiently), progressive challenge (as the patient regains control over motion, the robot reduces assistance, continually challenging the patient to improve further), quantifiable feedback (the exoskeleton

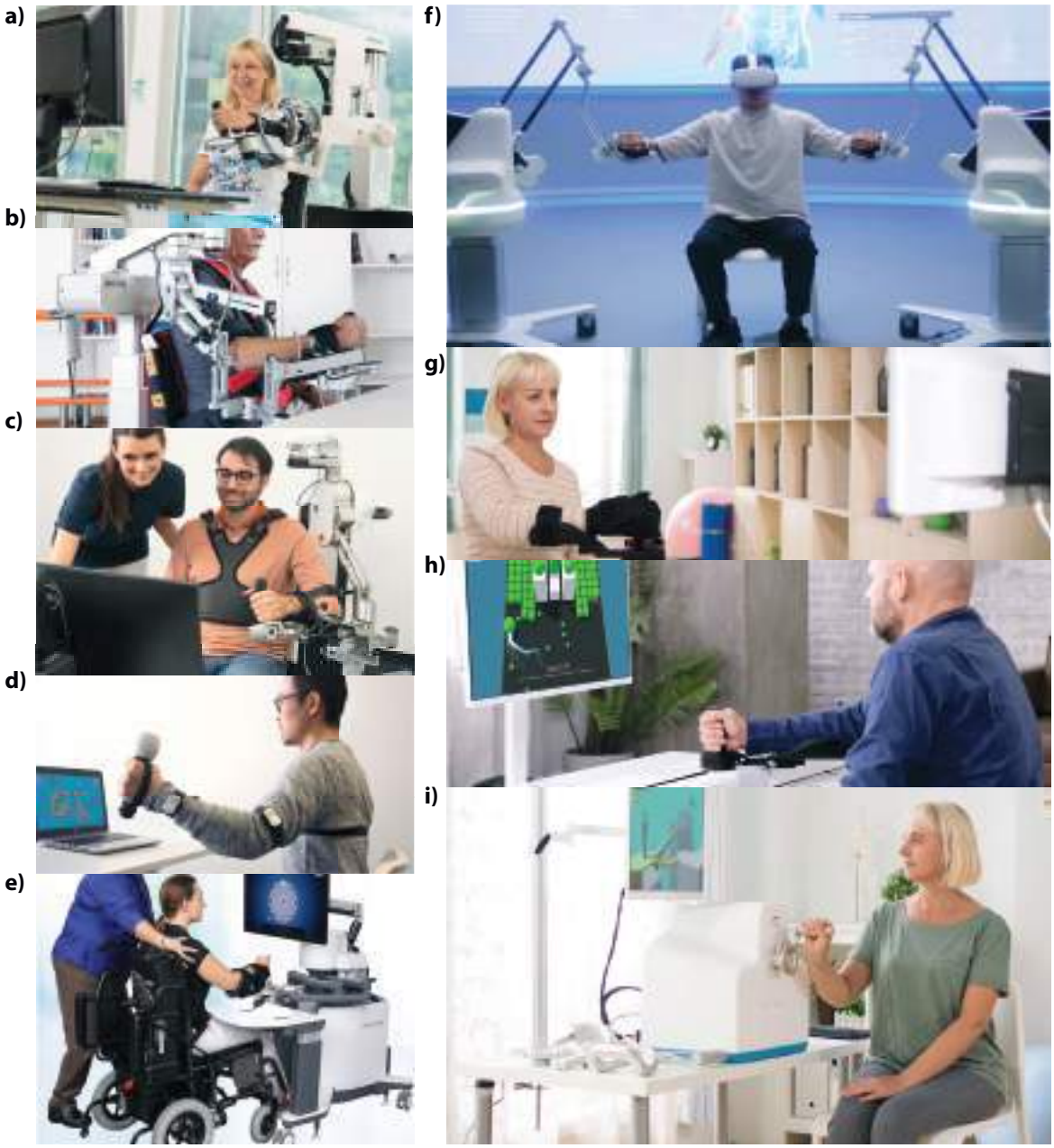

Figure 2.14: Upper limb commercial rehabilitation platforms (examples on the current market – 2024). ***Hocoma products:*** ***a)*** *Armeo Power (Arm-P);* ***b)*** *Armeo Spring (Arm-Sp);* ***c)*** *Armeo Spring Pro (Arm-Spro);* ***d)*** *Armeo Senso (Arm-Sens).* ***Bionik products:*** ***e)*** *Bionik InMotion Arm (InM).* ***Fourier Intelligence products:*** ***f)*** *Arm Motus EMU (AM-EMU);* ***g)*** *Arm Motus M2 Gen (AM-M2);* ***h)*** *Arm Motus M2 Pro (AM-M2pro);* ***i)*** *Wrist Motus M1-W (WM-M1).*

provides measurable feedback on the patient's progress and performance, allowing for precise, tracking, and adjustment of the rehabilitation process). All these capabilities enhance the effectiveness of therapy, ensuring that patients receive tailored, and dynamic support that evolves with their recovery.

- *Fourier Intelligence products*: Between the various choice of these devices, the ones for the upper limb are described below [57].

  f) The *Arm Motus EMU* is a cutting-edge 3D back-drivable upper limb rehabilitation robot for advanced therapeutic applications. It is designed for addressing upper limb disabilities caused by neurological or musculoskeletal disorders (such as stroke, spinal cord injuries or fractures, tendon injuries). A key feature is the advanced force feedback technology, which allows the device to simulate the tactile and supportive functions of a therapist's hands during rehabilitation exercises. This technology enables the Arm Motus EMU to provide tailored assistance or resistance and suit varying therapeutic goals depending on the user's needs. This adaptability makes the device a versatile tool in the rehabilitation process, providing personalized therapy that can enhance recovery outcomes. The system can be used in different modes: passive, for creating conscious linkage, assistive, for inducing passive participation, active, for optimizing motor control, and resistive, for improving muscular power. The Arm Motus EMU embeds a cable-driven mechanism combined with a parallel structure made of lightweight carbon fibre rods. This design reduces friction and inertia within the device, allowing for smoother and more responsive movements, thus, enhancing the control system performance enabling it to respond and execute commands more efficiently. This, in turn, improves the robot compliance in human-machine interactions, making it more adaptable and responsive to the patient's movements. As a result, the device provides a more effective and comfortable rehabilitation experience, helping patients regain upper limb function through precise and adaptive robotic assistance.

  g) The *Arm Motus M2* is designed to facilitate comprehensive and task-oriented rehabilitation training for upper limb recovery. This device is capable of performing a wide range of exercises that target different aspects of movement, such as strength, speed, and accuracy. By accurately and objectively quantifying each movement, the device ensures that both therapists and patients can monitor progress with precision.

Moreover, the device offers an immersive interactive experience, which engages users more deeply in their rehabilitation process. This interactive approach not only makes therapy more engaging but also accelerates improvements in motor function. By continuously challenging the user with diverse tasks and providing real-time feedback, the Arm Motus M2 plays a crucial role in reshaping and restoring upper limb functionality. Also, the system integrates multiple functional training modes to provide a comprehensive approach to upper limb recovery. This innovative system combines motor control with cognitive, muscle strength, and ROM training. Thus, Arm Motus M2 ensures that patients receive a holistic treatment that addresses not only the physical aspects of rehabilitation but also the cognitive processes involved in motor control. This multifaceted approach is designed to enhance the effectiveness of therapy, promoting quicker and more robust recovery of upper limb function.

h) The *Arm Motus M2 Pro* represents a new generation of upper limb rehabilitation robotics, featuring a compact and sleek all-in-one design. This advanced device utilizes a state of the art force feedback algorithm and a high-performance motor to create an optimal mechanical environment for users. The precise simulation provided by the device enhances the rehabilitation experience, making it more effective and user-friendly, while maintaining a smaller and more streamlined profile. The system offers a variety of training modes and customized trajectories to create limitless possibilities. Moreover, it features a high-performance motion control card that delivers high-quality audio, visual, and kinesthetic feedback to users. This cutting-edge device integrates immersive and interactive games into the rehabilitation process, offering goal-oriented training with progressively increasing difficulty. Additionally, it provides accurate evaluation and data analysis, making it a comprehensive tool for enhancing upper limb rehabilitation through engaging and effective methods.

i) The *Wrist Motus M1-W* is designed specifically for targeting the wrist joint, offering training that simulates Activities of Daily Living (ADLs). It provides exercises for key wrist movements, including PS, RUD, and FE. This device complements the Arm Motus M2 Gen and Pro by focusing on gross motor training for the upper limb, ensuring a comprehensive rehabilitation experience. The Wrist Motus M1-W is integrated with a variety of functional training modes, making it suitable for users with muscle

power ranging from 0 to 5. It combines motion control with cognitive training, and muscle strength with ADLs training, so to ensure that users can progressively improve both their cognitive and physical abilities through targeted and effective rehabilitation exercises. Moreover, the system offers an interactive game experience and a series of accessories for different functions depending on the users' needs.

Even if the above-mentioned companies have been already placed in the market, there is a need of spreading this kind of technology to improve therapy efficacy. Since detailed information about the mechanical structure of these devices is hard to be found due to commercial issues, a review on assistive robotics for upper limb rehabilitation available in the scientific literature has been made (see [41, 47, 58]), with focus on the state of the art on wrist exoskeletons [59, 60]. The most relevant examples of the upper limb exoskeletons for rehabilitation are illustrated in Figure 2.15 and described in the next list:

a) *CADEN-7* [9] is a 7-DOFs powered robotic neurorehabilitation device. The exoskeleton design, featuring proximal placement of motors and distal placement of cable-pulley reductions, optimizes its performance by ensuring low inertia and high stiffness in its links, having an overall weight of around $6.8\ kg$. This arrangement re-

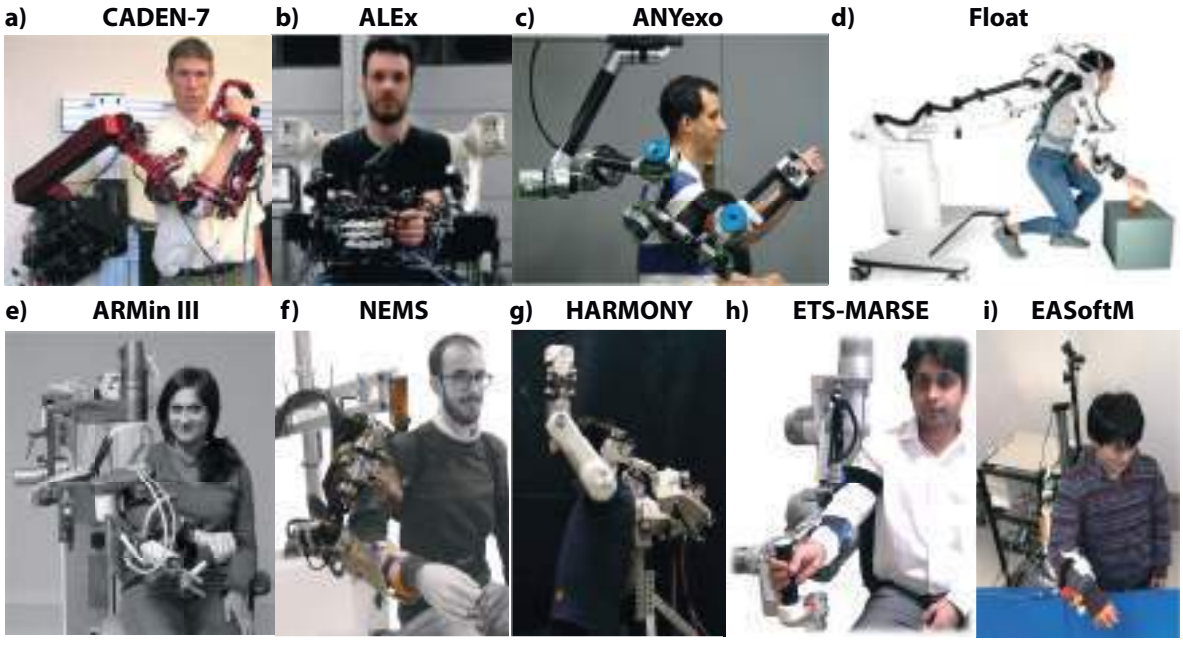

Figure 2.15: Upper limb exoskeletons for rehabilitation (examples from 2007 to 2022): ***a)*** *CADEN-7 [9];* ***b)*** *ALEx [10, 11];* ***c)*** *ANYexo [12];* ***d)*** *Float [13];* ***e)*** *ARMin III [14];* ***f)*** *NEMS [15];* ***g)*** *HARMONY [16];* ***h)*** *ETS-MARSE [17];* ***i)*** *EASoftM [18].*

sults in backdrivable transmissions with zero backlash, allowing for smooth, precise movements and enhanced user control. The design facilitates full functionality of the shoulder, elbow, and wrist joints, enabling a wide range of upper limb movements. CADEN-7 finds application as a therapeutic and diagnostic device for physiotherapy to assist in the rehabilitation of patients by providing targeted support and resistance, thus, allowing for accurate tracking and assessment of patient progress. However, the device can be also exploited as assistive device (it serves as a power amplification device for individuals with reduced muscle strength, helping them performing ADLs with less effort), haptic device (it can be integrated into VR systems to provide realistic force feedback, enhancing the immersive experience by allowing users to feel virtual objects), and master device (in teleoperation, it serves as the master device that controls a remote robotic arm, allowing precise manipulation of objects in hazardous or remote environments).

b) *ALEx* [10, 11] is a 6-DOFs exoskeleton for the upper limb: it allows 3-DOFs for the shoulder, and 1-DOF for the elbow via four active joints (four brushless torque motors are located in the backpack), whereas it includes two passive joints for the wrist PS and FE, thus, reproducing around the 90% of the human arm workspace. The high-level control system offers three distinct operational modalities designed to cater to different levels of user interaction and assistance. 1) With the passive mode, the user moves the upper limb freely, while the exoskeleton sensors monitor and measure the movements. The robot does not actively intervene but provides data on the motion, which can be used for assessment or feedback purposes. 2) Via the assistive mode, the device takes a more active role, guiding the user's upper limb through specific movements. This mode is particularly beneficial for users who need support in executing movements due to weakness or impaired motor control. 3) In the assisted-when-needed mode the exoskeleton monitors the user's intent to move and waits for him/her to initiate a movement. If the user does not start the movement within three seconds, the robot automatically steps in to guide the arm to the target position. This mode encourages the user to engage in the movement process while ensuring that assistance is provided when necessary. In any case, in all modes, the control system compensates for the moving parts weight, the mechanical transmission friction, and the links and motors

inertia, thus, ensuring smooth, precise, and natural movements, enhancing the user's experience and the effectiveness of the exoskeleton assistance.

c) *ANYexo* [12] is an upper limb exoskeleton based on low-impedance torque controllable series elastic actuators, specifically designed for therapy of patients with a neural impairment. The kinematic structure of the robot consists in six active DOFs (two for the shoulder girdle joint, three for the glenohumeral joint, and one for the elbow joint) plus one passive DOF for the link arm length adjustment. The system has been optimized for a broad ROM for performing ADLs and precise force control, aiming to closely replicate the compliant and accurate haptic feedback provided by human therapists. The modified modular series elastic actuators are essential for delivering the necessary power and precise torque control; they are designed to provide high performance in terms of both power-to-weight ratio and torque control, crucial for ensuring smooth and accurate movements, especially at high speeds. A feed-forward torque controller based on a precise dynamic model ensures an accurate and responsive control, improving the system transparency.

d) *Float* [13] is a 5-DOFs shoulder exoskeleton, designed to move the human upper limb in the 3D space, allowing the simulation of ADLs. Passive joints between links permits the regulation over different size of the user's arm. The exoskeleton is connected to a wheeled mobile base via a poly-articulated passive arm; this mechanical solution allows the device to be released from a fixed position, thus, enabling the user to receive support during complex functional activities. By disengaging the device from a fixed position, the user gains greater freedom of movement, that is particularly important for tasks requiring dynamic and coordinated whole-body actions, rather than just isolated limb movements. Thanks to its structure, including an active part of $10.0\ kg$, Float can assist the user in more complex functional activities, which may involve multiple joints and body parts working together. However, the control need to be further improved, since the friction compensation represents a preliminary solution to guarantee a transparent behaviour of the exoskeleton system, and the gravity compensation of the exoskeleton weight need to be implemented.

e) The *ARMin III* [14] robot is designed to assist with upper limb rehabilitation by offer-

ing precise control and movement across several key joints; it provides three actuated DOFs for the shoulder, and one for the elbow joint. The device can be easily switched from right-arm to left-arm use, and an additional module can be attached to provide actuated control over wrist PS and FE. It is known for the shoulder actuation mechanism (simple, slightly more complex than the ball-and-socket joint) and the passive weight compensation of the arm elevation through a spring that needs to be periodically readjusted in tension. However, the system is bulky, weighting around $18.7\ kg$ and constraining the user to sit in a wheelchair; since it only has position sensors, inertia effects cannot be measured and compensated.

f) *NEMS* [15] is a shoulder-elbow exoskeleton for upper limb neurological rehabilitation. The system is equipped with four active DOFs that facilitate key shoulder and elbow movements, and eight passive DOFs, which allow for precise alignment of the motor axes with the user's joint axes. So, the exoskeleton can be adjusted to accommodate different body sizes and shapes, providing a personalized fit for each user. The active joints utilize series elastic actuators, which introduce a level of compliance in the system, enabling the device to operate in both position and torque control mode, offering versatility in how the exoskeleton responds to user inputs. The ability to control the exoskeleton in torque mode is particularly beneficial for rehabilitation, as it allows for the fine-tuning of assistance levels, making the device adaptable to the patient's progress and needs. The exoskeleton is supported by a wheeled platform, which houses a box containing the control and interface electronics, centralizing the exoskeleton operational components; so, the entire setup weighs approximately $136\ kg$. This design provides a balance between functionality and stability, ensuring that the exoskeleton can offer substantial support while being manoeuvrable within different settings.

g) *HARMONY* [16] is an upper body exoskeleton for rehabilitation providing natural coordinated motions on the shoulder with a wide ROM via force and impedance control. It has a shoulder mechanism with five active DOFs, 1-DoF for the elbow, and a wrist mechanism powered by series elastic actuators. The device has very low impedance at both the joint and workspace level, imposing little resistance on the users' free movements. The implementation of task-space force or impedance control plays a crucial

role in delivering effective, task-oriented, training. Thanks to the system transparency and backdrivability, the assist-as-needed paradigm can be implemented, allowing the patient to exert as much voluntary effort as possible. Also, the gravity compensation allows patients who might struggle to lift their arms or maintain certain postures due to weakness or motor impairments.

h) *ETS-MARSE* [17] is a redundant 7-DOFs robot (three for the shoulder, one for the elbow, three for the wrist) for the rehabilitation of the impaired human upper limb, based on backstepping non linear control to reject or counteract the forces generated by the user's muscular activity: the controller actively compensates for any force exerted by the user's muscles, effectively minimizing its impact on the exoskeleton movement. The robot kinematics has been inspired by the human arm structure (it is redundant to allow the performance of several movements) and a control algorithm has been developed to achieve stability and robustness with passive trajectories in the 3D space.

i) *EASoftM* [18] assists the reaching motion of the upper limb, supporting the movement of the elbow and shoulder; it can record trajectories of hand reaching a target based on the visual feedback control. The device has been designed to meet specific conditions crucial for effective wearable assistive robotics: 1) it has a limited number of DOFs (this simplifies its design and control, making it easier to use and more focused on essential movements); 2) it ensures precise motion control, which is essential for rehabilitation and assistance, allowing for accurate replication of natural joint movements; 3) it is designed to be wearable and comfortably worn by users for extended periods; 4) it provides compliant assistance, so, it can adapt to the user's movements and apply force in a way that is safe and comfortable. This is achieved through soft modules located at the joint positions, which are actuated by pneumatic systems. The soft actuators use the visco-elastic properties of materials like plastic and rubber, allowing the device to mimic the dynamics of natural movement and provide a more intuitive and responsive assistance. Overall, the EASoftM is aligned with the anatomical structure of the body, ensuring to work harmoniously with the user's natural movements while providing the necessary support and assistance in a compliant and comfortable manner. As further works, the system need to be portable and wearable.

Table 2.2: Upper limb commercial rehabilitation platforms and upper limb exoskeletons for rehabilitation main features. From Figure 2.14: ***Hocoma products: a)*** *Armeo Power (Arm-P);* ***b)*** *Armeo Spring (Arm-Sp);* ***c)*** *Armeo Spring Pro (Arm-Spro);* ***d)*** *Armeo Senso (Arm-Sens).* ***Bionik products: e)*** *Bionik InMotion Arm (InM).* ***Fourier Intelligence products: f)*** *Arm Motus EMU (AM-EMU);* ***g)*** *Arm Motus M2 Gen (AM-M2);* ***h)*** *Arm Motus M2 Pro (AM-M2pro);* ***i)*** *Wrist Motus M1-W (WM-M1). From Figure 2.15:* ***a)*** *CADEN-7 [9]);* ***b)*** *ALEx [10, 11];* ***c)*** *ANYexo [12];* ***d)*** *Float [13];* ***e)*** *ARMin III [14];* ***f)*** *NEMS [15];* ***g)*** *HARMONY [16];* ***h)*** *ETS-MARSE [17];* ***i)*** *EASoftM [18]. The Degree Of Freedom (DOF) column indicates if the device is for the Shoulder (S), Elbow (E), and/or Wrist (W) joint (if available, there is the exact number of DOFs); the adjustment refers to the exoskeleton's ability to adapt to the user's body shape, posture, or activity; the integrability feature indicates whether the wrist exoskeleton can be integrated with shoulder, elbow, and hand exoskeletons for a full-body solution.*

Device	DOF	Actuation	Weight [∼kg]	Feedback	Adjustment	Power Supply	Device type	Integrability
Arm-P	S-E-W	Motors	5.5	Force sensors	Y	External	Desktop	Y
Arm-Sp	S-E-W	Springs	4.0	Force sensors	Y	External	Desktop	Y
Arm-Spro	S-E-W	Hybrid	5.0	Force sensors	Y	External	Desktop	Y
Arm-Sens	S-E-W	Motors	1.5	Force + Torque sensors	Y	External	Desktop	Y
InM	S-E	Motors	25.0	Force + Torque sensors	Y	Battery	Portable	Y
AM-EMU	S-E-W	Motors	12.8	Torque sensors	Y	External	Portable	Y
AM-M2	S-E-W	Motors	14.0	Torque sensors	Y	Battery	Portable	Y
AM-M2pro	S-E-W	Motors	16.0	Torque sensors	Y	Battery	Portable	Y
WM-M1	W (2)	Motors	4.0	Force sensors	Y	Battery	Portable	Y
CADEN-7	S-E-W (7)	Motors	25	Force sensors	Y	Battery	Portable	Y
ALEx	S-E (3)	Motors	20	Force sensors	Y	External	Desktop	Y
ANYexo	S-E-W	Motors	15	Force + Torque sensors	Y	Battery	Portable	Y
Float	S-E-W	Springs	5.0	None	N	None	Portable	N
ARMin III	S-E-W	Motors	15	Force + Torque sensors	Y	External	Desktop	Y
NEMS	S-E-W	Motors	9.0	Force sensors	Y	Battery	Portable	Y
HARMONY	S-E-W	Motors	15	Force + Torque sensors	Y	Battery	Portable	Y
ETS-MARSE	S-E-W	Motors	15	Force sensors	Y	External	Desktop	Y
EASoftM	S-E-W	Motors	12	Force sensors	Y	External	Desktop	Y

*Table 2.3: 3-Degrees of freedom wrist exoskeletons main features (examples from 2007 to 2024). From Figure 2.16: **a)** Open Wrist (OW) [19]; **b)** Rice Wrist-S (RW-S) [20]; **c)** MIT Wrist Robot (MIT-WR) [21]; **d)** Wrist Grimbal (WG) [22]; **e)** IIT Wrist (IIT-W) [23]; **f)** Rice Wrist (RW) [24]; **g)** Wrist Robot (WR) [25]; **h)** WristBot (WB) [26]; **i)** M3Rob (M3R) [27]; **l)** PowRobot (PR) [28]; **m)** Gopura Exos (GE) [29], **n)** WRES [10]. The Degree Of Freedom (DOF) column indicates the wrist joint number of motions; the adjustment refers to the exoskeleton's ability to adapt to the user's body shape, posture, or activity; the integrability feature indicates whether the wrist exoskeleton can be integrated with shoulder, elbow, and hand exoskeletons for a full-body solution.*

Device	DOFs	Actuation	Weight [∼kg]	Feedback	Adjustment	Power Supply	Device type	Integrability
OW	3	Tendon-driven	1.5	Force sensors	Y	Battery	Portable	Y
RW-S	3	Direct-drive	2.0	Torque + force sensors	Y	Battery	Desktop	Y
MIT-WR	3	Cable-driven	1.8	Force sensors	Y	External	Desktop	Y
WG	3	Passive	1.2	None	N	None	Desktop	N
IIT-W	3	Cables + gears	2.5	Force sensors	Y	External	Portable	Y
RW	3	Cable-driven	2.0	Torque + force sensors	Y	External	Desktop	Y
WR	3	Cable-driven	2.2	Force sensors	Y	External	Desktop	Y
WB	3	Cable-driven	2.3	Force sensors	Y	Battery	Desktop	Y
M3R	3	Gear-based	2.0	Torque sensors	Y	Battery	Portable	Y
PR	3	Direct-drive	2.1	Torque sensors	Y	Battery	Desktop	Y
GE	3	Direct-drive	1.8	Torque sensors	Y	Battery	Desktop	Y
WRES	3	Cable-driven	2.4	Torque sensors	N	External	Portable	Y

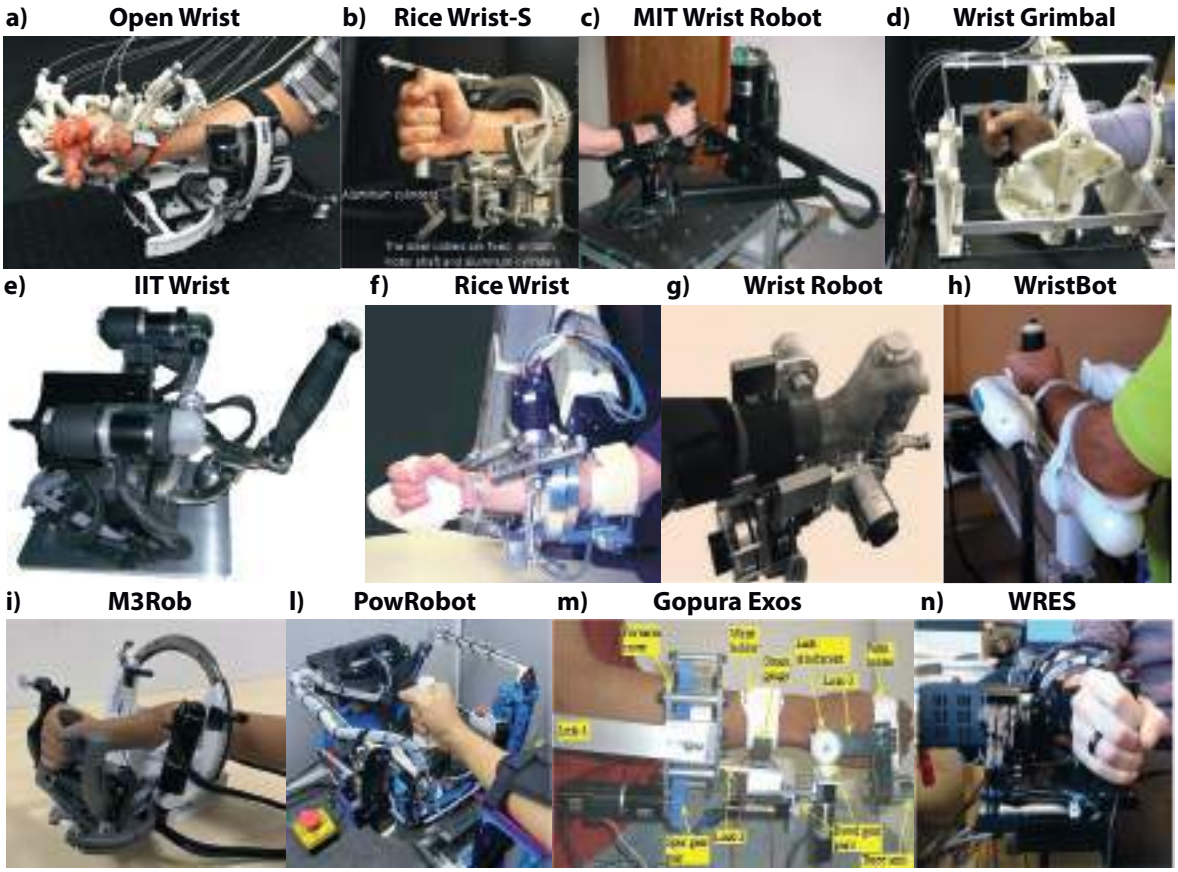

Figure 2.16: 3-Degrees of freedom wrist exoskeletons state of the art (examples from 2007 to 2024): ***a)*** *Open Wrist (OW) [19];* ***b)*** *Rice Wrist-S (RW-S) [20];* ***c)*** *MIT Wrist Robot (MIT-WR) [21];* ***d)*** *Wrist Grimbal (WG) [22];* ***e)*** *IIT Wrist (IIT-W) [23];* ***f)*** *Rice Wrist (RW) [24];* ***g)*** *Wrist Robot (WR) [25];* ***h)*** *WristBot (WB) [26];* ***i)*** *M3Rob (M3R) [27];* ***l)*** *PowRobot (PR) [28];* ***m)*** *Gopura Exos (GE) [29],* ***n)*** *WRES [10].*

To sum up, the main features of devices from Figure 2.14 and Figure 2.15 have been summarised in Table 2.2. The same features have been identified in Table 2.3 for the most relevant wrist exoskeletons with three DOFs available in the literature and illustrated in Figure 2.16. The next list describes in detail the devices of Figure 2.16:

a) *Open Wrist* [19]: It is realized via a serial chain of three rotational joints and is actuated via a capstan-based cable transmission system. The device is an improved version of the Rice Wrist-S [20] exoskeleton: designed to be used on a bench, it can be worn more easily thanks to its open structure. The first joint is made by means of a semi-circular guide at the device bottom: the user can position the limb by inserting it from the device top. This exoskeleton can be integrated with the Maesto hand exoskeleton ensuring movement in the complete hand and wrist workspace. Other notable features

are: the usage of ideal pulleys, that keeps the drive system cables in tension maintaining contact points, the coating of components in polymer-ceramic material, the possibility of changing right or left hand configuration by easily reversing the components position, and the addition of a passive DOF to compensate for any misalignment.

b) *Rice Wrist-S* [20]: This exoskeleton is a serial mechanism with 3-DOFs designed for rehabilitation purposes; it produces sufficient torque values to simulate movements in the full workspace of the human wrist and ensures minimal backlash and inertial loads by actuating the RUD and FE joints using cable routing. This latter enables remote positioning of the actuators, minimizing gravitational and inertial loads acting on the user. The addition of a redundant DOF allows the resolution of any misalignment between the human and exoskeleton joints.

c) *MIT Wrist Robot* [21]: The exoskeleton has three active DOFs; it can be used as a stand alone device or mounted at the tip of the MIT MANUS, thus allowing five active (plus two passive) DOFs for the shoulder, elbow, and wrist. It has been designed as a desktop device and finds application in the rehabilitation of the upper limb, its structure being thought to be easily used by the therapist and patients. One important feature is the low endpoint impedance and hardware backdrivability: when a patient attempts to backdrive the robot, the effective friction, inertia, and stiffness are low enough to feel as if no robot is connected.

d) *Wrist Grimbal* [22]: This cable-driven exoskeleton has three active DOFs for the wrist joint rehabilitation. Its kinematics is similar to the Rice Wrist-S [20] and the IIT Wrist [23]. Wrist Grimbal has a high mechanical rigidity due to the use of support bearings to enable the implementation, testing, and acceptance in clinical settings. The joints stiffness is of particular interest in the rehabilitation field: indeed, the device must not flex during the simulation of a movement and must not transmit high forces on the human wrist, creating discomfort during motion. The majority of the parts have been manufactured in ABS with a 3D printer, to reduce the device costs and inertia, while keeping the structure as rigid as needed; whereas, the main frame has been produced in aluminium, building a lightweight but affordable structure.

e) *IIT Wrist* [23]: It consists of a serial kinematic chain implemented by four geared motors. The radial-elbow deviation movement is actuated by two motors coupled in parallel. The device allows the reproduction of the complete human wrist ROM, providing torque levels comparable to those of an adult subject's wrist. This solution emphasizes high backdrivability and ensures weight and inertia compensation to avoid muscle contraction or hypertonia in the user.

f) *Rice Wrist* [24]: The exoskeleton is a 4-DOFs device, made of one rotational DOF for the elbow and three revolute-prismatic-spherical serial-in-parallel kinematic chain for the wrist joint. It consists of a compact structure: a basic, fixed, platform is linked to another, movable, platform via three extensible links driven by direct-current actuators arranged along the links. The RiceWrist is designed to deliver kinesthetic feedback during motor skill training or rehabilitation of reaching movements, allowing easy measurement of human joint angles; its design permits the delivery of high torque and guarantees low friction, zero backlash and high stiffness characteristics.

g) *Wrist Robot* [25]: This exoskeleton allows the reproduction of the wrist three DOFs and, thanks to its backdrivability, ensures smooth haptic interaction between the robot and the patient, allowing for a more natural and responsive rehabilitation experience. Its primary goal is to provide kinesthetic feedback during the training of motor skills or the rehabilitation of reaching movements. The device mechanics and electronics are modular, to facilitate possible integration into a more comprehensive haptic bimanual arm-wrist-hand system with up to 12-DOFs. This flexibility allows for the potential expansion and customization of the system to meet more complex rehabilitation needs. Also, the scalable software architecture makes it easier to integrate additional functionalities or expand the system as needed.

h) *WristBot* [26]: This robot has been designed for applications in motor control and rehabilitation studies of the human wrist. It is fully backdrivable with 3-DOFs and has low inertia to emulate the fluency of natural movements. Each DOF can be actuated singularly or simultaneously to others, being measured by high resolution incremental encoders and actuated by one brushless motor or two, providing both gravity compensation and continuous torque values necessary to manipulate the human wrist joints.

The system, integrated with a VR environment, can be used in the active modality, requiring only the subject's active muscle work, or in the assistive/passive mode, which is implemented via a real-time impedance control scheme.

i) *M3Rob* [27]: This rehabilitation robot allows the simulation of the three active DOFs of the wrist, offering the possibility to move also the hand fingers. An additional prismatic passive joint allows adjustments depending on the user's forearm dimensions. The motors are strategically positioned to minimize gravitational and inertial loads, allowing for smoother independent axis movement and providing protection from external factors. By placing the actuators remotely, a cable routing and guidance system is employed to transmit motion to the joints, offering a dependable solution as long as the cable tension is properly maintained. Designed to perform ADLs, the device is portable and ergonomic, to be used at home and in clinics. The performance of active rehabilitation ensures accurate position feedback and precise measurements of force and torque thanks to the force/torque sensor in the handle.

l) *PowRobot* [28]: This low-cost, portable, 3-DOFs exoskeleton can be used both at home and physical therapy centres. Indeed, the whole robot system, which is used as a desktop device, is designed as a bag-like structure that can be easily transported. Direct-current motors are used for the actuation of each joint: the RUD is actuated by bevel gears, whereas the FE is powered via a belt-pulley mechanism. As most of the wrist exoskeletons, a passive DOF is included under the FE joint to avoid misalignment problems. Passive, active/assistive and active exercises can be performed within this system, which includes a force sensor for human-robot interaction during the therapy session.

m) *Gopura Exos* [29]: It is a 3-DOFs wrist exoskeleton actuated by direct-current motors and gear pairs. The last link of the device, i.e., the end-effector, is attached to the palm of the user and is equipped with a force sensor. The robot potential control methods are force control, using force/torque sensors located at wrist and forearm, and electromyographic signals based control, using skin surface signals of forearm and wrist muscles.

n) *WRES* [10]): This wrist exoskeleton has three rotational DOFs; it is realized via a serial spherical mechanism of three revolute joints and is actuated via a cable drive system. The first joint allows the PS wrist movement, the second and third joints reproduce the RUD and FE movements respectively. The device is characterized by a simple setup: it is easy to wear thanks to its open structure and the lateral arrangement of its components; adjustable straps allow the centring of the axes of the human wrist joint with those of the exoskeleton. The mechanical design is intended to make the exoskeleton usable in rehabilitation, but also for other activities such as teleoperation and interaction with virtual environments. Aspects such as integrability with exoskeletons of the hand and upper limb to create a complete exoskeleton system capable of performing bimanual tasks led to the definition of stringent requirements in terms of compactness and bulkiness. Characterized by features such as high transparency and low weight, the WRES was designed to be mounted on the upper limb exoskeleton ALEx [11] and to accommodate the hand exoskeleton realized in the PERCRO laboratory [32]. The complete robotic arm thus realized allows the free reproduction of bimanual tasks: bringing the user's arms closer until the hands touch allows interaction with real or virtual objects.

Within this context, the present thesis aimed at developing a wrist exoskeleton to overcome limitations of the current devices. A detailed discussion of the above-mentioned exoskeletons has been provided in Chapter 4, to support the development of the proposed, novel, device.

Chapter 3

SEES: Shoulder-Elbow ExoSkeleton

This Chapter aims to present a versatile, fast and efficient methodology to design an accurate and light, wearable 6-DOFs passive shoulder-elbow exoskeleton capable of keeping a good alignment with the human body and to compensate for the gravity loads through the use of passive elements only. By pursuing features such as lightness and accuracy, the proposed device has been designed for the industrial sector, but may become useful also in the medical field, e.g., for treating patients with neuromuscular diseases and for rehabilitation [61, 62].

3.1. Project Requirements

Focusing on industrial workers forced to perform repetitive overhead tasks every day, this chapter aims to design a passive shoulder-elbow exoskeleton that conforms to the following specifications:

1. *ROM*: The device ROM must to fulfil the one of the natural human upper limb, allowing the simulation of typical industrial overhead tasks. To check that the complete upper limb workspace can be reached, three specific law of motions have been chosen and reported in Table 3.2 (see the kinematic model of Section 3.5.1 for explanations on each parameter set).

2. *Maximum load to be balanced*: The exoskeleton, being fully passive, need to balance at least the weight of the user's arm (around $3.3\ kg$), and its own weight. Then, a load to be lifted can be added depending on the application.

3. *Compactness and lightness*: The system ought to be manoeuvrable, minimizing its encumbrance, and light, since its weight is completely carried by the user.

4. *Agility and portability*: The exoskeleton has to be easy to be worn and carried, allowing the user to move without obstructions in the industrial environment.

5. *Reduced costs and number of components*: The system need to be competitive on the market offering a performing and affordable, but also simple and low-cost product to find application in the industrial sector.

These challenging specifications have been tackled exploiting advanced tools, aiming at optimally design a product that can be custom depending on the needs.

3.2. Design Considerations

Given the design principles reported in Section 2.3.2, the exoskeleton design is strongly influenced by the biomechanics of the human body, especially for upper limbs exoskeletons, owing to the small size and wide ROM of the limb itself [63]. A kinematic chain that correctly reproduces the human limb DOFs may be employed, allowing the exoskeleton to properly follow the human body movements avoiding the generation of undesired forces [64, 65]. The choice on how to represent the kinematics of the shoulder need to be evaluated in detail. In the literature, several configurations are studied, ranging from the simple ball-and-socket joint [9] to serial chains of Revolute (R) joints, like, for example, 3R [61, 66], 4R or 5R [65, 67, 68]. The usage of a serial chain allows for accurately reproducing the motion trajectory of the shoulder centre of rotation, whereas the inclusion of extra DOFs overcomes possible singularity configurations [67, 68].

To the best of the authors' knowledge, few 6-DOFs passive upper limbs exoskeletons have been designed in academia or industry. For instance, a recent study developed a 6-DOFs exoskeleton conceived as a hybrid device that reaches the static balancing via the combined action of direct current motors and springs [30] (Figure 3.1a). In this case, passive elements partly support the gravitational load so that motors become necessary to reach a complete equilibrium. Within the present paper, the pursuit of a full passive balancing provides the exoskeleton compactness improvement, reducing its weight and cost, similarly to [69]. However, the type of achievable tasks is limited since the exoskeleton design strongly depends on the performed movement. In fact, due to the complexity of compensating for the gravity load of a device without any active component, usually, passive exoskeletons available in the literature are designed for a specific motion and with a low number of DOFs (e.g., Figure 3.1b [31]).

Figure 3.1: Upper limb exoskeletons examples from the literature with passive springs. ***a)*** *6-Degrees Of Freedom (DOFs) hybrid shoulder-elbow exoskeleton [30].* ***b)*** *1-DOF passive shoulder exoskeleton [31].*

In this context, a design tool leveraging a comprehensive analytical model and allowing the computation of optimal exoskeleton parameters for a given set of design requirements (i.e., performed movement, user's upper limb mass and dimensions) is proposed. Building on such a model, the correct spring dimensioning can be achieved via an efficient optimization process for each movement in the human upper limb workspace. To clarify the capabilities of the proposed methodology, the current work presents a 6-DOFs passive exoskeleton designed for three overhead motions, the configuration of the springs being optimal for one specific movement only. However, the exoskeleton is verified to keep a reasonable level of balance for the remaining movements. During the tests, a single set of anthropometric parameters (taken from the literature) has been assigned to the exoskeleton, although the proposed parametric model can be rapidly updated to match different design inputs.

3.3. System Overview

Figure 3.2 shows the novel portable upper limb 6-DOFs exoskeleton (5-D0Fs for the shoulder joint (two displacements plus three rotations), 1-DOF for the elbow joint) conceived to mediate between motion capabilities and lightweight [70]. The exoskeleton is designed based on the human upper limb kinematics and ROM to keep good alignment during the upper limb motion [71]. The exoskeleton main features are compactness, agility and reduced total weight; its primary aim is to support the human upper limb gravitational load acting on each joint. The static balancing is achieved via the action of passive elements only, and, depending on the type of balancing springs which are implemented, the device consists in

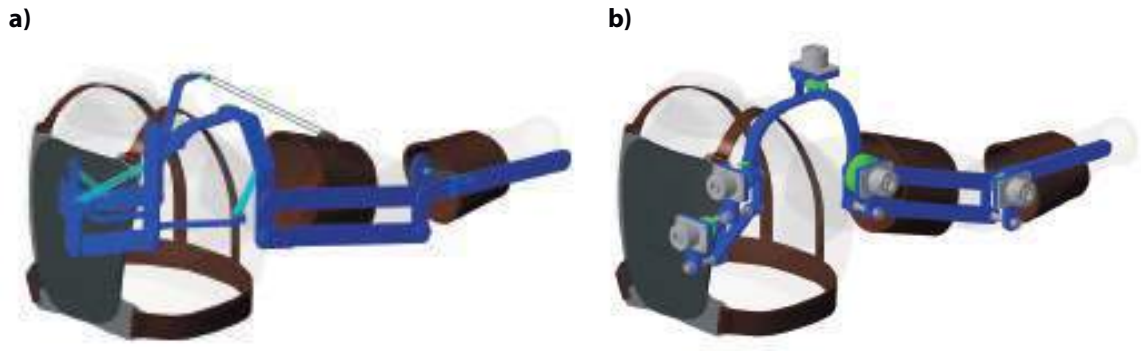

Figure 3.2: Passive 6-degrees of freedom Shoulder-Elbow ExoSkeleton (SEES) Computer Aided Design (CAD) model. Two configurations: ***a)*** *SEES balanced via five elastic bands (light blue elements);* ***b)*** *SEES balanced through five torsional springs (green elements). For each spring, the grey elements are commercial bi-direction clutches to provide the desired preload.*

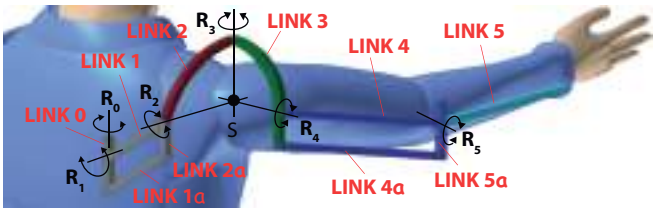

Figure 3.3: 6-Degrees of freedom exoskeleton kinematic model: six Revolute (R) joints (R_0, R_1, R_2, R_3, R_4, R_5), six main links ($0, 1, 2, 3, 4, 5$), four auxiliary links ($1a, 2a, 4a, 5a$).

two configurations: the exoskeleton can be balanced via linear springs (Figure 3.2a), or torsional springs (Figure 3.2b). Note that, similarly to existing commercial exoskeletons [72], elastic bands are used instead of classic linear springs (Figure 3.2a, light blue components), and custom torsional springs are implemented for each exoskeleton DOF (Figure 3.2b, green elements) [73].

The exoskeleton schematic model is illustrated in Figure 3.3: six main links are connected to form a kinematic serial chain with 6R joints. Then, extra links ($1a, 2a, 4a, 5a$) are added to obtain two decoupling systems (grey and blue parallelogram mechanisms), which make the rotations of R_1, R_2 and R_4, R_5 joints independent [74]. The overall structure is wearable and fixed on the operator's back through straps, whereas the human arm and forearm are attached to link 4 and link 5 with two holders (Figure 3.2).

The detailed design elements of the exoskeleton have been chosen so as to reduce the weight of structure at best and maximize the gravity compensation accuracy. Thus, the rest of this chapter focuses on the next main points:

- The development of a comprehensive, parametric, and accurate 6-DOFs exoskeleton analytical model to study the exoskeleton behaviour for different users' features within the overall workspace.
- The establishment of a versatile and efficient tool to help the designer in the preliminary design stage to evaluate the optimal exoskeleton configuration.
- The proposal of a first prototype, including custom and commercial elements, designed and optimally sized exploiting the developed methodology.

The first point includes the exoskeleton static analysis by considering the gravitational load acting on each joint due to both the human upper limb and the exoskeleton weights. After, the passive balancers theory is exploited to assess correct stiffness and position of each spring. In the present case, R_0 is not compensated, being fixed to the exoskeleton chassis, and it is assumed to have a constantly vertical oriented axis (Figure 3.3). If using linear springs, R_1 and R_5 joints are balanced through the classic 1-DOF balancer [75], whereas, due to the complexity of the considered 6-DOFs exoskeleton model that includes the user's limb, the shoulder joint (i.e., the kinematic chain involving R_2, R_3, R_4) is balanced through the development of a novel 3-DOFs balancer model. Specifically, the static balancing is reached by five linear springs [76]. Considerations on the choice of the spring type usage (Zero Free Length (ZFL) or Non-Zero Free Length (NZFL)) and materials are made to realize the first prototype of the exoskeleton. Also, for practicability, the implementation of torsional springs is considered instead of linear elements. In this case, each R joint of the SEES can be balanced by a spring centred in the joint itself and specifically preloaded.

3.4. Background on Passive Balancers

This work started from the balancer models shown in Figure 3.4 to reach the exoskeleton static balancing.

3.4.1. Linear Spring 1-DOF Balancer

The 1-DOF balancer [75] consists of one linear spring and one link of null density with an external mass m placed at a distance a from the R joint (Figure 3.4a). The static balancing

can be achieved via the use of a classic linear spring, as clearly explained in [30, 75]: the resultant gravity torque M that need to be externally provided in R is calculated via Eq. 3.1, and the balancing torque, including the spring stiffness constant, is determined as in Eq. 3.2:

$$M = mga\sin(\theta) \tag{3.1}$$

$$\begin{cases} M_k = kbe\left(1 - \frac{d_0}{d}\right)\cos(\theta) \\ k = \frac{mga}{be\left(1-\frac{d_0}{d}\right)} \\ d = \sqrt{b^2 + e^2 - 2be\cos(\theta)} \end{cases} \tag{3.2}$$

where m is the external mass, g is the gravity acceleration, a is the mass lever-arm. Concerning the spring configuration shown in Figure 3.4a, $b,\ e$ are the installation distances and $d,\ d_0$ are the final and initial lengths, being d defined through the cosine theorem. By considering the condition $|2be/(b^2 + e^2)| \leq 1$, the formulation of d becomes $d = \sqrt{b^2 + e^2}$, losing the θ dependence. The generic case of a NZFL spring can be simplified under the assumption of ZFL springs, where $d_0 = 0\ mm$.

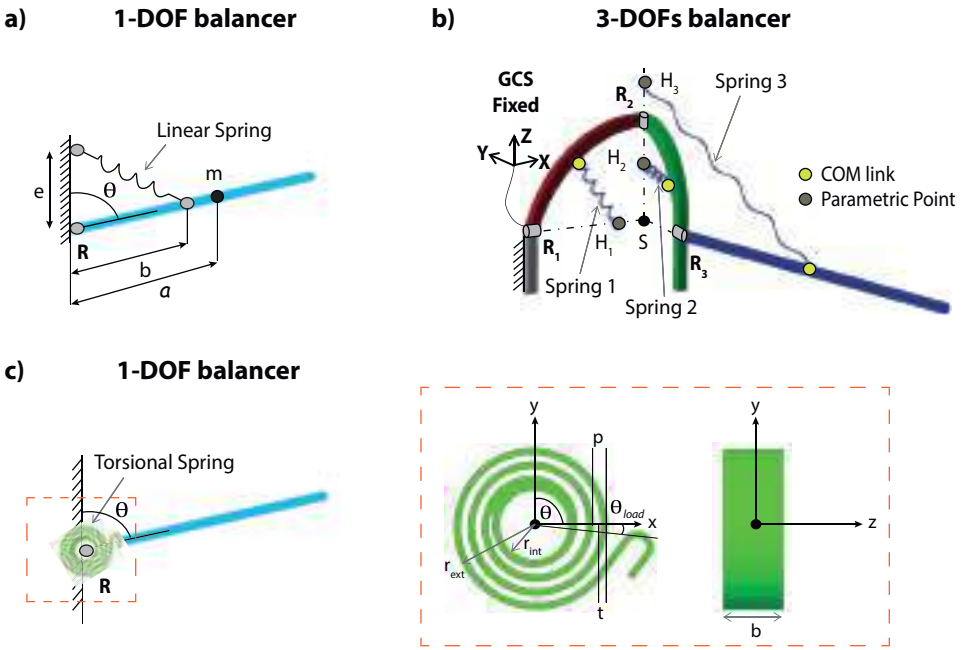

Figure 3.4: Passive balancers. ***a)*** *Linear spring: 1-Degree Of Freedom (DOF) architecture (Revolute (R) joint).* ***b)*** *Linear springs: 3-DOFs architecture (3R joint).* ***c)*** *Torsional spring: 1-DOF architecture (R joint).*

3.4.2. Linear Springs 3-DOFs Balancer

Figure 3.4b shows the spherical 3-DOFs balancer described in [77]. It is realized with a three links kinematic chain fixed to a frame: the 3R axes intersect in the joint centre of rotation (point S, fixed in the design space). The static balancing is achieved using three springs, one for each link. Every spring is connected between the link Centre Of Mass (COM) and a parametric point $H_i = [h_{ix};\ h_{iy};\ h_{iz}]$ ($i \in [1,3]$), expressed in the fixed GCS. As outlined in [77], the system is statically balanced when $H_1 = [h_{1x};\ 0;\ m_1 g/k_1]$, $H_2 = [0;\ 0;\ m_2 g/k_2]$ and $H_3 = [0;\ 0;\ m_3 g/k_3]$, where $k_i,\ m_i$ ($i \in [1,3]$) are the springs constants and the links masses respectively. Thus, spring 1 parametric point (H_1) can be at any point of the GCS (x, z) plane, whereas the other parametric points ($H_2,\ H_3$) lye on the vertical axis passing through the spherical joint centre of rotation (point S).

3.4.3. Torsional Spring 1-DOF Balancer

A practical solution for the 1-DOF balancer can be featured by using torsional springs, like in e.g., [73]. In this case, as shown in Figure 3.4c, the position of the spring is constrained, being centred into the R joint of interest, and its end is fixed to the link free of rotating around the R joint. The static balancing is reached thanks to the torque provided by the deformation of the spring during the motion and computed as in Eq. 3.3:

$$M_t = k_t(\triangle\theta_i - \theta_{i,load}) \tag{3.3}$$

where k_t is the torsional spring coefficient, $\triangle\theta_i$ is the angular ROM, and $\theta_{i,load}$ is the spring preload (i.e., the position of the spring in the initial configuration).

In [73], an interesting method to optimally size the spring is presented, where the stress generated by the spring deformation must not exceed the limit set by the material used to prototype the spring. The main parameters involved in the spring design are: the spring width b (along the z-axis), thickness t, initial position θ_{load}, the internal and external radius r_{int} and r_{ext}. Also, the effective spiral length L_e, which depends on the spiral pass p and the spring number of coils n_c, need to be considered. Indeed, the stiffness constant of the spring k_t can be computed as in Eq. 3.4:

$$k_t = \frac{Ebt^3}{12L_e} \tag{3.4}$$

being E the material Young modulus.

The stress due to the spring deformation is defined as in Eq. 3.5:

$$\sigma = \frac{6M_t}{bt^3} \tag{3.5}$$

being M_t computed as in Eq. 3.3.

So, by following the theoretical methodology presented in [73], a torsional spring can be optimally sized achieving a specific stiffness, not exceeding the material yield stress, and respecting specific space constraints.

3.5. SEES Virtual Prototyping

This section presents the proposed exoskeleton analytical model. The exoskeleton functional schematic is shown in Figure 3.5a, and the considered geometrical and mass parameters are listed in Table 3.1. These have been defined in accordance with a male user, whose body mass and height are $80\ kg$ and $1.8\ m$ [71]. However, the model is fully parametric, so as it can be customized as desired. The masses m_1 and m_2 represent the human arm and forearm, whereas the remaining masses are related to the exoskeleton parts. In particular, a density of 2700 kg/m^3 (Aluminium alloy) is assigned to each link. The exoskeleton initial configuration, namely the one visible in Figure 3.5a, is reported in Table 3.2 in terms of joints positions θ_i. The same table provides the rotation assigned to each R joint to generate the three movements considered in the study and shown in Figure 3.5b. For the sake of clearness, the imposed movements start from the upper limb forward extension, although any other configuration within the exoskeleton workspace can be utilized as the exoskeleton initial position. Concerning Figure 3.5a, the GCS is placed at the origin of the kinematic chain, whereas the GCS_2 is fixed to link $2a$ at the beginning of the spherical joint (R_2, R_3, R_4). The local systems CS_n ($n \in [0, 5]$) are placed in the centre of each R joint, with axes having the directions of the GCS axes. Note that $CS_{4'}$ and $CS_{5'}$ are rotated so as their x-axis is aligned with links 4 and link 5 respectively.

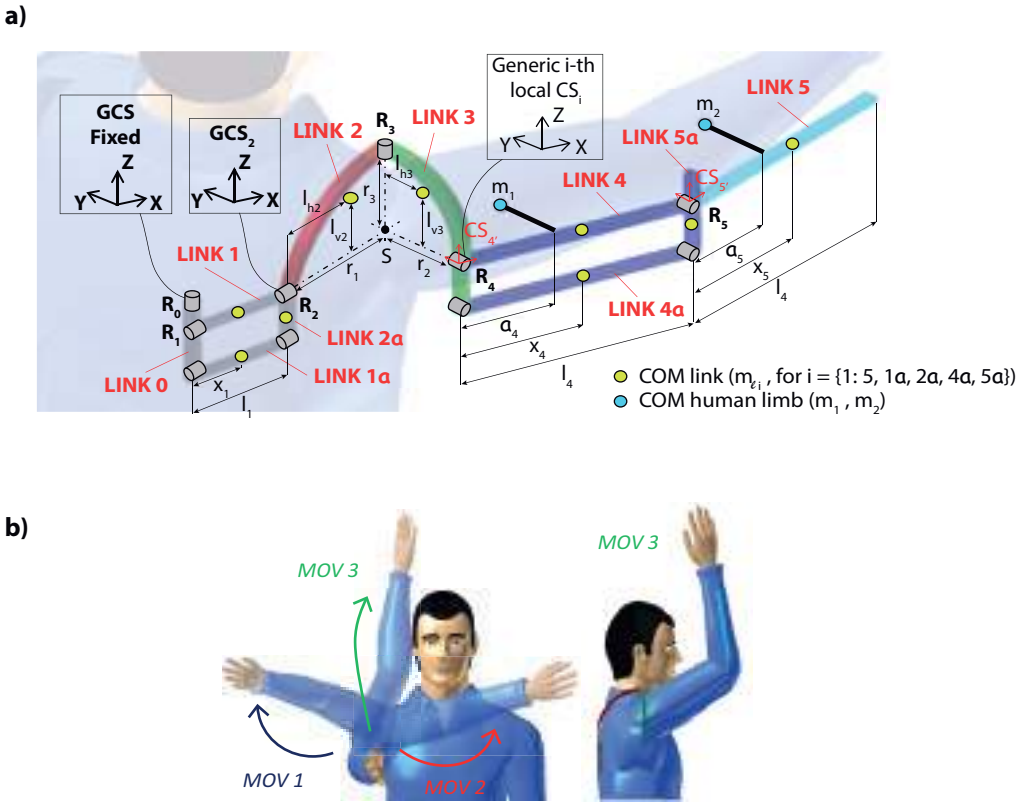

Figure 3.5: ***a)*** *Shoulder-elbow exoskeleton parametric model (initial configuration).* ***b)*** *Simulated movements: starting from the upper limb initial position in forwarding extension, the first movement (MOV 1) consists in the upper limb opening, the second (MOV 2) in the closure towards the chest, and the third (MOV 3) in the upward lift with the bent elbow (in detail on the right).*

3.5.1. Kinematic Analysis

The exoskeleton kinematic model has been developed to know the position of the end-effector during an imposed movement. Referring to the well-known theory and exploiting the DH method [78], the homogeneous matrix A_i ($i \in [1, 5]$) is defined as follows:

$$A_i = \begin{bmatrix} r_{11} & r_{12} & r_{13} & q_x \\ r_{21} & r_{22} & r_{23} & q_y \\ r_{31} & r_{32} & r_{33} & q_z \\ 0 & 0 & 0 & 1 \end{bmatrix} \tag{3.6}$$

where A_i is the matrix that relates the reference system i and the reference system $i-1$; $A_i(1:3, 1:3) = A_{i,rot}$ is the rotation matrix; $A_i(1:3, 4) = A_q$ is the translation vector (by convention, the notation $A(rows, columns)$ is for selecting the number of $rows$ and

$columns$ of interest, thus, extracting a sub-matrix from the matrix A).

The end-effector position in the GCS is defined bt the vector $Q = [X; Y; Z; 1]$ and is computed as in Eq. 3.7:

$$Q = Aq^6 \tag{3.7}$$

where $q^6 = [0; 0; 0; 1]$ is the vector position of the end-effector in the local CS_6, and A is the total transformation matrix from the CS_5 to the GCS, being computed as follows:

$$A = A_0 A_1 A_2 A_3 A_4 A_5 \tag{3.8}$$

where A_i, $i \in [1, 5]$ is the homogeneous matrix for the transformation from the CS_i to the CS_{i-1}.

Table 3.1: Main shoulder-elbow exoskeleton geometrical and mass parameters (the definition of each parameter is provided in Figure 3.5a).

LINK 1	*LINK 2*	*LINK 3*
$l_1 = 121\ mm$	$r_1 = 125\ mm$	$r_2 = 75\ mm$
$x_1 = 0.5\ l_1$	$r_3 = 95\ mm$	$r_3 = 95\ mm$
$m_{\ell 1} = 0.035\ kg$	$l_{h2} = 52\ mm$	$l_{h3} = 57\ mm$
	$l_{v2} = 61\ mm$	$l_{v3} = 54\ mm$
	$m_{\ell 2} = 0.051\ kg$	$m_{\ell 3} = 0.062\ kg$
LINK 4	*LINK 5*	*UPPER LIMB*
$l_4 = 307\ mm$	$l_5 = 225\ mm$	$a_4 = 0.44\ l_4$
$x_4 = 0.5\ l_4$	$x_5 = 0.5\ l_5$	$m_1 = 2.1\ kg$
$m_{\ell 4} = 0.085\ kg$	$m_{\ell 5} = 0.063\ kg$	$a_5 = 0.425\ l_5$
		$m_2 = 1.2\ kg$

Table 3.2: Shoulder-elbow exoskeleton parameters in terms of angular positions for each Revolute (R) joint R_i ($i \in [1, 5]$) of the exoskeleton. $\theta_{0,i}$ is the position of each R_i joint when the exoskeleton is in the initial configuration (as showed in Figure 3.5a); $\triangle\theta_i$ is the angle range covered by each R_i joint during the imposed movements (MOV 1, MOV 2, MOV 3, as illustrated in Figure 3.5b).

JOINT R_i	*INITIAL POSITION* $\theta_{0,i}[deg]$	*MOV 1* $\triangle\theta_i[deg]$	*MOV 2* $\triangle\theta_i[deg]$	*MOV 3* $\triangle\theta_i[deg]$
R_0	0	-5	10	0
R_1	-38	-10	-10	-15
R_2	0	-20	-15	-5
R_3	0	-40	35	15
R_4	106	-20	-30	-45
R_5	90	-10	-25	-100

Depending on the exoskeleton kinematics, each matrix defined in Eq. 3.8 is formulated as in the next equations:

$$A_0 = \begin{bmatrix} \cos\theta_0 & -\sin\theta_0 & 0 & 0 \\ \sin\theta_0 & \cos\theta_0 & 0 & 0 \\ 0 & 0 & 1 & 0 \\ 0 & 0 & 0 & 1 \end{bmatrix} \tag{3.9}$$

$$A_1 = \begin{bmatrix} 1 & 0 & 0 & 0 \\ 0 & 1 & 0 & -l_1\cos\theta_1 \\ 0 & 0 & 1 & -l_1\sin\theta_1 \\ 0 & 0 & 0 & 1 \end{bmatrix} \tag{3.10}$$

$$A_2 = \begin{bmatrix} 1 & 0 & 0 & r_1 \\ 0 & \cos\theta_2 & -\sin\theta_2 & -r_3\sin\theta_2 \\ 0 & \sin\theta_2 & \cos\theta_2 & r_3\cos\theta_2 \\ 0 & 0 & 0 & 1 \end{bmatrix} \tag{3.11}$$

$$A_3 = \begin{bmatrix} \cos\theta_3 & -\sin\theta_3 & 0 & r_2\sin\theta_3 \\ \sin\theta_3 & \cos\theta_3 & 0 & -r_2\cos\theta_3 \\ 0 & 0 & 1 & -r_3 \\ 0 & 0 & 0 & 1 \end{bmatrix} \tag{3.12}$$

$$A_4 = \begin{bmatrix} 1 & 0 & 0 & l_4\sin\theta_4 \\ 0 & 1 & 0 & 0 \\ 0 & 0 & 1 & l_4\cos\theta_4 \\ 0 & 0 & 0 & 1 \end{bmatrix} \tag{3.13}$$

$$A_5 = \begin{bmatrix} \cos\theta_5 & 0 & \sin\theta_5 & l_5\sin\theta_5 \\ 0 & 1 & 0 & 0 \\ -\sin\theta_5 & 0 & \cos\theta_5 & l_5\cos\theta_5 \\ 0 & 0 & 0 & 1 \end{bmatrix} \tag{3.14}$$

where $r_1,\ r_2,\ r_3,\ l_1,\ l_4,\ l_5$ are geometric parameters from Table 3.1, and θ_i ($i \in [1,5]$) is the angular rotation of the exoskeleton R_i joint.

Referring to Table 3.2, it is worth noting that the SEES final configuration θ_i ($i \in [1,5]$) in terms of joint rotations is defined as in Eq. 3.15:

$$\theta_i = \theta_{0,i} + \triangle\theta_i, \ _{i\in [1,5]} \tag{3.15}$$

where $\theta_{0,i}$ ($i \in [1,5]$) is the initial position of the joint R_i, and $\triangle\theta_i$ is the variation angle from the initial to the final time of the imposed motion.

Equation 3.10 and Eq. 3.13 do not involve a rotational contribution when passing from the CS_1 to the CS_0 and from the CS_4 to the CS_3. This happens due to the SEES structure involving two decoupling systems (grey and blue parallelogram mechanisms, Figure 3.5). The link 1 rotation θ_1 does not influence the angular position of the rest of the mechanism. Indeed, the link 2a is always in vertical position, regardless the SEES configuration, and it translates only. This is highlighted by the rotation matrix, which is an identity matrix, and the translation vector of Eq. 3.10. The same happens for the decoupling system involving link 4 and link 4a (see Eq. 3.13).

Given an initial configuration and assigning a specific motion law according to the parameters reported in Table 3.2, the SEES assumes a specific position in the 3D space. Figure 3.6 shows the workspace of the exoskeleton; in this case, for visualization purpose, it has been assumed a value of θ_5 equal to $\theta_{0,5}$.

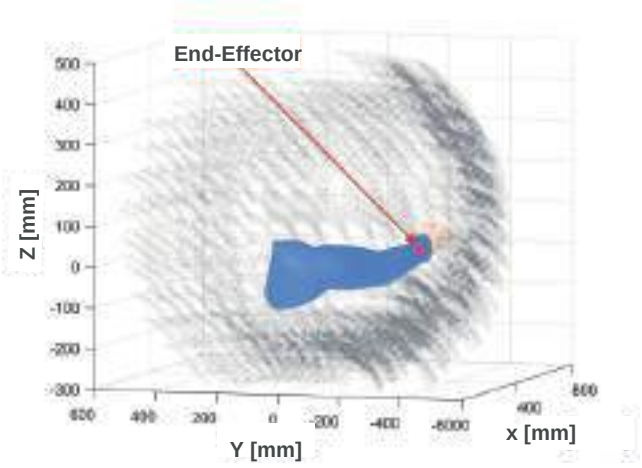

Figure 3.6: Shoulder-elbow exoskeleton workspace: position of the end-effector in the 3-dimensional space (X, Y, Z axes).

3.5.1.1. Numerical Validation

Figure 3.7 reports the position of the end-effector in the GCS for each imposed movement (MOV 1, MOV 2, MOV 3, Table 3.2, Figure 3.5). Theoretical equations have been implemented in the software *Matlab* and validated in the software *RecurDyn* (a commercial multi-body solver capable of performing kinetic-dynamic analyses of complex systems starting from their CAD representation [79]). Each plot shows the position of the end-effector (i.e., its displacements in terms of the GCS x-, y-, z-axis) over the imposed movement (the motion is considered in its percentage progress), that overlaps for both software, thus, validating the SEES kinematic model.

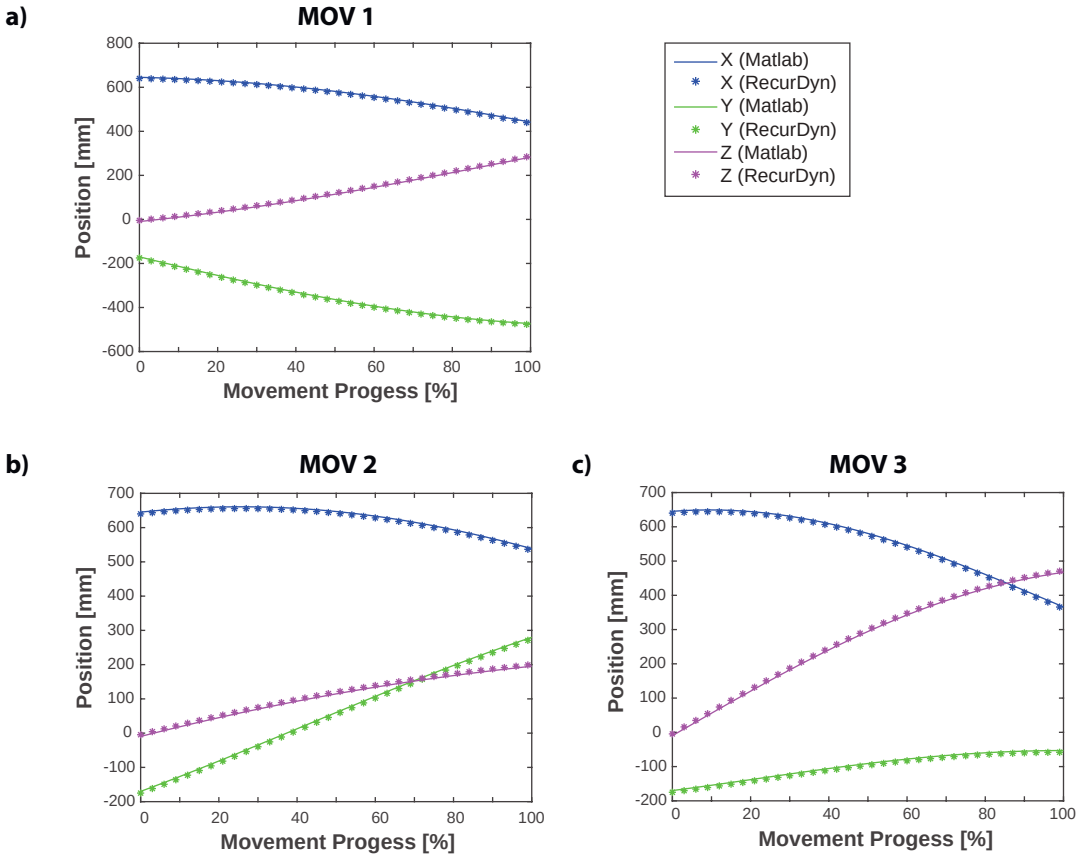

Figure 3.7: Kinematics validation of the shoulder-elbow exoskeleton: Matlab vs RecurDyn results. End-effector X, Y, Z position [mm] during the movement progress [%] with respect to the Global Coordinate System (GCS) for the three simulated movements: ***a)*** *MOV 1,* ***b)*** *MOV 2,* ***c)*** *MOV 3.*

3.5.2. Static Analysis

A parametric, static, model has been developed to compute, for a generic exoskeleton configuration, the resulting reaction torque at each R joint. This preliminary analysis is conducted by considering the human upper limb and the exoskeleton weight as the only external forces acting on the system, i.e., by neglecting other possible contributions. The model can be easily updated based on the user upper limb features and the investigated task. For instance, additional mass can be included when simulating the lifting operation of heavy components.

3.5.2.1. Gravity Torque Calculation

Let one define the variable θ_i as the generic R_i joint position. The gravity torque for each R_i ($i \in [1,5]$) joint (as already specified, there is no gravity torque in R_0) is computed by evaluating the mass lever-arm for each contribution (i.e., the horizontal h_i and vertical v_i component for the mass i). The analysis can be simplified for the gravity torque calculation in $R_3,\ R_4,\ R_5$, involving the matrices $A_2,\ A_3,\ A_4,\ A_5$, which depend on the R_i rotation θ_i ($i \in [2,5]$) [78], as studied in Section 3.5.1 (from Eq. 3.11 to Eq. 3.14). The force vector $f_{i,GCS} = [0;\ 0;\ -m_i g]$ ($i = \{1,2,\ell3,\ell4,\ell5,\ell4a,\ell5a\}$) defines the gravitational load for each mass $m_1,\ m_2,\ m_{\ell3},\ m_{\ell4},\ m_{\ell5},\ m_{\ell4a},\ m_{\ell5a}$ in GCS. Being $f_{i,CS_n} = [f_{ix,CS_n};\ f_{iy,CS_n};\ f_{iz,CS_n}]$ the force vector due to the mass i in CS_n, the resultant gravity forces with respect to the local CS_n ($n \in [3,5]$) are defined as in Eq. 3.16, Eq. 3.17, Eq. 3.18:

$$f_{i,CS_3} = (A_2 A_3)^T f_{i,GCS},\ _{i=\{1,2,\ell3,\ell4,\ell5,\ell4a,\ell5a\}} \tag{3.16}$$

$$f_{i,CS_4} = (A_2 A_3 A_4)^T f_{i,GCS},\ _{i=\{1,2,\ell4,\ell5,\ell4a,\ell5a\}} \tag{3.17}$$

$$f_{i,CS_5} = (A_2 A_3 A_5)^T f_{i,GCS},\ _{i=\{2,\ell5\}} \tag{3.18}$$

where the gravitational load of $m_2,\ m_{\ell5}$ is involved in Eq. 3.16, Eq. 3.17, Eq. 3.18, the one of $m_1,\ m_{\ell4},\ m_{\ell4a},\ m_{\ell5a}$ compares on both Eq. 3.16, Eq. 3.17, and the one of $m_{\ell3}$ is only in Eq. 3.16. Also, Eq. 3.16 is function of $\theta_2,\ \theta_3$, Eq. 3.17 of $\theta_2,\ \theta_3,\ \theta_4$, and Eq. 3.18 of $\theta_2,\ \theta_3,\ \theta_5$.

Referring to Figure 3.5 and Table 3.1, the following equations provide the gravity torque

for each R_i ($i \in [1,5]$) joint: the gravity torques in R_1, R_2 are given by Eq. 3.19, Eq. 3.20; multiplying the force vector (Eq. 3.16, Eq. 3.17, Eq. 3.18) by the lever-arm of each mass, the resultant gravity torques at $R_3,\ R_4,\ R_5$ are as in Eq. 3.21, Eq. 3.22, Eq. 3.23:

$$M_1 = \left[x_1 \left(m_{\ell 1} + m_{\ell 1a} \right) + l_1 \sum_i m_i \right] g \cos\left(\theta_1\right), \ _{i=\{\ell 2,\ell 3,\ell 4,\ell 5,\ell 2a,\ell 4a,\ell 5a,1,2\}} \tag{3.19}$$

$$\begin{aligned} M_2 = g \sum_i h_{2,i} m_i + r_2 \cos\left(\theta_2\right) \cos\left(\theta_3\right) g \sum_{ii} m_{ii} + [l_{h3} \cos\left(\theta_2\right) \cos\left(\theta_3\right) + \\ + \left(r_3 - l_{v3}\right) \sin\left(\theta_2\right)] m_{\ell 3} g + l_{v2} \sin\left(\theta_2\right) m_{\ell 2} g, \ _{i=\{1,2,ii\},\ ii=\ \{\ell 4,\ell 5,\ell 4a,\ell 5a\}} \end{aligned} \tag{3.20}$$

$$\begin{aligned} M_3 = \sum_{i=\ell 4,\ell 5,\ell 4a,\ell 5a} \left(\sqrt{{v_{3,i}}^2 + {h_{3,i}}^2} f_{iy,CS_3} + r_2 f_{ix,CS_3} \right) + \\ + \sum_{i=1,2} \left(\sqrt{{v_{3,i}}^2 + {h_{3,i}}^2} f_{iy,CS_3} \right) + l_{h3} f_{\ell 3x,CS_3} \end{aligned} \tag{3.21}$$

$$M_4 = x_4 \sum_{i=\ell 4,\ell 4a} f_{ix,CS_4} + l_4 \sum_{i=2,\ell 5,\ell 5a} f_{ix,CS_4} + a_4 f_{1x,CS_4} \tag{3.22}$$

$$M_5 = a_5 f_{2x,CS_5} + x_5 f_{\ell 5x,CS_5} \tag{3.23}$$

where:

- The geometric quantities are defined in Table 3.1.
- Concerning Eq. 3.19, x_1 and l_1 are the lever-arms with respect to R_1 of the masses $m_{l1},\ m_{l1a}$ and of the masses m_i ($i = \{\ell 2, \ell 3, \ell 4, \ell 5, \ell 2a, \ell 4a, \ell 5a, 1, 2\}$).

- Concerning Eq. 3.20, regarding Figure 3.8a:

$$\begin{cases} h_{2,i} = j\rho_i \cos\left(\theta_2 + \arctan\left(-\frac{v_{4,i}}{h_{3,i}}\right)\right) \\ \rho_i = \sqrt{{h_{3,i}}^2 + {v_{4,i}}^2}, \ i=\{1,\ell4,\ell4a,\ell5a\} \end{cases}$$

$$\begin{cases} h_{2,i} = j\rho_i \cos\left(\theta_2 + \arctan\left(-\frac{v_4+v_{5,i}}{h_{3,i}}\right)\right) \\ \rho_i = \sqrt{{h_{3,i}}^2 + \left(v_4 + v_{5,i}\right)^2}, \ i=\{2,\ell5\} \end{cases}$$

$$j = 1 \text{ for } \triangle\theta_3 \geq 0; \ j = -1 \text{ for } \triangle\theta_3 \leq 0$$

- Concerning Eq. 3.20, Eq. 3.21, Eq. 3.22:
  - $h_{3,i}$, $v_{3,i}$ are referred to Figure 3.8b and defined as:

$$\begin{aligned} h_{3,1} &= h_{4,1}\sin(\theta_3) & v_{3,1} &= h_{4,1}\cos(\theta_3) \\ h_{3,2} &= (h_4 + h_{5,2})\sin(\theta_3) & v_{3,2} &= (h_4 + h_{5,2})\cos(\theta_3) \\ h_{3,\ell4} &= h_{3,\ell4a} = h_{4,\ell4}\sin(\theta_3) & v_{3,\ell4} &= v_{3,\ell4a} = h_{4,\ell4}\cos(\theta_3) \\ h_{3,\ell5} &= (h_4 + h_{5,\ell5})\sin(\theta_3) & v_{3,\ell5} &= (h_4 + h_{5,\ell5})\cos(\theta_3) \\ h_{3,\ell5a} &= h_4\sin(\theta_3) & v_{3,\ell5a} &= h_4\cos(\theta_3) \end{aligned}$$

  - $h_{4,i}$, $v_{4,i}$, $h_{5,i}$, $v_{5,i}$ are illustrated in Figure 3.8b, Figure 3.8c and formulated as:

$$\begin{aligned} h_4 &= l_4\sin(\theta_4) & v_4 &= -l_4\cos(\theta_4) \\ h_{4,1} &= a_4\sin(\theta_4) & v_{4,1} &= -a_4\cos(\theta_4) \\ h_{4,\ell4} &= x_4\sin(\theta_4) & v_{4,\ell4} &= -x_4\cos(\theta_4) \\ v_{4,\ell4a} &= v_{4,\ell4} + l_{5a} & v_{4,\ell5a} &= v_4 + l_{v5a} \\ h_{5,2} &= a_5\sin(\theta_5) & v_{5,2} &= -a_5\cos(\theta_5) \\ h_{5,\ell5} &= x_5\sin(\theta_5) & v_{5,\ell5} &= -x_5\cos(\theta_5) \end{aligned}$$

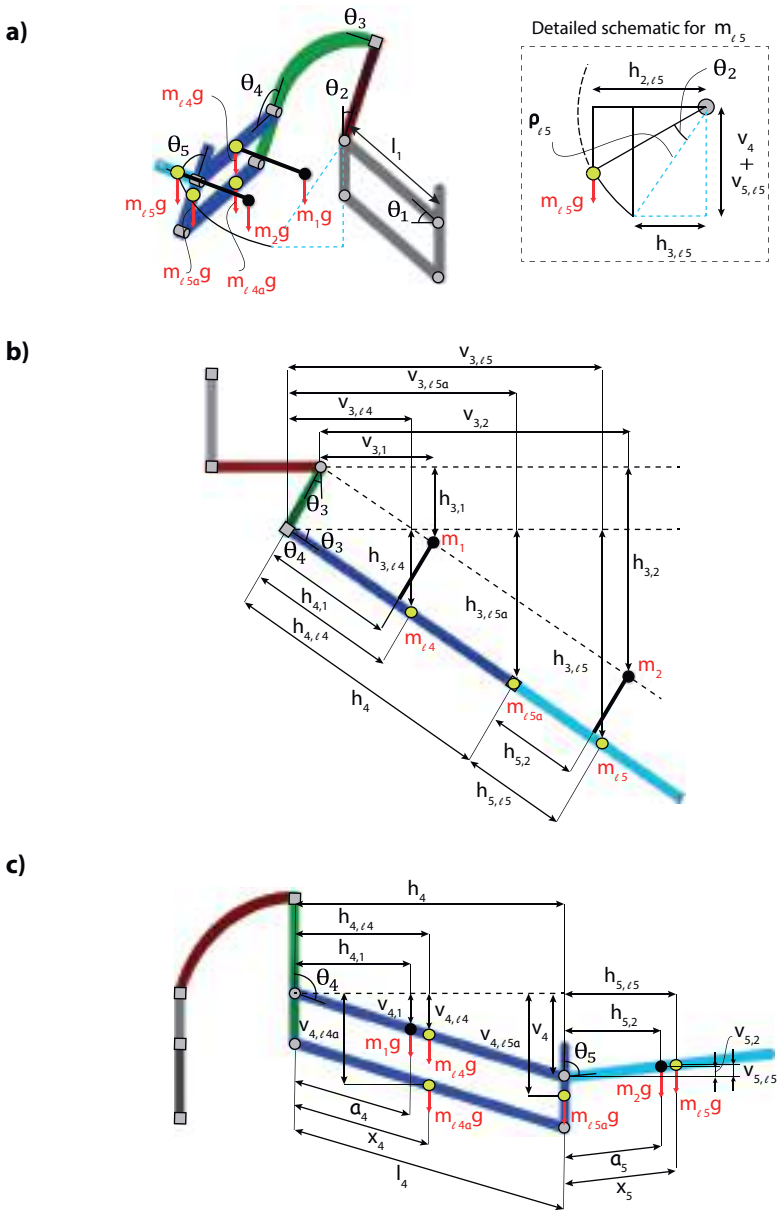

Figure 3.8: Schematics of the shoulder-elbow exoskeleton: influence of the position angle ***a)*** θ_2, ***b)*** θ_3, *and* ***c)*** θ_4, θ_5 *on the gravity torque* M_2 *(Eq. 3.20).*

3.5.2.2. Balancing Torque Calculation

Implementing two 1-DOF balancers and one 3-DOFs balancer, the exoskeleton is statically balanced via the action of five springs, namely one for each R_i ($i \in [1,5]$) joint.

Linear Spring 1-DOF Balancer: Leveraging the model presented in Section 3.4.1, the spring balancing torque $M_{i,s}$ in R_1 and R_5 is calculated as in Eq. 3.24:

$$\begin{cases} M_{i,s} = k_i b_i e_i \left(1 - \frac{d_{0i}}{d_i}\right) \cos(\theta_i), \ _{i=\{1,5\}} \\ k_i = \frac{N_i}{b_i e_i \left(1 - \frac{d_{0i}}{d_i}\right)} g, \ _{i=\{1,5\}} \\ d_i = \sqrt{b_i^2 + e_i^2}, \ _{i=\{1,5\}} \\ N_1 = x_1 (m_{\ell 1} + m_{\ell 1a}) + l_1 \sum_{ii} m_{ii}, \ _{ii=\{1,2,\ell 2,\ell 3,\ell 4,\ell 5,\ell 2a,\ell 4a,\ell 5a\}} \\ N_5 = a_5 m_2 + x_5 m_{\ell 5} \end{cases} \tag{3.24}$$

where, k_i ($i = \{1,5\}$) is the i^{th} spring coefficient, b_i, e_i are the installation distances, d_{0i}, d_i are the initial and final spring length, and x_1, l_1, a_5, x_5 are from Table 3.1. $m_{\ell 1}$, $m_{\ell 1a}$, m_{ii} ($ii = \{1, 2, \ell 2, \ell 3, \ell 4, \ell 5, \ell 2a, \ell 4a, \ell 5a\}$) contribute to the $M_{1,s}$ formulation, whereas m_2, $m_{\ell 5}$ influence the $M_{5,s}$ calculation.

Linear Springs 3-DOFs Balancer: To balance the R_2, R_3, R_4 joints, the 3-DOFs model introduced in Section 3.4.2 is considered. However, since the exoskeleton shoulder joint shown in Figure 3.9 is more complex than the three links kinematic chain studied in [77], proper model modifications are needed. The novel 3-DOFs balancer formulation takes into account that:

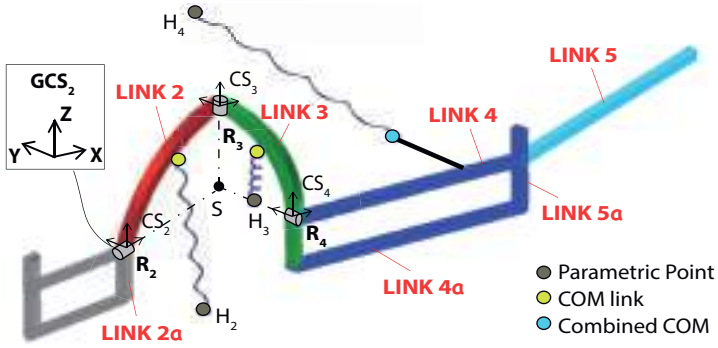

Figure 3.9: Parametric model of the 3-degrees of freedom balancer for the shoulder joint of the exoskeleton.

- Differently from [77], the exoskeleton spherical joint is not constrained in position and moves according to R_0 and R_1 joints (being the SEES structure a serial kinematic chain).
- The overall mass to be balanced comprises both the human upper limb and the exoskeleton structure.
- NZFL springs are required in the current application.

At first, the gravitational load of link 2, link 3, link 4, link 5, link 4a, link 5a and of the human upper limb may be evaluated. By summing each mass after R_4 joint, one can calculate a new combined COM as in Eq. 3.25:

$$m_{4tot} = m_{\ell 4} + m_{\ell 5} + m_{\ell 4a} + m_{\ell 5a} + m_1 + m_2 \tag{3.25}$$

As previously introduced, the employed 3-DOFs balancer consists of three springs (Figure 3.9). The springs connected to link 2 (*SPRING 2*) and link 3 (*SPRING 3*) have their first extremity in the links COM and their second extremity in the parametric points H_2 and H_3. The last spring (*SPRING 4*) is connected between the combined COM and the parametric point H_4. As a design choice, two models (*MODEL 1* and *MODEL 2*) have been investigated and explained in the next points, differing from the considered reference frame for the parametric point of each spring.

- *MODEL 1*: According to [77], a first model considers H_2, H_3, H_4 fixed to a single chassis (link 2a). So, *SPRING 2* balances R_2, *SPRING 3* acts on both R_2, R_3 joints, and *SPRING 4* influences the balancing of the overall spherical joint (R_2, R_3, R_4). The spring force F_{k_i,CS_n} ($i \in [2,4]$) expressed in the generic CS_n is evaluated as in Eq. 3.26:

$$\begin{cases} F_{k_i,CS_n} = k_i \left(PH_{i,CS_n} - D_{0i,CS_n} \right), \ _{i\in [2,4]} \\ PH_{i,CS_n} = P_{i,CS_n} - H_{i,CS_n}, \ _{i\in [2,4]} \end{cases} \tag{3.26}$$

  where k_i ($i \in [2,4]$) is the spring elastic constant, PH_{i,CS_n} is the vector of the spring final length, being P_{i,CS_n} the connection point to the i^{th} COM, and H_{i,CS_n} the i^{th} parametric point. Also, D_{0i,CS_n} is the vector of the spring initial length. Exploiting

the exoskeleton kinematic model, the full computation of Eq. 3.26 is provided in the SEES Equation Appendix (Section 3.9).

Defining the position vector P_{i,CS_n} ($i \in [2,4]$) and the force vector F_{k_i,CS_n} in the generic CS_n as:

$$P_{i,CS_n} = [P_{ix,CS_n};\ P_{iy,CS_n};\ P_{iz,CS_n}]\ ,\ _{i\in\ [2,4]} \tag{3.27}$$

$$F_{k_i,CS_n} = [F_{k_ix,CS_n};\ F_{k_iy,CS_n};\ F_{k_iz,CS_n}]\ ,\ _{i\in\ [2,4]} \tag{3.28}$$

the balancing torque $M_{i,s}$ in R_i ($i \in [2,4]$) provided by the springs is computed as in Eq. 3.29, Eq. 3.30, Eq.3.31:

$$M_{2,s} = \sum_{i=2,3,4} (F_{k_iz,GCS_2}\ P_{iy,GCS_2} - F_{k_iy,GCS_2}\ P_{iz,GCS_2}) \tag{3.29}$$

$$M_{3,s} = \sum_{i=3,4} (F_{k_iy,CS_3}\ P_{ix,CS_3} - F_{k_ix,CS_3}\ P_{iy,CS_3}) \tag{3.30}$$

$$M_{4,s} = F_{k_4x,CS_4}\ P_{4z,CS_4} - F_{k_4z,CS_4}\ P_{4x,CS_4} \tag{3.31}$$

Note as the torque $M_{2,s}$ acting in R_2 is a combination of the *SPRING 2*, *SPRING 3*, *SPRING 4* action; the torque $M_{3,s}$ registered in R_3 is caused by the balancing effect of both *SPRING 3* and *SPRING 4*; whereas $M_{4,s}$ balances R_4 through the *SPRING 4* effect only.

- *MODEL 2*: For simplicity, a second model is investigated by connecting each spring between two consecutive links, thus, considering the parametric point H_i ($i \in [2,4]$) of the i^{th} spring regarding the $(i-1)^{th}$ local system (Figure 3.9). In this case, every spring acts only upon the link where it is attached. Hence, compared to *MODEL 1*, the balancing torques of Eq. 3.29, Eq. 3.30, Eq. 3.31 can be rewritten and so streamlined, as in Eq. 3.32, Eq. 3.33, Eq. 3.34:

$$M_{2,s} = F_{k_2z,GCS_2}\ P_{2y,GCS_2} - F_{k_2y,GCS_2}\ P_{2z,GCS_2} \tag{3.32}$$

$$M_{3,s} = F_{k_3y,CS_3}\ P_{3x,CS_3} - F_{k_3x,CS_3}\ P_{3y,CS_3} \tag{3.33}$$

$$M_{4,s} = F_{k_4x,CS_4}\ P_{4z,CS_4} - F_{k_4z,CS_4}\ P_{4x,CS_4} \tag{3.34}$$

In this case, Eq. 3.32, Eq. 3.33, Eq. 3.34 are influenced by the only effect of *SPRING 2*, *SPRING 3*, *SPRING 4*, respectively. The model if fully implemented in the SEES Equation Appendix (Section 3.9).

Torsional Spring 1-DOF Balancer: Basing upon the theoretical model presented in Section 3.4.3, the spring torque $M_{i,t}$ ($i \in [1,5]$) for each R_i joint of the SEES can be simply computed as in Eq. 3.35:

$$M_{i,t} = k_{i,t}(\triangle\theta_i - \theta_{i,load}), \ _{i\in\,[1,5]} \tag{3.35}$$

where $k_{i,t}$ ($i \in [1,5]$) is the torsional spring coefficient, $\triangle\theta_i$ is defined in Table 3.2, and $\theta_{i,load}$ is the spring preload. Note that, in this case, the preload is in terms of rotation angle, but can be computed also in terms of torque $L_{i,load}$ as $k_{i,t}\theta_{i,load}$ ($i \in [1,5]$). So, Eq. 3.35 becomes Eq. 3.36:

$$M_{i,t} = k_{i,t} \triangle \theta_i - L_{i,load}, \ _{i\in\,[1,5]} \tag{3.36}$$

3.5.2.3. Resultant Torque Calculation

The resultant balanced torque $M_{i,b}$, in R_i ($i \in [1,5]$) is achieved by subtracting the spring balancing torque to the gravity torque for each R joint as in the next points:

- **Linear springs**
  - **1-DOF balancer**: Eq. 3.24 (for R_1 or R_5) minus Eq. 3.19 (for R_1) and Eq. 3.23 (for R_5).
  - **3-DOFs balancer**, *MODEL 1*: Eq. 3.29 minus Eq. 3.20 (for R_2), Eq. 3.30 minus Eq. 3.21 (for R_3), Eq. 3.31 minus Eq. 3.22 (for R_4).
  - **3-DOFs balacner**, *MODEL 2*: Eq. 3.32 minus Eq. 3.20 (for R_2), Eq. 3.33 minus Eq. 3.21 (for R_3), Eq. 3.34 minus Eq. 3.22 (for R_4).
- **Torsional springs**
  - **1-DOF balancer**: Eq. 3.35 (for R_1 or R_2 or R_3 or R_4 or R_5) minus Eq. 3.19, Eq. 3.20, Eq. 3.21, Eq. 3.22, Eq. 3.23 (for R_1, R_2, R_3, R_4, R_5 respectively).

3.5.2.4. Numerical Validation

The SEES gravity torque has been plotted in Figure 3.10 for each imposed motion (MOV 1, MOV 2, MOV 3, Table 3.2, Figure 3.5). In all cases, results form *Matlab* and *RecurDyn* overlap during all the movement progress. The resultant torques due to the spring balancing effect will be plotted in the next sections after the optimization process aiming at sizing the SEES springs, either linear or torsional, to fully balance the exoskeleton.

3.6. Springs Design Optimization, Results, and Discussions

3.6.1. Linear Springs

By leveraging the analytical models developed in Section 3.5, an optimization study is carried out to determine the best spring configuration that balances the complete exoskeleton.

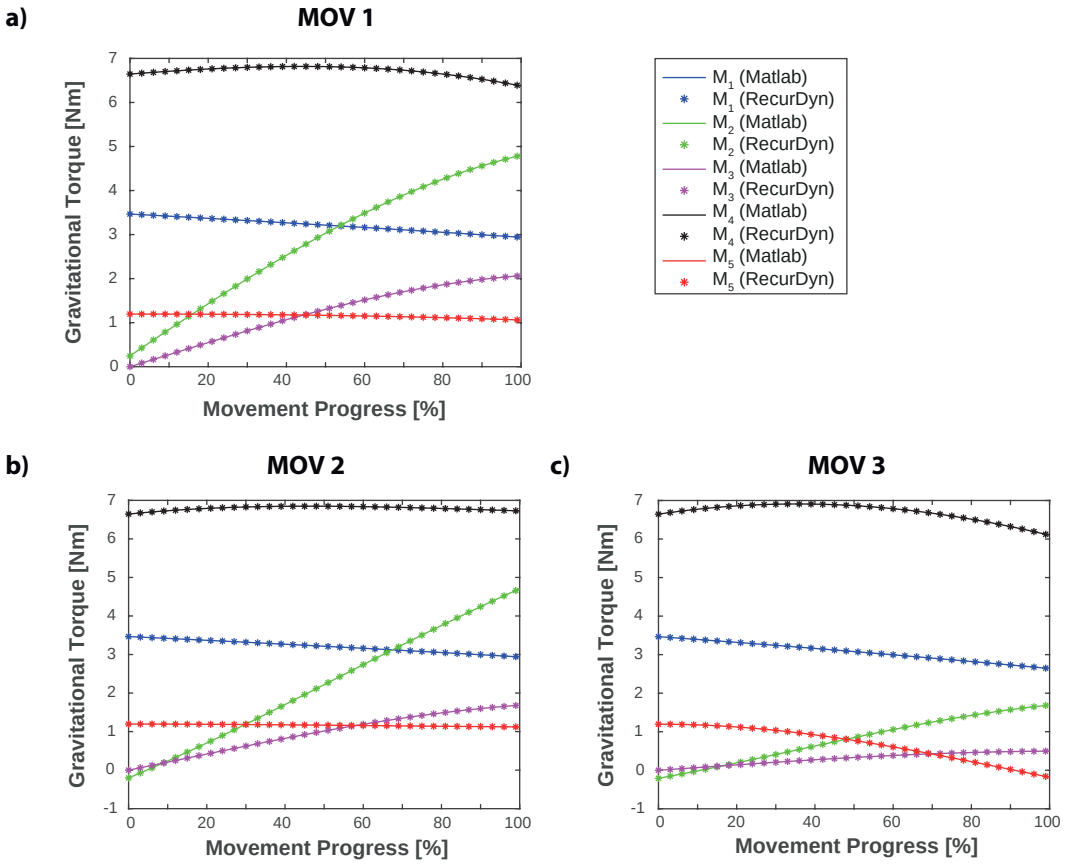

Figure 3.10: Statics validation of the shoulder-elbow exoskeleton: Matlab vs RecurDyn results. Gravitational reaction torques [Nm] during the movement progress [%] in each exoskeleton Revolute (R) joint R_i ($i \in [1,5]$) during the three simulated movements: ***a)*** *MOV 1,* ***b)*** *MOV 2,* ***c)*** *MOV 3.*

The system variables relevant for this study are listed below:

- Spring connection points: $H_2,\ H_3,\ H_4$ for the 3-DOFs spherical joint (Figure 3.9), installation distances b_1, e_1, b_5, e_5 for the 1-DOF R_1 and R_5 joints (Figure 3.4a).
- Spring elastic constants $k_2,\ k_3,\ k_4$ ($k_1,\ k_5$ are theoretically defined in Eq. 3.24).
- Spring initial lengths: $d_{01},\ d_{02},\ d_{03},\ d_{04},\ d_{05}$.

To reach a computationally efficient optimization routine, some of the variables which do not significantly influence the solution have been fixed as in the following points:

- $b_1 = l_1,\ b_5 = l_5$ (Table 3.1), $e_1 = e_5 = 30\ mm$.
- $d_{0i} = 30\ mm$ for NZFL springs, or $d_{0i} = 0\ mm$ for ZFL springs ($i \in\ [1, 5]$).

Therefore, only the exoskeleton spherical joint is involved in the optimization process, which may be formulated as follows:

$$\begin{aligned} \textbf{minimize}\ & \sum_{i=2}^{4} rms\ (M_{i,b}) \\ \textbf{with respect to}\ & H_i = [h_{ix};\ h_{iy};\ h_{iz}],\ k_i\ (i \in\ [2, 4]) \\ \textbf{subject to}\ & |H_i| \leq 200\ mm\ \ 0.1\ \frac{N}{mm} \leq k_i \leq 5\ \frac{N}{mm} \end{aligned}$$

where the objective function is the sum of the balanced torques root mean squares values, and the optimization parameters are twelve, namely the spring constants $k_2,\ k_3,\ k_4$ and the position of the parametric points $H_2,\ H_3,\ H_4$ (three coordinates (for the x-, y-, z-axis) for each parametric point). The explored design domain is in accord with the human upper limb workspace. However, specific constraints have to be defined since the position of the springs may interfere with the human upper limb or other parts of the human body, e.g., the head. By considering this, the design domain is further confined for each spring by adding non-linear constraints, e.g., the volume of a cylinder with a radius of $65\ mm$ and centred in the combined COM.

The problem is solved in *Matlab* for each of the input movements (MOV) specified in Figure 3.5 through the deterministic algorithm *fmincon*. To avoid local minima, several starting points are enforced in the optimization by adopting the *GlobalSearch* option within

the *fmincon* routine, and a tolerance of 10^{-6} is set. The presented methodology allowed to run different optimization studies, investigating several aspects to evaluate the best solution under the provided design requirements, e.g., the user's features and the motion law.

By comparing the balancing springs type to be employed (ZFL and NZFL), some of the obtained results are presented in Section 3.6.1.1 and Section 3.6.1.2 by evaluating the next points:

- Different 3-DOFs balancer optimal configurations (*SOLUTION 1*, *SOLUTION 2*).
- The task to be reproduced (*MOV 1*, *MOV 2*, *MOV 3*).
- The exoskeleton material properties (HyPothesis (HP): Aluminium alloy links, Carbon Fibre links, null mass links).

3.6.1.1. Zero Free Length Springs

As a first step, the HP of ZFL springs is considered. In this case, being $d_{0i} = 0\ mm$ ($i \in [1, 5]$), the theoretical model formulation is simplified (Eq. 3.24, Eq. 3.26).

The results obtained from the optimization routine are reported in Table 3.3: the solution varies based on the considered input movement. For validation purposes, each parameter set is verified with the multi-body software *RecurDyn*. This method, explained in detail in Figure 3.11, allows a rapid model visualization thanks to the motion animations and facilitates the designer in the preliminary design stage. By changing the springs parametric point coordinates under the obtained results of the optimization study carried out in *Matlab*, the model developed in *RecurDyn* can be rapidly updated. Each R joint of the exoskeleton is activated with the position law related to the prescribed movement (Table 3.2) and, to avoid undesired dynamic effects, the static analytical model validation has been conducted in *RecurDyn* by running kinetic-dynamic analyses with a total duration of $5\ s$. Referring to Table 3.1 and Table 3.2, the input parameters can be easily changed under the project specifications, e.g., the user's features or the specific task.

3.6.1.1.1. 3-DOFs Balancer Optimal Configuration

Figure 3.12a shows how the position of the combined COM (calculated through Eq. 3.25 and considered for the first optimization routine, the results of which are presented in Ta-

ble 3.3) falls within the human limb, and thus, it cannot be considered a connection point for the spring in real applications. Two possibilities are evaluated and shown in Figure 3.12b to solve this issue; the *SPRING 4* connection point fixed on link 4 is moved from the combined COM to:

- A point fixed to the arm holder (*SOLUTION 1*).
- The COM of link 4 (*SOLUTION 2*).

Table 3.3: Optimal results of the 3-degrees of freedom balancer for the shoulder joint of the exoskeleton (hypothesis: zero free length springs, Aluminium alloy links). The combined center of mass to be balanced is computed as in Eq. 3.25; each set of the springs optimization parameters (i.e., the position of the points of attachment h_{ix}, h_{iy}, h_{iz} and the linear elastic constant k_i ($i \in [2, 4]$)) is computed for each optimized (OPT.) movement (MOV 1, MOV 2, MOV 3).

	SPRING	*2*	*3*	*4*
	$h_{ix}\ [mm]$	52.200	107.700	124.000
OPT.	$h_{iy}\ [mm]$	−35.300	43.800	1.800
MOV 1	$h_{iz}\ [mm]$	−95.900	39.900	52.500
	$k_i\ [N/mm]$	0.347	0.220	0.566
	$h_{ix}\ [mm]$	−152.900	114.500	120.800
OPT.	$h_{iy}\ [mm]$	7.800	−71.500	1.900
MOV 2	$h_{iz}\ [mm]$	68.700	31.700	170.000
	$k_i\ [N/mm]$	0.481	0.141	0.175
	$h_{ix}\ [mm]$	18.700	124.900	118.000
OPT.	$h_{iy}\ [mm]$	37.200	−12.700	0.700
MOV 3	$h_{iz}\ [mm]$	38.900	−115.200	198.600
	$k_i\ [N/mm]$	4.249	1.363	0.150

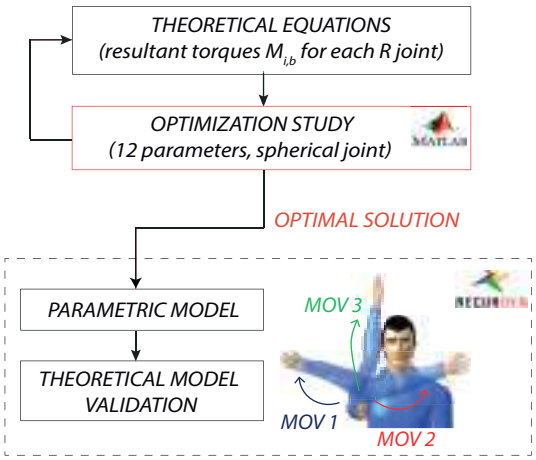

Figure 3.11: Balancing approach for the shoulder-elbow exoskeleton: optimization process and numerical validation.

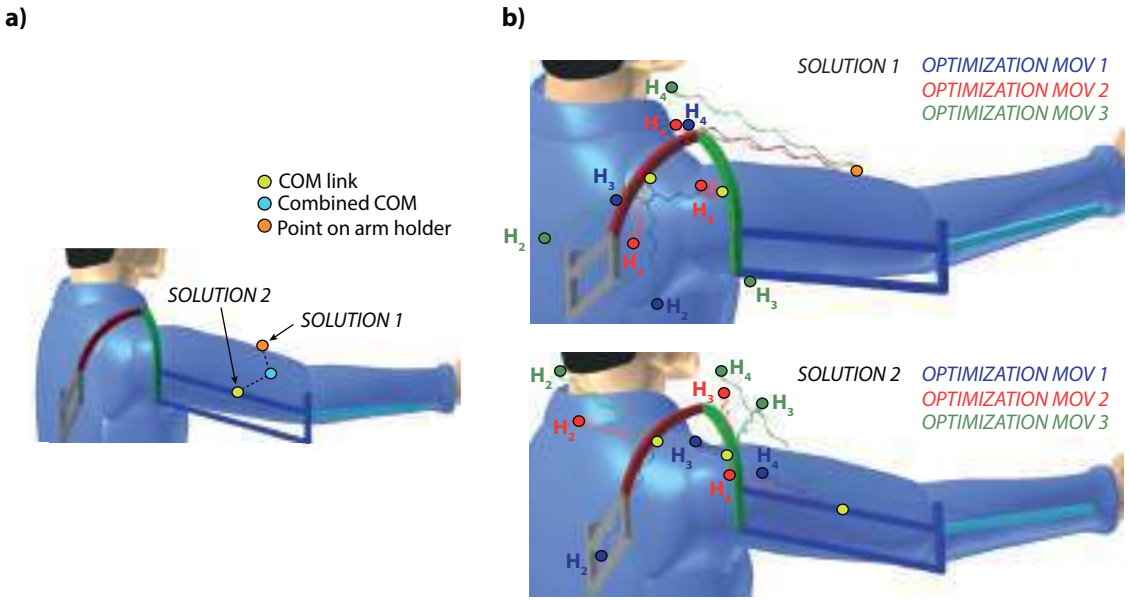

Figure 3.12: Configurations of the 3-Degrees Of Freedom (DOFs) balancer for the shoulder joint of the exoskeleton. ***a)*** *Evaluation of the spring connection point with reference to link 4.* ***b)*** *Optimal results of the 3-DOFs balancer (hypothesis: zero free length springs, Aluminium alloy links) for each simulated movement (MOV 1, MOV 2, MOV 3): top, SOLUTION 1 (MODEL 1), below, SOLUTION 2 (MODEL 2).*

After updating the analytical model by exploring both *MODEL 1* and *MODEL 2* (Section 3.5.2.2) for each solution, a new optimization study is launched in *Matlab*. The obtained configurations consistent with the design space are reported in Figure 3.12b. As expected, a balancer configuration is completely appropriate for one specific movement only. So, to enable different movements, every optimal configuration has also been tested by imposing the remaining non-optimized movements. The torque reduction evaluation reported in Table 3.4 may be useful to select the best solution.

Referring to Table 3.4, for both *SOLUTION 1* and *SOLUTION 2*, and for each 3-DOFs balancer configuration found after the i^{th} optimization process enforcing the i^{th} *MOV* one at a time (*OPT. MOV* $\boldsymbol{i}$), the first column from the left indicates the simulated movement *MOV* $\boldsymbol{i}$ ($i \in [1, 3]$). Regarding *SOLUTION 1*, the cases of *OPT. MOV 2* and *OPT. MOV 3* present a good torque reduction for all the considered movements (blue and green values), whereas the *OPT. MOV 1* case has a negative effect (i.e., a 14% overall torque increase) when enforcing *MOV 3*. As for *SOLUTION 2*, its quality strongly depends on the assigned movement: in most cases, the non-optimized movements produce rising resultant torques (negative values in red).

Table 3.4: Optimal results of the 3-degrees of freedom balancer for the shoulder joint of the exoskeleton: torque reduction [%] at each Revolute (R) joint R_i ($i \in [2,4]$) due to the balancing effect of the passive elements (hypothesis: zero free length springs, Aluminium alloy links) during the considered movement (MOV 1, MOV 2, MOV 3): SOLUTION 1 vs SOLUTION 2 (as illustrated in Figure 3.12b). Optimal values in blue, good in green, bad in red.

TORQUE RED. [%]	*SOLUTION 1*			*SOLUTION 2*		
	R_2	R_3	R_4	M_2	M_3	M_4
	OPT. MOV 1			*OPT. MOV 1*		
MOV 1	99.69	99.68	99.99	95.37	95.54	99.07
MOV 2	55.29	71.36	92.76	−48.29	−49.43	95.83
MOV 3	−14.00	61.51	85.06	−53.10	−55.09	92.32
	OPT. MOV 2			*OPT. MOV 2*		
MOV 1	50.93	67.15	97.11	−53.28	−45.16	97.41
MOV 2	99.64	95.52	99.89	99.00	99.29	99.63
MOV 3	80.10	69.60	98.20	73.11	49.27	99.19
	OPT. MOV 3			*OPT. MOV 3*		
MOV 1	71.10	73.85	94.00	−58.18	−35.26	97.02
MOV 2	81.46	84.66	99.24	76.56	66.25	99.22
MOV 3	98.19	97.43	99.69	95.93	92.51	99.84

*Table 3.5: **CASE STUDY 1**: Optimal results of the 3-degrees of freedom balancer for the shoulder joint of the exoskeleton (hypothesis: zero free length springs, Aluminium alloy links). NOTE: the proposed configuration is optimized for one specific movement (OPT. MOV 3).*

	SPRING	*2*	*3*	*4*
	$h_{ix}\ [mm]$	−63.710	141.700	77.600
OPT.	$h_{iy}\ [mm]$	54.830	−79.400	−12.500
MOV 3	$h_{iz}\ [mm]$	−7.400	−68.000	165.700
	$k_i\ [N/mm]$	1.231	0.569	0.178

The final solution is chosen considering the position of the springs under the available exoskeleton workspace and the possibility of reproducing multiple tasks while keeping a good balance. Being the exoskeleton specially developed for the industrial sector, a complete balancing is not required since the operator owns enough force to move the arm. Therefore, the *SOLUTION 1*, *OPT. MOV 3* case is chosen for further development (Table 3.4) (for simplicity, will be referred as **CASE STUDY 1** in the rest of the thesis).

Table 3.5 reports the numerical values of the optimized parameters for the **CASE STUDY 1**, shown in Figure 3.12b. Being this design influenced by the arm holder geometry, aspects like ergonomics and comfort need to be investigated.

3.6.1.1.2. Numerical Validation

For validation purposes, Figure 3.13 reports the gravity and balanced torques (M_i and $M_{i,b}$ ($i \in [1,5]$)) in each exoskeleton joint theoretically calculated in *Matlab* matching the ones obtained in *RecurDyn*. After the optimization process, thanks to the **CASE STUDY 1** balancer configuration, the exoskeleton is fully balanced since the resultant torque for each R joint is decreased to zero (Figure 3.13, null green values).

Material Properties: Once the 3-DOFs balancer optimal design is defined (**CASE STUDY 1**), the complete exoskeleton is tested by changing its material properties, i.e., reducing the links density by 40%. The new density falls within the typical range of Carbon Fibre. In such a case, the solution previously achieved with Aluminium alloy links (Table 3.5) is still applicable. Referring to Figure 3.14, the gravity torques M_i and the resultant balanced torques $M_{i,b}$ in each R_i joint ($i \in [1,5]$) are plotted during the movement progress for links of different materials. Each resultant torque is almost equally balanced since it cannot be considerably distinguished from the presented graph. In fact, being the exoskeleton designed to be light, its weight is the 12.1% (HP Aluminium alloy links) or the 7.5% (HP Carbon Fibre links) of the overall weight that need to be balanced (consisting in the exoskeleton proper weight plus the human upper limb weight). The maximum deviation from zero ($250\ Nmm$, exoskeleton in Carbon Fibre and $50\ Nmm$, exoskeleton in Aluminium) occurs in R_4 since *SPRING 4* has to support most of the weight (Eq. 3.25). Also, being the exoskeleton a serial chain, each R joint has to balance different percentage of the overall weight, and so, it reacts in different ways under a change of the design parameters.

As the last verification, to strengthen the accuracy of the proposed method, a 100% link density reduction is applied (i.e., the link mass is neglected), thus, streamlining the theoretical model of Section 3.5.2.1. The gravity torques calculated with the complete analytical model and the simplified model are compared: according to Table 3.6, assuming null density links, a maximum error of 12.22% occurs. So, the modelling accounting for the exoskeleton proper weight results in more precision.

Zero Free Length vs Non-Zero Free Length Springs: Although examples of ZFL springs realization have been reported in previous works [77, 80, 81], NZFL springs have been considered, due to their widespread use and practicability. To test the usability of the

model with NZFL springs, the proposed solution reported in Table 3.5 (**CASE STUDY 1**) has been updated by simply changing the springs initial length ($d_{0i} = 30\ mm\ (i \in [1,5])$), i.e., without running a new optimization process or changing the springs position and elastic constants.

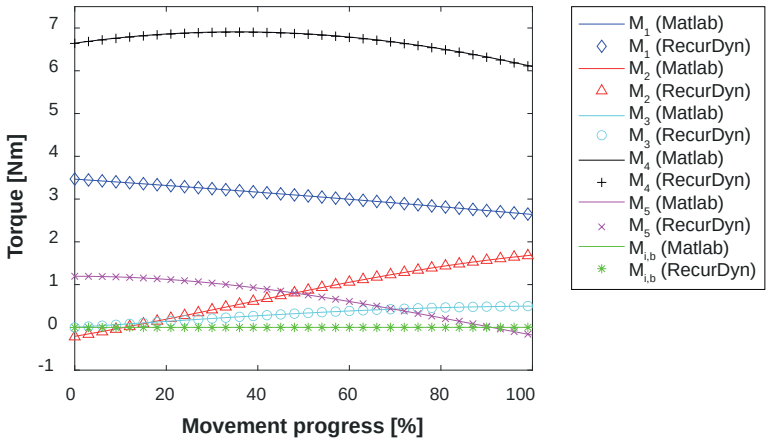

*Figure 3.13: Statics validation of the shoulder-elbow exoskeleton: Matlab vs RecurDyn results (hypothesis: zero free length springs, Aluminium alloy links). Gravity reaction torques M_i, and balanced torques $M_{i,b}$ in the Revolute (R) joint R_i ($i \in [1,5]$) during the optimized (OPT.) movement (MOV 3). Exoskeleton full balancing: overlapping of $M_{i,b}$ ($i \in [1,5]$). The balancer configuration for the exoskeleton consists in one 1-Degree Of Freedom (DOF) balancer for the R_1 joint, one 1-DOF balancer for R_5, and one 3-DOFs balancer (**CASE STUDY 1**) for $R_2,\ R_3,\ R_4$.*

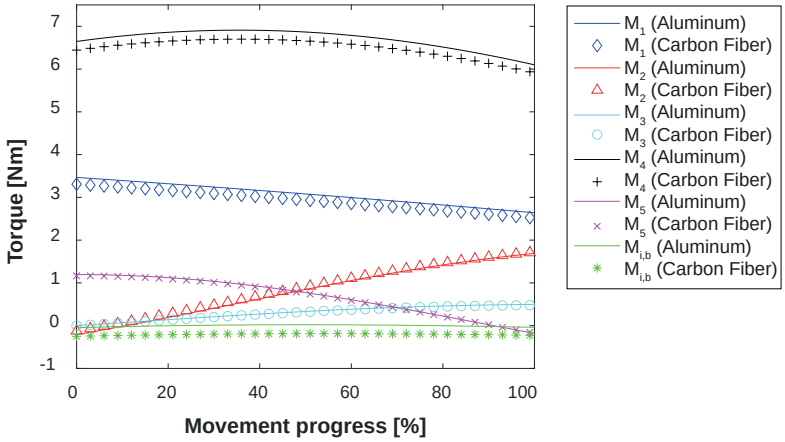

*Figure 3.14: Statics validation of the shoulder-elbow exoskeleton: links in Aluminium alloy (density: 2700 kg/m^3) vs links in Carbon Fibre (density: 1600 kg/m^3) results (hypothesis: zero free length springs). Gravity reaction torques M_i, and balanced torques $M_{i,b}$ in the Revolute (R) joint R_i ($i \in [1,5]$) during the optimized (OPT.) movement (MOV 3). The balancer configuration for the exoskeleton consists in one 1-Degree Of Freedom (DOF) balancer for the R_1 joint, one 1-DOF balancer for R_5, and one 3-DOFs balancer (**CASE STUDY 1**) for $R_2,\ R_3,\ R_4$.*

Table 3.6: Results of the shoulder-elbow exoskeleton due to the balancing effect of the passive elements: error [%] at each Revolute (R) joint R_i ($i \in [1, 5]$) of the gravity torques M_i between the approximated model (hypothesis: null links density) and the complete model (hypothesis: Aluminium alloy links) during the considered movement (MOV 1, MOV 2, MOV 3).

ERROR [%]	R_1	R_2	R_3	R_4	R_5
MOV 1	11.27	12.22	5.75	7.47	5.80
MOV 2	11.28	1.42	8.48	7.47	5.80
MOV 3	11.28	9.74	8.00	7.47	5.80

*Table 3.7: Results of the 3-degrees of freedom balancer for the shoulder joint of the exoskeleton: torque reduction [%] at each Revolute (R) joint R_i ($i \in [2, 4]$) (**CASE STUDY 1** with assumption of non-zero free length springs) during the considered movement (MOV 1, MOV 2, MOV 3). Optimal values in blue, good in green, bad in red.*

TORQUE RED. [%]	R_2	R_3	R_4
MOV 1	61.91	74.42	84.49
MOV 2	71.32	71.69	95.43
MOV 3	71.77	84.17	88.46

Table 3.7 shows how the percentage torque reduction for each R joint is lower comparing to Table 3.4. In detail, the simulation of the optimized movement (*MOV 3*) results in a good, but not complete, exoskeleton balancing (the percentage torque reduction for the shoulder joint drops, on average, from around 98% to 81%). This discrepancy is highlighted in Figure 3.15, which reports the registered torque for each exoskeleton R joint during the *MOV 3* progress for the above-mentioned cases. Being *SPRING 4* strictly influenced by the design parameters (it supports the main part of the overall weight computed in Eq. 3.25), the worst leftover torque occurs in R_4 (around $800\ Nmm$). However, the simulation of the non-optimized movements is still acceptable (Table 3.7, green values).

To sum up, for the 1-DOF balancers (R_1, R_5), the assumption of ZFL or NZFL springs influences the solution, but not considerably for the full balance reaching. The reduction torque drops from 100% to 92.9% in R_1 and from 98.5% to 97.9% in R_5. Thus, the 1-DOF R joints of the exoskeleton may be considered fully balanced also in the presence of NZFL springs. Conversely, the 3-DOFs balancer needs to be optimized under the HP of NZFL springs (see Section 3.6.1.2).

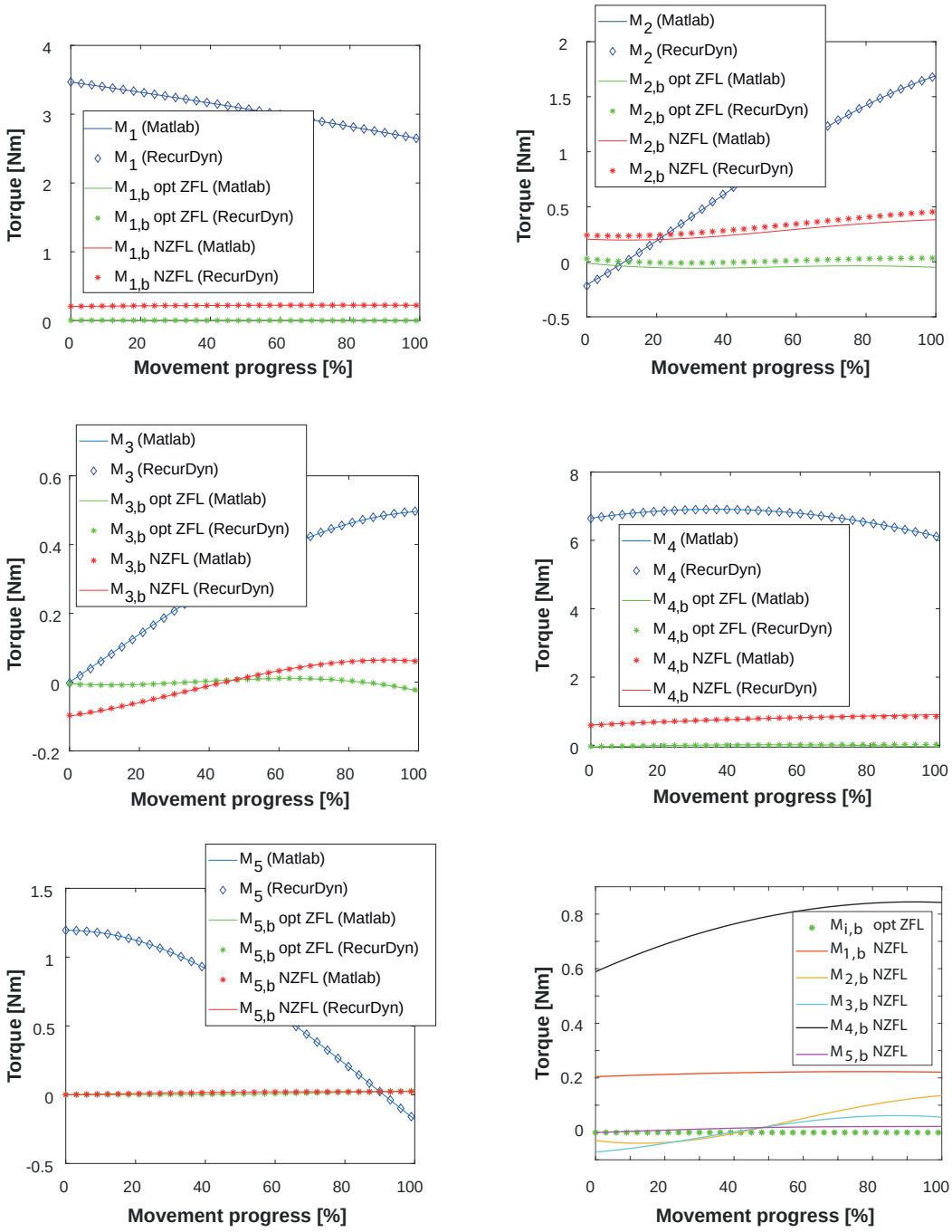

*Figure 3.15: Statics validation of the shoulder-elbow exoskeleton: Matlab vs RecurDyn results (Zero Free Length (ZFL) vs Non-Zero Free Length (NZFL) springs). Reaction torques in each exoskeleton Revolute (R) joint R_i ($i \in [1,5]$) during the optimized (OPT.) movement (MOV 3): gravity torques M_i, resultant torques $M_{i,b}$ ($i \in [1,5]$) balanced through ZFL springs (**CASE STUDY 1, optimal solution**) and NZFL springs (**CASE STUDY 1**, assumption of NZFL springs). The balancer configuration for the exoskeleton consists in one 1-Degree of Freedom (DOF) balancer for the R_1 joint, one 1-DOF balancer for R_5, and one 3-DOFs balancer (**CASE STUDY 1**) for $R_2,\ R_3,\ R_4$.*

3.6.1.2. Non-Zero Free Length Springs

3.6.1.2.1. 3-DOFs Balancer Optimal Configuration

To shorten the design process, in this case, the same conditions (i.e., *SOLUTION 1*, *OPT. MOV 3*) chosen in Section 3.6.1.1.1 for the proposed **CASE STUDY 1** has been used to find a new balancer configuration involving NZFL springs (this optimal solution will be referred as **CASE STUDY 2** in the rest of the thesis). A new optimization study has been run to reach the exoskeleton complete balancing by NZFL springs: a latest 3-DOFs balancer configuration, in terms of springs position and elastic constant, is found (Table 3.8) and shown in Figure 3.16. As clearly pointed out from the comparison between Figure 3.12b and Figure 3.16, Table 3.5 and Table 3.8, the optimal 3-DOFs balancer configuration with *HP NZFL* springs differs from the one with *HP ZFL* springs.

The torques percentage reduction for each movement is reported in Table 3.9. For the optimized movement (*MOV 3*), the 3-DOFs balancer with *HP NZFL* springs is completely balanced (blue values), as it was for the case of *HP ZFL* (Table 3.4). To enable the other non-optimized movements simulation, the exoskeleton in the optimal configuration for *MOV 3* is

Table 3.8: ***CASE STUDY 2****: Optimal results of the 3-degrees of freedom balancer for the shoulder joint of the exoskeleton (hypothesis: non-zero free length springs, Aluminium alloy links). NOTE: the proposed balancer configuration is optimized for one specific movement (OPT. MOV 3).*

	SPRING	*2*	*3*	*4*
	$h_{ix}\ [mm]$	-19.300	145.500	58.400
OPT.	$h_{iy}\ [mm]$	65.400	-69.000	-27.700
MOV 3	$h_{iz}\ [mm]$	-158.800	-10.300	197.400
	$k_i\ [N/mm]$	0.857	1.805	0.163

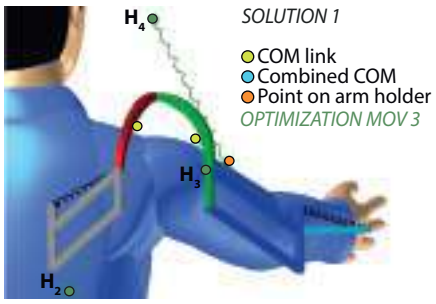

Figure 3.16: ***CASE STUDY 2****: Optimal results of the 3-degrees of freedom balancer for the shoulder joint of the exoskeleton (hypothesis: non-zero free length springs, Aluminium alloy links) for the simulation of the optimized movement (OPT. MOV 3).*

*Table 3.9: **CASE STUDY 2**: Optimal results of the 3-degrees of freedom balancer for the shoulder joint of the exoskeleton: torque reduction [%] at each Revolute (R) joint R_i ($i \in [2, 4]$) due to the balancing effect of the passive elements during the considered movement (MOV 1, MOV 2, MOV 3). Optimal values in blue, good in green, bad in red.*

TORQUE RED. [%]	R_2	R_3	R_4
MOV 1	58.11	−8.15	91.22
MOV 2	78.79	87.99	98.94
MOV 3	99.33	97.53	99.77

also tested by enforcing *MOV 1* and *MOV 2*. As outlined in Table 3.9, the proposed solution is still applicable for the simulation of *MOV 2* (green values), but the reproduction of *MOV 1* ends in a rising torque in the R_2 joint (red value).

3.6.1.2.2. Numerical Validation

For the presented solution with *HP NZFL* springs, the resultant torque for each exoskeleton R joint is plotted during the movement progress for the optimized movement in Figure 3.17. Now, compared to Figure 3.15, the leftover torque $M_{4,b}$ in R_4 is closer to zero, thus reaching the exoskeleton balancing.

Spring Damping Effect: To simulate the real spring behaviour, the damping effect has been considered. Figure 3.18 shows the hysteresis due to the springs damping: a gap in the balancing occurs between the simulation of the forward (GO) and downward (BACK) motion. Similarly to [82], a damping coefficient has been evaluated so that the hysteresis effect is lower than 10% for each R joint, thus, not significantly influencing the balancing effect. The worst impact occurs in R_4 joint since the SPRING 4 balances most of the weight due to the upper arm.

3.6.2. Torsional Springs

Theoretical models studied in Section 3.5 have been exploited to optimally size the torsional springs to balance the full exoskeleton. The system variables relevant for this study are listed below:

- Spring elastic constants: $k_{i,t}$ ($i \in [1, 5]$) (defined in Eq. 3.35).
- Spring preload: $\theta_{i,load}$ ($i \in [1, 5]$) (introduced in Eq. 3.35).

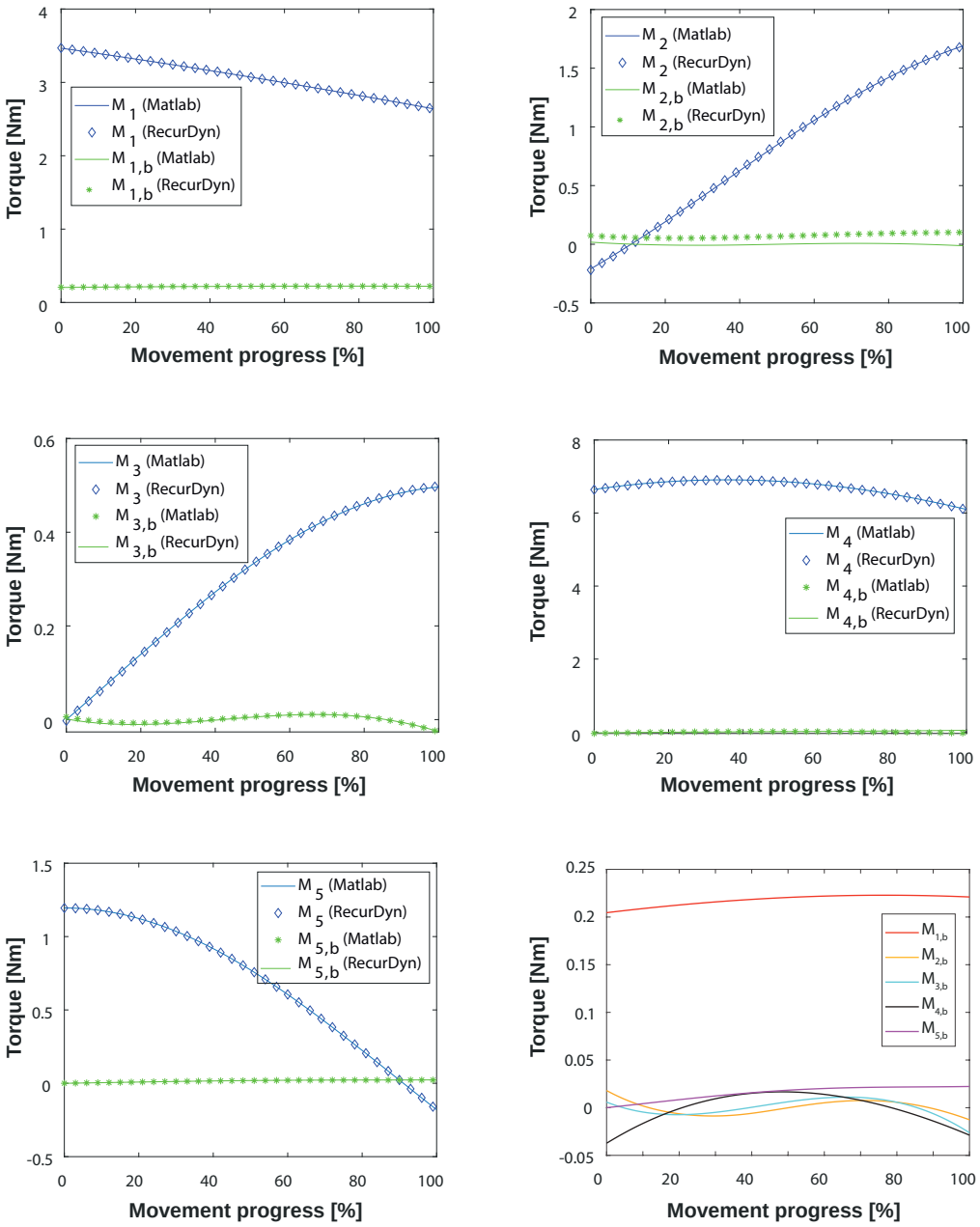

*Figure 3.17: Statics validation of the shoulder-elbow exoskeleton: Matlab vs RecurDyn results (hypothesis: Non-Zero Free Length (NZFL) springs, Aluminium alloy links). Reaction torques in each exoskeleton Revolute (R) joint R_i ($i \in [1,5]$) during the optimized (OPT.) movement (MOV 3): gravity torques M_i, balanced torques $M_{i,b}$ ($i \in [1,5]$). The balancer configuration for the exoskeleton consists in one 1-Degrees of Freedom (DOF) balancer for the R_1 joint, one 1-DOF balancer for R_5, and one 3-DOFs balancer (**CASE STUDY 2**) for $R_2,\ R_3,\ R_4$.*

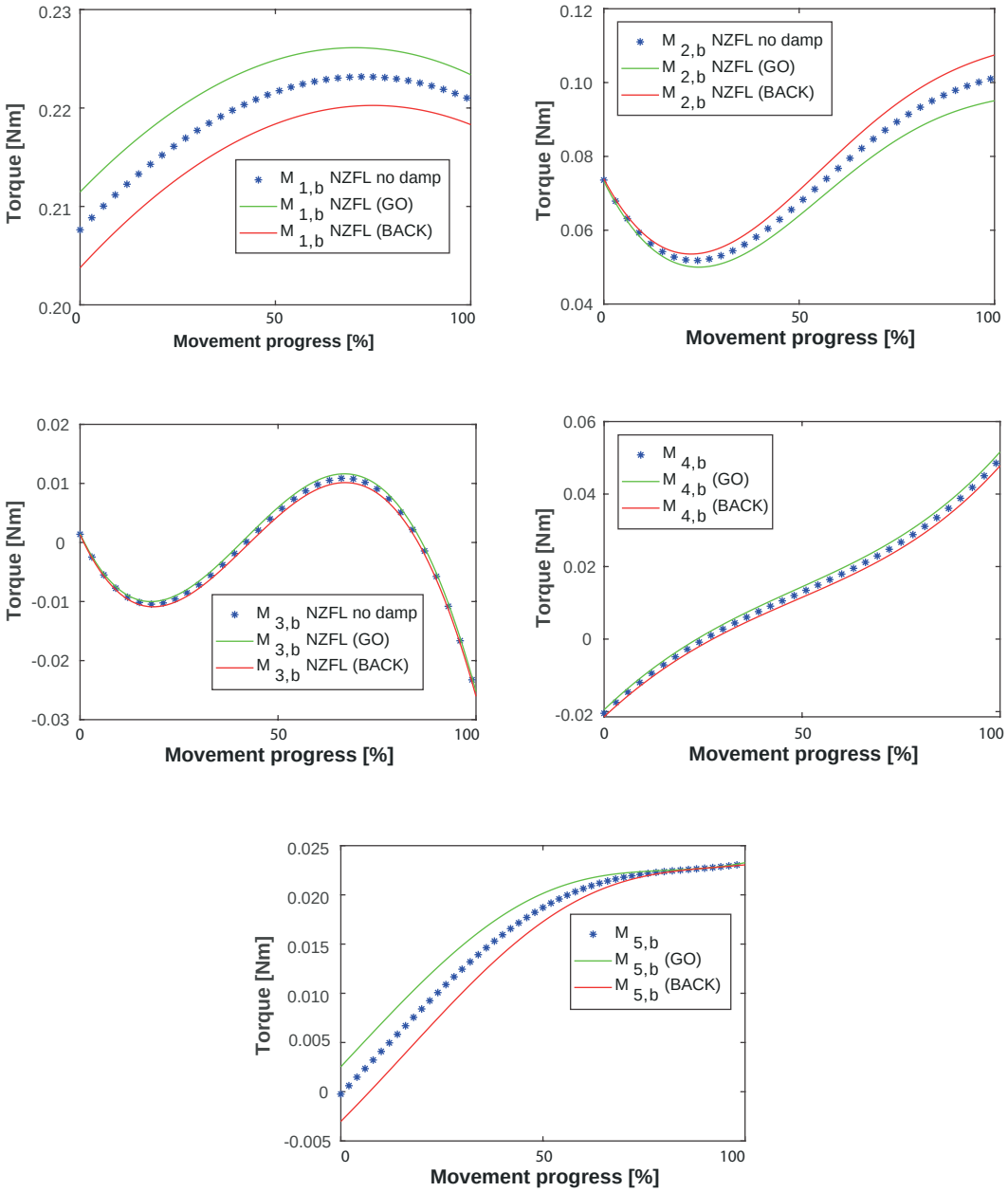

*Figure 3.18: Hysteresis effect on the balanced torques $M_{i,b}$ ($i \in [1,5]$) in each exoskeleton Revolute (R) joint R_i during the movement progress (MOV 3): $M_{i,b}$ for springs with the hypothesis of no damping, $M_{i,b}$ GO and BACK for springs with the hypothesis of damping. The balancer configuration for the exoskeleton consists in one 1-Degrees of Freedom (DOF) balancer for the R_1 joint, one 1-DOF balancer for R_5, and one 3-DOFs balancer (**CASE STUDY 2**) for $R_2,\ R_3,\ R_4$.*

So, the optimization process can be formulated as follows:

$$\begin{aligned}
\textbf{minimize} \quad & \sum_{i=1}^{5} rms\left(M_{i,b}\right) \\
\textbf{with respect to} \quad & K_t = [k_{1,t};\ k_{2,t};\ k_{3,t};\ k_{4,t};\ k_{5,t}]; \\
& \theta_{load} = [\theta_{1,load}; \theta_{2,load}; \theta_{3,load}; \theta_{4,load}; \theta_{5,load}] \\
\textbf{subject to} \quad & 0.1\ \frac{Nmm}{rad} \leq k_{i,t} \leq 20000\ \frac{Nmm}{rad};\ \ |\theta_{i,load}| \leq \pi\ rad
\end{aligned}$$

where the objective function is the sum of the balanced torques root mean squares values, and the optimization parameters are ten (two for each spring, namely five elastic constants plus five preloads).

The same design strategy presented in Section 3.6.1 (see Figure 3.11) has been adopted; the optimization process has been implemented in *Matlab*, investigating several aspects to evaluate the best solution under the provided design requirements. In case of torsional springs, the choice of the mounting configurations is easier, each spring being, for practical reasons, centred in the R joints of the exoskeleton. So, after simply running the optimization routine, optimal configurations can be found, and the exoskeleton parametric model can be updated in *RecurDyn* to better visualize the system. It is worth noting that, by considering the spring preload, the HP of NZFL, which is the most likely replicable in practice, is applied (i.e., unlike linear springs, which have been studied under the HP of ZFL and NZFL, the torsional springs will be optimally dimensioned under the HP of NZFL only).

3.6.2.1. 1-DOF Balancer Optimal Configuration

Not to be repetitive, in this case, the simulation of one movement only has been reported, (i.e., *MOV 3*), considering the SEES links in Carbon Fibre. Table 3.10 lists the values found after the optimization process of the torsional springs; the proposed configuration will be named as **CASE STUDY 3** in the rest of the thesis.

3.6.2.2. Numerical Validation

Results have been validated in the multi-body software *RecurDyn*; as visible from Figure 3.19, which reports the torque for each exoskeleton R_i joint ($i \in [1, 5]$) before (M_i)

Table 3.10: ***CASE STUDY 3****: Optimal results of the torsional springs in terms of stiffness k_i and angular preload $\theta_{i,load}$ for balancing the shoulder-elbow exoskeleton (one spring for each Revolute (R) joint R_i ($i \in [1,5]$)). NOTE: the proposed balancer configuration is optimized for one specific movement (OPT. MOV 3).*

	SPRING	*1*	*2*	*3*	*4*	*5*
OPT.	$k_i\ [Nmm/rad]$	3015	20000	1919	2351	811
MOV 3	$\theta_{i,load}\ [deg]$	-63	0	0	-180	97

and after ($M_{1,b}$) the balancing effect of the torsional springs, a good balance can be reached also in this case. The balancing of R_4 is the hardest to be achieved, since this joint carries on the overall weight of the upper limb. Even if the gravitational moment occurring in R_4 is not fully reduced to the zero value, this solution allows an easier realization considering the physical prototyping of the SEES in practice. Indeed, the design with torsional springs is more compact and the optimization process involves less parameters, the analytical model being simpler.

3.7. Summary

In this Chapter, a virtual prototype of a 6-DOFs, passive, upper limb exoskeleton is developed by pursuing the advances of mechanism efficiency and the aspects of simplified assembly, lightweight, and low production costs. To the best of the author's knowledge, there are no fully passive upper limbs exoskeletons with 6-DOFs reported in the literature. This is primarily due to the challenges of achieving balance, which are intricately tied to the nature of the tasks being performed. For instance, the 6-DOF exoskeleton from [30] can closely replicate the human arm kinematics but is designed as a hybrid system. Such device achieves static balancing through a combination of motors and springs. In this case, passive components partially counteract gravitational loads, but the addition of motors, despite increasing the system's weight, becomes essential for achieving full equilibrium. Conversely, fully passive exoskeletons in the current state of the art suffer from limited precision and are restricted to very simple kinematic designs, such as the 1-DOF device described in [31]. To overcome current limitations, this thesis developed a theoretical approach allowed the exoskeleton static balancing through passive elements only. Both linear and torsional springs have been considered, evaluating the feasibility of the proposed balancers considering specific criteria, e.g., body interference, workspace, and balancer configuration (the *Matlab* code

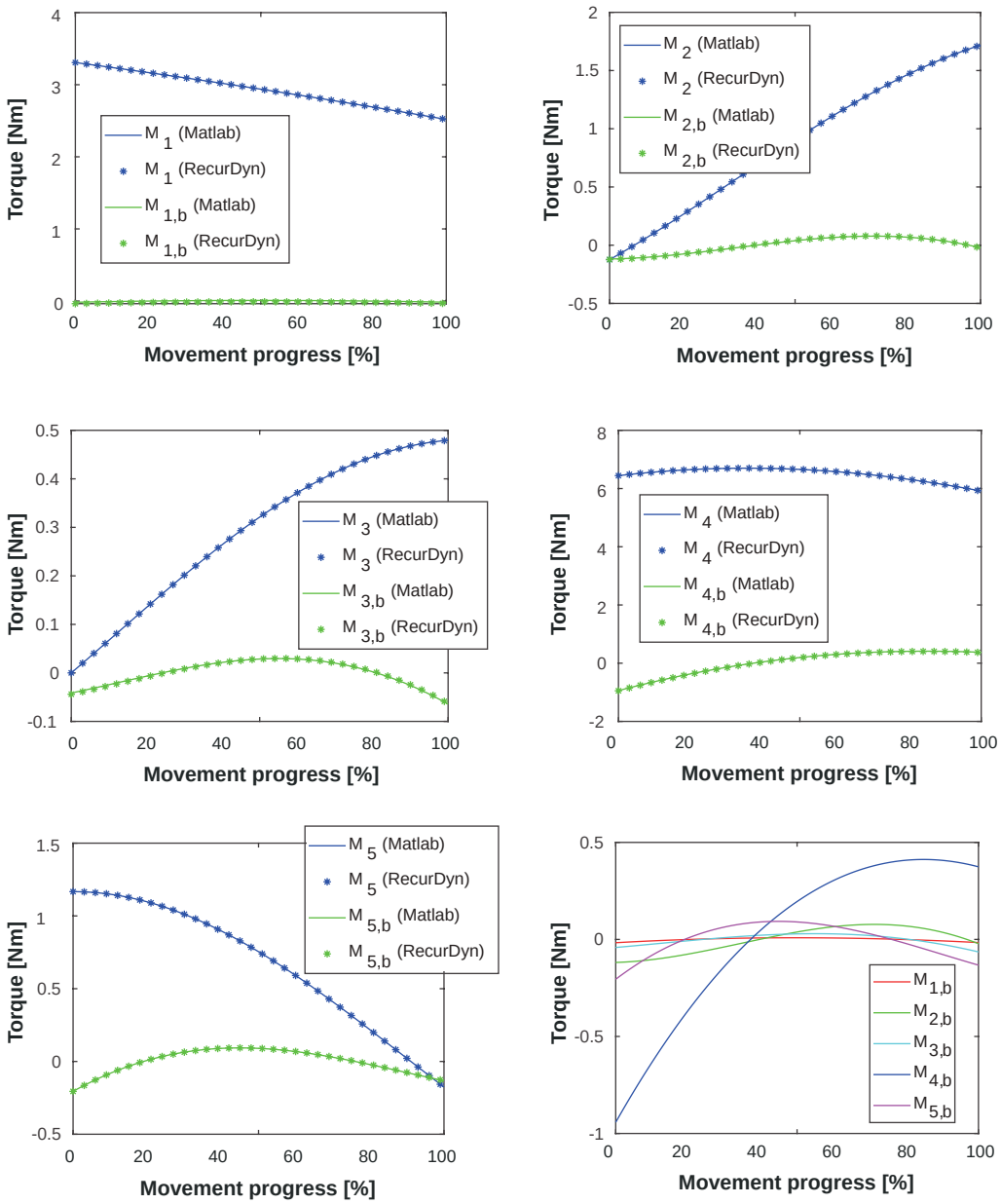

*Figure 3.19: Statics validation of the shoulder-elbow exoskeleton: Matlab vs RecurDyn results. Reaction torques in each exoskeleton Revolute (R) joint R_i ($i \in [1,5]$) during MOV 3: gravity torques M_i, balanced torques $M_{i,b}$ ($i \in [1,5]$). The balancer configuration consists in one torsional spring (1-degrees of freedom balancer) for each R joint (**CASE STUDY 3**).*

for the proposed design tool has been reported in Appendix A).

Concerning linear springs, two of the exoskeleton joints are compensated via the classic 1-DOF balancer, whereas a novel 3-DOFs balancer is designed for the shoulder joint, thus, running several optimization studies and correctly sizing the springs. Different exoskeleton configurations have been investigated, varying the complexity of the analytical model, e.g., implementing idealized ZFL or more practical NZFL springs and changing the reference frame of the spring connection points.

Then, torsional springs have been evaluated; this solutions came up as a more practical design aiming at physically prototyping the system. Even if it involves less optimization parameters and, thus, achieve a less accurate balancing respect to the case of linear springs, it is easier to be manufactured and more compact, embodying a practical structure that ensure a good balance without the risk of interference between the device and users during the motion. Commercial elements can be easily integrated with the custom springs, ensuring the correct positioning and preload of the optimized passive elements.

All models have been validated with commercial software for three specific overhead movements, assuming various conditions, e.g., links with different densities. Its versatility permits to easily change the input motion law to reproduce every movement in the exoskeleton design space, and to customize the geometric and mass parameters according to the user's limb size.

To sum up, this research reached a parametric, accurate and fast analytical model that may be useful during the preliminary design stages. Further feasibility studies would need to be conducted to implement the exoskeleton physical prototype, focusing on the user's features, tasks, and exoskeleton load capacity. Interesting applications to overcome possible collisions between the user and the device during motion are investigated in [82] and will be considered as further applications. As a case study, the proposed exoskeleton balancer configurations ensure a compact encumbrance around the exoskeleton structure and allows a complete balance during a movement which simulates the upper limb lift, a typical action to perform manual overheads tasks.

3.8. SEES Notations

For the linear spring 3-DOFs balancer, the notations below are considered:

- *MODEL 1*: springs connected between the COM of interest and one single chassis (link $2a$). Thus, all the parametric points are expressed in GCS_2 (Section 3.5.2.2, Figure 3.9).

- *MODEL 2*: springs connected between two consecutive links (the i^{th} COM and the i^{th} parametric point fixed to the $(i-1)^{th}$ link). Thus, the parametric point H_i is expressed in the local $CS_{(i-1)}$ (Section 3.5.2.2, Figure 3.9).

- *SOLUTION 1*: *SPRING 4* connected between a point fixed on the arm holder and the parametric point H_4 (Section 3.6.1.1.1, Figure 3.12).

- *SOLUTION 2*: *SPRING 4* connected between the link 4 COM and the parametric point H_4 (Section 3.6.1.1.1, Figure 3.12).

- *SPRING 2/ 3*: spring connected between the link 2/ 3 COM and the parametric point H_2/ H_3 (Section 3.5.2.2, Figure 3.9).

- *SPRING 4*: spring connected to link 4 (during the study development, the connection point will be moved in different positions, all fixed to link 4: from the combined COM (Eq. 3.25, Figure 3.9), to one point fixed to the harm holder (*SOLUTION 1*), or to the link 4 COM (*SOLUTION 2*).

For the assumptions made in the optimization process and the results presented in Section 3.6.1, the following marks are used:

- *HP ZFL/NZFL*: 3-DOFs balancer optimal configuration after the optimization run with HP of ZFL/NZFL springs.

- *MOV* i: simulated movement, regardless of the 3-DOFs balancer optimal configuration.

- *OPT. PARAM.*: optimization parameter.

- *OPT. MOV* $\boldsymbol{i}$: 3-DOFs balancer optimal configuration after the optimization process run by enforcing MOV i.

The proposed case studies are the following:

- **CASE STUDY 1**: *SOLUTION 1, OPT. MOV. 3* (linear springs, *HP ZFL*)
- **CASE STUDY 2**: *SOLUTION 1, OPT. MOV. 3* (linear springs, *HP NZFL*)
- **CASE STUDY 3**: torsional springs with preload (i.e., with *HP NZFL*).

3.9. SEES Equation Appendix

Referring to Figure 3.9, to compute Eq. 3.26, i.e., to calculate the force provided by the 3-DOFs balancer springs for the exoskeleton shoulder joint, and, thus, to find the resultant balancing torques $M_{2,s},\ M_{3,s},\ M_{4,s}$ in $R_2,\ R_3,\ R_4$ (from Eq. 3.29 to Eq. 3.34), each vector position may be expressed for the required reference system. Concerning the exoskeleton 3-DOFs balancer, the masses of interest are the ones of link 2 ($m_{\ell 2}$), link 3 ($m_{\ell 3}$), and the combined COM (m_{4tot}, Eq. 3.25). The position vectors of $m_{\ell 2}$, $m_{\ell 3}$, m_{4tot}, expressed in the local CS_2, CS_3, $CS_{4'}$ shown in Figure 3.5a are:

$$p_{2,CS_2} = [l_{h2};\ 0;\ l_{v2}] \tag{3.37}$$

$$p_{3,CS_3} = [0;\ -l_{h3};\ -l_{v3}] \tag{3.38}$$

$$p_{4tot,CS'_4} = [n_x;\ n_y;\ n_z] \tag{3.39}$$

where $l_{h2},\ l_{v2},\ l_{h3},\ l_{v3}$ are from Table 3.1, and $[n_x;\ n_y;\ n_z] = [231;\ 69;\ 8]\ mm$ (the m_{4tot} position has been measured from the parametric exoskeleton model designed in the software *RecurDyn*).

- Referring to *MODEL 1*, Eq. 3.40, Eq. 3.41, Eq. 3.42 concern *SPRING 2*:

$$P_{2,GCS_2} = (T_2\ \ [p_{2,CS_2}; 1])_{1:3} \tag{3.40}$$

$$H_{2,GCS_2} = [h_{2x};\ h_{2y};\ h_{2z}]\ (\textit{OPT. PARAM.}) \tag{3.41}$$

$$D_{2,GCS_2} = d_{02}\frac{P_{2,GCS_2} - H_{2,GCS_2}}{|P_{2,GCS_2} - H_{2,GCS_2}|} \tag{3.42}$$

Calculations from Eq. 3.43 to Eq. 3.48 refer to *SPRING 3*:

$$P_{3,CS_3} = T_3\ [p_{3,CS_3}; 1] \tag{3.43}$$

$$P_{3,GCS_2} = (T_2\ P_{3,CS_3})_{1:3} \tag{3.44}$$

$$H_{3,GCS_2} = [h_{3x};\ h_{3y};\ h_{3z}]\ (\textit{OPT. PARAM.}) \tag{3.45}$$

$$H_{3,CS_3} = (T_{2,rot})^T H_{3,GCS_2} - [r_1; 0; r_3] \tag{3.46}$$

$$D_{3,GCS_2} = d_{03}\frac{P_{3,GCS_2} - H_{3,GCS_2}}{|P_{3,GCS_2} - H_{3,GCS_2}|} \tag{3.47}$$

$$D_{3,CS_3} = (T_{2,rot})^T D_{3,GCS_2} - [r_1; 0; r_3] \tag{3.48}$$

Formulas from Eq. 3.49 to Eq. 3.57 interest *SPRING 4* (in this case, connected between the combined COM and the parametric point H_4):

$$P_{4,CS_4} = [n_x s_4 - n_z \cos(\theta_4)\,;\ n_y;\ n_x \cos(\theta_4) + n_z] \tag{3.49}$$

$$P_{4,CS_3} = T_3\ [P_{4,CS_4} - [0;\ r_2;\ r_3]; 1] \tag{3.50}$$

$$P_{4,GCS_2} = (T_2\ P_{4,CS_3})_{1:3} \tag{3.51}$$

$$H_{4,GCS_2} = [h_{4x};\ h_{4y};\ h_{4z}]\ (\textit{OPT. PARAM.}) \tag{3.52}$$

$$H_{4,CS_3} = (T_{2,rot})^T H_{4,GCS_2} - [r_1; 0; r_3] \tag{3.53}$$

$$H_{4,CS_4} = (T_{3,rot})^T H_{4,CS_3} + [0; r_2; r_3] \tag{3.54}$$

$$D_{4,GCS_2} = d_{04}\frac{P_{4,GCS_2} - H_{4,GCS_2}}{|P_{4,GCS_2} - H_{4,GCS_2}|} \tag{3.55}$$

$$D_{4,CS_3} = (T_{2,rot})^T D_{4,GCS_2} \tag{3.56}$$

$$D_{4,CS_4} = (T_{3,rot})^T D_{4,CS_3} \tag{3.57}$$

where the notation $(...)_{1:3}$ is for extracting the vector of dimension 1x3. $T_2,\ T_3$ are the transformation matrices from the local $CS_2,\ CS_3$ to GCS_2 (DH method [78]) defined as follows:

$$T_2 = \begin{bmatrix} 1 & 0 & 0 & 0 \\ 0 & \cos\theta_2 & -\sin\theta_2 & 0 \\ 0 & \sin\theta_2 & \cos\theta_2 & 0 \\ 0 & 0 & 0 & 1 \end{bmatrix} \tag{3.58}$$

$$T_3 = \begin{bmatrix} \cos\theta_3 & -\sin\theta_3 & 0 & r_1 \\ \sin\theta_3 & \cos\theta_3 & 0 & 0 \\ 0 & 0 & 1 & r_3 \\ 0 & 0 & 0 & 1 \end{bmatrix} \tag{3.59}$$

where T_2 involves the rotational matrix $T_{2,rot}$ around the x-axis (dependent on the rotation θ_2 of R_2); T_3 contains the z-axis rotational matrix $T_{3,rot}$ (dependent on the rotation θ_3 of R_3) and the translation vector $[r_1;\ 0;\ r_3]$ (Table 3.1).

Knowing the local position of the connection points P_{i,CS_n} (Eq. 3.37, Eq. 3.38, Eq. 3.39), to compute Eq. 3.40, Eq. 3.43, Eq. 3.44, Eq. 3.49, Eq. 3.50, Eq. 3.51, the direct kinematic implementation is needed (form the local CS_n to the global GCS_2). Indeed, imposing the parametric points (Eq. 3.41, Eq. 3.45, Eq. 3.52), and defining the initial length of the springs (Eq. 3.42, Eq. 3.47, Eq. 3.55) concerning GCS_2, the remaining equations involve the inverse kinematic (from the global GCS_2 to the local CS_n). The initial length d_{0i} for each of the i^{th} spring is evaluated in the 3D space via the vector $D_{0i} = d_{01}v_i/\left|v_i\right|$, where $|v_i|$ is the module of the vector v_i through the i^{th} spring connection point. Note that one of the two connection points of each spring is the parametric point that needs to be optimized to reach the exoskeleton balancing; thus, it is previously unknown and is indicated as *OPT. PARAM.*

Concerning *MODEL 1*, all the *OPT. PARAM.* are regarding GCS_2. Also, to complete the definition of Eq. 3.26, the spring elastic constants $k_2,\ k_3,\ k_4$ may be considered as optimization parameters (Section 3.6.1).

- Referring to *MODEL 2*, still vale Eq. 3.40, Eq. 3.41, Eq. 3.42, whereas formulas from Eq. 3.43 to Eq. 3.48 are simplified in Eq. 3.60, Eq. 3.61, Eq. 3.62, and formulas from Eq. 3.49 to Eq. 3.57 become Eq. 3.63, Eq. 3.64, Eq. 3.65. In this case, the *OPT. PARAM.* for *SPRING 3* and *SPRING 4* changed the reference system (H_3 is concerning

CS_3, H_4 is regarding CS_4).

$$P_{3,CS_3} = (T_3 \ [p_{3,CS_3}; 1])_{1:3} \tag{3.60}$$

$$H_{3,CS_3} = [h_{3x};\ h_{3y};\ h_{3z}] \ (\textit{OPT. PARAM.}) \tag{3.61}$$

$$D_{3,CS_3} = d_{03}\frac{P_{3,CS_3} - H_{3,CS_3}}{|P_{3,CS_3} - H_{3,CS_3}|} \tag{3.62}$$

$$P_{4,CS_4} = [n_x \sin(\theta_4) - n_z \cos(\theta_4)\ ;\ n_y;\ n_x \cos(\theta_4) + n_z] \tag{3.63}$$

$$H_{4,CS_4} = [h_{4x};\ h_{4y};\ h_{4z}] \ (\textit{OPT. PARAM.}) \tag{3.64}$$

$$D_{4,CS_4} = d_{04}\frac{P_{4,CS_4} - H_{4,CS_4}}{|P_{4,CS_4} - H_{4,CS_4}|} \tag{3.65}$$

Chapter 4

W-EXOS: Wrist EXOSkeleton

Within this Chapter, a 3-DOFs, cable-driven, wrist exoskeleton is developed to fulfil the needs of robot-assisted rehabilitation. The mechanical design is presented in detail, starting from theoretical modelling to experimental evaluation. By involving a custom VR serious game with an assistive control strategy and a system of sensors to monitor the rehabilitation process while creating an engaging environment for the patient, the proposed research offers a complete device to be used aside from human capabilities, concerning both the user and therapist. Tests have been conducted on thirteen healthy subjects, providing valuable insights into the functionality and potential of the system. However, to thoroughly evaluate its performance and reliability, testing on a larger and more diverse population is essential. This would help ensure that the system can accommodate a wide range of user needs, including variations in physical characteristics, strength, and movement capabilities. Furthermore, as part of future research, a clinical trial is planned to investigate the therapeutic benefits of robot-assisted therapy in real patients. This trial will focus on assessing the system's effectiveness in aiding rehabilitation, its usability in clinical environments, and its impact on recovery outcomes. These additional steps will be crucial for validating the system's readiness for widespread clinical application and real-world use.

4.1. Project Requirements

Focusing on orthopaedic and post-stroke patients' rehabilitation of upper limbs, this chapter aims to design a wrist exoskeleton that conforms to the following specifications, which will be referred to as SPEC. X (X$\in [1:6]$) in the rest of the manuscript:

1. *ROM and maximum torque*: The device ROM has to allow the simulation of a complete rehabilitation process involving the maximum movement for each of the three wrist joints (i.e., $\pm 90\ deg$, $+15/-45\ deg$, $\pm 85\ deg$ for PS, RUD, FE [38]). It is worth noting

that this ROM is wider than the one for performing ADLs [9]. The torque at each joint can be the minimum to realize at least passive movements of the wrist, overcoming gravity and passive joint elasticity (i.e., $6\ Nm$ for PS and $1.5\ Nm$ for RUD and FE).

2. *Integrability*: The wrist exoskeleton needs to be versatile in its flanges of attachment to be used as a stand-alone device, but, also, combined with a shoulder-elbow and a hand exoskeleton, to get a complete upper limb rehabilitation system.

3. *Bimanual task performance*: The device structure should allow the development of a symmetric system to simulate bimanual tasks exploiting its workspace without interference with the user.

4. *Safety and product conformity*: The exoskeleton must be equipped with covers to be ready for the market and comply with medical certifications.

5. *VR implementation*: A custom VR serious game may be developed to involve the user via an immersive context, relieving the effort in performing repetitive tasks during the rehabilitation process.

6. *Sensor integration*: The system needs to be sensorized to add features to the VR environment and, also, to collect measurements during the rehabilitation process for the post-processing of data.

4.2. Design Considerations

As studied in Chapter 2, in the scientific literature, a variety of systems have been proposed in the last decades [41, 59, 60]. There are different devices for the upper limbs, but only a few include a 3-DOFs wrist module (e.g., [9]). To the authors' knowledge, other available wrist exoskeletons lack some features (e.g., the number of DOFs and/or the achievable ROM, the level of assistance, the versatility of being integrated into a monitored and comfortable environment for the patient) to provide optimal conditions for a complete wrist rehabilitation system. For instance, the eWrist [83] offers surface electromyography-based force control for wrist stroke treatment via an assist-as-needed support strategy, but it includes only 1-DOF (i.e., the wrist extension), whereas [84] presents a 3-DOFs soft robotic

orthosis for wrist rehabilitation at home, which supports all the three DOFs of the wrist, even if not in their full ROM, but it excludes the therapist from the rehabilitation process and it does not provide a station to save and evaluate parameters during the motion.

Looking at rigid wrist exoskeletons, some of the pioneers can be found in [10, 19–29, 85, 86]. Mostly, they have been designed for performing ADLs allowing the PS, RUD and FE simulation. However, these systems present different features that, even if combined, miss one or more of the specs listed in Section 4.1. Even if most of the devices can satisfy SPEC. 1, the fulfilment of SPEC. 2 and SPEC. 3 narrow the list of compatible systems. Indeed, devices presented in [19, 20, 23, 24] may host the hand exoskeleton and could be mounted on an upper limb exoskeleton but, being designed as desktop devices, they would not allow the performance of bimanual tasks, hampered by interference between parts and the user and by their downward high mass distribution. M3Rob [27] involves the integration of a hand exoskeleton but does not provide the attachment for an upper limb exoskeleton. Devices proposed in [21, 22, 25, 26, 28, 29] are limited to ground usage, the ones of [85, 86] could be portable but are designed as desktop devices and do not provide attachments for supporting other upper limb joints, whereas the wrist modulus of [9] is already connected to the shoulder-elbow module but cannot host the hand exoskeleton. An interesting solution is proposed in [10], the device meeting SPEC. 1 (partially), SPEC. 2 and SPEC. 3. Its specifications have been defined according to the minimum ROM and torque for each joint to perform ADLs, guaranteeing enough torque for each joint, but partial ROM (81% PS, 47% RUD, and 44% FE) compared to the human wrist full motion capabilities [38].

Hence the necessity to develop a novel device that fulfils all specs derived from the needs of robot-aided rehabilitation, aiming at overcoming barriers of traditional therapy at a clinical level, reducing the gap between technology and usability, and offering a high-level solution to improve rehabilitation efficacy. The system performances, qualitative and quantitative, have been assessed via the following metrics: wearability, integrability with different devices, theoretical ROM evaluation through a position control test, and usage in typical rehabilitation scenarios including the device interaction with VR serious games.

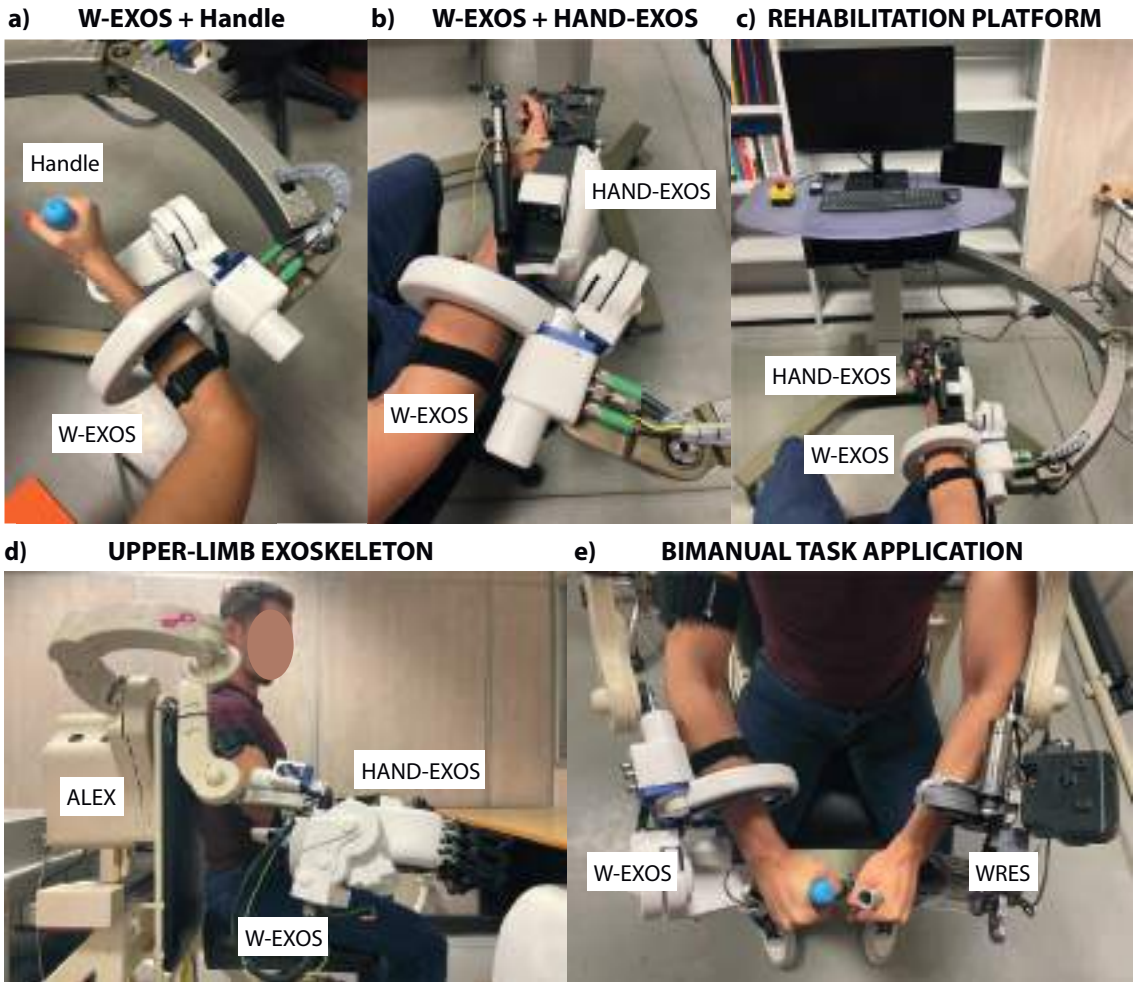

Figure 4.1: Physical prototype and layout configurations. ***a)*** *Wrist EXOSkeleton (W-EXOS) with the sensorized handle.* ***b)*** *W-EXOS with the hand exoskeleton [32].* ***c) Rehabilitation platform****: W-EXOS with the hand exoskeleton (the same configuration can be obtained by replacing the hand exoskeleton with the handle, as in a)). The station includes a screen for the virtual reality serious game visualization, a tablet for setting the therapy parameters, a central telescopic column for adjusting the station height, a robotic arm to support the W-EXOS, an emergency bottom (in red) for safety.* ***d) Upper limb exoskeleton****: W-EXOS with the hand exoskeleton attached to the 4-degrees of freedom shoulder-elbow ALEX [11] (the same configuration can be obtained by replacing the hand exoskeleton with the handle, as in e)).* ***e)*** *Bimanual task performance: ALEX hosts the W-EXOS on the right arm and the WRES [10] on the left arm. The user can move both arms until the end-effectors touch each other without interference between the device parts and the user's body.*

4.3. System Overview

The novel, versatile, 3-DOFs cable-driven W-EXOS with coupled joints is shown in Figure 4.1a equipped with a handle as end-effector. It allows the PS, RUD and FE movement within the physiological wrist ROM (SPEC. 1). According to SPEC. 2 and SPEC. 3, the

device is versatile in practice: designed to be used as part of a rehabilitation platform, where it is integrated on a working station equipped with a movable arm (Figure 4.1a,c), it can also be a module of a complete upper limb system, i.e., it can be attached to the 4-DOFs shoulder-elbow ALEX [11] (Figure 4.1d,e) taking application in both rehabilitation and teleoperation, allowing the simulation of bimanual tasks and the manipulation of virtual and real objects, similarly to [10]. In any case, the W-EXOS handle can be replaced by the hand exoskeleton [32], thus, allowing the wrist-hand combined motion (Figure 4.1b,c,d).

W-EXOS differs from the devices available in the literature thanks to its novel kinematics, explained in detail in Section 4.4.1, and the integrability with different structures while being compact and light to accommodate the end-effector, i.e., the handle or the hand exoskeleton. Indeed, the W-EXOS total weight is $2.7\ kg$ ($3.0\ kg$ with covers (SPEC. 4)), and, as detailed explained in Section 4.4.2, all parts, motors and transmission elements have been optimally sized and positioned on the external part of the device, thus, allowing simultaneous motion of both arms (SPEC. 3). The combination of these features has been achieved through the design of an efficient cable system transmission, deeply investigated in Section 4.4.2.1. Aspects such as ergonomics, reduced setup time and adaptability to limbs of different sizes have been considered to design the end-effector and the user interface; in detail, the handle can be mounted in a translation guide adding a passive DOF to the W-EXOS. So, the user's hand position can be regulated and the human wrist rotation centre can match the device one, thus, avoiding undesired forces during the motion. Once the user's and the device axis are aligned, the patient's forearm can be fixed to the support equipped with a comfortable neoprene cushion via elastic straps, correctly positioning the art. Also, a non-immersive VR serious game has been developed (SPEC. 5); it allows the performance of specific tasks creating a motivational environment for the user and improving the recovery efficacy in wrist skills, accelerating the patient's reintegration into social life and employment. Exercises can be calibrated and customized depending on the patient's needs to change the game difficulty. Moreover, the handle includes a pressure sensor to measure forces applied by the user on the device while performing a task, thus monitoring the therapy process (SPEC. 6).

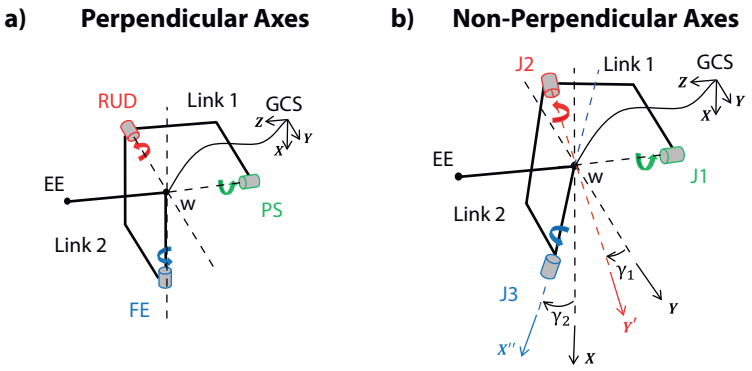

Figure 4.2: Kinematic schemes: three rotational joints with competing axes in the centre of rotation (point W). ***a)*** *Human wrist: perpendicular axes (Pronation Supination (PS), Radial Ulnar Deviation (RUD), Flexion Extension (FE)).* ***b)*** *Wrist exoskeleton: non-perpendicular axes (J1, J2, J3: rotation γ_1 in the YZ plane of the Global Coordinate System (GCS), rotation γ_2 in the XZ' plane, being Z' the new Z after the rotation γ_1).*

4.4. W-EXOS Virtual and Physical Prototyping

4.4.1. Kinematic Analysis

With the definition of a fast and versatile theoretical model in the choice of design parameters, the device workspace has been investigated for multiple tasks under SPEC. 1. The human wrist has been modelled as an equivalent exoskeleton with a 3-DOFs serial kinematic chain of three rotational joints (i.e., PS, RUD and FE) whose perpendicular axes intersect at one point (i.e., the wrist rotation centre). The W-EXOS consists of a first joint (J1) corresponding to PS, and other two joints (J2, J3) having an offset angle for RUD, and FE, thus, resulting in a spherical joint with non-perpendicular axes.

The kinematic schemes of both systems (i.e., the human wrist and the W-EXOS) are presented in Figure 4.2, where q_i represents the DOF of the wrist (i =PS, RUD, FE) and the device (i =J1, J2, J3). Starting from the kinematics with perpendicular axes (Figure 4.2a), the one of W-EXOS (Figure 4.2b) consists in a serial rotation of RUD and FE around point W: being J1 coincident with PS, J2 is obtained rotating RUD around the x-axis (GCS) of γ_1; then, J3 is achieved rotating FE around y'-axis (i.e., the new axis after the γ_1 rotation) of γ_2. This solution ensures the device full ROM performance keeping a reduced footprint. Indeed, γ_1 has been set as the minimum required to allow the full wrist extension avoiding interference between the user hand and link 1; whereas γ_2 enables the full wrist ulnar deviation preventing the end-effector from hurting the user's forearm.

By setting $\gamma_1 = 10\ deg$ and $\gamma_2 = 15\ deg$, pulleys and capstans embodying J2, and J3 can be realized with angular sectors up to $360\ deg$ depending on the ROM specs for each joint and the encumbrance of the other device parts. The classic kinematics with perpendicular axes would have let the same ROM at the expense of the device compactness and dynamic performances, since it may involve an increase in the length of link 1 and link 2 along the y- and x-axis respectively. Also, the device footprint and inertia growth go against SPEC. 2 and SPEC. 3. On the other hand, the proposed scheme causes the loss of matching between the human wrist and W-EXOS joints. In this case, project requirements relative to the perpendicular axes of the wrist need to be redefined under the W-EXOS novel kinematics. This limitation can be easily solved through theoretical model investigation: to perform a specific motion of the wrist, correspondent rotations of the W-EXOS can be derived and, then, set through control.

Kinematics models have been computed via the DH method [78] and compared evaluating effects due to the non-perpendicularity of the W-EXOS axes. DH parameters are reported in Table 4.1; note that a_i and d_i, $i =$ J1, J2, J3, are null, the GCS origin having in the wrist rotation centre. The complete model for deriving the exoskeleton joint rotations given a specific human wrist motion are provided in Appendix B.

Imposing a given motion law for the wrist rotations, positions and torques at W-EXOS joints have been evaluated. Figure 4.3 shows the coupling of the W-EXOS joints: each DOF of the wrist has been activated once at a time to simulate a pure **a)** PS, **b)** RUD, and **c)** FE movement (a sinusoidal motion law with frequency $f = 0.2\ Hz$ has been imposed). Then, the behaviour of the W-EXOS has been derived. As shown in Figure 4.3a, J1 is independent: the PS movement simulation results in the same rotation of J1 (note that RUD, FE, J2, and J3 are null (red, and blue continuous/dotted lines)). However, the reproduction of a pure RUD or FE movement (Figure 4.3b,c continuous lines) can be achieved via the activation of all the W-EXOS joints (Figure 4.3b,c dotted lines). Thus, several combinations of motion joints, i.e., actuation of a single joint or combination of two/three joints, have been considered to set the W-EXOS ROM under the physiological wrist specs.

The simultaneous activation of PS, RUD, and FE joints resulted in the following max/min values for J1, J2, and J3 respectively: $+106/-110\ deg$, $+46/-16\ deg$, $+72/-94\ deg$. So, the W-EXOS ROM has been set accordingly, thus satisfying SPEC. 1: the overall range per-

Table 4.1: Denavit Hartemberg parameters of the wrist exoskeleton (i = J1, J2, J3).

	q_{J1}	q_{J2}	q_{J3}
α_i	0	$\pi/2+\gamma_1$	$-\pi/2$
a_i	0	0	0
d_i	0	0	0
θ_i	$\theta_1=0$	$\theta_2=0$	$\theta_3=\pi/2+\gamma_2$

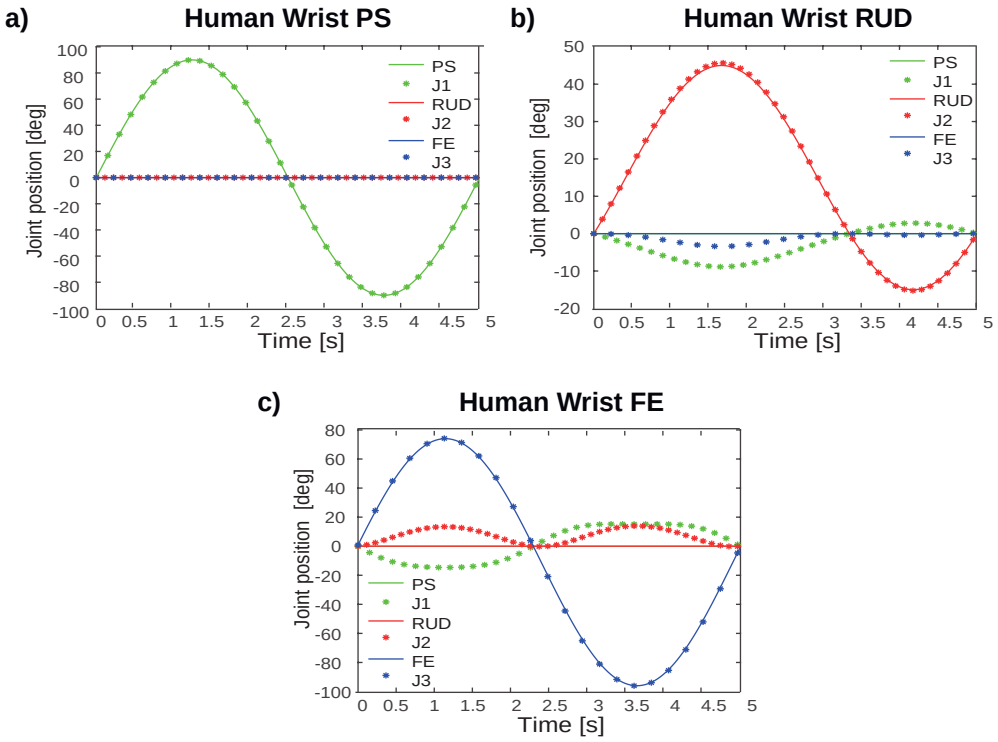

Figure 4.3: Kinematic models validation: human wrist (Pronation Supination (PS), Radial Ulnar Deviation (RUD), Flexion Extension (FE), continuous lines) vs Wrist EXOSkeleton (W-EXOS, J1, J2, J3, dotted lines) joints position [deg] in time [s]. Simulation of a single human wrist joint actuation and consequent coupling of the W-EXOS joints: ***a)*** *PS movement (i.e., RUD, FE null): J1 coincides with PS, J2 and J3 are null;* ***b)*** *RUD movement (i.e., PS, FE null): activation of all W-EXOS joints;* ***c)*** *FE movement (i.e., PS, RUD null): activation of all W-EXOS joints.*

formed by the device is 220 deg, 62 deg, 159 deg for J1, J2, J3. Concerning the human wrist workspace (i.e., ± 90 deg, $+15/-45$ deg, ± 85 deg for PS, RUD, FE from SPEC. 1), the J1 ROM is increased by 22.2%, whereas those of J2, and J3 have not noticeably changed ($+3.3\%$, -6.5%). Within this configuration, the device covers the 93.3% workspace of the wrist; indeed it allows the complete wrist ROM, except for the extension movement due to the occurrence of interference.

4.4.2. Mechanical Design

The CAD of the W-EXOS (the proposed 3-DOFs cable-drive wrist exoskeleton activated by brushless gear motors) is shown in Figure 4.4, highlighting the connection flanges to be replaced to reach the desired configuration. A comparison can be made with the configurations of the physical prototype shown in Figure 4.1: the device has been designed so to achieve different layouts by simply choosing the right flange of connection (Figure 4.4a). In particular, Figure 4.4b and Figure 4.4c show the possibility of having the handle and the hand exoskeleton as the end-effector of the W-EXOS. In detail, the W-EXOS can be identified as made of two main sub-assemblies:

- MODULE 1 reproduces the fixed part which supports the overall mechanism and is shown in Figure 4.4d.
- MODULE 2, illustrated in Figure 4.4e, contains the differential transmission for the activation of J2, and J3.

The merging of the two modules realizes J1, made of an inner ring fixed to the base, and a rotating outer ring. Two bearings realize a close, lightweight, circular guide mounted via the back-to-back configuration, thus, avoiding the device twisting during motion.

MODULE 1 includes the first motor selected to provide enough torque to hold the whole device weight. The support of motor 1 (Figure 4.4d, base) provides the flange to connect the device to the working station or the upper limb exoskeleton, being attached to the J1 inner ring. This latter hosts the connection for the forearm support (in white), ergonomically designed to ensure the device usability and acceptance.

Concerning MODULE 2, link 1 (Figure 4.4e, light blue) connects J1 to the differential transmission involving J2 and J3, and houses motor 2 and motor 3. The design choice of placing motors for powering J2 and J3 after J1 (i.e., they are not grounded) simplifies the cable transmission, at the expense of perceived inertia on joints. So, parts have been positioned close to the fixed base, whereas capstans and pulleys have been designed to keep the overall mechanism structure compact. This scheme features a device fully equipped with actuation and transmission systems, which can be integrated with a movable arm, not being constrained to be used as a desktop device (SPEC. 2, SPEC. 3). Indeed, the W-EXOS is

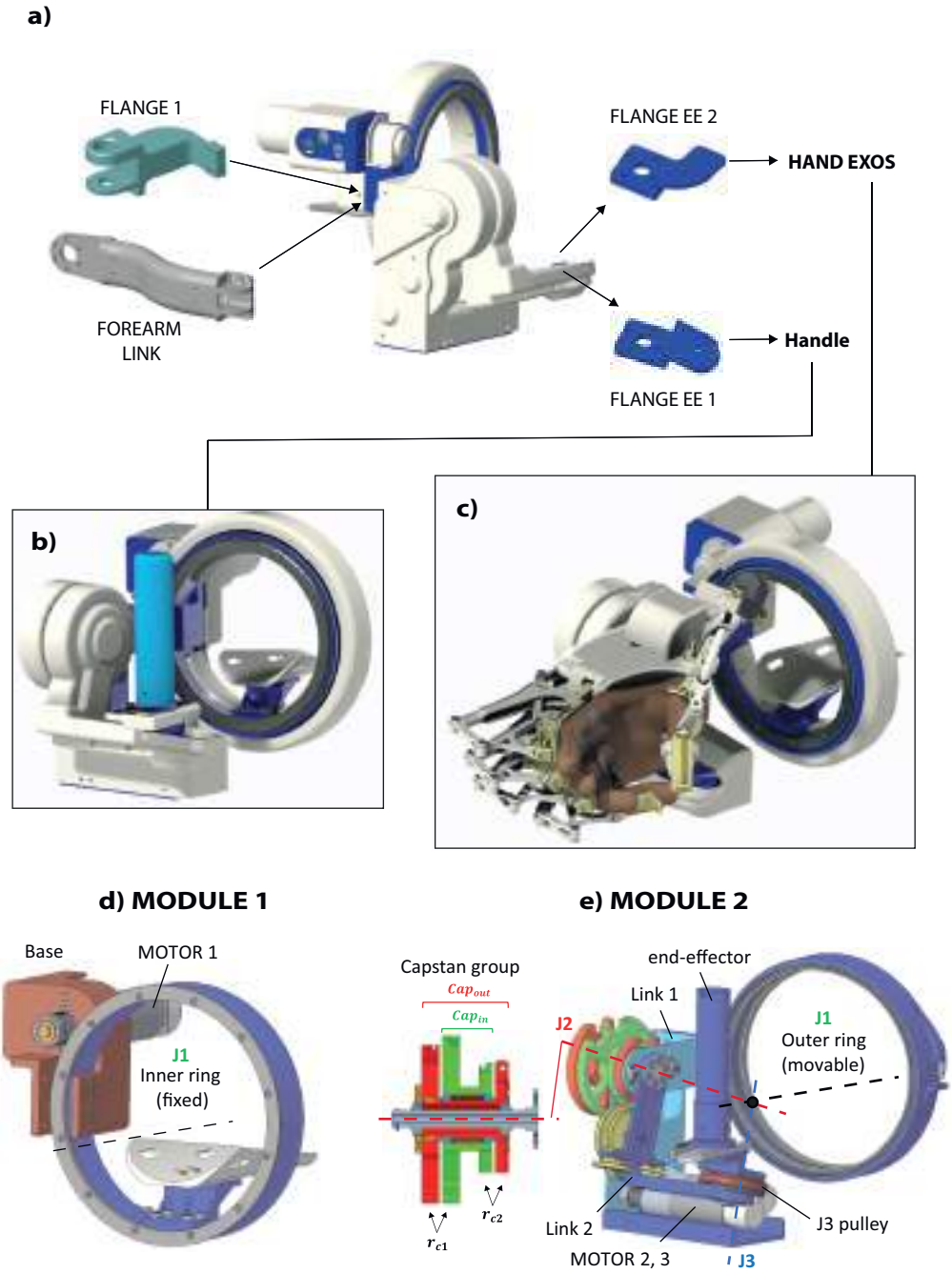

Figure 4.4: Wrist-EXOSkeleton (W-EXOS) Computer Aided Design (CAD) model with covers. ***a)*** *The W-EXOS end-effector can be switched between the handle (Figure 4.1a) and the hand exoskeleton (Figure 4.1b) through FLANGE EE 1 and FLANGE EE 2. The W-EXOS, regardless of the type of end-effector, can be mounted on the rehabilitation platform (Figure 4.1c) or the shoulder-elbow exoskeleton (Figure 4.1d) via FLANGE 1 or FOREARM LINK.* ***b)*** *W-EXOS with the handle as end-effector (Figure 4.1a).* ***c)*** *W-EXOS with the hand exoskeleton as end-effector (Figure 4.1b).* ***d)*** *W-EXOS MODULE 1: fixed base and J1 inner ring.* ***e)*** *W-EXOS MODULE 2: J1 outer ring and differential transmission with J2, J3 (capstans group in section).*

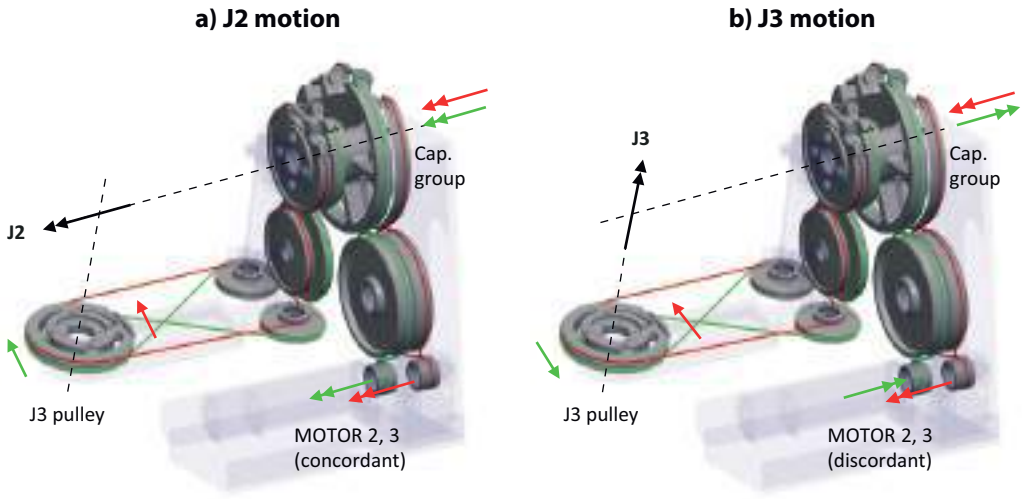

Figure 4.5: Wrist exoskeleton differential transmission (capstans, free pulleys and J3 pulley in grey). The red/green cable starts from motor 2/motor 3 and goes through the free pulleys, the capstan group, till the J3 pulley. The single/double arrow is for the force/moment acting on the element of interest (red/green is due to motor 2/motor 3). The double black arrow indicates the actuated degree of freedom (J2 or J3). ***a)*** *J2 motion is allowed by the concordant rotation of motor 2 and motor 3, i.e., of capstans;* ***b)*** *J3 motion is due to the discordant rotation of motor 2 and motor 3, i.e., of capstans.*

notable for its differential transmission, which is designed and described in detail in the next paragraph.

4.4.2.1. Differential Transmission

Concerning Figure 4.4e, J2 hosts two capstans mounted on a drive shaft including link 2. This latter realizes the J2 motion and hosts the J3 pulley, which fulfils the J3 rotation. The outer capstans ($Cap_{out,1}$ and $Cap_{out,2}$, with radius r_{c1} and r_{c2}, in red) are rigidly coupled with a hollow shaft. The inner capstans ($Cap_{in,1}$ and $Cap_{in,2}$, with radius r_{c1} and r_{c2}, in green), feature a mono-component. Capstans with radius r_{c1} are activated by the parallel coupling of motor 2 and motor 3; capstans with radius r_{c2} move accordingly, being rigidly coupled to the driven capstans.

Figure 4.5 explains the routing cable $2-$stage transmission which couples in parallel motors 2 and motor 3: the red cable connects motor 2 to Cap_{out}, reaching the J3 pulley via a system of passive pulleys. In the same way, the green cable connects motor 3 to Cap_{in} and J3 pulley. For both routing, the first stage (transmission ration τ_2) pairs motors to capstans with radius r_{c1}, and the second stage (transmission ration τ_3) connects capstans with radius

r_{c2} and the J3 pulley (radius $r_{p,j3}$). If motors rotation is concordant (Figure 4.5a), J2 is activated (i.e., same rotation of Cap_{out} and Cap_{in}); otherwise (Figure 4.5b), the motion of J3 occurs (i.e., motors discordant, opposite rotation of Cap_{out} and Cap_{in}). This behaviour is highlighted by the structure of the reduction matrix k_m, computed as in Eq. 4.1, which pairs motors to W-EXOS joints:

$$k_m = inv(k_g k_r k_t) = \begin{bmatrix} \frac{1}{k_1 \tau_1} & 0 & 0 \\ 0 & \frac{1}{2k_2\tau_2} & \frac{1}{2k_2\tau_2\tau_3} \\ 0 & \frac{1}{2k_2\tau_2} & -\frac{1}{2k_2\tau_2\tau_3} \end{bmatrix} \tag{4.1}$$

being k_g, k_r, k_t defined as follows:

$$k_g = \begin{bmatrix} k_1 & 0 & 0 \\ 0 & k_2 & 0 \\ 0 & 0 & k_3 \end{bmatrix} \tag{4.2}$$

$$k_r = \begin{bmatrix} \tau_1 & 0 & 0 \\ 0 & \tau_2 & 0 \\ 0 & 0 & \tau_2 \end{bmatrix} \tag{4.3}$$

$$k_t = \begin{bmatrix} 1 & 0 & 0 \\ 0 & 1 & 1 \\ 0 & \tau_3 & -\tau_3 \end{bmatrix} \tag{4.4}$$

where k_g is the reduction matrix between motors and gears, k_r is the coupling matrix between motors angular velocities and capstans of radius r_{c1}, and k_t is the coupling matrix between capstans of radius r_{c2} and J3 pulley. $\tau_1 = 8.6$, $\tau_2 = 5.3$, $\tau_3 = 1$, are the device transmission ratios where, concerning Figure 4.4d,e, τ_1 refers to J1 and is between motor 1 and the outer ring, whereas τ_2 and τ_3 are for the $2-$stage differential transmission.

The motor position vector $\boldsymbol{q_m}$ is computed as in Eq. 4.5:

$$\boldsymbol{q_m} = k_m \boldsymbol{q} \tag{4.5}$$

being $\boldsymbol{q} = [q_{J1};\ q_{J2};\ q_{J3}]$ the W-EXOS joints vector position, and k_m defined in Eq. 4.1.

The exoskeleton dynamics has been studied to know the motor torques required to simulate wrist movements and evaluate inertial torques perceived by the user due to motors and joint coupling (see the kinematic model in Section 4.4.1). The effects of motor 2 and motor 3 are distributed differently at respective joints, depending on accelerations encountered during a specific motion. When simulating a movement, even the single joint actuation of the human wrist resulted in distributed inertial torques on all W-EXOS joints (this aspect will be further explained in the discussion of results, Section 4.6). Thus, the W-EXOS DOFs coupling resulted in greater perceived inertia at each joint (as expected, J1 is affected by the highest torque since it supports the overall mechanism).

In the rehabilitation context, motors are fully exploited to reach a high assistance level when performing a passive wrist movement, thus, under the hypothesis of static conditions. In this case, the user is passive and the motion is guided through motors, since the system inertia is negligible. The latter may assume a significant contribution with the active involvement of the user, who can move joints faster, but also, applies forces on the device, making unnecessary the full exploitation of deliverable motor torque to complete a task. So, dynamic effects can be compensated by the remaining motor torque. Consequently, the joint coupling due to the novel kinematics does not considerably affect the motor size.

4.4.2.2. Technical Specifications

The W-EXOS total weight is $2.7\ kg$ ($3.0\ kg$ with covers). Its structural parts are in S136 MOLD STEEL and other components (i.e., links, free pulleys, capstans) in hard anodized 7075-T6 Aluminium Alloy. Covers have been printed via rapid prototyping powder sintering technology in poly amide-based plastic with glass fibre filler; they have been designed to optimize the device overall dimensions and ensure a complete ROM avoiding interference during motion and hosting power cables electronics (SPEC. 4).

The device is equipped with FAULHABER brushless motors, encoders IE3-1024 to monitor the joints position, and efficient, light, gearboxes to achieve high reduction ratios limiting the overall system footprint. Motor 1 (3242G024BX4) has a maximum torque of $53\ mNm$ and is equipped with one gearbox 32/3R 14:1. Motor 2 and motor 3 (2250X024BX4) deliver a maximum torque of $32\ mNm$ each, having gearboxes 22GPT 6,6:1. The transmission ca-

ble (CarlStahl, TECHNOCABLES) has a diameter of $1\ mm$, whereas, the bearings realizing J1 are KAYDON-SKF ultra slim type A, angular contact. The end-effector passive DOF consists of the igus-drylin N compact linear guide and is equipped with the pressure sensor Adafruit 1075.

Despite the strict requirements on the reduced encumbrance, the W-EXOS design proved to be suitable for performing ADLs and typical rehabilitation tasks. It is capable of simulating a full (around the 93%) human wrist ROM, ensured not to be exceeded by mechanical stoppers for each joint, and provides a maximum continuous torque of $6.38\ Nm$ on PS, and $2.24\ Nm$ for both RUD and FE, having high torque-weight ($2.41\ Nm/kg$) and torque-volume ($0.91x10^{-5}\ Nm/mm^3$) ratios. Risk analysis and electrical safety tests have been carried out to make the device compliant with medical certification.

4.5. Performance Assessment and Experiments

Theoretical models have been validated through experiments evaluating the device performance on the effective ROM and torque at each joint. Aspects such as usability, ergonomics, and applicability have been qualitatively investigated considering different assistive control strategies. Two tests have been carried out: one for exploring the achievable device workspace via a position control strategy, allowing the comparison of results with theoretical ones (Section 4.5.1); and another for analysing an actual setup where the device is worn by healthy subjects performing a VR serious game under an assistive control strategy (Section 4.5.2).

4.5.1. Position Control Test

The theoretical device ROM has been validated via a position control test, imposing a wrist movement and transforming it under the proposed device kinematics (Section 4.4.1). A standard position loop in the joint space using a proportional and derivative controller for all drivers has been implemented with the control law reported in Eq. 4.6:

$$u(t) = K_p e(t) + K_v \frac{d}{dt} e(t) \tag{4.6}$$

where $u(t)$ is the control signal over time and $e(t)$ is the position error between the reference signal and the measured one, being $K_p = 100$, $K_v = 1$ for motor 1, and $K_p = 50$, $k_v = 0.5$ for motor 2, motor 3. Proportional (K_p) and derivative (K_v) control coefficients have been empirically set to ensure the control loop stability.

The experiment consisted of three tests, with no subject wearing the exoskeleton, to reproduce a pure wrist **a)** PS, **b)** RUD, and **c)** FE movement. Sinusoidal motion laws with frequency $f = 0.2\ Hz$ repeated five times have been imposed at the W-EXOS joints within ranges consistent with SPEC. 1.

4.5.2. Virtual Reality Test

W-EXOS has been tested in the rehabilitation platform configuration (Figure 4.1c) with the handle as end-effector (Figure 4.1a) and worn by humans during a preliminary pseudo-rehabilitation task. The user had to perform orientation tasks by piloting an aircraft towards specific targets in a VR environment while receiving assistance from the device. The assistive strategy and the orientation tasks have been designed in collaboration with physical rehabilitation experts, and are described in detail in the next sections.

4.5.2.1. Participants

Thirteen healthy subjects (ten males, and three females) voluntarily joined the experiment and signed the informed consent before starting the test. Their mean features are as follows: 29.5 ± 3.2 years old, $175.8 \pm 11.2\ cm$ height, $24.7 \pm 7.8\ cm$ forearm length (elbow-wrist rotation centre distance), $19.1 \pm 1.4\ cm$ hand length (wrist rotation centre-middle fingertip distance). The study has been conducted under the World Medical Association Declaration of Helsinki guidelines and approved by the joint Scuola Superiore Sant'Anna and Scuola Normale Superiore ethical committee.

4.5.2.2. Experimental Setup

As visible from the CAD model of the system and the physical setup shown in Figure 4.6 and Figure 4.7, the W-EXOS in its basic configuration, i.e., having the handle as end-effector, has been integrated into the rehabilitation platform. The experimental setup is made of the following main components:

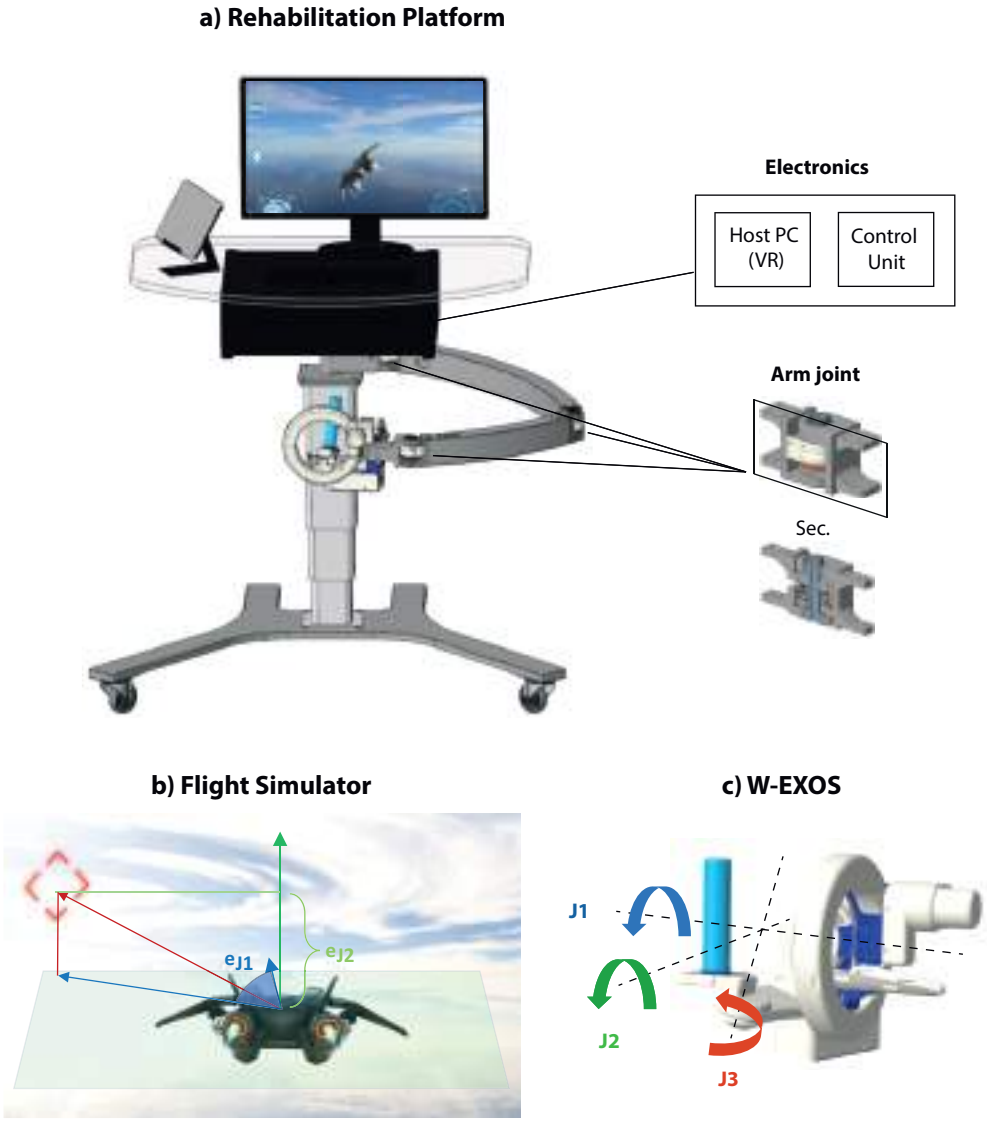

Figure 4.6: ***a)*** *Rehabilitation platform Computer Aided Design (CAD) model: Wrist-EXOSkeleton (W-EXOS) integrated into an adjustable working station with screen and keyboard for virtual reality implementation and tablet for therapist's rehabilitation monitoring (on the right, electronics box, arm joint and its section).* ***b)*** *Flight Simulator game aircraft Degrees of Freedom (DOFs) (roll and pitch). Correspondence between the W-EXOS DOFs and the aircraft DOFs: pronation-supination and radial-ulnar deviation orientation errors (e_{J1}, e_{J2}) (the green vector indicates the vertical direction of the aircraft, being normal to the green plane; the blue one is the pointing vector to the target (red dashed rhomboid); the red one connects the aircraft to the target).* ***c)*** *W-EXOS DOFs (J1, J2, J3).*

- Wrist exoskeleton.
- Control unit.
- Host Personal Computer (PC).

Figure 4.7: Experimental setup of the rehabilitation platform: subject wearing the wrist exoskeleton and performing the Flight Simulator serious game.

The W-EXOS is mounted on the extremity of a planar 3-DOFs aluminium arm, part of a wheeled structure which contains also the control unit. The system can be placed where preferred in the room and is equipped with a telescoping column to adjust the height according to the patient's comfortable posture. A table placed above the electronic housing supports the monitor, the tablet, and the keyboard to visualize the VR and check the therapy state. The arm is made of two hollow links connected in series with three revolute joints, allowing hosting cables, which connect the exoskeleton mounted in peripheral to the related electronics and control PC, and expanding the workspace in virtual environments. As visible from the section of Figure 4.6, each joint (passive) is equipped with a magnetic encoder to monitor the system during motion.

The control unit drives the exoskeleton motors through three commercial drivers (FAULHABER CONTROLLER MC5005 S ET) that implement a current closed-loop; it contains all the electronic components for the acquisition of the joints encoders and Hall sensors data, plus a set of relays for startup/shutdown routines, a 230/230V insulator transformer and a set of peripherals to connect the system to a local network and to an external debug/programmer PC.

The host PC runs a serious game called Flight Simulator and features an i7 13-gen, 32

Gb random-access-memory, and an Nvidia GTX 1660Ti graphic card. The Flight Simulator game has been developed using Unity 3D integrated development environment. The virtual environment features an aircraft, that flies with a constant velocity, and a set of targets that has to be reached piloting through the wrist exoskeleton as a sort of cloche: the user is asked to complete several orientation tasks driving the aircraft with the correct rotations of the wrist. In this application, only PS and RUD have been mapped to the aircraft piloting system (i.e., roll and pitch), being the yaw aircraft DOF (i.e., FE of the wrist exoskeleton) not actuated in an actual piloting setting (Figure 4.6). However, the user is free to move the FE joint, being this DOF coupled to the RUD one, due to the wrist kinematics deeply investigated in Section 4.4.1.

4.5.2.3. Experimental Protocol

As the experiment starts, the subject sits in front of the screen at $1\ m$ away from it and wears the wrist exoskeleton. The system features a neoprene cushion with lateral Velcro strap bands to secure the forearm in position on a soft surface. Before fixing the arm, the subject has to align the wrist rotation centre with the one of the exoskeleton, inserting the arm into the circular guide constituting the PS joint. Then the subject can grasp the handle, regulating its distance from the hand palm using its passive linear guide. The platform height is adjustable to match an angle of $90\ deg$ on the user's elbow and an approximately zero angle on the shoulder abduction. Once the user sits comfortably in the system, the experiment supervisor can set the therapy parameters tailored to the patient and start the serious game. The subject has to accomplish a sequence of orientation tasks guiding the aircraft flying at a constant speed through the wrist exoskeleton and catching twenty total targets, which are placed in a random position one at a time. When reached, a new target appears in a different location till the end of the game.

To sum up, during the session, the user is asked to complete several orientation tasks with the correct wrist rotations while receiving assistance proportional to the orientation error. As depicted in Figure 4.6, in this application, J1 and J2 have been mapped to the aircraft piloting system (i.e., roll and pitch).

4.5.2.4. Assistive Control

The W-EXOS provides assistance to the subject during the orientation tasks through a closed-loop control. Let once define the angular position vector $\mathbf{q} \in \mathbb{R}^3$ of the exoskeleton as in Eq. 4.7:

$$\mathbf{q} = [q_{J1}\ q_{J2}\ q_{J3}]^T \tag{4.7}$$

where $q_{J1},\ q_{J2},\ q_{J3}$ are the angular positions of the PS, RUD, and FE joints.

Knowing the device kinematics and dynamics (theoretical models have been developed based on the DH method [78]), the control strategy has been developed into three layers schematised in Figure 4.8. The lower layer provides ripple torque compensations ($\boldsymbol{\tau}_r$), constructed on the base of a look-up table having joint positions as inputs, and friction torque compensation ($\boldsymbol{\tau}_f$), computed as in Eq. 4.8:

$$\boldsymbol{\tau}_f(\dot{\mathbf{q}}) = \begin{cases} K_{f1,Ji}\dot{\mathbf{q}}, & \text{if } |\dot{\mathbf{q}}| <= V_{ft,Ji},\ i = 1,2,3 \\ K_{f2,Ji}\dot{\mathbf{q}}, & \text{if } |\dot{\mathbf{q}}| > V_{ft,Ji}\ ,\ i = 1,2,3 \end{cases} \tag{4.8}$$

being $\dot{\mathbf{q}}$ the joint velocity vector; $K_{f1,Ji} = [0.3,\ 0.01,\ 0.01]$, $K_{f2,Ji} = [0.7,\ 0.01,\ 0.01]$, for $i = 1,2,3$, the slope coefficients; and $V_{ft,Ji} = [0.7,\ 11.0,\ 11.0]\ deg/s$, for $i = 1,2,3$, the speed boundary value between coefficients.

Gravity compensation is provided by the middle layer, fed by joint positions. The torque $\boldsymbol{\tau}_{ML}$ including both the lower and the middle layer compensations is defined in Eq. 4.9:

$$\boldsymbol{\tau}_{ML} = \mathbf{g}(\mathbf{q}) + \boldsymbol{\tau}_f(\dot{\mathbf{q}}) + \boldsymbol{\tau}_r(\mathbf{q}) \tag{4.9}$$

where $\mathbf{q}$ and $\dot{\mathbf{q}}$ are the joint position and velocity vectors, $\mathbf{g}$ is the gravity torque vector, $\boldsymbol{\tau}_f$ and $\boldsymbol{\tau}_r$ are the friction and the ripple torque compensation vectors.

The high-level control provides assistance (if enabled) during the orientation tasks on the

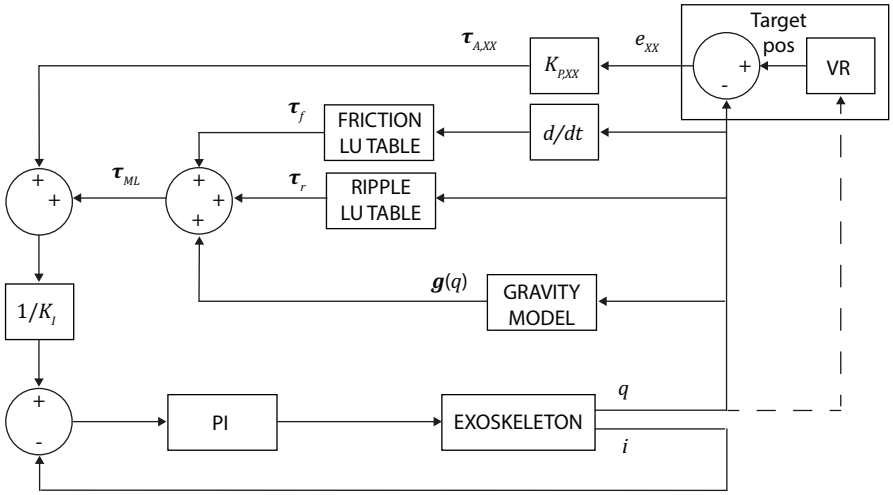

Figure 4.8: Control scheme: XX stands for both J1 and J2, collapsed in a single signal to optimize labels. LU Table stands for Look-Up Table. K_I is the torque constant. Other symbols have been defined from Eq. 4.8 to Eq. 4.11.

J1 and J2 DOFs with a simple proportional control computed as in Eq. 4.10:

$$\begin{cases} \boldsymbol{\tau}_{A,J1} = K_{P,J1}\, e_{J1} \\ \boldsymbol{\tau}_{A,J2} = K_{P,J2}\, e_{J2} \end{cases} \tag{4.10}$$

where $\boldsymbol{\tau}_{A,J1}$ and $\boldsymbol{\tau}_{A,J2}$ are the assistive torques on the J1 and J2 DOFs; $K_{P,J1} = 0.016\, Nm/deg$ and $K_{P,J2} = 0.010\, Nm/ud$ (being ud the Unity distance) are the gain coefficients of the motors driving the J1 and J2 joints, with a saturation value of the output torque equal to $2\, Nm$. e_{J1} and e_{J2} are the J1 and J2 orientation errors: as visible from Figure 4.6, e_{J1} is the angle between the aircraft pointing vector (in blue) and the vector that links the aircraft position to the target one (in red), projected onto the horizontal Unity plane (in green), with positive counter clockwise direction; whereas e_{J2} is the distance between the target and the aircraft vertical position.

Thus, the total torque can be formulated as in Eq. 4.11:

$$\boldsymbol{\tau} = \boldsymbol{\tau}_{ML} + \boldsymbol{\tau}_{A,J1} + \boldsymbol{\tau}_{A,J2} \tag{4.11}$$

4.5.2.5. Data Analysis and Statistics

Aiming at evaluating the efficacy of the device assistance during the performance of orientation tasks, for each session (made of twenty targets), the next data have been recorded:

- Exoskeleton joint angles, velocities, and accelerations.
- Joint assistive torques, i.e., torques provided by the device for the orientation task (Eq 4.10), and joint total torques, i.e., the sum of the assistive and compensation torques (Eq 4.11), to supervise the device assistance level and the user's effort.
- Grasping force due to the user's hand grip on the sensorized handle, to measure the effort in wearing and driving the device.
- Aircraft orientation errors, i.e., the difference between the device position and the one of the targets to be reached, to check the accuracy of the user's movement (Eq. 4.10, Figure 4.6).
- Game status to segment all session data for each of the twenty targets.

Data has been split into different trials being segmented between one target hit and the next one. After this segmentation, the following features have been extracted on each trial and used in the analysis: trial duration, maximum of grasping force, mean and standard deviation of joint angles, mean aircraft orientation errors, maximum of joint velocities. The maximum of some of the measurements has been used to better highlight the difference between conditions that a classic average could not achieve due to the nature of the orientation task: once oriented towards the target, the subject has to keep a correct trajectory until the target is reached without any further active motion, thus, flattening the values of features on a long-lasting trial.

Non-parametric two-sided Wilcoxon Signed-Rank test with repeated measures has been used to compare the two conditions, namely performing the Flight Simulator game with assistance or with no assistance, across all repetitions (twenty targets), having first assessed non-normality properties of distributions of the measured data through the Shapiro-Wilk test. The significance threshold of the p-value (p) has been set to $\alpha = 0.05$.

4.6. Results and Discussions

4.6.1. Position Control Test Results

Concerning the position control test, W-EXOS joints position and position error have been reported in Figure 4.9. Results match the theoretical ones presented in Figure 4.3: as

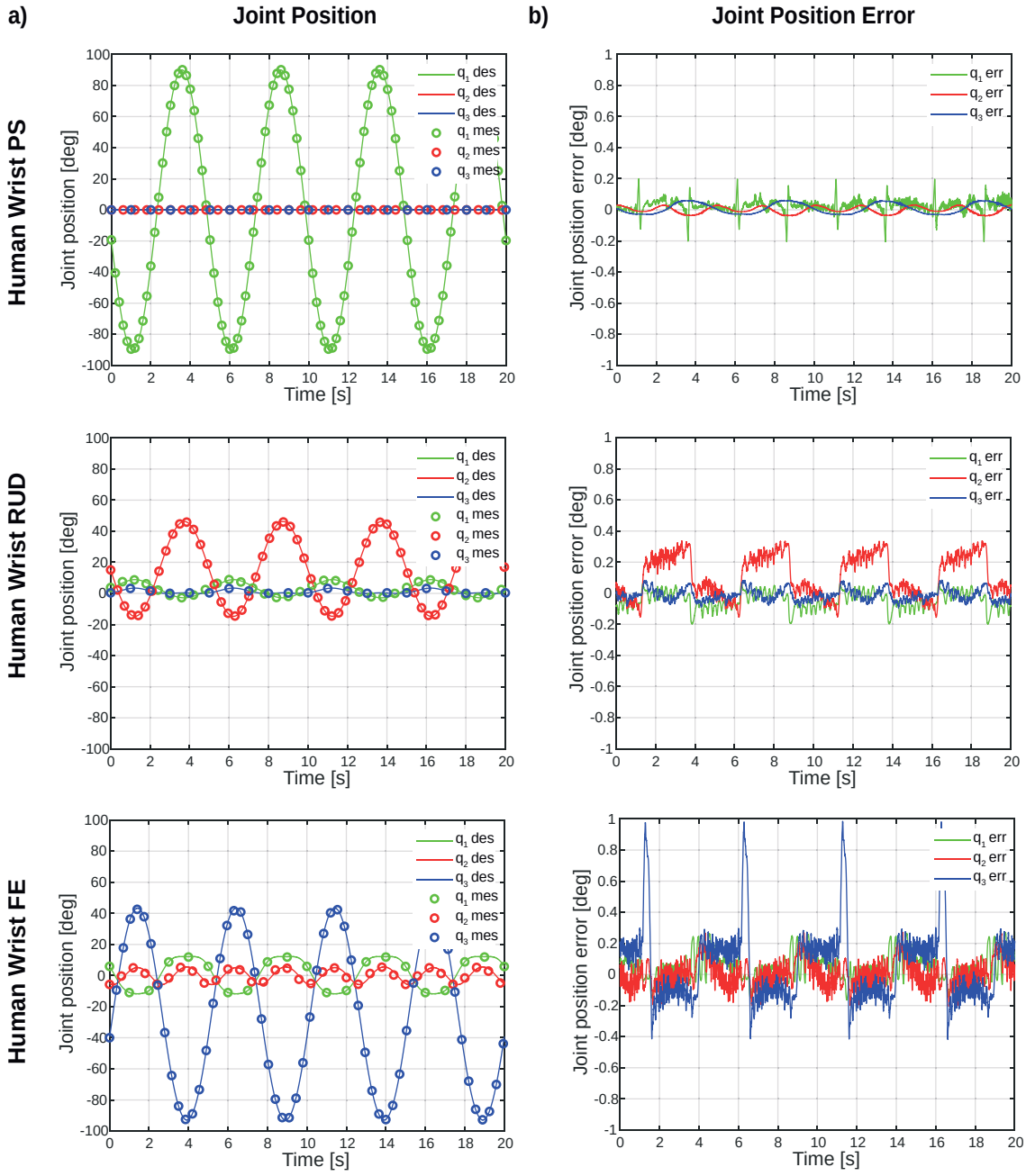

Figure 4.9: Position control test results. Performance achieved by the wrist exoskeleton to reproduce the wrist single motion of the Pronation Supination (PS), Radial Ulnar Deviation (RUD), and Flexion Extension (FE) joint (from up to down). ***a)*** *Joint position [deg] in time [s]: desired (q_i des, $i = 1, 2, 3$, continuous lines) vs measured (q_i mes, $i = 1, 2, 3$, bubble lines).* ***b)*** *Position error [deg] in time [s] for each joint concerning the imposed (desired) position (q_i err, $i = 1, 2, 3$).*

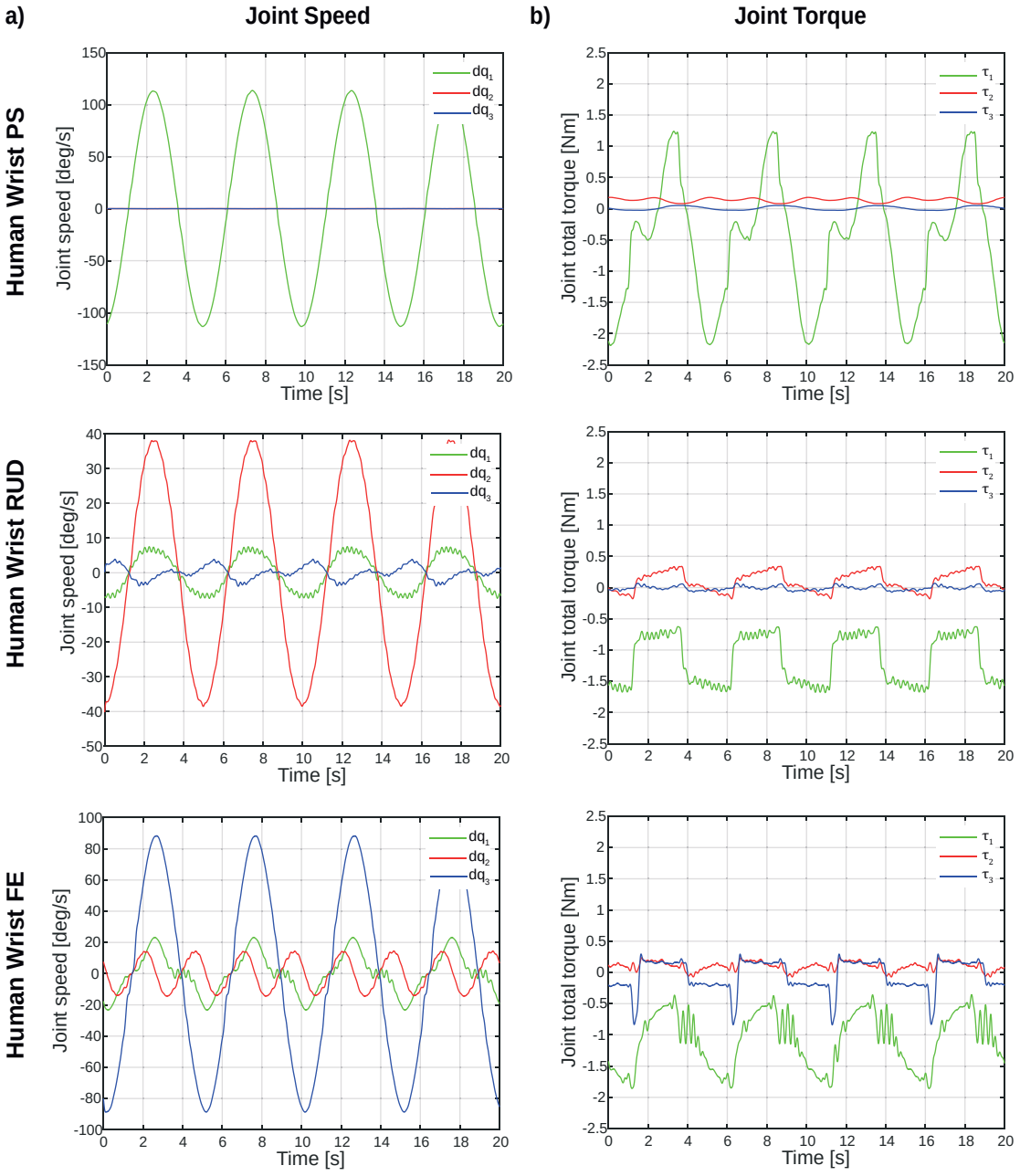

Figure 4.10: Position control test results. Performance achieved by the the wrist exoskeleton to reproduce the wrist single motion of the Pronation Supination (PS), Radial Ulnar Deviation (RUD), and Flexion Extension (FE) joint (from up to down). ***a)*** *Joint measured speeds [deg/s] in time [s] (dq_i, $i = 1, 2, 3$).* ***b)*** *Joint total torques [Nm] in time [s] (τ_i, $i = 1, 2, 3$).*

expected, J1 is independent (PS is achieved with the J1 rotation only), whereas the pure motion of RUD or FE involves the combination of all W-EXOS joints. The desired and measured positions for each movement overlap (continuous and bubble lines) and good performances of the position control have been reached, assessing an error minor than $1\ deg$ in all tests.

Figure 4.10 reports the W-EXOS joints speed and torque for each joint: the speed resulted in a maximum range of around $\pm 110\ deg/s$, $\pm 39\ deg/s$, and $\pm 83\ deg/s$ at J1, J2, and J3 (Figure 4.10a), whereas the total torque range is $+1.3/-2.3\ Nm$, $+0.4/-0.2\ Nm$ and $+0.3/-0.8\ Nm$ for J1, J2, and J3 (Figure 4.10b). As said in Section 4.4.2, dynamics effects due to joints coupling occur for the simulation of a pure human wrist motion (i.e., reproducing a PS, RUD, or FE human wrist motion requires torque in all W-EXOS joints). In any case, J1 involves the highest torque, holding most of the device weight.

4.6.2. Virtual Reality Test Results

The most relevant results between all measurements taken in Wilcoxon Signed-Rank test have been reported in Figure 4.11 and Figure 4.12. Differences across experimental conditions (i.e., assist, no-assist) regarding the analysed metrics have been plotted for the following measurements:

- Maximum (Max) angles of PS and RUD.
- Standard (Std) deviation of PS and RUD.
- Mean aircraft orientation error for PS and RUD.
- Maximum speeds of PS and RUD joints.
- Trial duration.
- Maximum grasping force.

The duration of trials did not show any difference among conditions (Figure 4.12b, $p = 0.11$, median: $46.0\ s/45.5\ s$ for assist/no-assist). Indeed, the measurement of handle grasping peaks across trials resulted in statistical significance between assist and no-assist conditions (Figure 4.12c, $p < 0.01$, median: $2.5\ N/2.8\ N$ for assist/no-assist). Figure 4.11a,b plot

the maximum and standard deviation of joint angles: only maximum values of PS showed a significant difference among conditions (PS: $p < 0.01$, RUD: $p = 0.82$, with a median value around zero for both DOFs), whereas standard deviations did for RUD only (PS: $p = 0.40$, median: $4.9\ deg$/$6.8\ deg$ and RUD: $p < 0.01$, median: $7.2\ deg$/$4.7\ deg$ for assist/no-assist). An important outcome concerned the PS and RUD aircraft orientation errors (Figure 4.11c, $p < 0.01$ for both PS and RUD, PS median: $3.2\ deg$/$6.2\ deg$, RUD median: $29.7\ deg$/$44.4\ deg$ for assist/no-assist). Figure 4.12a reports the comparison of the joints maximum speeds: the PS one was statistically relevant ($p = 0.05$), unlike that of the RUD ($p = 0.54$), both having a mean value around zero.

Figure 4.13a,b report the total (red) and assistive (green) torque on PS, and RUD joints of the subjects' wrist (since, in this application, the FE joint was not involved in any active action, the related submitted torque is almost zero). Data have been plotted considering the standard deviation of all subjects and trials (light band) and the mean (thick line). In both cases, a mean value different from zero, given by model compensations, occurs (it is higher for the PS due to the device kinematics). The assist torque reaches a mean (thick green) of $0.13\ Nm \pm 0.12\ Nm$ on PS, and of $0.22\ Nm \pm 0.10\ Nm$ on RUD. Concerning the mean total torque (tick red), the PS one constantly oscillates around $0.55\ Nm$ due to subjects' orientation adjustments, whereas, once the correct height of the target has been reached, the RUD torque almost assumes a null value. This highlights the two error computation strategies (Section 4.5.2.4). Offsets between the total and the assist torque for both PS and RUD show the main contribution of gravity compensation.

Figure 4.13c shows the theoretical ROM (grey ellipsoid), and the ROM reached by subjects (transparent red band) with its mean (red line), considering maximum joint angle values for each trial. These values depend on the target random position, according to which a certain PS or RUD rotation has to be performed. Higher values occurred during Pronation (P) rather than Supination (S), whereas the whole potential wrist ROM of the RUD was covered.

4.6.3. Discussions

4.6.3.1. Achieved Requirements

The device characterization justified the project design choices of the present research. Referring to Figure 4.14, it can be noticed that W-EXOS is suitable in the rehabilitation

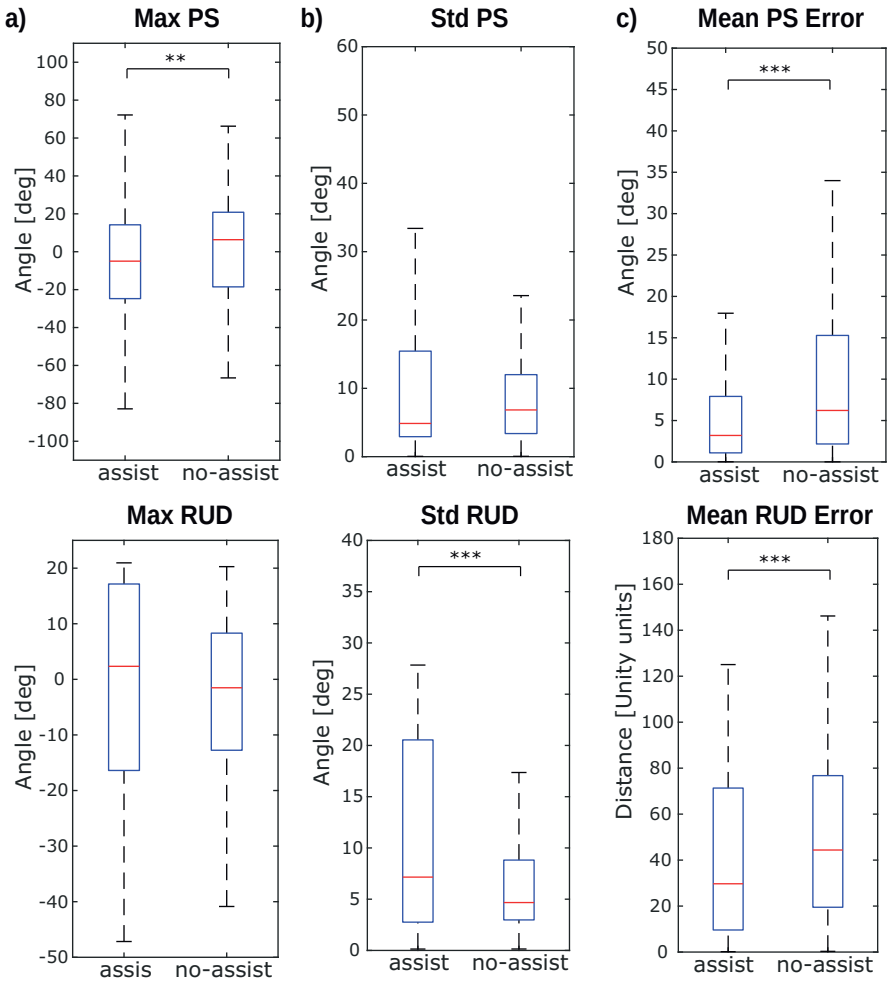

Figure 4.11: Virtual reality test results. Metrics distribution in assist and no-assist conditions (two columns for each box plot). ***a)*** *Maximum Pronation Supination (PS) and Radial Ulnar Deviation (RUD) positions (angle [deg]);* ***b)*** *Standard deviation of the PS and RUD positions (angle [deg]);* ***c)*** *PS and RUD aircraft mean orientation error (angle [deg], and Unity distance [ud]). For each plot, the red horizontal line in the blue box represents the data distribution median, whereas the blue box itself represents the second quartile. Lower and upper whiskers (black horizontal lines) show the first and third quartiles respectively. Asterisks represent the statistical significance of differences between conditions: * is for $p < .1$, ** is for $p < .05$, and *** is for $p < .01$ (plots with no asterisks show a not statistically significant comparison between conditions).*

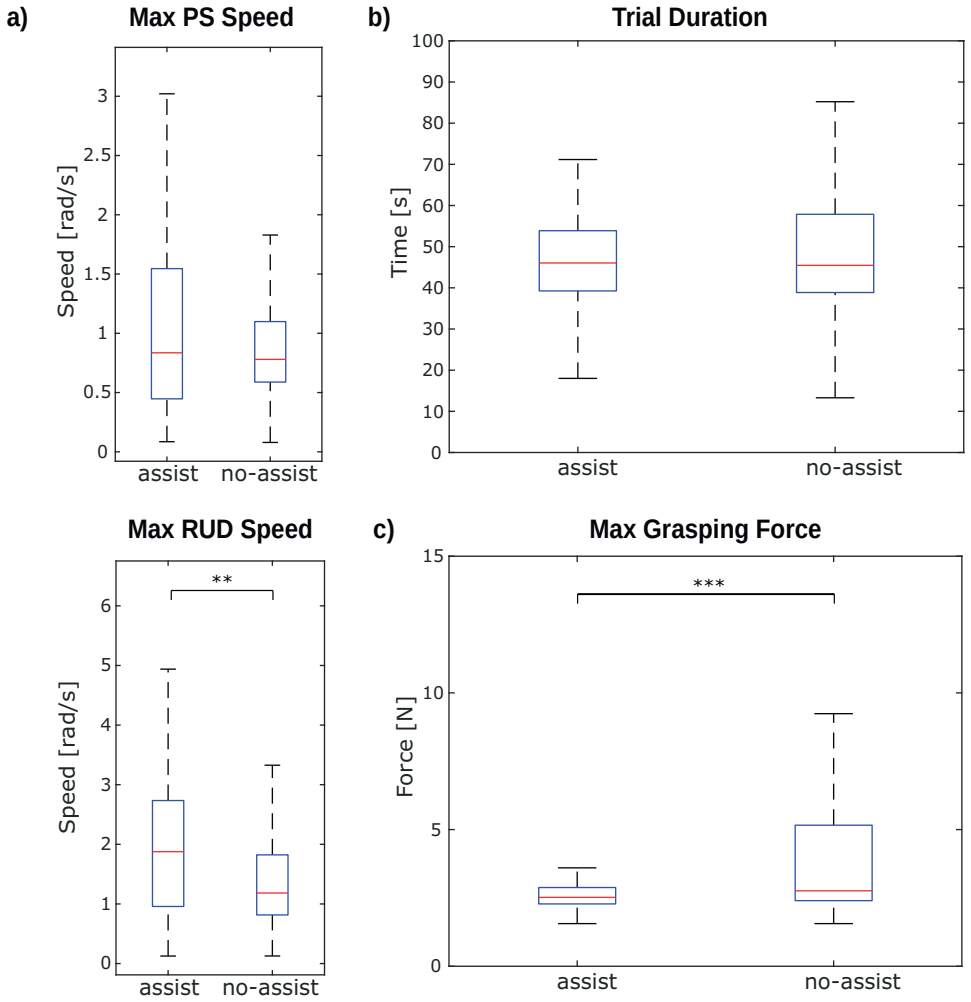

Figure 4.12: Virtual reality test results. Metrics distribution in assist and no-assist conditions (two columns for each box plot). ***a)*** *Maximum Pronation Supination (PS) and Radial Ulnar Deviation (RUD) speeds [rad/s];* ***b)*** *Trial duration (time [s]);* ***c)*** *Maximum grasping force made by the user on the device handle [N]. For each plot, the red horizontal line in the blue box represents the data distribution median, whereas the blue box itself represents the second quartile. Lower and upper whiskers (black horizontal lines) show the first and third quartiles respectively. Asterisks represent the statistical significance of differences between conditions: * is for $p < .1$, ** is for $p < .05$, and *** is for $p < .01$ (plots with no asterisks show a not statistically significant comparison between conditions).*

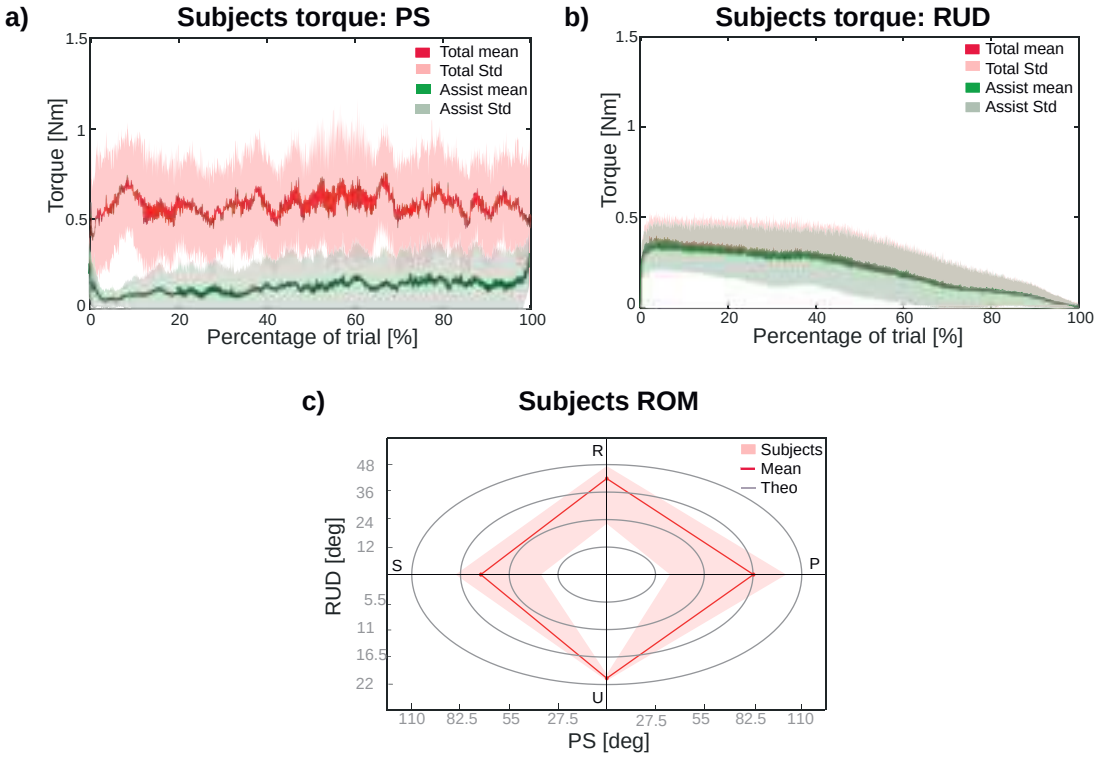

*Figure 4.13: Virtual reality test results. Mean value over thirteen subjects of the torque [Nm] during the percentage of trial [%] on **a)** Pronation Supination (PS) and **b)** Radial Ulnar Deviation (RUD) while playing the serious game (measured wrist exoskeleton joint torques transformed into wrist space). Mean (thick red and green line) and standard deviation (Std, transparent red and green band) of total (assistive + compensation, in red) and assistive (in green) torque. **c)** Range Of Motion (ROM) [deg] reached while playing the serious game and receiving the exoskeleton assistance across all subjects and trials (Subjects, transparent red band); mean values (red line); theoretical ROM (Theo, grey ellipsoids: the grey scale in PS and RUD axes is relative to the ellipsoid limit values).*

protocol, satisfying the human wrist requirements (HW req., continuous horizontal lines) in terms of ROM and maximum continuous torque, without oversize the system. The W-EXOS joints torque (full-colour blocks contoured in black) and the RU ROM (light green block) match the HW req.; the PS ROM (light orange block, 220 deg) exceeds the HW req. (light orange horizontal line, 180 deg), whereas, the FE ROM (light blue block, 159 deg) is lower than the HW req. (light blue horizontal line, 170 deg). This is due to the new kinematics and the W-EXOS joints coupling (Section 4.4.1); however, this ROM ensures the wrist natural movement. Most devices have been designed for ADLs, requiring lower performances than HW req.: e.g., only [22] fulfils the HW req. (except for the PS torque), whereas [27] provides enough PS and RU ROM, not enough FE ROM, and more than needed torque for all joints.

As reported in Section 4.2, the fulfilment of all SPECs identifies the WRES [10] as the most relevant device among previous works. Compared to the WRES, the W-EXOS has a wider ROM, similar maximum torque for the PS, and higher maximum torque for the RUD, and FE joints. These features have been achieved thanks to the novel kinematics and design choices for both customized and commercial parts. Indeed, W-EXOS weights $2.7\ kg$ (vs $2.9\ kg$ [10]) and has more performing torque-weight and torque-volume ratios ($2.41\ Nm/kg$ and $0.91x10^{-5}\ Nm/mm^3$ vs $2.38\ Nm/kg$ and $0.87x10^{-5}\ Nm/mm^3$ [10]) with the same motors. Even if the PS joint of the W-EXOS is a close circular guide, the device wearability has been secured thanks to the KAYDON-SKF ultra slim bearings, having an internal and external radius of $150\ mm$ and $156\ mm$ (vs $113\ mm$ and $175\ mm$ [10]) (i.e., the internal encumbrance has been augmented and the external one has been reduced). Basically, the W-EXOS design aimed at decreasing the number of components to lower costs and ease the mounting phase. Moreover, the device includes additional features, like a set of covers under medical certification, a sensorized end-effector, and a custom VR serious game.

As visible from Figure 4.1e, W-EXOS and WRES [10] have been mounted in the shoulder-

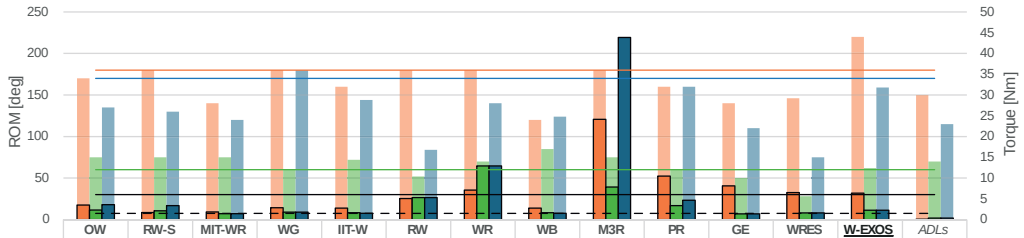

	OW	RW-S	MIT-WR	WG	IIT-W	RW	WR	WB	M3R	PR	GE	WRES	W-EXOS	ADLs
PS ROM	170	180	140	180	160	180	180	120	180	160	140	146	220	150
RUD ROM	75	75	75	60	72	52	70	85	75	60	50	28	62	70
FE ROM	135	130	120	180	144	84	140	124	115	160	110	75	159	115
PS Torque	3.5	1.69	1.85	2.87	2.77	5.08	7.1	2.77	24.16	10.46	8.1	6.52	6.38	0.06
RUD Torque	2.3	2.11	1.43	1.77	1.63	5.3	12.9	1.63	7.85	3.36	1.38	1.62	2.24	0.35
FE Torque	3.6	3.37	1.43	1.77	1.53	5.3	12.9	1.53	43.86	4.63	1.38	1.62	2.24	0.35
PS ROM (HW req.)	180	180	180	180	180	180	180	180	180	180	180	180	180	180
RUD ROM (HW req.)	60	60	60	60	60	60	60	60	60	60	60	60	60	60
FE ROM (HW req.)	170	170	170	170	170	170	170	170	170	170	170	170	170	170
PS Torque (HW req.)	6	6	6	6	6	6	6	6	6	6	6	6	6	6
RUD, FE Torque (HW req.)	1.5	1.5	1.5	1.5	1.5	1.5	1.5	1.5	1.5	1.5	1.5	1.5	1.5	1.5

Figure 4.14: Capabilities in terms of Range Of Motion (ROM) [deg] (light-colour, left vertical axis) and maximum torque [Nm] (full-colour contoured in black, right vertical axis) for each joint (Pronation Supination (PS) in orange, Radial Ulanr Deviation (RUD) in green, Flexion Extension (FE) in blue) of the most relevant devices in the literature (Open Wrist [19], Rice Wrist-S [20], MIT Wrist Robot [21], Wrist Grimbal [22], IIT Wrist [23], Rice Wrist [24], Wrist Robot [25], WristBot [26], M3Rob [27], PowRobot [28], Gopura Exos [29], WRES [10]), the novel Wrist EXOSkeleton (W-EXOS) and the Activities of Daily Living (ADLs) [9]. For each capability, the continuous line (same colours) is for the Human Wrist requirement (HW req.) in rehabilitation.

elbow exoskeleton [11] so that they can be compared. The W-EXOS higher performances have been achieved by keeping a similar encumbrance to the WRES. By wearing the full system, the user can touch both hands, being able to perform bimanual tasks including real and virtual object manipulation. Also, the W-EXOS has been integrated with the hand exoskeleton [32] and attached to ALEX [11] (Figure 4.1d), thus proving its versatility in the integration with different systems. Indeed, all configurations visible in Figure 4.1 can be easily achieved by simply choosing the connection flange, as depicted in Figure 4.4.

Considering the challenge of performing bimanual tasks, an interesting device is presented in [87]. The UULE is a 4-DOFs upper limb exoskeleton providing the shoulder and elbow flexion-extension, and the wrist PS and FE. The study reported in [87] compares available systems highlighting the importance of the device weight. Most devices range from $1.78\ kg$ to $18.75\ kg$, depending on which body part they target, either the wrist or the whole upper limb. The UULE weights $1.78\ kg$ only, but the wrist modulus is just 2-DOFs, being the RUD movement not provided.

Like studied in e.g., [10, 27–29], the inclusion of sensors can be examined. The pressure sensor embedded in the W-EXOS end-effector allows adding functionalities for the exoskeleton and the serious game interaction, e.g., for virtual object grasping. It lets indirect measurements, like the user's muscular stress during the VR test, thus, monitoring the rehabilitation process. In addition to offering the possibility of assessing practical device usage, the VR integration, like done in e.g., [21, 25, 26, 28, 85, 86], is important to create a playful environment for patients during the rehabilitation session. For this purpose, just having a game-like interface could not be sufficient to stimulate the user's focus and attention. In all previous VR integration, serious games employ a simple 2D environment with a static scenario that cannot be explored, showing basic scenes and graphics (e.g., tasks like repetitive sinusoidal trajectory following [85] or 2D target reaching [25]). In this work, the VR integration featured a more complex VR setting, with advanced graphics, realistic objects and visual feedback, also providing a high degree of versatility for customization (e.g., interactions with objects or obstacle avoidance). From a pure force/torque interaction point of view, most of the VR settings, including the proposed ones, ask the user to perform a standard set of movements and/or to apply a force towards the exoskeleton. Control strategies here often employ assist as needed algorithms, to support patients in their movement in

case of absence of active movements [26, 88]. In the proposed system, the control strategies perform a custom and proportional assistive action based on how much the subject is getting away from the target, continuously supporting the user's movement during the task. Also, complex VR environments allow therapy customization by choosing the difficulty level via the serious game settings.

Concerning safety, mechanical stoppers have been designed to prevent the exoskeleton ROM from exceeding the human joints one, thus, avoiding hurting the user. Also, the therapist can push the emergency button to switch off the overall platform in case of malfunctions.

4.6.3.2. Assistance Strategy

The assistance strategy of the proposed wrist exoskeleton has been compared to the no-assistance condition to evaluate the performance difference during an orientation task in a serious game. The study gave interesting results on the main effects of such assistance on healthy subjects (see Section 4.6.2).

Referring to Figure 4.11a,b and analysing the difference in the PS and RUD angles maximum and standard deviation, even if results were not always statistically significant (see whether there are asterisks or not), the plots showed an increasing trend in the assist condition exploring the exoskeleton ROM (see longer box plot whiskers), exploiting one of the device strengths. Indeed the exoskeleton has been developed to allow the complete human ROM (93.3%) for rehabilitation purposes. Comparisons can be performed with other works in the literature that experimented with orientation/trajectory following tasks with a similar device: for example, in [89], a 3-DOFs wrist exoskeleton has been tested in several tasks monitoring its performance. Particular attention has been put to the ROM and trajectory tests, in which, although the device was able to follow the submitted references, the covered ROM was much smaller than the one achieved by the system of this study.

Looking at the maximum of joints velocity graph in Figure 4.12a, the assist condition showed higher values than the other one, even if not all significant (see whether there are asterisks or not). A similar increasing trend can be noted among conditions: this is linked to the ability of the subject to rapidly understand the amount of the aircraft turn, following the perceived assistance torque.

Relevant results have been found for the mean orientation error along each trial, and the

grasping force (see the three asterisks for both measurements, Figure 4.11c, Figure 4.12c). The first confirmed the efficacy of the orientation aid given by the device for both the PS and RUD since lower mean PS and RUD errors occurred when the assistance was enabled. The second considered the peak for all trials: under the assist condition, the grasping force was significantly lower, with a maximum value less than $5\ kg$, also with a lower variability across trials (referring to shorter box plot whiskers), than the no-assist condition, in which the force was around $10\ kg$. This occurred since subjects perceiving the assistance during the orientation tasks used it as an orientation hint limiting the force applied with their contractions, thus relaxing their muscles, and focusing on using their ROM, meeting one of the therapy aims. Indeed, the level of assistance has been chosen to not replace the active wrist movement of the subject, being, in any case, useful as an orientation hint. The decreasing trend of muscle activity is a typical metric of the assistance control efficacy; for instance, in [90] the authors showed how an electromyography-based control can be used in an assist-as-needed control to decrease the wrist muscles contraction level during full-range wrist movements. Although, in this case, the monitored muscles set was different, a substantial decrease in grasping force has been detected under the assist condition, being the robot handle the device joints driver. Considering a rehabilitation context, having the possibility to regulate the level of assistance while playing the serious game is a vantage point for therapists, who can engage in muscle activities in patients, thus, tailoring the therapy to their needs.

Concerning the duration of the trials shown in Figure 4.12b, no differences have been detected between the two conditions (except for a little higher variance in data), even considering lower orientation errors for the assist condition, probably motivated by the average high distance between two consecutive targets, leaving the users enough time to adjust the aircraft orientation and to hit the target.

It is worth noting that tests have been carried out on healthy voluntary subjects; each completed the experiments without reporting any discomfort. As a first step, results from the VR test provide a reference for the mechanism performances and potential efficacy during orientation tasks, showing the device readiness to be tested in clinics. The tested assistive strategy showed the actual performance of a typical rehabilitation scenario where the active action of a robotic exoskeleton aids a motion task. Different assistive strategies can be used under specific clinical conditions: the proposed one is a simple approach to provide such

an orientation hint as intuitive assistance without considering the subject's effort, showing the device functionalities with a human in the loop. As a next step, data collected from real patients would be determinant to prove the system efficacy during a real rehabilitation session.

4.7. Summary

This chapter presented a 3-DOFs active cable-driven wrist exoskeleton versatile in its usage, light and compact while performing around the 93% of the physiological wrist ROM. It is powered via electric motors through an effective cable transmission, resulting in a backlash-free, optimized torque-weight ratio device. It presents an optimal mass distribution, all its components being disposed on the external side with the motors and transmission system embedded into covers. W-EXOS is versatile to be exploited in different contexts in a single/integrated configuration, allowing the user's upper limbs free motion. It provides connections, on one side, for a handle or a hand exoskeleton, on the other side, for a robotic arm part of a rehabilitation platform or a shoulder-elbow exoskeleton.

Theoretical models allowed the evaluation of the joint coupling effect due to the non-perpendicular axes kinematics. After detailing mechanical and constructive features, analytical models have been validated via a position control strategy, investigating the device ROM without human presence. Then, a VR experiment involved healthy subjects wearing the device and playing a serious game in a robotic rehabilitation-like session under an assistive control strategy. Considering a rehabilitation context, having the possibility of performing wrist movements in its full physiological range is of great importance for the therapy efficacy. The integrated VR allows therapists to engage in patients' muscle activities by regulating the assistance level during the serious game, thus, customizing the treatment to the patient's needs. Also, the system is capable of recording a large set of data: the device joint positions, velocities, accelerations, and torques (e.g., compensation and assistive torque), the grasping force due to the user's hand grip on the handle, so to monitor and assess the system efficacy. In the future, these measurements can be exploited to feed AI-based predictive models together with clinical and demographic data [88, 91], thus, improving the estimation of the system performance. Next, the device will be tested with patients in orthopaedic and post-stroke clinical scenarios, evaluating the effects of robot-assisted therapy. In the mean-

time, the exoskeleton got the CE marking from the G.S.D. S.r.l (Certified in accordance with UNI EN ISO 9001:2015 by TUV Rheinland Italia S.r.l. - Certificate N. 39 00 1850509; Test Report N. 23408).

According to [59], lately, simple and low-cost rehabilitation robots (e.g., [86]) seem to be the innovative solution for recovering wrist functionalities by individually addressing its three DOFs. On the contrary, traditional methods include complex systems that can provide focused and effective rehabilitation strategies involving simultaneous movements. The proposed device aims at providing flexibility in both the complexity of the overall structure (being usable on its own or integrated with other systems) and of the therapy (each DOF can be activated independently or combined with others under different conditions, e.g., speed, kind of motion and sequence).

Chapter 5

Conclusions

By following an in-depth analysis of the latest advancements in upper limbs exoskeletons design, this thesis provided the SEES, a 6-DOFs shoulder-elbow exoskeleton, and the W-EXOS, a 3-DOFs wrist exoskeleton, to be used in industrial and medical contexts for aiding workers and injured individuals while reproducing specific movements. As visible from Figure 5.1, the exoskeletons cover the reproduction of the complete workspace of the human upper limb joints, namely, the shoulder (5-DOFs), elbow (1-DOF), and wrist (3-DOFs). The devices, sharing common objectives from the current state of the art, have been developed as stand alone devices, to highlight the potential of each individual technology, combining traditional robotics methods and advanced optimization tools.

The SEES and the W-EXOS have been presented in Chapter 3 and Chapter 4 respectively. The SEES has been designed via a virtual prototype focusing on improving the mechanism efficiency while ensuring a simplified assembly, a lightweight design, and low production costs. To do so, the device has been designed fully passive, being suitable for the industrial

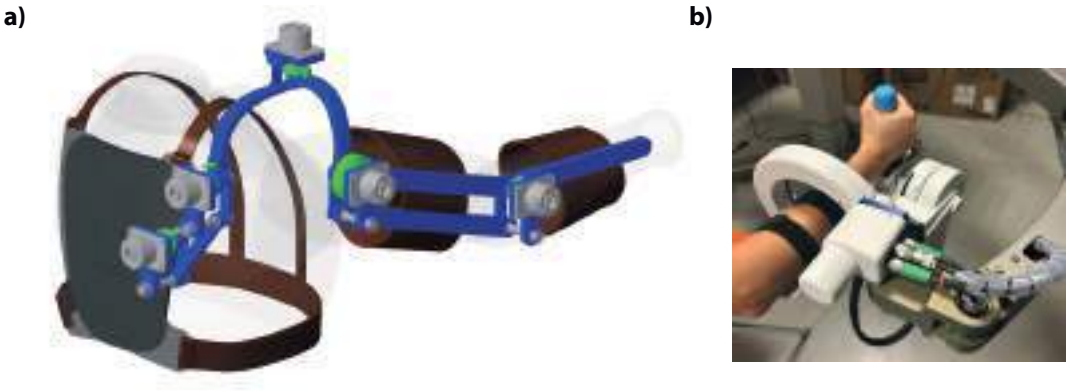

Figure 5.1: Upper limb exoskeletons proposed in the present thesis. ***a)*** *Virtual prototype of the 6-Degrees of Freedom (DOFs), passive, Shoulder-Elbow ExoSkeleton (SEES) with five torsional springs (green elements).* ***b)*** *Physical prototype of the 3-DOFs, active, Wrist-EXOSkeleton (W-EXOS) driven via a cable transmission and three brushless motors (one for each DOF).*

environment. A parametric, accurate, and fast analytical model that could prove valuable during the preliminary design stages of passive upper limbs exoskeletons has been provided so to be tested for different layouts depending on the needs. The W-EXOS has been designed via both virtual and physical prototyping; it is an active, cable-driven, device to be highly versatile in the integration with other systems, lightweight, and compact, while achieving approximately the 93% of the physiological wrist ROM. The device has been designed for versatility, making it adaptable for use in various contexts, whether as a stand alone device or integrated into larger systems: on one side, it can be equipped with a handle or a hand exoskeleton, on the other side, it can be connected to a robotic arm as part of a rehabilitation platform or a shoulder-elbow exoskeleton. This flexibility enables the W-EXOS to find application in both rehabilitation and assistive scenarios, enhancing its overall functionality and allowing the user's upper limbs to move freely within the natural workspace of the arm.

Concerning the SEES, a theoretical approach has been used to achieve the static balancing of the exoskeleton using passive elements alone. Both linear and torsional springs have been considered: the firsts allow the analysis of various parameters, achieving an optimal balance for each joint; the seconds are easier to be manufactured and assembled in practice, reducing the device footprint at the expense of the balancing accuracy. In any case, the feasibility of the proposed balancers has been evaluated based on specific criteria, such as body interference, workspace, and balancer configuration. All models have been validated using commercial software for three specific overhead movements, considering various conditions, such as links with differing densities. The model versatility allows for easy adjustment of the input motion laws, enabling the reproduction of any movement within the exoskeleton design space. Additionally, the geometric and mass parameters can be customized to match the user's limb size, further enhancing the adaptability and personalization of the exoskeleton.

By setting specific project requirements, the W-EXOS has been realized with a more traditional approach: it is powered by electric motors utilizing an efficient cable transmission system, offering backlash-free performance and an optimized torque-weight ratio. Its components are strategically distributed to ensure an ideal mass balance, with the motors and the transmission system embedded within external covers, enhancing both functionality and user's comfort. Theoretical models have been employed to assess the joint coupling effects caused by the non-perpendicular axes kinematics. After thoroughly outlining the mechanical

and structural aspects, the analytical models have been validated through a position control strategy, allowing for the device ROM evaluation in the absence of a human user. Subsequently, a VR experiment has been conducted with healthy participants wearing the device. They engaged in a serious game simulating a robotic rehabilitation session under an assistive control strategy to further assess the system performance.

So, the present research proposed two different approaches for designing upper limbs exoskeletons that aids the human arm preventing and/or treating injuries. Although the developed devices embody evident advances in the current literature, additional studies may be carried out to pursue the research in this field of technology. As a case study, the proposed balancer configurations of the SEES successfully ensure compactness and achieve full balance during a specific movement simulating upper limb lifting, which is essential for performing overhead manual tasks. Further feasibility considerations are required to implement a physical prototype of the SEES, with a focus on user's characteristics, task requirements, and load capacity. Instead, the W-EXOS provided a novel platform to deliver a playful and efficient environment to carry out recovery of the injured wrist joint, offering an advanced solution as alternative to the traditional therapy. Next, the device will undergo testing with patients in orthopaedic and post-stroke clinical settings to evaluate the effects of robot-assisted therapy. Metrics such as the grasping force generated by the user's grip on the handle, along with additional data on joint positions and torques, will be monitored. This information can then be utilized to inform AI-based predictive models that incorporate clinical and demographic data, ultimately assessing the system efficacy.

Bibliography

[1] COMAU. https://www.comau.com/en/our-offer/products-and-solutions/wearable-robotics-exoskeletons/. Accessed: 2024-08-17.

[2] LEVITATE. https://www.levitatetech.com/. Accessed: 2024-08-17.

[3] skelex. https://www.skelex.com/it. Accessed: 2024-08-17.

[4] AGADE. https://agade-exoskeletons.com/. Accessed: 2024-08-17.

[5] ShoulderX. https://exoskeletonreport.com/product/shoulderx/. Accessed: 2024-08-17.

[6] exoBIONICS. https://eksobionics.com/ekso-evo/. Accessed: 2024-08-17.

[7] Ottoock. https://corporate.ottobock.com/en/company/newsroom/new-exoskeleton-for-comfortable-overhead-work. Accessed: 2024-08-17.

[8] Van der Have, A., Rossini, M., Rodriguez-Guerrero, C., Van Rossom, S., and Jonkers, I., 2022. "The Exo4Work Shoulder Exoskeleton Effectively Reduces Muscle and Joint Loading During Simulated Occupational Tasks Above Shoulder Height". *ELSEVIER Applied Ergonomics,* **103**(103800).

[9] Perry, J. C., Rosen, J., and Burns, S., 2007. "Upper-Limb Powered Exoskeleton Design". *IEEE/ASME Transaction on Mechatronics,* **12**(4), pp. 408–417.

[10] Buongiorno, D., Sotgiu, E., Leonardis, D., Marcheschi, S., Solazzi, M., and Frisoli, A., 2018. "WRES: A Novel 3 DoF WRist ExoSkeleton with Tendon-Driven Differential Transmission for Neuro-Rehabilitation and Teleoperation". *IEEE Robotics and Automation Letters,* **3**(3), pp. 2152–2159.

[11] Pirondini, E., Coscia, M., Marcheschi, S., Roas, G., Salsedo, F., Frisoli, A., Bergamasco, M., and Micera, S., 2016. "Evaluation of the Effects of the Arm Light Exoskeleton on Movement Execution and Muscle Activities: A Pilot Study on Healthy Subjects". *Journal of NeuroEngineering and Rehabilitation,* **13**(9), pp. 1–21.

[12] Zimmermann, Y., Forino, A., Riener, R., and Hutter, M., 2019. "ANYexo: A Versatile and Dynamic Upper-Limb Rehabilitation Robot". *IEEE Robotics and Automation Letters,* **4**(4), pp. 3649–3656.

[13] Buccelli, S., Tessari, F., Fanin, F., De Guglielmo, L., Capitta, G., Piezzo, C., Bruschi, A., Van Son, F., Scarpetta, S., Succi, A., Rossi, P., Maludrottu, S., Barresi, G., Creatini, I., Taglione, E., Laffranchi, M., and De Michieli, L., 2022. "A Gravity-Compensated Upper-Limb Exoskeleton for Functional Rehabilitation of the Shoulder Complex". *Applied Sciences,* **12**(7).

[14] Nef, T., Guidali, M., and Riener, R., 2009. "ARMin III - Arm Therapy Exoskeleton with an Ergonomic Shoulder Actuation". *Applied Bionics and Biomechanics,* **6**(2), pp. 127–142.

[15] Crea, S., Cempini, M., Moisé, M., Baldoni, A., Trigili, E., Marconi, D., Cortese, M., Giovacchini, F., Posteraro, F., and Vitiello, N., 2016. "A Novel Shoulder-Elbow Exoskeleton with Series Elastic Actuators". *IEEE International Conference on Biomedical Robotics and Biomechatronics*, pp. 1248–1253.

[16] Kim, B., and Deshpande, A. D., 2017. "An Upper-Body Rehabilitation Exoskeleton Harmony with an Anatomical Shoulder Mechanism: Design, Modeling, Control, and Performance Evaluation". *The International Journal of Robotics Research,* **36**(4), pp. 414–435.

[17] Brahmi, B., Saad, M., Rahman, M. H., and Ochoa-Luna, C., 2019. "Cartesian Trajectory Tracking of a 7-DOF Exoskeleton Robot Based on Human Inverse Kinematics". *IEEE Transactions on Systems, Man, and Cybernetics: Systems,* **49**(3), pp. 600–611.

[18] Oguntosin, V. W., Mori, Y., Kim, H., Nasuto, S. J., Kawamura, S., and Hayashi, Y., 2017. "Design and Validation of Exoskeleton Actuated by Soft Modules toward Neurorehabilitation-Vision-Based Control for Precise Reaching Motion of Upper Limb". *Frontier in Neuroscinece,* **11**(352).

[19] Pezent, E., Rose, C. G., Deshpande, A. D., and O'Malley, M. K., 2017. "Design and Characterization of the OpenWrist: A Robotic Wrist Exoskeleton for Coordinated Hand-Wrist Rehabilitation". *IEEE International Conference on Rehabilitation Robotics*, pp. 720–725.

[20] Pehlivan, A. U., Sergi, F., Erwin, A., Yozbatiran, N., Francisco, G. E., and O'Malley, M. K., 2014. "Design and Validation of the RiceWrist-S Exoskeleton for Robotic Rehabilitation after Incomplete Spinal Cord Injury". *Robotica,* **32**(8), pp. 1415–1431.

[21] Krebs, Hermano Igo, V. B. T., Williams, D., Celestino, J., Charles, S. K., Lynch, D., and Hogan, N., 2007. "Robot-Aided Neurorehabilitation: A Robot for Wrist Rehabilitation". *IEEE Transactions on Neural Systems and Rehabilitation Engineering,* **15**(3), pp. 327–335.

[22] Martinez, J. A., Ng, P., Lu, S., Campagna, M. S., and Celik, O., 2013. "Design of Wrist Gimbal: A Forearm and Wrist Exoskeleton for Stroke Rehabilitation". *IEEE International Conference on Rehabilitation Robotics*, pp. 1–6.

[23] Cappello, L., Elangovan, N., Contu, S., Khosravani, S., Konczak, J., and Masia, L., 2015. "Robot-Aided Assessment of Wrist Proprioception". *Frontiers in Human Neuroscience,* **9**.

[24] Gupta, A., O'Malley, M. K., Patoglu, V., and Burgar, C., 2008. "Design, Control and Performance of RiceWrist: A Force Feedback Wrist Exoskeleton for Rehabilitation and Training". *The International Journal of Robotics Research,* **27**(2), pp. 233–251.

[25] Masia, L., Casadio, M., Psiche, G., Sandini, G., and Morasso, P., 2009. "Performance Adaptive Training Control Strategy for Recovering Wrist Movements in Stroke Patients: A Preliminary, Feasibility Study". *Journal of Neuroengineering and Rehabilitation,* **6**(44).

[26] Albanese, G. A., Taglione, E., Gasparini, C., Grandi, S., Pettinelli, F., Sardelli, C., Catitti, P., Sandini, G., Masia, L., and Zenzeri, J., 2021. "Efficacy of Wrist Robot-Aided Orthopedic Rehabilitation: A Randomized Controlled Trial". *Journal of Neuro-Engineering and Rehabilitation,* **18**.

[27] Alonso-Linaje, G., Cisnal, A., Fraile, J. C., and Turiel, J. P., 2024. "Design and Analysis of the M3Rob: A Robotic Platform for Wrist and Hand Rehabilitation". *IEEE Access,* **12**, pp. 30472–30481.

[28] Mayetin, U., and Kucuk, S., 2022. "Design and Experimental Evaluation of a Low Cost, Portable, 3-DOF Wrist Rehabilitation Robot with High Physical Human-Robot Interaction". *Springer Journal of Intelligent and Robotic Systems,* **106**(65).

[29] Gopura, R., and Kiguchi, K., 2007. "Development of an Exoskeleton Robot for Human Wrist and Forearm Motion Assist". *International Conference on Industrial and Information Systems*, pp. 535–540.

[30] Bilancia, P., and Berselli, G., 2021. "Conceptual Design and Virtual Prototyping of a Wearable Upper Limb Exoskeleton for Assisted Operations". *Springer International Journal on Interactive Design and Manufacturing,* **15**, pp. 525–539.

[31] Tschiersky, M., Hekman, E. E. G., Herder, J. L., and Brouwer, D. M., 2022. "Gravity Balancing Flexure Spring Mechanisms for Shoulder Support in Assistive Orthoses". *IEEE Transactions on Medical Robotics and Bionics*, pp. 1–1.

[32] Sarac, M., Solazzi, M., Sotgiu, E., Bergamasco, M., and Frisoli, A., 2017. "Design and Kinematic Optimization of a Novel Underactuated Robotic Hand Exoskeleton". *Meccanica,* **52**, pp. 749–761.

[33] Nikhil, G., Yedukondalu, G., and Rao, S., 2019. "Robotic Exoskeletons: A Review on Development". *International Journal of Mechanical and Production Engineering Research and Development,* **9**(4), pp. 529–542.

[34] Zhou, L., Li, Y., and Bai, S., 2017. "A Human-Centered Design Optimization Approach for Robotic Exoskeletons Through Biomechanical Simulation". *Robotics and Autonomous Systems,* **91**, pp. 337–347.

[35] Castro, M. N., Rasmussen, J., Bai, S., and Andersen, M. S., 2019. "The Reachable 3-D Workspace Volume is a Measure of Payload and Body-Mass-Index: A Quasi-Static Kinetic Assessment". *Applied Ergonomics,* **75**, pp. 108–119.

[36] Netter, F. H., 2022. "Netter Atlas of Human Anatomy: A Systems Approach-E-Book: paperback+ eBook". *Elsevier Health Sciences*.

[37] Tortora, G. J., and Derrickson, B. H., 2018. "Principles of Anatomy and Physiology". *John Wiley & Sons*.

[38] Kapandji, A., 1982. "The Physiology of the Joints. Volume 1 Upper Limb". *Churchill Livingstone, Edinburgh London Melbourne and New York*.

[39] Mordor Intelligence. https://www.mordorintelligence.com/. Accessed: 2024-04-12.

[40] Marchal-Crespo, L., and Reinkensmeyer, D. J., 2009. "Review of Control Strategies for Robotic Movement Training after Neurologic Injury". *Journal of NeuroEngineering and Rehabilitation,* **6**(1), pp. 1–15.

[41] Maciejasz, P., Eschweiler, J., Gerlach-Hahn, K., Jansen-Troy, A., and Leonhardt, S., 2014. "A Survey on Robotic Devices for Upper Limb Rehabilitation". *Journal of NeuroEngineering and Rehabilitation,* **11**(1), pp. 1–29.

[42] Cohen, Y., Naseraldin, H., Chaudhuri, A., and Pilati, F., 2019. "Assembly Systems in Industry 4.0 Era: A Road Map to Understand Assembly 4.0". *Springer International Journal of Advanced Manufacturing and Technology,* **105**(9), pp. 4037–4054.

[43] Hyun, D. J., Bae, K., Kim, K., Nam, S., and Lee, D. H., 2019. "A Light-Weight Passive Upper Arm Assistive Exoskeleton Based on Multi-Linkage Spring-Energy Dissipation Mechanism for Overhead Tasks". *Elsevier Robotics and Autonomous Systems,* **122**, p. 103309.

[44] Bances, E., Schneider, U., Siegert, J., and Bauernhansl, T., 2020. "Exoskeletons Towards Industrie 4.0: Benefits and Challenges of the IoT Communication Architecture". *Elsevier Procedia Manufacturing International Conference on Industry 4.0 and Smart Manufacturing.,* **42**, pp. 49–56.

[45] Gómez, M. M., 2020. "Prediction of Work-Related Musculoskeletal Discomfort in the Meat Processing Industry Using Statistical Models". *Elsevier International Journal of Industrial Ergonomics,* **75**, p. 102876.

[46] Huysamen, K., Power, V., and O'Sullivan, L., 2020. "Kinematic and Kinetic Functional Requirements for Industrial Exoskeletons for Lifting Tasks and Overhead Lifting". *Ergonomics,* **63**(7), pp. 818–830.

[47] Gull, M. A., Bai, S., and Bak, T., 2020. "A Review on Design of Upper Limb Exoskeletons". *MDPI Robotics,* **9**(1).

[48] Jalal, M. F. A., Harith, H. H., Hasan, W. Z. W., Salim, M. S. F., and Lin, T. T., 2024. "Exoskeletons for Elderly Activity of Daily Living Assistance: A Review of Upper Limb Exoskeletons and Assessments". *International Journal of Integrated Engineering,* **16**(1), pp. 87–105.

[49] Jin, T., Chifu, Y., Feng, J., Changbin, C., Yingjie, L., and Chunzhi, Y., 2024. "A Systematic Review of Occupational Shoulder Exoskeletons for Industrial Use: Mechanism Design, Actuators, Control, and Evaluation Aspects". *ELSEVIER SSRN*.

[50] MAX. https://www.newequipment.com/home/product/55105088/68991-modular-agile-exoskeleton. Accessed: 2024-08-17.

[51] SUITX. https://www.suitx.com/en/home. Accessed: 2024-08-17.

[52] Ottoock Shoulder. https://orthexo.de/en/exoskeletons/industrial-exoskeletons/paexo-shoulder/. Accessed: 2024-08-17.

[53] Bosch, T., van Eck, J., Knitel, K., and de Looze, M., 2016. "The Effects of a Passive Exoskeleton on Muscle Activity, Discomfort and Endurance Time in Forward Bending Work". *Applied Ergonomics,* **54**, pp. 212–217.

[54] Pacifico, I., Scano, A., Guanziroli, E., Moisé, M., Morelli, L., Chiavenna, A., Romo, D., Spada, S., Colombina, G., Molteni, F., Giovacchini, F., Vitiello, N., and Crea, S., 2020. "An Experimental Evaluation of the Proto-MATE: A Novel Ergonomic Upper-Limb Exoskeleton to Reduce Workers' Physical Strain". *IEEE Robotics & Automation Magazine,* **27**(1), pp. 54–65.

[55] DIH Medical. https://www.dih.com/products-solutions/. Accessed: 2023-04-24.

[56] Bionik. https://bioniklabs.com/. Accessed: 2023-04-24.

[57] Fourier Intelligence. https://fourierintelligence.com/. Accessed: 2023-04-24.

[58] Guatibonza, A., Solaque, L., Velasco, A., and Penuela, L., 2024. "Assistive Robotics for Upper Limb Physical Rehabilitation: A Systematic Review and Future Prospects". *Chinese Journal of Mechanical Engineering*.

[59] Garcia, G. F., Goncalves, R. S., and Carbone, G., 2024. "A Review of Wrist Rehabilitation Robots and Highlights Needed for New Devices". *Machines,* **12**(5).

[60] Pitzalis, R. F., Park, D., Caldwell, D. G., Berselli, G., and Ortiz, J., 2023. "State of the Art in Wearable Wrist Exoskeletons Part I: Background Needs and Design Requirements". *Machines,* **11**(4).

[61] Trigili, E., Crea, S., Moisé, M., Baldoni, A., Cempini, M., Ercolini, G., Marcon, D., Posteraro, F., Carrozza, M. C., and Vitiello, N., 2019. "Design and Experimental Characterization of a Shoulder-Elbow Exoskeleton with Compliant Joints for Post-Stroke Rehabilitation". *IEEE/ASME Transactions on Mechatronics,* **24**(4), pp. 1485–1496.

[62] Gunn, M., Shank, T. M., Eppes, M., Hossain, J., and Rahman, T., 2015. "User Evaluation of a Dynamic Arm Orthosis for People with Neuromuscular Disorders". *IEEE Transactions on Neural Systems and Rehabilitation Engineering,* **24**(12), pp. 1277–1283.

[63] Hsieh, H., Chien, L., and Lan, C., 2015. "Mechanical Design of a Gravity-Balancing Wearable Exoskeleton for the Motion Enhancement of Human Upper Limb". pp. 4992–4997.

[64] Jarrasse, N., and Morel, G., 2012. "Connecting a Human Limb to an Exoskeleton". *IEEE Transactions on Robotics,* **28**(3), pp. 697–709.

[65] Hsieh, H. C., Chen, D. F., Chien, L., and Lan, C. C., 2017. "Design of a Parallel Actuated Exoskeleton for Adaptive and Safe Robotic Shoulder Rehabilitation". *IEEE/ASME Transactions on Mechatronics,* **22**(5), pp. 2034–2045.

[66] Sui, D., Fan, J., Jin, H., Cai, X., Zhao, J., and Zhu, Y., 2017. "Design of a Wearable Upper-Limb Exoskeleton for Activities Assistance of Daily Living". *IEEE International Conference on Advanced Intelligent Mechatronics*, pp. 845–850.

[67] Lo, H. S., and Xie, S., 2014. "Optimization and Analysis of a Redundant 4R Spherical Wrist Mechanism for a Shoulder Exoskeleton". *Cambridge University Press Robotica,* **32**(8), pp. 1191–1211.

[68] Lo, H. S., and Xie, S. S., 2014. "An Upper Limb Exoskeleton with an Optimized 4R Spherical Wrist Mechanism for the Shoulder Joint". *IEEE/ASME International Conference on Advanced Intelligent Mechatronics*, pp. 269–274.

[69] Wu, Q., Wang, X., and Du, F., 2016. "Development and Analysis of a Gravity-Balanced Exoskeleton for Active Rehabilitation Training of Upper Limb". *Proceedings of the Institution of Mechanical Engineers, Part C: Journal of Mechanical Engineering Science,* **230**(20), pp. 3777–3790.

[70] Vazzoler, G., Bilancia, P., Berselli, G., Fontana, M., and Frisoli, A., 2021. "Preliminary Analysis and Design of a Passive Upper Limb Exoskeleton". *IEEE International Conference on Advanced Robotics*, pp. 569–574.

[71] Dempster, W. T., and Gaughran, G. R., 1967. "Properties of Body Segments Based on Size and Weight". *American Journal of Anatomy,* **120**(1), pp. 33–54.

[72] JAECO-WREX. https://performancehealth.com/jaeco-wrex-supports. Accessed: 2024-08-17.

[73] Scarcia, U., Berselli, G., Melchiorri, C., Ghinelli, M., and Palli, G., 2016. "Optimal Design of 3D Printed Spiral Torsion Springs". p. V002T03A020.

[74] Cheng, Z., Foong, S., Sun, D., and Tan, U.-X., 2015. "Towards a multi-DOF Passive Balancing Mechanism for Upper Limbs". *IEEE International Conference on Rehabilitation Robotics*, pp. 508–513.

[75] Nathan, R., 1985. "A Constant Force Generation Mechanism". *ASME Journal of Mechanisms Transmissions ans Automation in Design,* **107**(4), pp. 508–513.

[76] Herder, J. L., 2001. "Energy-Free Systems; Theory, Conception and Design of Statically Balanced Spring Mechanisms". *Just Herder*.

[77] Wang, J., and Kong, X., 2019. "A Geometric Approach to the Static Balancing of Mechanisms Constructed Using Spherical Kinematic Chain Units". *Elsevier Mechanism and Machine Theory,* **140**, pp. 305–320.

[78] Siciliano, B., Sciavicco, L., Villani, L., and Oriolo, G., 2010. "Robotics: Modelling, Planning and Control". *Springer Science & Business Media*.

[79] RecurDyn Overview. https://functionbay.com/en/page/single/2/recurdyn-overview. Accessed: 2024-08-17.

[80] Streit, D. A., and Gilmore, B. J., 1989. "Perfect Spring Equilibrators for Rotatable Bodies". *ASME Journal of Mechanical Transmission and Automation Design,* **111**(4), pp. 451–458.

[81] Delissen, A. A., Radaelli, G., and Herder, J. L., 2017. "Design and Optimization of a General Planar Zero Free Length Spring". *Elsevier Mechanism and Machine Theory,* **117**, pp. 56–77.

[82] Dunning, A. G., 2016. "Slender Spring Systems, for a close-to-body dynamic arm support for people with Duchenne muscular dystrophy". *TU Delft, Doctoral Thesis*.

[83] Lambelet, C., Lyu, M., Woolley, D., Gassert, R., and Wenderoth, N., 2017. "The eWrist - A Wearable Wrist Exoskeleton with sEMG-based Force Control for Stroke Rehabilitation". *IEEE International Conference on Rehabilitation Robotics*, pp. 726–733.

[84] Bartlett, N. W., Lyau, V., Raiford, W. A., Holland, D., Gafford, J. B., Ellis, T. D., and Walsh, C. J., 2015. "A Soft Robotic Orthosis for Wrist Rehabilitation". *ASME Journal of Medical Devices,* **9**(3).

[85] Khor, K. X., Chin, P. J. H., Hisyam, A. R., Yeong, C. F., Narayanan, A. L. T., and Su, E. L. M., 2014. "Development of CR2-Haptic: A Compact and Portable Rehabilitation Robot for Wrist and Forearm training". *IEEE Conference on Biomedical Engineering and Sciences*, pp. 424–429.

[86] Goncalves, R. S., Brito, L. S. F., Moraes, L. P., Carbone, G., and Ceccarelli, M., 2020. "A Fairly Simple Mechatronic Device for Training Human Wrist Motion". *International Journal of Advanced Robotic Systems,* **17**(6).

[87] Kwok, T. M., and Yu, H., 2024. "A Novel Bilateral Underactuated Upper Limb Exoskeleton for Post-stroke Bimanual ADL Training". *IEEE Transactions on Neural Systems and Rehabilitation Engineering*, pp. 1–1.

[88] Camardella, C., Cappiello, G., Curto, Z., Germanotta, M., Aprile, I., Mazzoleni, S., Scoglio, A., and Frisoli, A., 2022. "A Random Tree Forest Decision Support System to Personalize Upper Extremity Robot-Assisted Rehabilitation in Stroke: A Pilot Study". *International Conference on Rehabilitation Robotics*, pp. 1–6.

[89] Yang, S., Li, M., Wang, J., Wang, T., Liang, Z., He, B., Xie, J., and Xu, G., 2021. "A Novel Wrist Rehabilitation Exoskeleton Using 3D-Printed Multi-Segment Mechanism". *IEEE International Conference on Engineering in Medicine and Biology Society*, pp. 4769–4772.

[90] Gopura, R., and Kiguchi, K., 2008. "A Human Forearm and Wrist Motion Assist Exoskeleton Robot with EMG-based Fuzzy-neuro Control". *IEEE International Conference on Biomedical Robotics and Biomechatronics*, pp. 550–555.

[91] Camardella, C., Germanotta, M., Aprile, I., Cappiello, G., Curto, Z., Scoglio, A., Mazzoleni, S., and Frisoli, A., 2023. "A Decision Support System to Provide an Ongoing Prediction of Robot-Assisted Rehabilitation Outcome in Stroke Survivors". *International Conference on Rehabilitation Robotics*, pp. 1–6.

Appendix

This appendix contains the *Matlab* code related to the study presented in Chapter 3 (Appendix A) and Chapter 4 (Appendix B). To run the tool, each *Matlab* file (*.m* format) must be saved, named as indicated, and run as explained (in all the appended scripts, % is for insert a comment). Also, a list of the activities related to the research period leading to the completion of the present thesis is included in Appendix C.

A. SEES Optimization Tool

In this appendix, the next files have been attached (a folder with the code for the proposed design tool can be freely downloaded at this **link**):

A.1. OPTIM_LS.m

A.2. PLOT_LS.m

A.3. F_LS.m

A.4. F_nlc.m

A.5. OPTIM_TS.m

A.6. PLOT_TS.m

A.7. F_TS.m

The file from A.1. to A.4. are for the SEES balanced via Linear Springs (LS). To start the optimization process, run the *OPTIM_LS.m* file. Then, to plot the optimization results, set the *xyopt* optimal value obtained from the A.1. file in the *PLOT_LS.m* file, and run the *PLOT_LS.m* file. It is worth noting that, before running the files, a check on the values of the *Indexes* in both the A.1. and A.2. files need to be done (i.e., they have to be the same). These parameters have been defined so that they can be changed accordingly to investigate the different proposed configurations. *F_LS.m* and *F_nlc.m* are functions called in the A.1. file (A.3. is for the optimization function, whereas A.4. contains a constraint function). The files from A.5. to A.7. are for the SEES balanced via Torsional Springs (TS) and can be run like the previous points (in this case, there is no constraint function).

A.1. OPTIM_LS.m

```
% Matlab code: optimization process
% This attachment contains the Matlab code implemented for the 6-DOFs passive upper limb exoskeleton with linear springs.

clear all
close all
clc

lmt=200;

%  [h2x;h2y;h2x;k2;          h3x;h3y;h3z;k3;        h4x;h4y;h4z;k4        ]
x0=[1;1;1;1;                 1;1;1;1;               1;1;1;1               ];
lb=[-100;-lmt;-lmt;0.1;    -lmt;-lmt;-lmt;0.1;    -lmt;-lmt;-lmt;0.1     ];
```

```
ub=[65;lmt;lmt;5;          lmt;lmt;lmt;5;          lmt;lmt;lmt;5          ];

nlc=@F_nlc; opt=[];

rng default
problem=createOptimProblem('fmincon','x0',x0,'objective',@F_LS,'lb',lb,'ub',ub,'nonlcon',nlc,'options',opt);

rs = RandomStartPointSet; ms = MultiStart;
[xyopt,fval]=run(ms,problem,rs);
xyopt
```

A.2. PLOT_LS.m

```
% Matlab code: results plot
% This attachment contains the Matlab code implemented for the 6-DOFs passive upper limb exoskeleton with linear springs.

% The code is divided in two main parts:
% MODEL 1 (itself divided into three possible solutions)
% MODEL 2

% The script contains the following indices:
% MOV, FL, MODEL, SOLUTION

% Let chose:

% MOV = 1 for enforcing the first movement
% MOV = 2 for enforcing the second movement
% MOV = 3 for enforcing the third movement

% MODEL = 1 for springs connected between the COM of interest and one common chassis (Link 2a).
% All the parametric points are expressed in the global system GCS2, and:
        % SOLUTION = 0 for spring 4 attached to the combined COM
        % SOLUTION = 1 for spring 4 attached to the arm holder
        % SOLUTION = 2 for spring 4 attached to the link 4 COM

% MODEL = 2 for springs connected between two consecutive links. The parametric point H_i is expressed in the local CS_(i-1)

% FL = 0 for ZFL springs
% FL = 1 for NZFL springs

% The used parameters have been defined from the exoskeleton parametric model implemented in the MBD software RecurDyn.
% By updating the parameters as desired the code can be automatically run.
% In the following, the parameters that may be changed as desired are indicated as follows: >>> PARAM >>>

clear all
close all
clc

% Indices
MOV=3; FL=1; MODEL=1; SOLUTION=1;

% xyopt is the optimization result obtained by running the file "OPTIM_LS.m"
% NOTE: check that the Indices are the same imposed in the "F_LS.m file"
xyopt=[-19.3373; 65.3982; -158.8283; 0.8570; 145.4564; -69.0450; -10.2691; 1.80519; 58.4413; -27.7204; 197.4187; 0.1630]

h2_x=xyopt(1); h2_y=xyopt(2);  h2_z=xyopt(3);  k2=xyopt(4);
h3_x=xyopt(5); h3_y=xyopt(6);  h3_z=xyopt(7);  k3=xyopt(8);
h4_x=xyopt(9); h4_y=xyopt(10); h4_z=xyopt(11); k4=xyopt(12);

% Constraints
g=9.81;       %[m/s^2]
DTOR=pi/180; %[rad/deg]

% Concentrated Masses [kg] >>> PARAM >>>
m1=2.1; m2=1.2;

% Link masses [kg] (density aluminium 2.7e-006 kg/mm^3) >>> PARAM >>>
m_1=3.48e-002;  m_4=8.49e-002;  m_5=6.28e-002;  m_1a=3.48e-002;
m_4a=8.49e-002; m_2a=1.56e-002; m_5a=2.37e-002; m_2=5.11e-002;
m_3=6.17e-002;  m_4t=(m_4+m_4a+m_5a+m1+m2+m_5); % Combined COM

% Geometric parameters [mm]  >>> PARAM >>>
dim1=75; dim2=95; r1=125; r2=75; r3=95;
l1=(dim1^2+dim2^2)^0.5; l4=307; l5=225; l5a=50; lv5a=10;

% Link COM position [mm]  >>> PARAM >>>
x1=l1/2; x4=l4/2; x5=l5/2; a4=0.44*l4; a5=0.425*l5;
lv2=61; lh2=52; lv3=54; lh3=57;

% Spring initial length [mm]
if FL == 0
d_01=0; d_02=0; d_03=0; d_04=0; d_05=0;
elseif FL == 1  % >>> PARAM >>>
d_01=30; d_02=30; d_03=30; d_04=30; d_05=30;
end

% Spring installation distances [mm]  >>> PARAM >>>
b1=l1; c1=30; b5=l5; c5=30;

% Elastic constants [N/mm]
```

```
k1=(x1*(m_1+m_1a) + l1*(m1+m2 + m_4+m_5 + m_4a + m_2a+m_5a + m_2+m_3))*g/(b1*c1*(1-d_01/(b1^2+c1^2)^0.5));
k5=((m2*a5+m_5*x5)*g)/(b5*c5*(1-d_05/(b5^2+c5^2)^0.5));

% Exoskeleton initial configuration  >>> PARAM >>>
t10=-atan(dim1/dim2); %[rad]
t40=106; t50=90;      %[deg]

% Input rotations for each MOV [deg]  >>> PARAM >>>
if MOV == 1
deltat0_max=-5;  deltat1_max=-10; deltat2_max=-20;
deltat3_max=-40; deltat4_max=-20; deltat5_max=-10;

elseif MOV == 2
deltat0_max=10; deltat1_max=-10; deltat2_max=-15;
deltat3_max=35; deltat4_max=-30; deltat5_max=-25;

elseif MOV == 3
deltat0_max=0;  deltat1_max=-15; deltat2_max=-5;
deltat3_max=15; deltat4_max=-45; deltat5_max=-100;
end

% Time vector
step=100; sim_time=100; time=0:sim_time/step:sim_time;

% Input joint rotation vectors
if deltat0_max==0
deltat0=zeros(1,step+1);
else
deltat0=(0:deltat0_max/step:deltat0_max)*DTOR;
end
t0=deltat0;
if deltat1_max==0
deltat1=zeros(1,step+1);
else
deltat1=(0:deltat1_max/step:deltat1_max)*DTOR;
end
t1=deltat1+t10;
if deltat2_max==0
deltat2=zeros(1,step+1);
else
deltat2=(0:deltat2_max/step:deltat2_max)*DTOR;
end
t2=deltat2;
if deltat3_max==0
deltat3=zeros(1,step+1);
else
deltat3=(0:deltat3_max/step:deltat3_max)*DTOR;
end
t3=deltat3;
if deltat4_max==0
deltat4=zeros(1,step+1);
else
deltat4=(0:deltat4_max/step:deltat4_max)*DTOR;
end
t4=deltat4+t40*DTOR;
if deltat5_max==0
deltat5=zeros(1,step+1);
else
deltat5=(0:deltat5_max/step:deltat5_max)*DTOR;
end
t5=deltat5+t50*DTOR;

% Kinematic and static analysis
h4_m1=a4*sin(t4); h4=l4*sin(t4);
h5_m2=a5*sin(t5); v4_m1=-a4*cos(t4);
v4=-l4*cos(t4); v5_m2=-a5*cos(t5);
h3_m1=h4_m1.*sin(t3); h3_m2=(h4+h5_m2).*sin(t3);
v3_m1=h4_m1.*cos(t3); v3_m2=(h4+h5_m2).*cos(t3);
r_m1=(h3_m1.^2+v4_m1.^2).^0.5; r_m2=(h3_m2.^2+(v4+v5_m2).^2).^0.5;

if deltat3_max >= 0
j=1;
else
j=2;
end

h2_m1=(-1)^j*r_m1.*cos(t2+atan(-v4_m1./h3_m1));
h2_m2=(-1)^j*r_m2.*cos(t2+atan(-(v4+v5_m2)./h3_m2));
h4m4=x4*sin(t4);
v4m4=-x4*cos(t4);
h5m5=x5*sin(t5);
v5m5=-x5*cos(t5);
h3m4=h4m4.*sin(t3);
v3m4=h4m4.*cos(t3);
h3m5=(h4+h5m5).*sin(t3);
v3m5=(h4+h5m5).*cos(t3);
rm4=(h3m4.^2+v4m4.^2).^0.5;
rm5=(h3m5.^2+(v4+v5m5).^2).^0.5;
h2m4=(-1)^j*rm4.*cos(t2+atan(-v4m4./h3m4));
h2m5=(-1)^j*rm5.*cos(t2+atan(-(v4+v5m5)./h3m5));
v4m4a=v4m4+l5a;
rm4a=(h3m4.^2+v4m4a.^2).^0.5;
h2m4a=(-1)^j*rm4a.*cos(t2+atan(-v4m4a./h3m4));
h3m5a=h4.*sin(t3);
v3m5a=h4.*cos(t3);
```

```
v4m5a=v4+lv5a;
rm5a=(h3m5a.^2+v4m5a.^2).^0.5;
h2m5a=(-1)^j*rm5a.*cos(t2+atan(-v4m5a/h3m5a));

% Torque in CS1
% M1 gravitational
M1_dec=((m_1 + m_1a)*x1 + l1*(m1+m2 + m_4+m_5 + m_4a + m_2a+m_5a))*g*cos(t1);
M1_dec=M1_dec + l1*(m_2+m_3)*g*cos(t1);
d1=(b1^2+c1^2+2*b1*c1*sin(t1)).^0.5;
% M1 spring
M1_spring=k1*b1*c1.*cos(t1).*(d1-d_01)./d1;
% M1 balanced
M1_balanced=M1_dec-M1_spring;

for i=1:1:step+1
ct0=cos(t0(i));st0=sin(t0(i)); ct1=cos(t1(i));st1=sin(t1(i));
ct2=cos(t2(i));st2=sin(t2(i)); ct3=cos(t3(i));st3=sin(t3(i));
ct4=cos(t4(i));st4=sin(t4(i)); ct5=cos(t5(i));st5=sin(t5(i));

% Rotation matrices
R_2=[1 0 0; 0 ct2 -st2; 0 st2 ct2]; R_3=[ct3 -st3 0; st3 ct3 0; 0 0 1];
R_4=[ct4 0 st4; 0 1 0; -st4 0 ct4]; R_5=[ct5 0 st5; 0 1 0 ; -st5 0 ct5];

% Force in CS0
f_m4=[0; 0; -m_4*g];    f_m3=[0; 0; -m_3*g]; f_m4a=[0; 0; -m_4a*g];
f_m5a=[0; 0; -m_5a*g]; f_m1=[0; 0; -m1*g];  f_m2=[0; 0; -m2*g];
f_m5=[0; 0; -m_5*g];

% Force in CS3
f_m4_CS3=transpose(R_2*R_3)*f_m4;    f_m3_CS3=transpose(R_2*R_3)*f_m3;
f_m4a_CS3=transpose(R_2*R_3)*f_m4a; f_m5a_CS3=transpose(R_2*R_3)*f_m5a;
f_m1_CS3=transpose(R_2*R_3)*f_m1;    f_m2_CS3=transpose(R_2*R_3)*f_m2;
f_m5_CS3=transpose(R_2*R_3)*f_m5;

% Force in CS4
f_m4_CS4=transpose(R_2*R_3*R_4)*f_m4;    f_m4a_CS4=transpose(R_2*R_3*R_4)*f_m4a;
f_m5a_CS4=transpose(R_2*R_3*R_4)*f_m5a; f_m1_CS4=transpose(R_2*R_3*R_4)*f_m1;
f_m2_CS4=transpose(R_2*R_3*R_4)*f_m2;    f_m5_CS4=transpose(R_2*R_3*R_4)*f_m5;

% Forces in CS5
f_m2_CS5=transpose(R_2*R_3*R_5)*f_m2; f_m5_CS5=transpose(R_2*R_3*R_5)*f_m5;

% Torque in CS2
% M2 gravitational
M2(i)=(h2m4(i) + r2*ct3*ct2)*m_4*g;
M2(i)=M2(i) + (h2m4a(i) + r2*ct3*ct2)*m_4a*g + (h2m5a(i) +r2*ct3*ct2)*m_5a*g;
M2(i)=M2(i) + ((lh3*ct3)*ct2+(r3-lv3)*st2)*m_3*g;
M2(i)=M2(i) + m1*g*h2_m1(i) + m2*g*h2_m2(i);
M2(i)=M2(i) + (h2m5(i) + r2*ct3*ct2)*m_5*g;

% Torque in CS3
% M3 gravitational
M3(i)=f_m4_CS3(2,1)*(v3m4(i)^2+h3m4(i)^2)^0.5 + f_m4_CS3(1,1)*r2;
M3(i)=M3(i) + f_m3_CS3(1,1)*lh3;
M3(i)=M3(i) + f_m4a_CS3(2,1)*(v3m4(i)^2+h3m4(i)^2)^0.5 + f_m4a_CS3(1,1)*r2;
M3(i)=M3(i) + f_m5a_CS3(2,1)*(v3m5a(i)^2+h3m5a(i)^2)^0.5 + f_m5a_CS3(1,1)*r2;
M3(i)=M3(i) + f_m1_CS3(2,1)*(v3_m1(i)^2+h3_m1(i)^2)^0.5 + f_m2_CS3(2,1)*(v3_m2(i)^2+h3_m2(i)^2)^0.5;
M3(i)=M3(i) + f_m5_CS3(2,1)*(v3m5(i)^2+h3m5(i)^2)^0.5 + f_m5_CS3(1,1)*r2;

% Torque in CS4
% M4 gravitational
M4_dec(i)=f_m4_CS4(1,1)*x4 + f_m5_CS4(1,1)*l4;
M4_dec(i)=M4_dec(i) + f_m4a_CS4(1,1)*x4 + f_m5a_CS4(1,1)*l4;
M4_dec(i)=M4_dec(i) + f_m1_CS4(1,1)*a4 + f_m2_CS4(1,1)*l4;

% Torque in CS5
% M5 gravitational
M5(i)=f_m2_CS5(1,1)*a5;
M5(i)=M5(i) + f_m5_CS5(1,1)*x5;
d5(i)=(b5^2+c5^2-2*b5*c5*cos(t5(i)))^0.5;
% M5 spring
M5_spring(i)=k5*b5*c5*sin(t5(i))*(d5(i)-d_05)/d5(i);
% M5 balanced
M5_balanced(i)=M5(i)-M5_spring(i);

% Transformation matrices
R2=[1 0 0 0; 0 ct2 -st2 0; 0 st2 ct2 0; 0 0 0 1];
R3=[ct3 -st3 0 r1; st3 ct3 0 0; 0 0 1 r3; 0 0 0 1];

if MODEL == 1 % global system

%%%%%%%%%%%%%%%%%%%%%%%%%%%%%%%%%%%%%%%%%%%%%%%%%%%%%%%%%%%%%%%%%%%%%%%%%%%%%%
%%%%%%%%%%%%%%%%%%%%%%%%% MODEL 1: SOLUTION 0, 1, 2 %%%%%%%%%%%%%%%%%%%%%%%%%
%%%%%%%%%%%%%%%%%%%%%%%%%%%%%%%%%%%%%%%%%%%%%%%%%%%%%%%%%%%%%%%%%%%%%%%%%%%%%%

% Spring with reference to LINK 2
%%%%%%%%%%%%%%%%%%%%%%%%%%%%%%%%%%%%%%
p_22=[lh2; 0; lv2];       % local system CS2
P_2=R2*[p_22; 1];         % global system GCS2

% Force of spring 2
H_2=[h2_x; h2_y; h2_z];  % global system GCS2
P_2=P_2(1:3);

v2=[P_2(1)-h2_x; P_2(2)-h2_y; P_2(3)-h2_z];
```

```
v2_m=sqrt(v2(1)^2+v2(2)^2+v2(3)^2);
v2_v=[v2(1)/v2_m; v2(2)/v2_m; v2(3)/v2_m];

D_2=v2_v*d_02; PH_2=(P_2 - H_2);
F_spring2=k2*(PH_2-D_2);

% Spring with reference to LINK 3
%%%%%%%%%%%%%%%%%%%%%%%%%%%%%%%%%%
p_33=[0; -lh3; -lv3]; P_3_cs3=R_3*p_33;   % local system CS3
P_3=R2*R3*[p_33; 1];                       % global system GCS2

% Force of spring 3
H_3=[h3_x; h3_y; h3_z];                    % global system GCS2
P_3=P_3(1:3);

v3=[P_3(1)-h3_x; P_3(2)-h3_y; P_3(3)-h3_z];
v3_m=sqrt(v3(1)^2+v3(2)^2+v3(3)^2);
v3_v=[v3(1)/v3_m; v3(2)/v3_m; v3(3)/v3_m];

D_3=v3_v*d_03; PH_3=(P_3 - H_3);
F_spring3=k3*(PH_3-D_3);

% Force of spring 3 in CS3
H_cs3=transpose(R2)*[H_3;1];
H_3_cs3=[H_cs3(1)-r1; H_cs3(2); H_cs3(3)-r3];

D3_cs3=transpose(R2)*[D_3;1];
F_spring3_cs3=k3*(P_3_cs3-H_3_cs3-D3_cs3(1:3));

% Spring with reference to LINK 4
%%%%%%%%%%%%%%%%%%%%%%%%%%%%%%%%%%
if SOLUTION == 0
nx_4=231.4; ny_4=69.6; nz_4=8.2;  % measure from RecurDyn >>> PARAM >>>
elseif SOLUTION == 1
nx_4=214.6; ny_4=69.6; nz_4=66.7; % measure from RecurDyn >>> PARAM >>>
elseif SOLUTION == 2
nx_4=x4; ny_4=0; nz_4=0;
end
X_4(i)=nx_4*st4-nz_4*ct4; Y_4(i)=ny_4; Z_4(i)=nx_4*ct4+nz_4;
P_4cs4=[X_4(i); Y_4(i); Z_4(i)];
P_4cs=[X_4(i); Y_4(i)-r2; Z_4(i)-r3];
P_4cs3=R_3*P_4cs;            % local system CS3
P_4cs2=R2*R3*[P_4cs;1];      % global system GCS2

% Force of spring 4 in GCS2
H_4=[h4_x; h4_y; h4_z];      % global system GCS2
P_4=P_4cs2(1:3);

v4=[P_4(1)-h4_x; P_4(2)-h4_y; P_4(3)-h4_z];
v4_m=sqrt(v4(1)^2+v4(2)^2+v4(3)^2);
v4_v=[v4(1)/v4_m; v4(2)/v4_m; v4(3)/v4_m];

D_4=v4_v*d_04; PH_4=P_4 - H_4;
F_spring4=k4*(PH_4-D_4);

% Force of spring 4 in CS3
H_cs3=transpose(R2)*[H_4;1];
H_4_cs3=[H_cs3(1)-r1; H_cs3(2); H_cs3(3)-r3];

D4_cs3=transpose(R2)*[D_4;1];
F_spring4_cs3=k4*(P_4cs3-H_4_cs3-D4_cs3(1:3));

% Force of spring 4 in CS4
H1=R_3'*H_4_cs3;
H_4_cs4=[H1(1); H1(2)+r2; H1(3)+r3];

D4_cs4=R_3'*D4_cs3(1:3);
F_spring4_cs4=k4*(P_4cs4-H_4_cs4-D4_cs4(1:3));

% Spring balancing torques
% M2 spring
M2_spring(i)=F_spring2(3,1)*P_2(2,1)-F_spring2(2,1)*P_2(3,1)+F_spring3(3,1)*P_3(2,1) ...
-F_spring3(2,1)*P_3(3,1)+F_spring4(3,1)*P_4(2,1)-F_spring4(2,1)*P_4(3,1);
% M3 spring
M3_spring(i)=-F_spring3_cs3(1,1)*P_3_cs3(2,1)+F_spring3_cs3(2,1)*P_3_cs3(1,1) ...
-F_spring4_cs3(1,1)*P_4cs3(2,1)+F_spring4_cs3(2,1)*P_4cs3(1,1);
% M4 spring
M4_spring(i)=-F_spring4_cs4(3,1)*P_4cs4(1,1) + F_spring4_cs4(1,1)*P_4cs4(3,1);

elseif MODEL == 2
%%%%%%%%%%%%%%%%%%%%%%%%%%%%%%%%%%%%%%%%%%%%%%%%%%%%%%%%%%%%%%%%%%%%%%%%%%%%%%%
%%%%%%%%%%%%%%%%%%%%%%%%%%%%%%%%%%%%%% MODEL 2 %%%%%%%%%%%%%%%%%%%%%%%%%%%%%%%%%%%%%%%%
%%%%%%%%%%%%%%%%%%%%%%%%%%%%%%%%%%%%%%%%%%%%%%%%%%%%%%%%%%%%%%%%%%%%%%%%%%%%%%%

% Spring with reference to LINK 2
%%%%%%%%%%%%%%%%%%%%%%%%%%%%%%%%%%
p_22=[lh2; 0; lv2]; % local system CS2
P_2=R2*[p_22; 1];

% Force of spring 2 in CS2
H_2=[h2_x; h2_y; h2_z]; P_2=P_2(1:3); PH_2=P_2 - H_2;
F_spring2=k2*PH_2;

% Spring with reference to LINK 3
%%%%%%%%%%%%%%%%%%%%%%%%%%%%%%%%%%
```

```
p_33=[0; -lh3; -lv3]; % local system CS3
P_3=R_3*p_33;

% Force of spring 3 in CS3
H_3=[h3_x; h3_y; h3_z]; P_3=P_3(1:3); PH_3=P_3-H_3;
F_spring3=k3*PH_3;

% Spring with reference to LINK 4
%%%%%%%%%%%%%%%%%%%%%%%%%%%%%%%%%%
nx_4=x4; ny_4=0; nz_4=0; % Spring attached to link 4 COM
X_4(i)=nx_4*st4-nz_4*ct4; Y_4(i)=ny_4; Z_4(i)=nx_4*ct4+nz_4;
P_4=[X_4(i); Y_4(i); Z_4(i)];

% Force of spring 4 in CS4
H_4=[h4_x; h4_y; h4_z]; P_4=P_4(1:3); PH_4=P_4-H_4;
F_spring4=k4*PH_4;

% Spring balancing torques
M2_spring(i)=F_spring2(3,1)*P_2(2,1) - F_spring2(2,1)*P_2(3,1);  % M2 spring
M3_spring(i)=-F_spring3(1,1)*P_3(2,1) + F_spring3(2,1)*P_3(1,1); % M3 spring
M4_spring(i)=-F_spring4(3,1)*P_4(1,1) + F_spring4(1,1)*P_4(3,1); % M4 spring

end

M2_balanced(i)=M2(i)-M2_spring(i);       % M2 balanced
M3_balanced(i)=M3(i)-M3_spring(i);       % M3 balanced
M4_balanced(i)=M4_dec(i)-M4_spring(i); % M4 balanced

end

% Plot of the gravitational and the balanced torque for each R joint
f1 = figure; plot(time,M1_dec,'b');
hold on
plot(time,M1_balanced,'*g','MarkerIndices',[1:3:100]);
xlabel('Movement progress [%]'); ylabel ('Torque [Nmm]')
legend('M_1 ','M_1_,_b')

f2 = figure; plot(time,-M2)
hold on
plot(time,-M2_balanced,'*g','MarkerIndices',[1:3:100])
xlabel('Movement progress [%]'); ylabel ('Torque [Nmm]')
legend('M_2','M_2_,_b')

f3 = figure; plot(time,M3)
hold on
plot(time,+M3_balanced,'*g','MarkerIndices',[1:3:100])
xlabel('Movement progress [%]'); ylabel ('Torque [Nmm]')
legend('M_3','M_3_,_b')

f4 = figure; plot(time,M4_dec)
hold on
plot(time,M4_balanced,'*g','MarkerIndices',[1:3:100])
xlabel('Movement progress [%]'); ylabel ('Torque [Nmm]')
legend('M_4','M_4_,_b')

f5 = figure; plot(time,M5)
hold on
plot(time,M5_balanced,'*g','MarkerIndices',[1:3:100])
xlabel('Movement progress [%]'); ylabel ('Torque [Nmm]')
legend('M_5','M_5_,_b')
```

A.3. F_LS.m

```
% Matlab code: optimized function
% This attachment contains the Matlab code implemented for the 6-DOFs passive upper limb exoskeleton with linear springs.

% The code is divided in two main parts:
% MODEL 1 (itself divided into three possible solutions)
% MODEL 2

% The script contains the following indices:
% MOV, FL, MODEL, SOLUTION

% Let chose:

% MOV = 1 for enforcing the first movement
% MOV = 2 for enforcing the second movement
% MOV = 3 for enforcing the third movement

% MODEL = 1 for springs connected between the COM of interest and one common chassis (Link 2a).
% All the parametric points are expressed in the global system GCS2, and:
% SOLUTION = 0 for spring 4 attached to the combined COM
% SOLUTION = 1 for spring 4 attached to the arm holder
% SOLUTION = 2 for spring 4 attached to the link 4 COM

% MODEL = 2 for springs connected between two consecutive links. The parametric point H_i is expressed in the local CS_(i-1)

% FL = 0 for ZFL springs
% FL = 1 for NZFL springs

% The used parameters have been defined from the exoskeleton parametric model implemented in the MBD software RecurDyn.
```

```
% By updating the parameters as desired the code can be automatically run.
% In the following, the parameters that may be changed as desired are indicated as follows: >>> PARAM >>>

function y = F_LS(X)

% Indices
MOV=3; FL=1; MODEL=1; SOLUTION=1;

global m_2 m_3 m_4t g time PH_2 PH_3 PH_4

h2_x=X(1); h2_y=X(2); h2_z=X(3); k2=X(4);
h3_x=X(5); h3_y=X(6); h3_z=X(7); k3=X(8);
h4_x=X(9); h4_y=X(10); h4_z=X(11); k4=X(12);

% Constants
g=9.81;        %[m/s^2]
DTOR=pi/180; %[rad/deg]

% Concentrated Masses [kg] >>> PARAM >>>
m1=2.1; m2=1.2;

% Link masses [kg] (density aluminium 2.7e-006 kg/mm^3) >>> PARAM >>>
m_1=3.48e-002;  m_4=8.49e-002;  m_5=6.28e-002;  m_1a=3.48e-002;
m_4a=8.49e-002; m_2a=1.56e-002; m_5a=2.37e-002; m_2=5.11e-002;
m_3=6.17e-002;  m_4t=(m_4+m_4a+m_5a+m1+m2+m_5); % Combined COM

% Geometric parameters [mm]  >>> PARAM >>>
dim1=75; dim2=95; r1=125; r2=75; r3=95;
l1=(dim1^2+dim2^2)^0.5; l4=307; l5=225; l5a=50; lv5a=10;

% Link COM position [mm]  >>> PARAM >>>
x1=l1/2; x4=l4/2; x5=l5/2; a4=0.44*l4; a5=0.425*l5;
lv2=61; lh2=52; lv3=54; lh3=57;

% Spring initial length [mm]
if FL == 0
d_01=0; d_02=0; d_03=0; d_04=0; d_05=0;
elseif FL == 1  % >>> PARAM >>>
d_01=30; d_02=30; d_03=30; d_04=30; d_05=30;
end

% Spring installation distances [mm]  >>> PARAM >>>
b1=l1; c1=30; b5=l5; c5=30;

% Elastic constants [N/mm]
k1=(x1*(m_1+m_1a) + l1*(m1+m2 + m_4+m_5 + m_4a + m_2a+m_5a + m_2+m_3))*g/(b1*c1*(1-d_01/(b1^2+c1^2)^0.5));
k5=((m2*a5+m_5*x5)*g)/(b5*c5*(1-d_05/(b5^2+c5^2)^0.5));

% Exoskeleton initial configuration  >>> PARAM >>>
t10=-atan(dim1/dim2); %[rad]
t40=106; t50=90;        %[deg]

% Input rotations for each MOV [deg]  >>> PARAM >>>
if MOV == 1
deltat0_max=-5;  deltat1_max=-10; deltat2_max=-20;
deltat3_max=-40; deltat4_max=-20; deltat5_max=-10;

elseif MOV == 2
deltat0_max=10; deltat1_max=-10; deltat2_max=-15;
deltat3_max=35; deltat4_max=-30; deltat5_max=-25;

elseif MOV == 3
deltat0_max=0;  deltat1_max=-15; deltat2_max=-5;
deltat3_max=15; deltat4_max=-45; deltat5_max=-100;
end

% Time vector
step=100; sim_time=100; time=0:sim_time/step:sim_time;

% Input joint rotation vectors
if deltat0_max==0
deltat0=zeros(1,step+1);
else
deltat0=(0:deltat0_max/step:deltat0_max)*DTOR;
end
t0=deltat0;
if deltat1_max==0
deltat1=zeros(1,step+1);
else
deltat1=(0:deltat1_max/step:deltat1_max)*DTOR;
end
t1=deltat1+t10;
if deltat2_max==0
deltat2=zeros(1,step+1);
else
deltat2=(0:deltat2_max/step:deltat2_max)*DTOR;
end
t2=deltat2;
if deltat3_max==0
deltat3=zeros(1,step+1);
else
deltat3=(0:deltat3_max/step:deltat3_max)*DTOR;
end
t3=deltat3;
if deltat4_max==0
```

```
deltat4=zeros(1,step+1);
else
deltat4=(0:deltat4_max/step:deltat4_max)*DTOR;
end
t4=deltat4+t40*DTOR;
if deltat5_max==0
deltat5=zeros(1,step+1);
else
deltat5=(0:deltat5_max/step:deltat5_max)*DTOR;
end
t5=deltat5+t50*DTOR;

% Kinematic and static analysis
h4_m1=a4*sin(t4); h4=l4*sin(t4);
h5_m2=a5*sin(t5); v4_m1=-a4*cos(t4);
v4=-l4*cos(t4); v5_m2=-a5*cos(t5);
h3_m1=h4_m1.*sin(t3); h3_m2=(h4+h5_m2).*sin(t3);
v3_m1=h4_m1.*cos(t3); v3_m2=(h4+h5_m2).*cos(t3);
r_m1=(h3_m1.^2+v4_m1.^2).^0.5; r_m2=(h3_m2.^2+(v4+v5_m2).^2).^0.5;

if deltat3_max >= 0
j=1;
else
j=2;
end

h2_m1=(-1)^j*r_m1.*cos(t2+atan(-v4_m1./h3_m1));
h2_m2=(-1)^j*r_m2.*cos(t2+atan(-(v4+v5_m2)./h3_m2));
h4m4=x4*sin(t4);
v4m4=-x4*cos(t4);
h5m5=x5*sin(t5);
v5m5=-x5*cos(t5);
h3m4=h4m4.*sin(t3);
v3m4=h4m4.*cos(t3);
h3m5=(h4+h5m5).*sin(t3);
v3m5=(h4+h5m5).*cos(t3);
rm4=(h3m4.^2+v4m4.^2).^0.5;
rm5=(h3m5.^2+(v4+v5m5).^2).^0.5;
h2m4=(-1)^j*rm4.*cos(t2+atan(-v4m4./h3m4));
h2m5=(-1)^j*rm5.*cos(t2+atan(-(v4+v5m5)./h3m5));

v4m4a=v4m4+l5a;
rm4a=(h3m4.^2+v4m4a.^2).^0.5;
h2m4a=(-1)^j*rm4a.*cos(t2+atan(-v4m4a./h3m4));
h3m5a=h4.*sin(t3);
v3m5a=h4.*cos(t3);
v4m5a=v4+lv5a;
rm5a=(h3m5a.^2+v4m5a.^2).^0.5;
h2m5a=(-1)^j*rm5a.*cos(t2+atan(-v4m5a/h3m5a));

% Torque in CS1
% M1 gravitational
M1_dec=((m_1 + m_1a)*x1 + l1*(m1+m2 + m_4+m_5 + m_4a + m_2a+m_5a))*g*cos(t1);
M1_dec=M1_dec + l1*(m_2+m_3)*g*cos(t1);
d1=(b1^2+c1^2+2*b1*c1*sin(t1)).^0.5;
% M1 spring
M1_spring=k1*b1*c1.*cos(t1).*(d1-d_01)./d1;
% M1 balanced
M1_balanced=M1_dec-M1_spring;

for i=1:1:step+1
ct0=cos(t0(i)); st0=sin(t0(i)); ct1=cos(t1(i)); st1=sin(t1(i));
ct2=cos(t2(i)); st2=sin(t2(i)); ct3=cos(t3(i)); st3=sin(t3(i));
ct4=cos(t4(i)); st4=sin(t4(i)); ct5=cos(t5(i)); st5=sin(t5(i));

% Rotation matrices
R_2=[1 0 0; 0 ct2 -st2; 0 st2 ct2]; R_3=[ct3 -st3 0; st3 ct3 0; 0 0 1];
R_4=[ct4 0 st4; 0 1 0; -st4 0 ct4]; R_5=[ct5 0 st5; 0 1 0 ; -st5 0 ct5];

% Force in CS0
f_m4=[0; 0; -m_4*g];   f_m3=[0; 0; -m_3*g]; f_m4a=[0; 0; -m_4a*g];
f_m5a=[0; 0; -m_5a*g]; f_m1=[0; 0; -m1*g];  f_m2=[0; 0; -m2*g];
f_m5=[0; 0; -m_5*g];

% Force in CS3
f_m4_CS3=transpose(R_2*R_3)*f_m4;   f_m3_CS3=transpose(R_2*R_3)*f_m3;
f_m4a_CS3=transpose(R_2*R_3)*f_m4a; f_m5a_CS3=transpose(R_2*R_3)*f_m5a;
f_m1_CS3=transpose(R_2*R_3)*f_m1;   f_m2_CS3=transpose(R_2*R_3)*f_m2;
f_m5_CS3=transpose(R_2*R_3)*f_m5;

% Force in CS4
f_m4_CS4=transpose(R_2*R_3*R_4)*f_m4;   f_m4a_CS4=transpose(R_2*R_3*R_4)*f_m4a;
f_m5a_CS4=transpose(R_2*R_3*R_4)*f_m5a; f_m1_CS4=transpose(R_2*R_3*R_4)*f_m1;
f_m2_CS4=transpose(R_2*R_3*R_4)*f_m2;   f_m5_CS4=transpose(R_2*R_3*R_4)*f_m5;

% Forces in CS5
f_m2_CS5=transpose(R_2*R_3*R_5)*f_m2; f_m5_CS5=transpose(R_2*R_3*R_5)*f_m5;

% Torque in CS2
% M2 gravitational
M2(i)=(h2m4(i) + r2*ct3*ct2)*m_4*g;
M2(i)=M2(i) + (h2m4a(i) + r2*ct3*ct2)*m_4a*g + (h2m5a(i) +r2*ct3*ct2)*m_5a*g;
M2(i)=M2(i) + ((l3*ct3)*ct2+(r3-lv3)*st2)*m_3*g;
M2(i)=M2(i) + m1*g*h2_m1(i) + m2*g*h2_m2(i);
M2(i)=M2(i) + (h2m5(i) + r2*ct3*ct2)*m_5*g;
```

```
% Torque in CS3
% M3 gravitational
M3(i)=f_m4_CS3(2,1)*(v3m4(i)^2+h3m4(i)^2)^0.5 + f_m4_CS3(1,1)*r2;
M3(i)=M3(i) + f_m3_CS3(1,1)*lh3;
M3(i)=M3(i) + f_m4a_CS3(2,1)*(v3m4(i)^2+h3m4(i)^2)^0.5 + f_m4a_CS3(1,1)*r2;
M3(i)=M3(i) + f_m5a_CS3(2,1)*(v3m5a(i)^2+h3m5a(i)^2)^0.5 + f_m5a_CS3(1,1)*r2;
M3(i)=M3(i) + f_m1_CS3(2,1)*(v3_m1(i)^2+h3_m1(i)^2)^0.5 + f_m2_CS3(2,1)*(v3_m2(i)^2+h3_m2(i)^2)^0.5;
M3(i)=M3(i) + f_m5_CS3(2,1)*(v3m5(i)^2+h3m5(i)^2)^0.5 + f_m5_CS3(1,1)*r2;

% Torque in CS4
% M4 gravitational
M4_dec(i)=f_m4_CS4(1,1)*x4 + f_m5_CS4(1,1)*l4;
M4_dec(i)=M4_dec(i) + f_m4a_CS4(1,1)*x4 + f_m5a_CS4(1,1)*l4;
M4_dec(i)=M4_dec(i) + f_m1_CS4(1,1)*a4 + f_m2_CS4(1,1)*l4;

% Torque in CS5
% M5 gravitational
M5(i)=f_m2_CS5(1,1)*a5;
M5(i)=M5(i) + f_m5_CS5(1,1)*x5;
d5(i)=(b5^2+c5^2-2*b5*c5*cos(t5(i)))^0.5;
% M5 spring
M5_spring(i)=k5*b5*c5*sin(t5(i))*(d5(i)-d_05)/d5(i);
% M5 balanced
M5_balanced(i)=M5(i)-M5_spring(i);

% Transformation matrices
R2=[1 0 0 0; 0 ct2 -st2 0; 0 st2 ct2 0; 0 0 0 1];
R3=[ct3 -st3 0 r1; st3 ct3 0 0; 0 0 1 r3; 0 0 0 1];

if MODEL == 1 % global system

%%%%%%%%%%%%%%%%%%%%%%%%%%%%%%%%%%%%%%%%%%%%%%%%%%%%%%%%%%%%%%%%%%%%%%%%%%%%%%%%%%
%%%%%%%%%%%%%%%%%%%%%%%%%%%% MODEL 1: SOLUTION 0, 1, 2 %%%%%%%%%%%%%%%%%%%%%%%%%%%%
%%%%%%%%%%%%%%%%%%%%%%%%%%%%%%%%%%%%%%%%%%%%%%%%%%%%%%%%%%%%%%%%%%%%%%%%%%%%%%%%%%

% Spring with reference to LINK 2
%%%%%%%%%%%%%%%%%%%%%%%%%%%%%%%%%%%%
p_22=[lh2; 0; lv2];      % local system CS2
P_2=R2*[p_22; 1];        % global system GCS2

% Force of spring 2
H_2=[h2_x; h2_y; h2_z];  % global system GCS2
P_2=P_2(1:3);

v2=[P_2(1)-h2_x; P_2(2)-h2_y; P_2(3)-h2_z];
v2_m=sqrt(v2(1)^2+v2(2)^2+v2(3)^2);
v2_v=[v2(1)/v2_m; v2(2)/v2_m; v2(3)/v2_m];

D_2=v2_v*d_02; PH_2=(P_2 - H_2);
F_spring2=k2*(PH_2-D_2);

% Spring with reference to LINK 3
%%%%%%%%%%%%%%%%%%%%%%%%%%%%%%%%%%%%
p_33=[0; -lh3; -lv3]; P_3_cs3=R_3*p_33;  % local system CS3
P_3=R2*R3*[p_33; 1];                     % global system GCS2

% Force of spring 3
H_3=[h3_x; h3_y; h3_z];                  % global system GCS2
P_3=P_3(1:3);

v3=[P_3(1)-h3_x; P_3(2)-h3_y; P_3(3)-h3_z];
v3_m=sqrt(v3(1)^2+v3(2)^2+v3(3)^2);
v3_v=[v3(1)/v3_m; v3(2)/v3_m; v3(3)/v3_m];

D_3=v3_v*d_03; PH_3=(P_3 - H_3);
F_spring3=k3*(PH_3-D_3);

% Force of spring 3 in CS3
H_cs3=transpose(R2)*[H_3;1];
H_3_cs3=[H_cs3(1)-r1; H_cs3(2); H_cs3(3)-r3];

D3_cs3=transpose(R2)*[D_3;1];
F_spring3_cs3=k3*(P_3_cs3-H_3_cs3-D3_cs3(1:3));

% Spring with reference to LINK 4
%%%%%%%%%%%%%%%%%%%%%%%%%%%%%%%%%%%%
if SOLUTION == 0
nx_4=231.4; ny_4=69.6; nz_4=8.2;  % measure from RecurDyn >>> PARAM >>>
elseif SOLUTION == 1
nx_4=214.6; ny_4=69.6; nz_4=66.7; % measure from RecurDyn >>> PARAM >>>
elseif SOLUTION == 2
nx_4=x4; ny_4=0; nz_4=0;
end
X_4(i)=nx_4*st4-nz_4*ct4; Y_4(i)=ny_4; Z_4(i)=nx_4*ct4+nz_4;
P_4cs4=[X_4(i); Y_4(i); Z_4(i)];
P_4cs=[X_4(i); Y_4(i)-r2; Z_4(i)-r3];
P_4cs3=R_3*P_4cs;           % local system CS3
P_4cs2=R2*R3*[P_4cs;1];     % global system GCS2

% Force of spring 4 in GCS2
H_4=[h4_x; h4_y; h4_z];     % global system GCS2
P_4=P_4cs2(1:3);

v4=[P_4(1)-h4_x; P_4(2)-h4_y; P_4(3)-h4_z];
```

```
v4_m=sqrt(v4(1)^2+v4(2)^2+v4(3)^2);
v4_v=[v4(1)/v4_m; v4(2)/v4_m; v4(3)/v4_m];

D_4=v4_v*d_04; PH_4=P_4 - H_4;
F_spring4=k4*(PH_4-D_4);

% Force of spring 4 in CS3
H_cs3=transpose(R2)*[H_4;1];
H_4_cs3=[H_cs3(1)-r1; H_cs3(2); H_cs3(3)-r3];

D4_cs3=transpose(R2)*[D_4;1];
F_spring4_cs3=k4*(P_4cs3-H_4_cs3-D4_cs3(1:3));

% Force of spring 4 in CS4
H1=R_3'*H_4_cs3;
H_4_cs4=[H1(1); H1(2)+r2; H1(3)+r3];

D4_cs4=R_3'*D4_cs3(1:3);
F_spring4_cs4=k4*(P_4cs4-H_4_cs4-D4_cs4(1:3));

% Spring balancing torques
% M2 spring
M2_spring(i)=F_spring2(3,1)*P_2(2,1)-F_spring2(2,1)*P_2(3,1)+F_spring3(3,1)*P_3(2,1) ...
-F_spring3(2,1)*P_3(3,1)+F_spring4(3,1)*P_4(2,1)-F_spring4(2,1)*P_4(3,1);
% M3 spring
M3_spring(i)=-F_spring3_cs3(1,1)*P_3_cs3(2,1)+F_spring3_cs3(2,1)*P_3_cs3(1,1)...
-F_spring4_cs3(1,1)*P_4cs3(2,1)+F_spring4_cs3(2,1)*P_4cs3(1,1);
% M4 spring
M4_spring(i)=-F_spring4_cs4(3,1)*P_4cs4(1,1) + F_spring4_cs4(1,1)*P_4cs4(3,1);

elseif MODEL == 2
%%%%%%%%%%%%%%%%%%%%%%%%%%%%%%%%%%%%%%%%%%%%%%%%%%%%%%%%%%%%%%%%%%%%%%%%%%%%%%%%
%%%%%%%%%%%%%%%%%%%%%%%%%%%%%%%%%%% MODEL 2 %%%%%%%%%%%%%%%%%%%%%%%%%%%%%%%%%%%%%
%%%%%%%%%%%%%%%%%%%%%%%%%%%%%%%%%%%%%%%%%%%%%%%%%%%%%%%%%%%%%%%%%%%%%%%%%%%%%%%%

% Spring with reference to LINK 2
%%%%%%%%%%%%%%%%%%%%%%%%%%%%%%%%%%%
p_22=[lh2; 0; lv2]; % local system CS2
P_2=R2*[p_22; 1];

% Force of spring 2 in CS2
H_2=[h2_x; h2_y; h2_z]; P_2=P_2(1:3); PH_2=P_2-H_2;
F_spring2=k2*PH_2;

% Spring with reference to LINK 3
%%%%%%%%%%%%%%%%%%%%%%%%%%%%%%%%%%%
p_33=[0; -lh3; -lv3]; % local system CS3
P_3=R_3*p_33;

% Force of spring 3 in CS3
H_3=[h3_x; h3_y; h3_z]; P_3=P_3(1:3); PH_3=P_3-H_3;
F_spring3=k3*PH_3;

% Spring with reference to LINK 4
%%%%%%%%%%%%%%%%%%%%%%%%%%%%%%%%%%%
nx_4=x4; ny_4=0; nz_4=0; % Spring attached to link 4 COM
X_4(i)=nx_4*st4-nz_4*ct4; Y_4(i)=ny_4; Z_4(i)=nx_4*ct4+nz_4;
P_4=[X_4(i); Y_4(i); Z_4(i)];

% Force of spring 4 in CS4
H_4=[h4_x; h4_y; h4_z]; P_4=P_4(1:3); PH_4=P_4-H_4;
F_spring4=k4*PH_4;

% Spring balancing torques
M2_spring(i)=F_spring2(3,1)*P_2(2,1) - F_spring2(2,1)*P_2(3,1);  % M2 spring
M3_spring(i)=-F_spring3(1,1)*P_3(2,1) + F_spring3(2,1)*P_3(1,1); % M3 spring
M4_spring(i)=-F_spring4(3,1)*P_4(1,1) + F_spring4(1,1)*P_4(3,1); % M4 spring

end

M2_balanced(i)=M2(i)-M2_spring(i);       % M2 balanced
M3_balanced(i)=M3(i)-M3_spring(i);       % M3 balanced
M4_balanced(i)=M4_dec(i)-M4_spring(i); % M4 balanced

end

y=rms(M2_balanced)+rms(M3_balanced)+rms(M4_balanced)+rms(M1_balanced)+rms(M5_balanced);

end
```

A.4. F_nlc.m

```
% Matlab Code: nonlinear constraint function
% The constraints have been defined in accordance with the exoskeleton parametric model implemented in the software RecurDyn.

function [c1,ceq1, c2,ceq2, c3,ceq3] = F_nlc(X)

r=65; xc=0; yc=-42.5;

eq_cyl_1=(X(2)-xc)^2+(X(3)-yc)^2;    c1=(r^2-eq_cyl_1); ceq1=[];
eq_cyl_2=(X(6)-xc)^2+(X(7)-yc)^2;    c2=(r^2-eq_cyl_2); ceq2=[];
```

```
eq_cyl_3=(X(10)-xc)^2+(X(11)-yc)^2; c3=(r^2-eq_cyl_3); ceq3=[];

end
```

A.5. OPTIM_TS.m

```
% Matlab code: optimization process
% This attachment contains the Matlab code implemented for the 6-DOFs passive upper limb exoskeleton with torsional springs.

clear all
close all
clc

lim=180;

% k_it is for the torsional constant, t_il is for the angular preload (theta % load) of the i-spring
%  [k_1t;k_2t;k_3t;k_4t;k_5t;       t_1l;t_2l;t_3l;t_4l;t_5l  ]
x0=[100;100;100;100;100;            0;0;0;0;0                 ];
lb=[0.1;0.1;0.1;0.1;0.1;           -lim;-lim;-lim;-lim;-lim   ];

ub=[20000;20000;20000;20000;20000; lim;lim;lim;lim;lim        ];

nlc=[]; opt=[];

rng default
problem=createOptimProblem('fmincon','x0',x0,'objective',@F_TS,'lb',lb,'ub',ub,'nonlcon',nlc,'options',opt);

rs = RandomStartPointSet; ms = MultiStart;
[xyopt,fval]=run(ms,problem,rs);
xyopt
```

A.6. PLOT_TS.m

```
% Matlab Code: optimized function
% This attachment contains the Matlab code implemented for the 6-DOFs passive upper limb exoskeleton with torsional springs.

% The script contains the index MOV

% Let chose:

% MOV = 1 for enforcing the first movement
% MOV = 2 for enforcing the second movement
% MOV = 3 for enforcing the third movement

% The used parameters have been defined from the exoskeleton parametric model implemented in the MBD software RecurDyn.
% By updating the parameters as desired the code can be automatically run.
% In the following, the parameters that may be changed as desired are indicated % as follows: >>> PARAM >>>

clear all
close all
clc

% Index
MOV=3;

% xyopt is the optimization result obtained by running the file "OPTIM_TS.m"
% NOTE: check that the Indices are the same imposed in the "F_TS.m file"
xyopt=[3014.9761;19999.9999;1918.6339;2350.8892;811.0103;-63.1718;-0.0155;-1.2385;-179.9999;-96.9350]

% Constants
g=9.81;       %[m/s^2]
DTOR=pi/180; %[rad/deg]

% Concentrated Masses [kg] >>> PARAM >>>
m1=2.1; m2=1.2;

% Link masses [kg] (density carbon fiber 1.6e-006 kg/mm^3) >>> PARAM >>>
m_1=2.06e-002;  m_4=5.03e-002;  m_5=3.72e-002;  m_1a=2.06e-002;
m_4a=5.03e-002; m_2a=9.25e-003; m_5a=1.40e-002; m_2=3.04e-002;
m_3=3.66e-002;  m_4t=(m_4+m_4a+m_5a+m1+m2+m_5); % Combined COM

% Geometric parameters [mm]  >>> PARAM >>>
dim1=75; dim2=95; r1=125; r2=75; r3=95;
l1=(dim1^2+dim2^2)^0.5; l4=307; l5=225; l5a=50; lv5a=10;

% Link COM position [mm]  >>> PARAM >>>
x1=l1/2; x4=l4/2; x5=l5/2; a4=0.44*l4; a5=0.425*l5;
lv2=61; lh2=52; lv3=54; lh3=57;

% Spring torsional constant [Nmm/rad]
k1r=xyopt(1); k2r=xyopt(2); k3r=xyopt(3); k4r=xyopt(4); k5r=xyopt(5);

% Exoskeleton initial configuration  >>> PARAM >>>
t10=-atan(dim1/dim2);          %[rad]
t20=0; t30=0; t40=106; t50=90; %[deg]

% Input rotations for each MOV [deg]  >>> PARAM >>>
```

```
if MOV == 1
deltat0_max=-5;  deltat1_max=-10; deltat2_max=-20;
deltat3_max=-40; deltat4_max=-20; deltat5_max=-10;

elseif MOV == 2
deltat0_max=10; deltat1_max=-10; deltat2_max=-15;
deltat3_max=35; deltat4_max=-30; deltat5_max=-25;

elseif MOV == 3
deltat0_max=0;  deltat1_max=-15; deltat2_max=-5;
deltat3_max=15; deltat4_max=-45; deltat5_max=-100;
end

% Spring angular initial position (preload) [deg]
deltat1_opt=xyopt(6); deltat2_opt=xyopt(7); deltat3_opt=xyopt(8); deltat4_opt=xyopt(9); deltat5_opt=xyopt(10);

% Spring angular initial position (preload) [rad]
deltat1_max_rad=deltat1_opt*DTOR; deltat2_max_rad=deltat2_opt*DTOR;
deltat3_max_rad=deltat3_opt*DTOR; deltat4_max_rad=deltat4_opt*DTOR;
deltat5_max_rad=deltat5_opt*DTOR;

% Time vector
step=100; sim_time=100; time=0:sim_time/step:sim_time;

% Input joint rotation vectors
if deltat0_max==0
deltat0=zeros(1,step+1);
else
deltat0=(0:deltat0_max/step:deltat0_max)*DTOR;
end
t0=deltat0;
if deltat1_max==0
deltat1=zeros(1,step+1);
else
deltat1=(0:deltat1_max/step:deltat1_max)*DTOR;
end
t1=deltat1+t10;
if deltat2_max==0
deltat2=zeros(1,step+1);
else
deltat2=(0:deltat2_max/step:deltat2_max)*DTOR;
end
t2=deltat2+t20*DTOR;
if deltat3_max==0
deltat3=zeros(1,step+1);
else
deltat3=(0:deltat3_max/step:deltat3_max)*DTOR;
end
t3=deltat3+t30*DTOR;
if deltat4_max==0
deltat4=zeros(1,step+1);
else
deltat4=(0:deltat4_max/step:deltat4_max)*DTOR;
end
t4=deltat4+t40*DTOR;
if deltat5_max==0
deltat5=zeros(1,step+1);
else
deltat5=(0:deltat5_max/step:deltat5_max)*DTOR;
end
t5=deltat5+t50*DTOR;

% Kinematic and static analysis
h4_m1=a4*sin(t4); h4=l4*sin(t4);
h5_m2=a5*sin(t5); v4_m1=-a4*cos(t4);
v4=-l4*cos(t4); v5_m2=-a5*cos(t5);
h3_m1=h4_m1.*sin(t3); h3_m2=(h4+h5_m2).*sin(t3);
v3_m1=h4_m1.*cos(t3); v3_m2=(h4+h5_m2).*cos(t3);
r_m1=(h3_m1.^2+v4_m1.^2).^0.5; r_m2=(h3_m2.^2+(v4+v5_m2).^2).^0.5;

if deltat3_max >= 0
j=1;
else
j=2;
end

h2_m1=(-1)^j*r_m1.*cos(t2+atan(-v4_m1./h3_m1));
h2_m2=(-1)^j*r_m2.*cos(t2+atan(-(v4+v5_m2)./h3_m2));
h4m4=x4*sin(t4);
v4m4=-x4*cos(t4);
h5m5=x5*sin(t5);
v5m5=-x5*cos(t5);
h3m4=h4m4.*sin(t3);
v3m4=h4m4.*cos(t3);
h3m5=(h4+h5m5).*sin(t3);
v3m5=(h4+h5m5).*cos(t3);
rm4=(h3m4.^2+v4m4.^2).^0.5;
rm5=(h3m5.^2+(v4+v5m5).^2).^0.5;
h2m4=(-1)^j*rm4.*cos(t2+atan(-v4m4./h3m4));
h2m5=(-1)^j*rm5.*cos(t2+atan(-(v4+v5m5)./h3m5));
v4m4a=v4m4+l5a;
rm4a=(h3m4.^2+v4m4a.^2).^0.5;
h2m4a=(-1)^j*rm4a.*cos(t2+atan(-v4m4a./h3m4));
h3m5a=h4.*sin(t3);
v3m5a=h4.*cos(t3);
```

```
v4m5a=v4+lv5a;
rm5a=(h3m5a.^2+v4m5a.^2).^0.5;
h2m5a=(-1)^j*rm5a.*cos(t2+atan(-v4m5a/h3m5a));

% Torque in CS1
% M1 graviational
M1_dec=((m_1 + m_1a)*x1 + l1*(m1+m2 + m_4+m_5 + m_4a + m_2a+m_5a))*g*cos(t1);
M1_dec=M1_dec + l1*(m_2+m_3)*g*cos(t1);
% M1 spring rot
M1_spring_rot=k1r.*(t1-t10-deltat1_max_rad);
% M1 balanced
M1_balanced=M1_dec-M1_spring_rot;

for i=1:1:step+1
ct0=cos(t0(i)); st0=sin(t0(i)); ct1=cos(t1(i)); st1=sin(t1(i));
ct2=cos(t2(i)); st2=sin(t2(i)); ct3=cos(t3(i)); st3=sin(t3(i));
ct4=cos(t4(i)); st4=sin(t4(i)); ct5=cos(t5(i)); st5=sin(t5(i));

% Rotation matrices
R_2=[1 0 0; 0 ct2 -st2; 0 st2 ct2]; R_3=[ct3 -st3 0; st3 ct3 0; 0 0 1];
R_4=[ct4 0 st4; 0 1 0; -st4 0 ct4]; R_5=[ct5 0 st5; 0 1 0 ; -st5 0 ct5];

% Force in CS0
f_m4=[0; 0; -m_4*g];    f_m3=[0; 0; -m_3*g]; f_m4a=[0; 0; -m_4a*g];
f_m5a=[0; 0; -m_5a*g]; f_m1=[0; 0; -m1*g];   f_m2=[0; 0; -m2*g];
f_m5=[0; 0; -m_5*g];

% Force in CS3
f_m4_CS3=transpose(R_2*R_3)*f_m4;    f_m3_CS3=transpose(R_2*R_3)*f_m3;
f_m4a_CS3=transpose(R_2*R_3)*f_m4a; f_m5a_CS3=transpose(R_2*R_3)*f_m5a;
f_m1_CS3=transpose(R_2*R_3)*f_m1;    f_m2_CS3=transpose(R_2*R_3)*f_m2;
f_m5_CS3=transpose(R_2*R_3)*f_m5;

% Force in CS4
f_m4_CS4=transpose(R_2*R_3*R_4)*f_m4;    f_m4a_CS4=transpose(R_2*R_3*R_4)*f_m4a;
f_m5a_CS4=transpose(R_2*R_3*R_4)*f_m5a; f_m1_CS4=transpose(R_2*R_3*R_4)*f_m1;
f_m2_CS4=transpose(R_2*R_3*R_4)*f_m2;    f_m5_CS4=transpose(R_2*R_3*R_4)*f_m5;

% Force in CS5
f_m2_CS5=transpose(R_2*R_3*R_5)*f_m2; f_m5_CS5=transpose(R_2*R_3*R_5)*f_m5;

% Momento in CS2
% M2 gravitational
M2(i)=(h2m4(i) + r2*ct3*ct2)*m_4*g;
M2(i)=M2(i) + (h2m4a(i) + r2*ct3*ct2)*m_4a*g + (h2m5a(i) +r2*ct3*ct2)*m_5a*g;
M2(i)=M2(i) + ((lh3*ct3)*ct2+(r3-lv3)*st2)*m_3*g;
M2(i)=M2(i) + m1*g*h2_m1(i) + m2*g*h2_m2(i);
M2(i)=M2(i) + (h2m5(i) + r2*ct3*ct2)*m_5*g;

% Torque in CS3
% M3 gravitational
M3(i)=f_m4_CS3(2,1)*(v3m4(i)^2+h3m4(i)^2)^0.5 + f_m4_CS3(1,1)*r2;
M3(i)=M3(i) + f_m3_CS3(1,1)*lh3;
M3(i)=M3(i) + f_m4a_CS3(2,1)*(v3m4(i)^2+h3m4(i)^2)^0.5 + f_m4a_CS3(1,1)*r2;
M3(i)=M3(i) + f_m5a_CS3(2,1)*(v3m5a(i)^2+h3m5a(i)^2)^0.5 + f_m5a_CS3(1,1)*r2;
M3(i)=M3(i) + f_m1_CS3(2,1)*(v3_m1(i)^2+h3_m1(i)^2)^0.5 + f_m2_CS3(2,1)*(v3_m2(i)^2+h3_m2(i)^2)^0.5;
M3(i)=M3(i) + f_m5_CS3(2,1)*(v3m5(i)^2+h3m5(i)^2)^0.5 + f_m5_CS3(1,1)*r2;

% Torque in CS4
% M4 gravitational
M4_dec(i)=f_m4_CS4(1,1)*x4 + f_m5_CS4(1,1)*l4;
M4_dec(i)=M4_dec(i) + f_m4a_CS4(1,1)*x4 + f_m5a_CS4(1,1)*l4;
M4_dec(i)=M4_dec(i) + f_m1_CS4(1,1)*a4 + f_m2_CS4(1,1)*l4;

% Torque in CS5
% M5 gravitational
M5(i)=f_m2_CS5(1,1)*a5;
M5(i)=M5(i) + f_m5_CS5(1,1)*x5;
% M5 spring
M5_spring_rot(i)=k5r*(t5(i)-t50*DTOR-deltat5_max_rad);
% M5 balanced
M5_balanced(i)=M5(i)-M5_spring_rot(i);

% Transformation matrices
R2=[1 0 0 0; 0 ct2 -st2 0; 0 st2 ct2 0; 0 0 0 1];
R3=[ct3 -st3 0 r1; st3 ct3 0 0; 0 0 1 r3; 0 0 0 1];

M2_spring_rot(i)=k2r*(t2(i)-deltat2_max_rad);           % M2 spring
M3_spring_rot(i)=k3r*(t3(i)-deltat3_max_rad);           % M3 spring
M4_spring_rot(i)=k4r*(t4(i)-t40*DTOR-deltat4_max_rad); % M4 spring

M2_balanced(i)=M2(i)-M2_spring_rot(i);      % M2 balanced
M3_balanced(i)=M3(i)-M3_spring_rot(i);      % M3 balanced
M4_balanced(i)=M4_dec(i)-M4_spring_rot(i); % M4 balanced

end

% Plot of the gravitational and the balanced torque for each R joint
f1 = figure; plot(time,M1_dec,'b');
hold on
plot(time,M1_balanced,'*g','MarkerIndices',[1:3:100]);
xlabel('Movement progress [%]'); ylabel ('Torque [Nmm]')
legend('M_1 ','M_1_,_b')

f2 = figure; plot(time,-M2)
```

```
hold on
plot(time,-M2_balanced,'*g','MarkerIndices',[1:3:100])
xlabel('Movement progress [%]'); ylabel ('Torque [Nmm]')
legend('M_2','M_2_,_b')

f3 = figure; plot(time,M3)
hold on
plot(time,+M3_balanced,'*g','MarkerIndices',[1:3:100])
xlabel('Movement progress [%]'); ylabel ('Torque [Nmm]')
legend('M_3','M_3_,_b')

f4 = figure; plot(time,M4_dec)
hold on
plot(time,M4_balanced,'*g','MarkerIndices',[1:3:100])
xlabel('Movement progress [%]'); ylabel ('Torque [Nmm]')
legend('M_4','M_4_,_b')

f5 = figure; plot(time,M5)
hold on
plot(time,M5_balanced,'*g','MarkerIndices',[1:3:100])
xlabel('Movement progress [%]'); ylabel ('Torque [Nmm]')
legend('M_5','M_5_,_b')
```

A.7. F_TS.m

```
% Matlab Code: optimized function
% This attachment contains the Matlab code implemented for the 6-DOFs passive upper limb exoskeleton with torsional springs.

% The script contains the index MOV

% Let chose:

% MOV = 1 for enforcing the first movement
% MOV = 2 for enforcing the second movement
% MOV = 3 for enforcing the third movement

% The used parameters have been defined from the exoskeleton parametric model implemented in the MBD software RecurDyn.
% By updating the parameters as desired the code can be automatically run.
% In the following, the parameters that may be changed as desired are indicated % as follows: >>> PARAM >>>

function y = F_TS(X)

% Index
MOV=3;

global m_2 m_3 m_4t g time

% Constants
g=9.81;       %[m/s^2]
DTOR=pi/180; %[rad/deg]

% Concentrated Masses [kg] >>> PARAM >>>
m1=2.1; m2=1.2;

% Link masses [kg] (density carbon fiber 1.6e-006 kg/mm^3) >>> PARAM >>>
m_1=2.06e-002;  m_4=5.03e-002;  m_5=3.72e-002;  m_1a=2.06e-002;
m_4a=5.03e-002; m_2a=9.25e-003; m_5a=1.40e-002; m_2=3.04e-002;
m_3=3.66e-002;  m_4t=(m_4+m_4a+m_5a+m1+m2+m_5); % Combined COM

% Geometric parameters [mm]  >>> PARAM >>>
dim1=75; dim2=95; r1=125; r2=75; r3=95;
l1=(dim1^2+dim2^2)^0.5; l4=307; l5=225; l5a=50; lv5a=10;

% Link COM position [mm]  >>> PARAM >>>
x1=l1/2; x4=l4/2; x5=l5/2; a4=0.44*l4; a5=0.425*l5;
lv2=61; lh2=52; lv3=54; lh3=57;

% Spring torsional constant [Nmm/rad]
k1r=X(1); k2r=X(2); k3r=X(3); k4r=X(4); k5r=X(5);

% Exoskeleton initial configuration  >>> PARAM >>>
t10=-atan(dim1/dim2);          %[rad]
t20=0; t30=0; t40=106; t50=90; %[deg]

% Input rotations for each MOV [deg]  >>> PARAM >>>
if MOV == 1
deltat0_max=-5;  deltat1_max=-10; deltat2_max=-20;
deltat3_max=-40; deltat4_max=-20; deltat5_max=-10;

elseif MOV == 2
deltat0_max=10; deltat1_max=-10; deltat2_max=-15;
deltat3_max=35; deltat4_max=-30; deltat5_max=-25;

elseif MOV == 3
deltat0_max=0;  deltat1_max=-15; deltat2_max=-5;
deltat3_max=15; deltat4_max=-45; deltat5_max=-100;
end

% Spring angular initial position (preload) [deg]
deltat1_opt=X(6); deltat2_opt=X(7); deltat3_opt=X(8);
deltat4_opt=X(9); deltat5_opt=X(10);
```

```
% Spring angular initial position (preload) [rad]
deltat1_max_rad=deltat1_opt*DTOR; deltat2_max_rad=deltat2_opt*DTOR;
deltat3_max_rad=deltat3_opt*DTOR; deltat4_max_rad=deltat4_opt*DTOR;
deltat5_max_rad=deltat5_opt*DTOR;

% Time vector
step=100; sim_time=100; time=0:sim_time/step:sim_time;

% Input joint rotation vectors
if deltat0_max==0
deltat0=zeros(1,step+1);
else
deltat0=(0:deltat0_max/step:deltat0_max)*DTOR;
end
t0=deltat0;
if deltat1_max==0
deltat1=zeros(1,step+1);
else
deltat1=(0:deltat1_max/step:deltat1_max)*DTOR;
end
t1=deltat1+t10;
if deltat2_max==0
deltat2=zeros(1,step+1);
else
deltat2=(0:deltat2_max/step:deltat2_max)*DTOR;
end
t2=deltat2+t20*DTOR;
if deltat3_max==0
deltat3=zeros(1,step+1);
else
deltat3=(0:deltat3_max/step:deltat3_max)*DTOR;
end
t3=deltat3+t30*DTOR;
if deltat4_max==0
deltat4=zeros(1,step+1);
else
deltat4=(0:deltat4_max/step:deltat4_max)*DTOR;
end
t4=deltat4+t40*DTOR;
if deltat5_max==0
deltat5=zeros(1,step+1);
else
deltat5=(0:deltat5_max/step:deltat5_max)*DTOR;
end
t5=deltat5+t50*DTOR;

% Kinematic and static analysis
h4_m1=a4*sin(t4); h4=l4*sin(t4);
h5_m2=a5*sin(t5); v4_m1=-a4*cos(t4);
v4=-l4*cos(t4); v5_m2=-a5*cos(t5);
h3_m1=h4_m1.*sin(t3); h3_m2=(h4+h5_m2).*sin(t3);
v3_m1=h4_m1.*cos(t3); v3_m2=(h4+h5_m2).*cos(t3);
r_m1=(h3_m1.^2+v4_m1.^2).^0.5; r_m2=(h3_m2.^2+(v4+v5_m2).^2).^0.5;

if deltat3_max >= 0
j=1;
else
j=2;
end

h2_m1=(-1)^j*r_m1.*cos(t2+atan(-v4_m1./h3_m1));
h2_m2=(-1)^j*r_m2.*cos(t2+atan(-(v4+v5_m2)./h3_m2));
h4m4=x4*sin(t4);
v4m4=-x4*cos(t4);
h5m5=x5*sin(t5);
v5m5=-x5*cos(t5);
h3m4=h4m4.*sin(t3);
v3m4=h4m4.*cos(t3);
h3m5=(h4+h5m5).*sin(t3);
v3m5=(h4+h5m5).*cos(t3);
rm4=(h3m4.^2+v4m4.^2).^0.5;
rm5=(h3m5.^2+(v4+v5m5).^2).^0.5;
h2m4=(-1)^j*rm4.*cos(t2+atan(-v4m4./h3m4));
h2m5=(-1)^j*rm5.*cos(t2+atan(-(v4+v5m5)./h3m5));
v4m4a=v4m4+l5a;
rm4a=(h3m4.^2+v4m4a.^2).^0.5;
h2m4a=(-1)^j*rm4a.*cos(t2+atan(-v4m4a./h3m4));
h3m5a=h4.*sin(t3);
v3m5a=h4.*cos(t3);
v4m5a=v4+lv5a;
rm5a=(h3m5a.^2+v4m5a.^2).^0.5;
h2m5a=(-1)^j*rm5a.*cos(t2+atan(-v4m5a/h3m5a));

% Torque in CS1
% M1 graviational
M1_dec=((m_1 + m_1a)*x1 + l1*(m1+m2 + m_4+m_5 + m_4a + m_2a+m_5a))*g*cos(t1);
M1_dec=M1_dec + l1*(m_2+m_3)*g*cos(t1);
% M1 spring rot
M1_spring_rot=k1r.*(t1-t10-deltat1_max_rad);
% M1 balanced
M1_balanced=M1_dec-M1_spring_rot;

for i=1:1:step+1
ct0=cos(t0(i)); st0=sin(t0(i)); ct1=cos(t1(i)); st1=sin(t1(i));
ct2=cos(t2(i)); st2=sin(t2(i)); ct3=cos(t3(i)); st3=sin(t3(i));
```

```
ct4=cos(t4(i)); st4=sin(t4(i)); ct5=cos(t5(i)); st5=sin(t5(i));

% Rotation matrices
R_2=[1 0 0; 0 ct2 -st2; 0 st2 ct2]; R_3=[ct3 -st3 0; st3 ct3 0; 0 0 1];
R_4=[ct4 0 st4; 0 1 0; -st4 0 ct4]; R_5=[ct5 0 st5; 0 1 0 ; -st5 0 ct5];

% Force in CS0
f_m4=[0; 0; -m_4*g];    f_m3=[0; 0; -m_3*g]; f_m4a=[0; 0; -m_4a*g];
f_m5a=[0; 0; -m_5a*g]; f_m1=[0; 0; -m1*g];   f_m2=[0; 0; -m2*g];
f_m5=[0; 0; -m_5*g];

% Force in CS3
f_m4_CS3=transpose(R_2*R_3)*f_m4;    f_m3_CS3=transpose(R_2*R_3)*f_m3;
f_m4a_CS3=transpose(R_2*R_3)*f_m4a; f_m5a_CS3=transpose(R_2*R_3)*f_m5a;
f_m1_CS3=transpose(R_2*R_3)*f_m1;    f_m2_CS3=transpose(R_2*R_3)*f_m2;
f_m5_CS3=transpose(R_2*R_3)*f_m5;

% Force in CS4
f_m4_CS4=transpose(R_2*R_3*R_4)*f_m4;    f_m4a_CS4=transpose(R_2*R_3*R_4)*f_m4a;
f_m5a_CS4=transpose(R_2*R_3*R_4)*f_m5a; f_m1_CS4=transpose(R_2*R_3*R_4)*f_m1;
f_m2_CS4=transpose(R_2*R_3*R_4)*f_m2;    f_m5_CS4=transpose(R_2*R_3*R_4)*f_m5;

% Force in CS5
f_m2_CS5=transpose(R_2*R_3*R_5)*f_m2; f_m5_CS5=transpose(R_2*R_3*R_5)*f_m5;

% Momento in CS2
% M2 gravitational
M2(i)=(h2m4(i) + r2*ct3*ct2)*m_4*g;
M2(i)=M2(i) + (h2m4a(i) + r2*ct3*ct2)*m_4a*g + (h2m5a(i) +r2*ct3*ct2)*m_5a*g;
M2(i)=M2(i) + ((lh3*ct3)*ct2+(r3-lv3)*st2)*m_3*g;
M2(i)=M2(i) + m1*g*h2_m1(i) + m2*g*h2_m2(i);
M2(i)=M2(i) + (h2m5(i) + r2*ct3*ct2)*m_5*g;

% Torque in CS3
% M3 gravitational
M3(i)=f_m4_CS3(2,1)*(v3m4(i)^2+h3m4(i)^2)^0.5 + f_m4_CS3(1,1)*r2;
M3(i)=M3(i) + f_m3_CS3(1,1)*lh3;
M3(i)=M3(i) + f_m4a_CS3(2,1)*(v3m4(i)^2+h3m4(i)^2)^0.5 + f_m4a_CS3(1,1)*r2;
M3(i)=M3(i) + f_m5a_CS3(2,1)*(v3m5a(i)^2+h3m5a(i)^2)^0.5 + f_m5a_CS3(1,1)*r2;
M3(i)=M3(i) + f_m1_CS3(2,1)*(v3_m1(i)^2+h3_m1(i)^2)^0.5 + f_m2_CS3(2,1)*(v3_m2(i)^2+h3_m2(i)^2)^0.5;
M3(i)=M3(i) + f_m5_CS3(2,1)*(v3m5(i)^2+h3m5(i)^2)^0.5 + f_m5_CS3(1,1)*r2;

% Torque in CS4
% M4 gravitational
M4_dec(i)=f_m4_CS4(1,1)*x4 + f_m5_CS4(1,1)*l4;
M4_dec(i)=M4_dec(i) + f_m4a_CS4(1,1)*x4 + f_m5a_CS4(1,1)*l4;
M4_dec(i)=M4_dec(i) + f_m1_CS4(1,1)*a4 + f_m2_CS4(1,1)*l4;

% Torque in CS5
% M5 gravitational
M5(i)=f_m2_CS5(1,1)*a5;
M5(i)=M5(i) + f_m5_CS5(1,1)*x5;
% M5 spring
M5_spring_rot(i)=k5r*(t5(i)-t50*DTOR-deltat5_max_rad);
% M5 balanced
M5_balanced(i)=M5(i)-M5_spring_rot(i);

% Transformation matrices
R2=[1 0 0 0; 0 ct2 -st2 0; 0 st2 ct2 0; 0 0 0 1];
R3=[ct3 -st3 0 r1; st3 ct3 0 0; 0 0 1 r3; 0 0 0 1];

M2_spring_rot(i)=k2r*(t2(i)-deltat2_max_rad);          % M2 spring
M3_spring_rot(i)=k3r*(t3(i)-deltat3_max_rad);          % M3 spring
M4_spring_rot(i)=k4r*(t4(i)-t40*DTOR-deltat4_max_rad); % M4 spring

M2_balanced(i)=M2(i)-M2_spring_rot(i);     % M2 balanced
M3_balanced(i)=M3(i)-M3_spring_rot(i);     % M3 balanced
M4_balanced(i)=M4_dec(i)-M4_spring_rot(i); % M4 balanced

end

y=rms(M2_balanced)+rms(M3_balanced)+rms(M4_balanced)+rms(M1_balanced)+rms(M5_balanced);

end
```

B. W-EXOS Kinematic Model

This appendix contains the following codes:

B.1. MAIN_KIN.m

B.2. F_KIN.m

B.3. F_DH.m

To compute the W-EXOS joints positions for a specific human wrist position, run the B.1. file. The B.2. file is a function called in the B.1. file containing the DH parameters and matrices to solve the device kinematics; whereas the B.3. file is a function called in the B.2. file (it is the matrix to be filled with the DH parameters).

B.1. MAIN_KIN.m

```
% This Matlab code computes the exskeleton rotations (J1, J2, J3) depending on a given human wrist rotations (PS, RUD, FE).

% By selecting the "Imposed Rotations" of the human wrist, the range of motion to be investigated is set.
% By selecting the index "joint", the kind of motion to impose is chosen (i.e., simple or combined motion).

% The optimization routine is set to compute the exoskeleton joint rotations.

DTOR=pi/180; %[rad/deg]

% Exoskeleton Initial Configuration: rotation human axis (PS,RU,FE) = (z,y,x)
z0=0; y0=0; x0=0; %[deg]

% Chose a value for the "Imposed Rotations" depending on the human wrist range of motion:
% PS [-90; 90], RU [-45; 15], FE [-85; 85]
% Imposed Rotations [deg]
ps_min=-10; ps_max=10; ru_min=-10; ru_max=10; fe_min=-10; fe_max=10;

% Sinusoidal motion law (y=a*sin(i+b)+c)
a1=abs(ps_max-ps_min)/2*DTOR; % PS
a2=abs(ru_max-ru_min)/2*DTOR; b2=(ru_max+ru_min)/2*DTOR;   phi2=-DTOR;  % RU
a3=abs(fe_max-fe_min)/2*DTOR; b3=(fe_max+fe_min)/2*DTOR;   phi3=-DTOR;  % FE

% Chose the index "joint"
joint = 1;      % = 1   for PS         (single joint motion)
                                % = 2   for RU         (single joint motion)
                                % = 3   for FE         (single joint motion)
                                % = 23  for RU, FE     (combined joint motion, two joints)
                                % = 231 for -RU, FE    (combined joint motion, two joints)
                                % = 232 for RU, -FE    (combined joint motion, two joints)
                                % 12    for PS, RU     (combined joint motion, two joints)
                                % 13    for PS, FE     (combined joint motion, two joints)
                                % 123   for PS, RU, FE (combined joint motion, all joints)

counter=1;
f=0.75;          % chose the motion speed in terms of frequency [Hz]
T=1/f;           % period of the sinusoidal motion law [sec]
w=2*pi/T;        % angular speed [rad/s]
time=[0:0.01:T]; % time vector [sec]
delta_t=0.01;

for t=0:delta_t:T %>>> start of cycle "for"
i=w*t;
% single joint motion
if joint==1 %PS
z=a1*sin(i); y=0*sin(i); x=0*sin(i);
elseif joint==2 %RU
z=0*sin(i); y=a2*(sin(i+phi2))+b2; x=0*sin(i);
elseif joint==3 %FE
z=0*sin(i); y= 0*sin(i); x=a3*sin(i+phi3)+b3;
% combined joint motion (two joints)
elseif joint==23 %RU, FE
z=0*sin(i); y=a2*(sin(i+phi2))+b2; x=a3*sin(i+phi3)+b3;
elseif joint==231 %-RU, FE
z=0*sin(i); y=-(a2*(sin(i+a2))-15*DTOR); x=a3*sin(i+phi3)+b3;
elseif joint==232 %RU, -FE
z=0*sin(i); y=a2*(sin(i+phi2))+b2; x=-(a3*sin(i-phi3)+11*DTOR);
elseif joint==12 %PS, RU
z=a1*sin(i); y=a2*(sin(i+phi2))+b2; x=0*sin(i);
elseif joint==13 %PS, FE
z=a1*sin(i); y=0*sin(i); x=a3*sin(i+phi3)+b3;
% combined joint motion (all joints)
elseif joint==123 %PS, RU, FE
z=a1*sin(i); y=a2*(sin(i+phi2))+b2; x=a3*sin(i+phi3)+b3;
end

% Optimization
q0=[0; 0; 0]; lb=[-pi; -pi; -pi]; ub=[pi; pi; pi];

options = optimoptions('fmincon','OptimalityTolerance',1e-18,'StepTolerance',1e-18);
[q,fval,exitflag]=fmincon(@(q)F_KIN(q,z,y,x),q0,[],[],[],[],lb,ub,[],options);

q_exos(:,counter)=q;         %Exoskeleton joints (non-perpendicular axes) [rad]
q_human(:,counter)=[z,y,x]; %Human joints (perpendicular axes) [rad]
counter=counter+1;

end %<<< end of cycle "for"

% Exoskeleton joints (non-perpendicular axes) [deg]
q_exos_deg =q_exos/DTOR;
ps_exos=q_exos_deg(1,:); ru_exos=-q_exos_deg(2,:); fe_exos=-q_exos_deg(3,:);

% Human joints (perpendicular axes) [deg]
```

```
q_human_deg=q_human/DTOR;
ps_human=q_human_deg(1,:); ru_human=q_human_deg(2,:); fe_human=q_human_deg(3,:);

% Plot of results
figure; plot(time, ps_human, 'g')
hold on
plot(time, ps_exos, '*g','MarkerIndices',[1:3:150]);
plot(time, ru_human, 'r')
plot(time, ru_exos, '*r','MarkerIndices',[1:3:150]);
plot(time, fe_human, 'b')
plot(time, fe_exos, '*b','MarkerIndices',[1:3:150]);
title('Human Wrist vs W-EXOS')
legend('PS', 'J1', 'RU', 'J2', 'FE', 'J3'); xlim([0 T]);
ylabel('joint position [deg]','FontWeight','bold','FontSize',12,'FontName','Calibri');
xlabel('time [s]','FontWeight','bold','FontSize',12,'FontName','Calibri');
```

B.2. F_KIN.m

```
% This Matlab code is the function called in the "wexos_kinematics" file in the optimization process

function F_sum = F_KIN(q,z,y,x)

DTOR=pi/180; %[rad/deg]
gamma_1=10*DTOR; gamma_2=15*DTOR; %[rad]

% Denavit Hartemberg method
DH.theta = [ 0       0                  pi/2+gamma_2 ];
DH.alfa  = [ 0       pi/2+gamma_1       -pi/2        ];
DH.q =     [ q(1)    q(2)               q(3)         ];
T = eye(3);
for i = 1:3
A(:,:,i) = F_DH([DH.theta(i) DH.alfa(i) DH.q(i)]);
T = T*A(:,:,i);
end
T_q=T;

DH.theta = [ 0       0                  pi/2+gamma_2 ];
DH.alfa  = [ 0       pi/2+gamma_1       -pi/2        ];
DH.q =     [ 0       0                  0            ];
T = eye(3);
for i = 1:3
A(:,:,i) = F_DH([DH.theta(i) DH.alfa(i) DH.q(i)]);
T = T*A(:,:,i);
end
T_0 = T;

T_tot = T_q*inv(T_0);

% Rotation matrixes (human wrist)
Rz = [cos(z) -sin(z) 0 ; sin(z) cos(z) 0 ; 0 0 1];
Ry = [cos(y) 0 sin(y) ; 0 1 0 ; -sin(y) 0 cos(y)];
Rx = [1 0 0 ; 0 cos(x) -sin(x) ; 0 sin(x) cos(x)];
Rzyx = Rx*Ry*Rz;

% Optimization function
F(1)=T_tot(:,1)'*Rzyx(:,1)-1;
F(2)=T_tot(:,2)'*Rzyx(:,2)-1;
F(3)=T_tot(:,3)'*Rzyx(:,3)-1;
F_sum=abs(F(1))+abs(F(2))+abs(F(3));

end
```

B.3. F_DH.m

```
% This Matlab code is the function called in the "F_KIN" file in the Denavit Hartemberg method

function R = F_DH(p)

% p = [theta alfa q]
Rz =[cos(p(1)) -sin(p(1)) 0 ; sin(p(1)) cos(p(1)) 0 ; 0 0 1];
Rx =[1 0 0 ; 0 cos(p(2)) -sin(p(2)) ; 0 sin(p(2)) cos(p(2))];
Rzq=[cos(p(3)) -sin(p(3)) 0 ; sin(p(3)) cos(p(3)) 0 ; 0 0 1];

R=Rz*Rx*Rzq;

end
```

C. Related Activities

This appendix mentions the major activities of interest carried out during the Doctor of Philosophy program.

C.1. Collaborations

The major of the work has been carried out between the Mechanical Computer Aided Engineering laboratory (MCAElab) - Department of Mechanical, Energy, Management and Transportation Engineering of the University of Genova, Italy, and the Institute of Mechanical Intelligence (IIM) of the Scuola Superiore Sant'Anna of Pisa, Italy.

Part of the research has been carried out at the Flexible Research Group - Mechanical and Aerospace Engineering Department of the University of California Los Angeles (UCLA), United States.

C.2. Awards

- *IDETC-CIE 2024 Compliant Mechanism Award*

  Vazzoler, G., Shimohara, S., Berselli, G., Hopkins, J.B., 2024. "Design Methodology and Physical Prototyping of a Binary Stiffness, Rotary Motion, Compliant Mechanism with Multiple, Decoupled, Degrees-of-Freedom". *International Design Engineering Technical Conferences & Computers and Information in Engineering Conference* - Published in the IDETC24 Special Issue, Journal of Mechanical Design, Transactions of the ASME - DOI.

- *Finalist for the I-RIM 2022 Best Paper Award*

  Vazzoler, G., Berselli, G., Frisoli, A., 2022. "A Concept for a Gravity-Balanced Upper-Limb Exoskeleton". *4th Italian Conference for Robotics and Intelligent Machines* - DOI.

- *FAIM 2022 Best Paper Award*

  Merlo, F., **Vazzoler, G.,** Berselli, G., 2022. "Eco-Programming of Industrial Robots for Sustainable Manufacturing". *31st International Conference on Flexible Automation and Intelligent Manufacturing* - DOI.

- *Master's Thesis Award 2021- ADM Special Mention*

  Master's degree in Mechanical Engineering - Design and Production, University of Genova, 2020. Thesis title: Preliminary Design and Virtual Prototyping of an Exoskeleton for Upper Limbs; Candidate: **G. Vazzoler**; Supervisors: Prog. Ing. G. Berselli, Dott. Ing. P. Bilancia. *National Association of Industrial Engineering Design and Methods*.

C.3. Teaching Support

- *Assistant Instructor*

  1. Master's Degree Course in Mechanical Engineering - Design and Production (Cod. 9269, class LM-33), University of Genova
     - Design of Automatic Machinery and Robots (Cod. 86927, Prof. G. Berselli, Italian language).

  - Design of Automatic Machinery and Robots (Cod. 98960, Prof. G. Berselli, English language).

2. $2nd$ Doctoral Summer School on Robotics and Intelligent Machines - DRIMS2, Scuola Superiore Sant'Anna, Pisa.

- *Member of the Examination Board*

1. Bachelor's Degree Course in Mechanical Engineering (Cod. 8720, class L-9), University of Genova:
   - Industrial Technical Design (Cod. 56657, Prof. G. Berselli, Italian language).
2. Master's Degree Course in Mechanical Engineering - Design and Production (Cod. 9269, class LM-33)), University of Genova:
   - Design of Automatic Machinery and Robots (Cod. 86927, Prof. G. Berselli, Italian language).
   - Design of Automatic Machinery and Robots (Cod. 98960, Prof. G. Berselli, English language).
   - Integrated CAD/CAE Mechanical Design (Cod. 108667, Prof. G. Berselli, Italian language).

- *Thesis Supervisor*

1. Bachelor Erasmus student Adrian-Mihail Neculae. Period: June 2022 - September 2022. Thesis tutor: Prof. G. Berselli (University of Genova).
2. Master student Edoardo Michele Migliano. Period: June 2022 - December 2023. Thesis tutor: Prof. G. Berselli (University of Genova).

C.4. Notable Projects

- *2024 - 2025* (under submission): PoC Instrument (Proof of Concept - Foundation Company of San Paolo) for the next patents (Italian patent granted):
  - *RE-Arm: Robotic solutions for advanced upper limb prostheses.* Project leader: Prof. G. Berselli. Patent application number 102023000019935 - Motorised upper limb prosthetic limb with optimised construction configuration.
  - *RE-Wrist: Robotic solutions for advanced wrist prostheses.* Project leader: Prof. G. Berselli. Patent application number 102023000027465 - Single and multi-degree-of-freedom joint with two or more of said advanced joints.

- *2023 - 2026* (ongoing): European Project SMERF: Small Medium Enterprise Ready for the Future. Interreg Central Europe, budget: EURO 2.49m. Partner: University of Genova.

- *2022 - 2026* (ongoing): European Project Fit4MedRob: Fit for Medical Robotics. Ministry of the University and Research (MUR, PNRR), budget: EURO 1.8m. Partner: University of Genova.

- *2022 - 2026* (ongoing): European Project IntelliMan: AI-Powered Manipulation System for Advanced Robotic Service, Manufacturing and Prosthetics. Budget: EURO 4.5m. Partner: University of Genova.
- *2020 - 2023*: National research project RoboGym: Robotic Gym for shoulder and upper limb rehabilitation. Budget: EURO 350 000. Partner: Scuola Superiore Sant'Anna of Pisa.

C.5. Roles in International Conferences and Communities

- *Chair*: SMASIS 2023 - ASME Premier Conference on Smart Materials, Adaptive Structures, and Intelligent Systems, Austin, Texas, USA, 10-13 Sept. 2023.
- *co-Chair*: SMASIS 2023 - ASME Premier Conference on Smart Materials, Adaptive Structures, and Intelligent Systems, Austin, Texas, USA, 10-13 Sept. 2023.
- *Leadership Team 2023 - 2024* for the Italy Section of ASME (American Society of Mechanical Engineering).